Validation Predictions of a 13 m/s Cross-wind Fire for Fuego and the University of Waterloo Dataset

Alexander L. Brown, Walter Gill, Greg Evans, Daniel Jarboe

Sandia National Laboratories

Validation Predictions of a 13 m/s Cross-wind Fire for Fuego and the University of Waterloo Dataset

Alexander L. Brown, Walter Gill
Fire & Aerosol Science Department 1532
Sandia National Laboratories
P.O. Box 5800
Albuquerque, NM 87185-1135

Gregory Evans, Daniel Jarboe
Department 8775
Sandia National Laboratories
P.O. Box 969
M.S. 9409
Livermore, CA 94551-0969

Abstract

Detailed herein are the results of a validation comparison.   The experiment involved a 2 meter diameter liquid pool of Jet-A fuel in a 13 m/s crosswind. The scenario included a large cylindrical blocking object just down-stream of the fire.   It also included seven smaller calorimeters and extensive instrumentation.   The experiments were simulated with Fuego. The model included several conduction regions to model the response of the calorimeters, the floor, and the large cylindrical blocking object. A blind comparison was used to compare the simulation predictions with the experimental data. The more upstream data compared very well with the simulation predictions. The more downstream data did not compare very well with the simulation predictions. Further investigation suggests that features omitted from the original model contributed to the discrepancies. Observations are made with respect to the scenario that are aimed at helping an analyst approach a comparable problem in a way that may help improve the potential for quantitative accuracy.

Acknowledgements

Contents

Table of Contents

List of Figures

List of Tables

This page is intentionally left blank

1. Introduction

Verification and validation of computer codes are essential processes that provide credibility to computational predictive results. They are specific processes among many software quality practices (Zepper et al 2002) that when combined permit predictions to be employed in a credible and sound scientific fashion. Validation is often used to mean various things, but herein is guided by the Advanced Simulation & Computing (ASC) guidelines for validation of computer codes. For the purposes of this document, validation is a process through which a computer code is evaluated through comparisons with experimental data. From Trucano et al (2002):

> …*validation* relies upon the process of comparing the results of [ASC] code calculations with the results of *physical experiments*, and has the primary goal of developing and quantifying sufficient *confidence* in the codes so that they can be used to predict a specified problem result.

The code in question for this work is the Fuego fire prediction code. It has been employed for several years at Sandia National Laboratories (SNL) to predict low-mach number fluid and heat transfer problems, and fire environments.

This present validation work stands on the back of the verification and validation activities previously performed for the tools employed in this study. The verification of the code is documented in the Verification Manual (2003). Validation that has been previously performed for the Fuego code resides in the categories listed in Oberkampf et al (2003; see Figure 3 therein) as unit problems, benchmark cases, and subsystem cases. This study is unique when compared to all previous validation studies in that it is an integral validation study. It is integral in the sense that a complete system is involved in the validation scenario. Most of the former verification and validation comparisons were not performed employing the full set of physical assumptions that are found in a typical fire environment. The fire environment of motivating interest to the development of this code involves a large (i.e. on the order of meters in dimension) spill of a liquid fuel and the subsequent heat transport to objects in the vicinity of the fire. Previous validation studies have been more limited in scope and size. This validation comparison was constructed to emulate an aircraft accident and subsequent fire under windy conditions. The calculation involves the full spectrum of physics models incorporated in the Fuego code to perform predictions. Chemistry, fluid dynamics, soot, participating media radiation heat transport, convection, and thermal conduction are all involved in this integral study.

With the goal of validation in mind, a repeatable and relevant test was designed to provide validation data for a fire in a cross-wind environment. The test was designed to meet the requirements of a comprehensive validation study. The size of the test objects, the scale of the fire, and the extent of instrumentation all lend to the quality of this test compared with other existing tests.

A challenge with this study is the maturity of Fuego as an analytical code. This project involved in many cases very new features to the code. Additionally, the scope of the calculations is large compared to other calculations formerly performed.
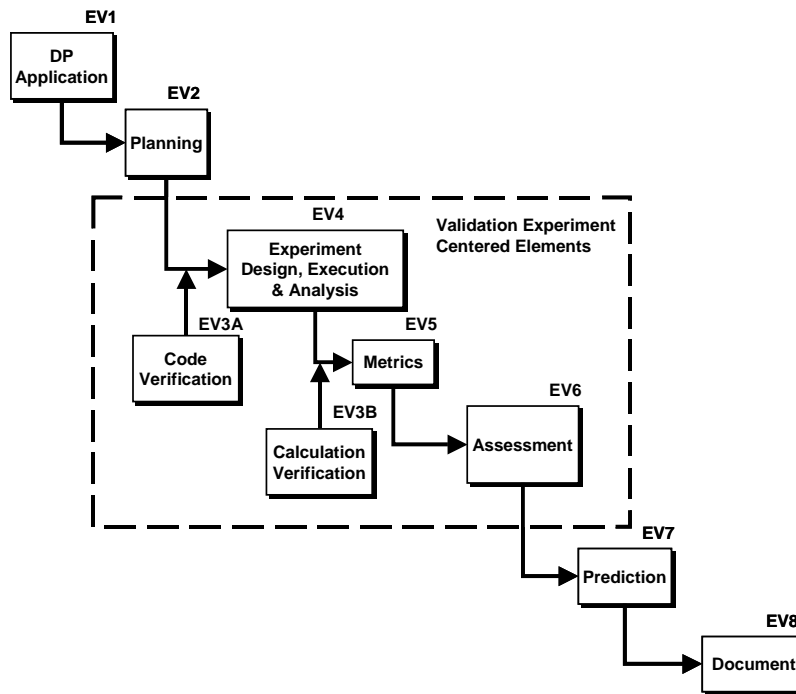
Figure 1-1 Elements (EV1–EV8) of a validation process (from Trucano, 2002)

Validation of multi-physics codes at the integral level requires specific applications. At this level, the processes that make up each sub-model have already been thoroughly verified and validated, and the objective is to verify that the processes work together as intended. A schematic of the process is found in Figure 1-1. These codes may perform well in certain fire scenarios and not at all in others. Therefore, Element EV1 is intended narrow the scope of the validation exercise to fire scenarios of specific interest, which in this case is the response of objects in fires with crosswinds.

Given the selected fire scenarios, in Element EV2 a Phenomena Identification and Ranking Table (PIRT) is developed to rank the physical phenomena to be modeled. The phenomena are ranked according to their expected importance for modeling the specific scenario set and analyzed for disparities between the needs and current modeling capabilities.

The aspects analyzed include the availability and quality of mathematical models, verified codes, validation data, and material properties for each physical phenomena of interest. For the present application, the PIRT included phenomena such as:
• Radiation Macro-Scale Transport
• Radiation Emission/Absorption Processes
• Soot Optical Properties
• Convective Heat Transfer
• Fuel Vaporization
• Fire/Object Coupling

A gap analysis between current SNL programs and specific needs identified both unplanned activities required for the application and activities that would not meet schedule demands for the application. Based on this analysis, the Fuel Vaporization and Fire/Object Coupling were determined as unmet needs and actions were planned to fill these gaps. The identified gaps set requirements both for specific numerical simulation tools (EV3) and specific V&V activities. The EV3 activities are discussed elsewhere. The needed V&V activities are in part addressed in this document. These include designing validation experiments (EV4), defining validation metrics (EV5), and establishing assessment criteria (EV6). This report also addresses discussion of model predictions (EV7) and documentation (EV8).

1-1. Experiments

The validation comparison focuses on data taken from a series of experiments performed at the University Waterloo at their Live Fire Research Facility (LFRF). The LFRF is a 20 meter long by 16.6 meter wide structure with a bank of six large fans at one end of the facility. A horizontal cross-section illustration is found in Figure 1-2. The fans covered an area of 8.2m wide by 5.8 m high (27' wide by 19' high), centered on one face of the facility opposite the large doorway. The fans are pictured in Figure 1-3. The fans blow external air into a pre-conditioning vestibule, through a straightening section with a series of 50 cm x 50 cm boxes, and into the facility. The down-stream end of the straightening boxes will be called the flow entrance to the test area for the purposes of this comparison.
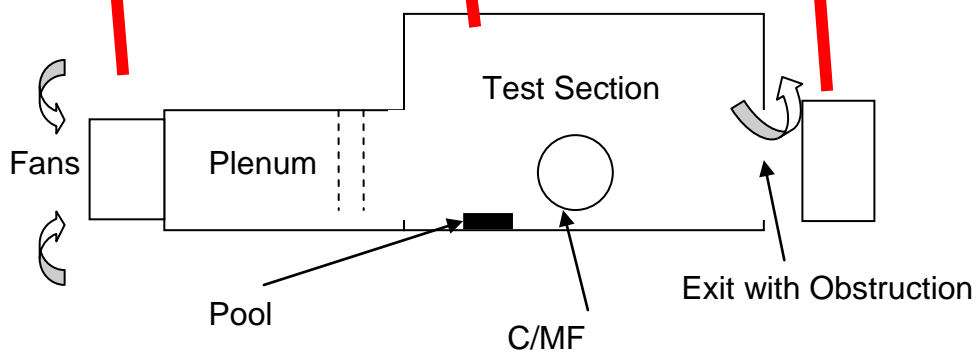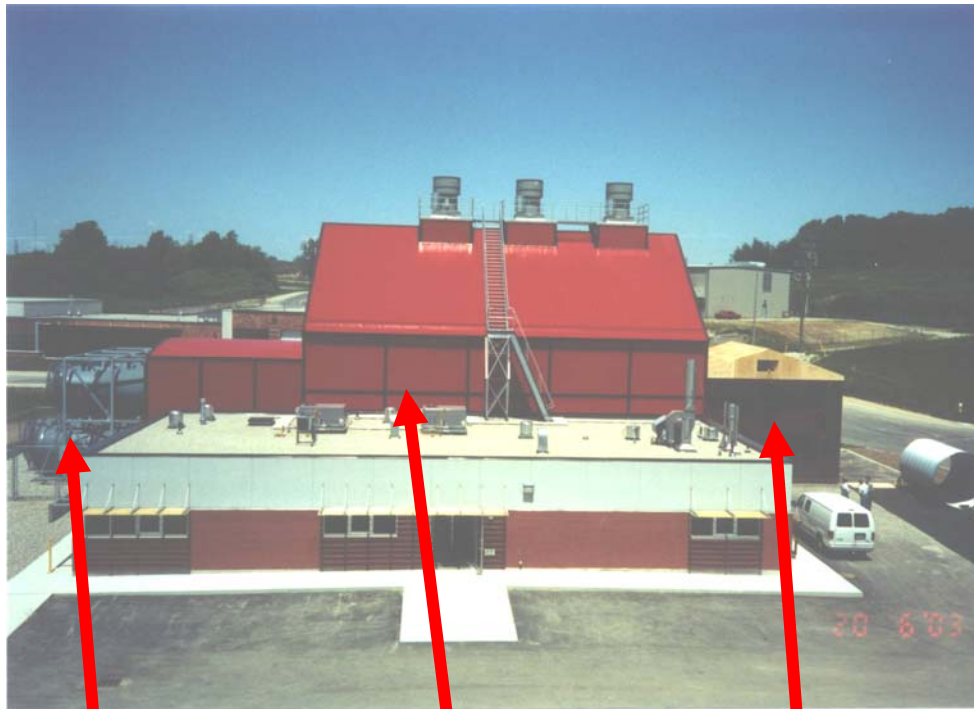
Figure 1-2 A schematic of the University of Waterloo LFRF

a. From outside the facility
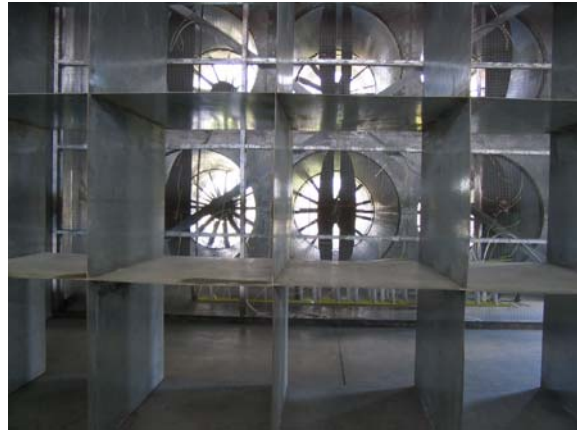
b. From inside the facility

Figure 1-3 Photographs of the LFRF Fans

Three series of fire test experiments were performed. While the documentation of the results of the experiments is still in progress, there exists substantial documentation on the tests. A student thesis (Lam, C.S., 2003) details results from the experiments and the experimental design and layout. The facility has also been characterized for flow, which is documented in Weisinger and Weckman, 2003 and Weisinger 2004. Herein, only the most significant details are documented. For further information on the tests and the facility, the reader is referred to this additional documentation.

A commonality between each series of tests was that Jet-A fuel was burned under a cross-wind condition within the LFRF (Figures 1-4 and 1-5). The Jet-A fuel was burned out of a metal pan that was enclosed by a pedestal. The pedestal was located about 14 ft (4.3 m) down-stream of the flow entrance to the test area, and was approximately 9 ft square (2.7 m). The pedestal was composed of cinder-block bricks over which a fire brick was laid. At the center of the pedestal was the 2 m diameter thin-walled steel pan. The pan was 18 cm deep. It was set on several load cells that were employed to measure the time-dependent weight of the pan and liquid to determine the fuel regression rate. The top lip of the pan and the top of the pedestal were at approximately the same height of 1 ft (30 cm) above the concrete floor of the facility. Around the pan there was a layer of 3 in (7.5 cm) high fire-brick that was intended to shield the concrete floor from the most severe parts of the fire and prevent

spalling. During a fire test, the pan was filled with 10 cm of water, with typically 22 gallons of Jet-A fuel on the top of the water (about 6.5 cm). There was on average a 7 cm gap between the top lip of the pool and the liquid pool during a burn.

Several objects were located within the facility. The most massive object was a 2.8 meter diameter thin walled corrugated steel culvert section that was composed of two segments of 6.096 and 9.144 meter (or 20 and 30 ft) in length. This calorimeter culvert (hereafter referred to as the cylinder/mock fuselage or C/MF) was well instrumented to allow post-test mapping the thermal environment. A test report document details the instrumentation and the layout of the C/MF (Lam, 2003). The C/MF was mounted on four stands composed primarily of 2" x 4" (5.08 cm x 10.16 cm) square tube steel. The stands were arranged symmetrically about the centerplane at 1.5 m and 3.7 m away from the centerplane. The two stands nearest the centerplane of the facility were protected by a thick layer of wire retained kaowool blanket insulation that increased the obtrusiveness of the stands in that region.

In addition to this C/MF, seven smaller 1 ft (30.48 cm) diameter by 2 ft (60.96 cm) long calorimeters were arranged at various locations throughout the facility. The location of these calorimeters was not static for all test series. Figure 1-4 shows a layout for the test series to which these comparisons are being made.

Fires were ignited by a team of fire fighters in protective gear with a torch. The four fans that were away from and above the nearest exit door were turned on. The fire fighter required about 30 seconds time with the torch waved over the fuel pool to ignite the fuel. Up to 30 more seconds were required before the fire covered the full surface area of the pan. During this time, the two remaining fans were turned on (the outside fan, and then the center fan 30 seconds later). For comparisons, the point of full flame coverage was noted as a reference point.

Extensive environmental data were taken at hundreds of locations during each test. This validation comparison is focusing on only a limited set of data points for validation comparisons.
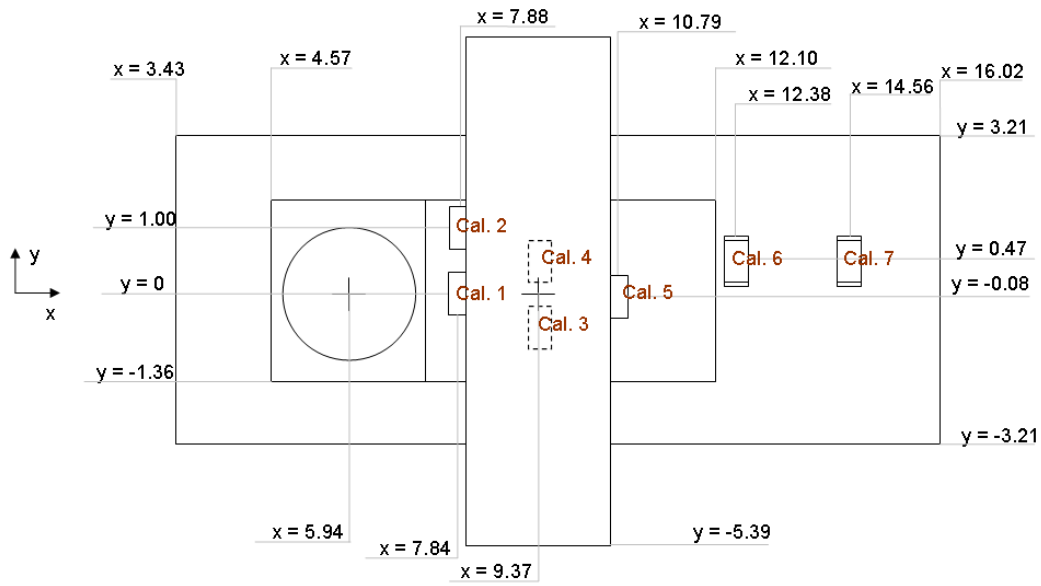
A. Top View – Flow is from left to right

Structure Dimensions:

Culvert-   ø2.75m x 10.78m
Calorimeters- ø0.30m x 0.61m
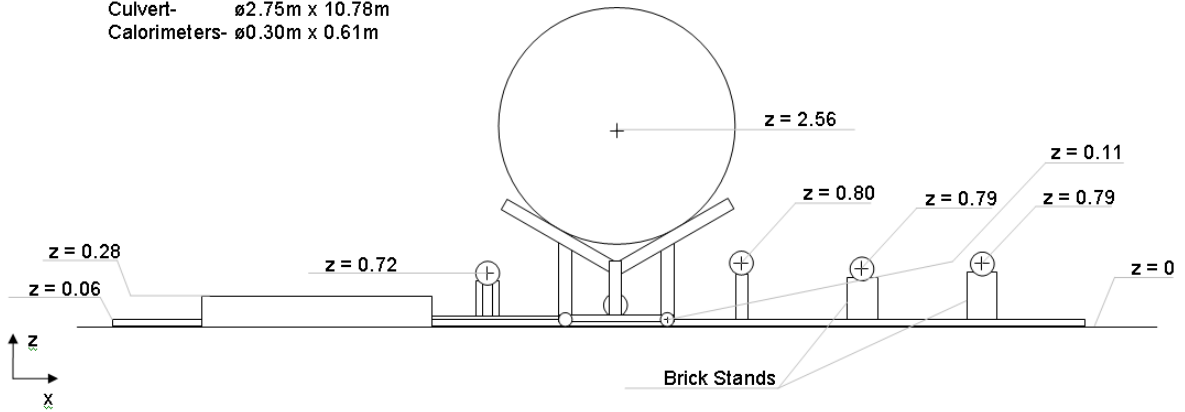
B. Side View – Flow is from left to right

Figure 1-4 Schematics of the test set-up
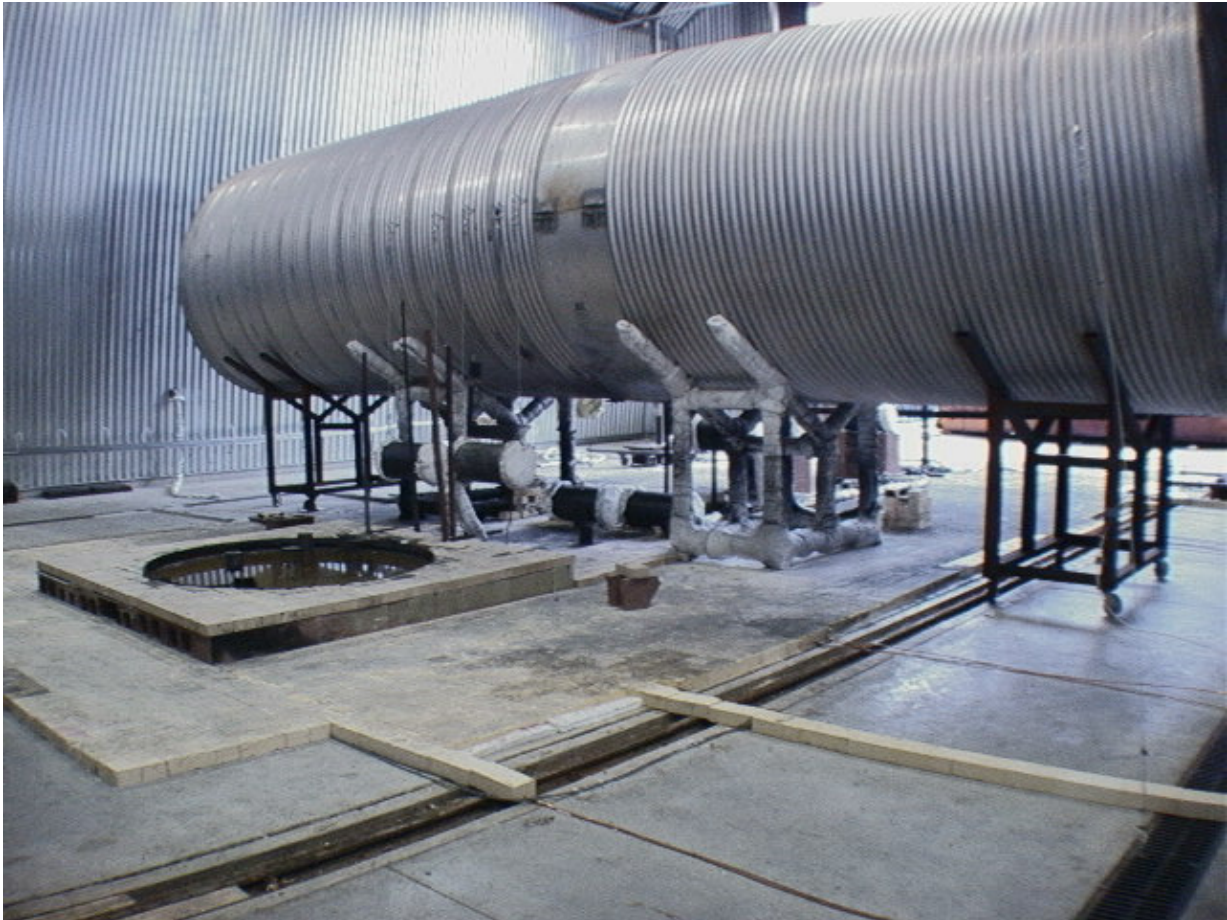
Figure 1-5 Photograph of the test set-up from up-wind side

1-2. Fuego/Syrinx

Fuego is a code developed under the ASC program at Sandia National Laboratories and is intended to be used to predict low-Mach number fires. Fuego resides under the Sierra architecture which is a common architecture that was created for engineering analysis codes. This promises to allow the various predictive codes to communicate with each other and solve coupled problems. For example, Fuego could be coupled to Calore, a tool for solving thermal conduction problems. The Calore tool would employ calculated estimates of the boundary conditions from the Fuego fire prediction code and in turn provide updated boundary conditions back to Fuego. The thermal profile could also be sent to Adagio, a solid mechanics model, and used to predict a structural response for an object in a fire.

Fuego contains a set of physical sub-models that are necessary to describe the physics of a fire. In many cases, multiple models are available to the user for predicting physics. A complete listing of the features is not practical here, but typically used sub-models include the Eddy Dissipation Concept model (EDC) for combustion of a mixing-limited fire, the k-epsilon model with wall functions for turbulence, the Magnussen model for soot, an Aztec

solver for solving momentum and continuity transport, etc. Extensive information is available in the user documentation for Fuego that is maintained on the Fuego web-page[1], or in a sourceforge repository (SIERRA/Fuego Theory Manual, 2002; SIERRA/Fuego Users Manual, 2004).

A typical Fuego simulation will involve not only predictions of the Fuego code, but also participating media radiation (PMR). PMR is calculated by Syrinx, a closely associated Sierra code that employs the discrete ordinates method (DO) to solve the equations of radiative transport. Since the Syrinx PMR code is not typically used in the sierra architecture outside the context of a fire, the fire/PMR solver package is often termed the Fuego/Syrinx code or just Fuego, and not designated as two separate ACS or Sierra codes.

The Fuego code is in flux as the development team continually adds to the capabilities of the code. The source code is maintained in a repository where changes are tracked and regression tests are persistently performed to verify the status of the software. Regular releases of the code occur. For this study, a feature that allowed extra non-linear iterations to be performed with certain equations that only existed in a cutting-edge 'version of the day' was used. For this reason, the test matrix calculations were performed with the version of the code extracted from the repository on September 8, 2005. A drawback of employing a non-standard version of the code is that it complicates the ability of future work to extract the exact version used and perform follow-up work. It also means that somebody using a different version of the code needs to be aware that there is not a guarantee that the results discovered with the version of the code employed for this study will be applicable to another version that might be employed for other purposes. It is generally a good practice to use a more standard version of the code for a study such as this. The use of a non-standard version of the code for this study is a consequence of the maturity of the code and the maturity of the code analysts' capability with respect to the use of the code.

1-3. Computing Resources

Performing a Fuego/Syrinx calculation involves an extensive array of other resources that must operate in harmony to provide predictions. A Fuego/Syrinx simulation in the Sierra architecture requires the use of a wide variety of additional codes. Furthermore, Fuego/Syrinx simulations require numerous second-party libraries be available and present to the user on the physical machine where on the code is run. Only specific platforms are supported on which calculations can be performed. Table 1-1 lists the systems employed for this study, a description of the system, and the use this project found for the machine.

---

[1] http://scico.sandia.gov/fuego/
This web page is for internal use only at the time of publication of this report.

Table 1-1 Systems employed in this study

System	OS	Description	Use
rogue	Red Hat Linux	A 814 CPU linux cluster with P-4 Xeon 2.4 or 3.06 GHz CPUs.	The calculation matrix was performed on this system, as well as many scoping and follow-up calculations.
renegade	Red Hat Linux	A 246 processor classified / unclassified linux cluster with P-4 Xeon 3.06 GHz CPUs.	Some scoping calculations that required large processor counts and quick turn-around were performed on this system that was more underutilized than rogue. Early scoping calculations were also performed here.
liberty	Red Hat Linux	A 246 node linux cluster with two P-4 Xeon 3.06 GHz CPUs per node	Scoping calculations were performed on this system.
sahp6595	Red Hat Linux	A desk-top linux workstation with 2 Pentium IV	Results are stored on two extra hard drives. Used to re-combine files, and to visualize output.
sass2889	Solaris Unix	A slow 64 processor sun system.	When cycles were needed for small jobs and other machines were full.
atlantis	IRIX Unix	A 64 processor SGI system for graphical processing	Mostly used as an intermediate machine for backing up files to the SMSS.
SMSS		A tape back-up system	Most results are archived on the SMSS system.
PC	Windows	A desk-top windows system.	Plotting results, creating meshes, some visualization, and documentation.

The use of the number of different machines and operating systems was driven by capability, availability, and intended use. Rogue, renegade and liberty were work-horse machines with many fast processors available for computing. The decision to run on a machine was mostly a function of availability to the user at the time the calculations were being performed. Renegade was employed predominantly during scoping phases while rogue was upgraded. After the rogue upgrade, renegade was ported to the classified network and thereafter used minimally. Local machines desk-top machines were used for most of the post-processing, and documentation. Atlantis and SMSS were employed to back-up results.

The number of codes employed to prepare and interpret simulations performed for this study is large. Table 1-2 lists the major codes employed for this study. A column in Table 1-2 suggests that most codes underwent revision during the period in which this work was performed. The majority of the new versions required modest to significant effort on the part of the analyst to update to the new version of the code. In the case of loadbal and sierra-concat, it is difficult to assess which versions had been used. During tests, the paths to the executables that had been employed were removed without notice, and it is unknown which versions were used prior to this point in time. In the majority of cases, multiple versions were used in the course of this study to take advantage of code improvements that were found in the more advanced versions.

Table 1-2 Codes employed for this study

Program	OS	Versions	Description	Developer	Typical Use
cubit	Windows or Linux/Unix	7.1-10	A code for generating meshes.	SNL	sahp6595 or a windows PC.
SolidWorks	Windows	2004	A solid geometry modeling package	Solid Works Corp.	windows PC
verde	Linux/Unix	2.5-2.6	A mesh verification code.	SNL	sahp6595
loadbal	Linux/Unix	Unknown	A mesh decomposition code for parallel simulations	SNL / SEACAS	sahp6595
sierra script	Linux/Unix	1.14-1.16	A script that decomposes meshes, launches the code, and concatenates results.	SNL / SNTools	rogue
Fuego	Linux/Unix	1.0-2.0beta	The fire dynamics simulation code	SNL	rogue
Syrinx	Linux/Unix	1.0	The PMR calculation code	SNL	rogue
sierra-concat	Linux/Unix	Unknown	Takes meshes decomposed for parallelization and re-combines the results.	SNL / SEACAS	rogue/ sahp6595
conex	Linux/Unix	2	Takes files from multiple restarts and re-combines them into a single file.	SNL / SEACAS	sahp6595
Ensight	Windows or Linux/Unix	7.6-8.0	Used to visualize, parse, and plot ExodusII output from simulations	CEI	sahp6595
Chemkin	Unix	Chemkin-III, vers. 6.20A 2000/07/07	A code that is used to describe chemically reacting species (reactions and thermodynamics properties of species)	SNL	sass3276a
Tranfit	Unix	v. 3.15A 00/02/01	Transport properties of species from kinetic theory		sass3276a

The list of codes above is not a comprehensive list of those available or useful to fire simulations with ASC codes. It only represents the limited set that was most commonly used to prepare and analyze the simulations.

2. Method

2-1. Validation Plan

Design of Experiments.

The series of experiments were designed following the principles set forth by Trucano *et al.* [2002] for the definition and design of validation experiments. These principles can be summarized in two parts, Experimental Design Requirements and Experimental Data Requirements:

Experimental Design Requirements are that the experiment:

1. Links to application objectives;
2. Addresses specific elements of the Phenomena Identification and Ranking Table (PIRT);
3. Is conducted in the domain of the application; and
4. Is organized in a pattern for analysis.

Experimental Data Requirements are that:

1. Observed data are robust and specific;
2. Boundary conditions are known and controlled;
3. Measurement uncertainties are understood, controlled and quantified.

To meet the Experimental Design Requirements, the setup represented an aircraft involved in a pool fire in the presence of a cross wind. This scenario is of interest in current weapon safety studies and it is expected that Fuego will be heavily employed as these studies develop. Heat flux instrumentation was selected to address the missing elements identified in PIRT. Small calorimeters are placed in the flow which have an appropriate dimension and geometry (0.3 m OD x 0.6 m long x 9.5 mm wall SS304 tube) to represent objects of current interest. The size and thermal characteristics of the calorimeter are mindful of the weapon systems under consideration as well as of a variety of small cargo hazardous materials packagings. The locations of the calorimeters in the fire test are based on environments that would be of interest. These are the environments and object orientations that result in non-uniform heating that fully exercise object safety theme performance in the domain of application. The experiment was designed with wind speed as the control variable, and performed multiple times to gather information on repeatability.

To provide the Experimental Data Requirements, the experiments were conducted in the University of Waterloo Cross Wind Facility. The facility is large enough to accommodate up to a 2 m diameter pool fire (which is within the limits of interest) and provides consistent repeatable boundary conditions. The facility is amenable to simulation because the domain is well defined and the boundaries are relatively simple to describe. Pre-test simulations (Appendix D) were used to estimate instrumentation response which allowed the design and

selection of appropriate diagnostics. Measurements uncertainties have been obtained as part of the data reduction as discussed in a later section.

System Response Measures.
Given the existing resource available for this effort, an analysis that was focused in scope to the most relevant system response measure to the applications of interest was performed. This included the thermal response of the calorimeters and the incident heat flux to the culvert for which substantial spatial and temporal data exist. For the calorimeters, a quantitative comparison of the local body temperature versus time and location was chosen along with the peak spatial thermal gradient around the calorimeter wall. For the culvert heat flux gages, the magnitudes of the incident radiative and convective flux was of interest. It was anticipated that as the surroundings heat in response to the fire that an increase in the incident flux to the culvert heat flux gages would be measured as it suggests the importance of the thermal response of nearby objects to the radiation field at a point. Table 2 summarizes the set of thermal system response measures for the computational study. These response measures are the comparison points between the model and the experiment. This requires prediction and measurement data with quantified uncertainties.

In the experiments, two calorimeters, listed in Table 2-1 were noticeably radiating in the visible spectrum for several minutes following each test. These are the two calorimeters listed in Table 2-1. The center-plane-upstream calorimeter that had not been painted (as all other calorimeters had been) was glowing on the bottom side following the tests. Figure 2-1 shows photographs of the calorimeters following a test. The top side remains coated with soot, while the bottom is not. The other calorimeter was the one underneath the culvert that was nearest the control room. These two calorimeters were therefore selected for comparison because of the significant response to the fire.

Table 2-1 Proposed thermal system response measures for the sensitivity analysis

System Response Measure	Instrument	Units
Max Calorimeter Thermal Difference	Calorimeter 1: Upstream/centerplane	K
Calorimeter Peak Temperature	Calorimeter 1: Upstream/centerplane	K
Max Calorimeter Thermal Difference	Calorimeter 3: Under culvert/control room side	K
Calorimeter Peak Temperature	Calorimeter 3: Under culvert/control room side	K
Time Averaged Total Heat Flux: 2-6 min[*]	Culvert heat flux gage, facing down	W/m^2
Total Heat Flux Slope (vs. time): 2-6 min[*]	Culvert heat flux gage, facing down	W/sm^2

*Since 6 minutes was difficult to achieve given available computer resource, the 2 minute point was used for comparison for most cases. Selected cases were run to 6 minutes.

The above-mentioned metrics are thermal and could potentially match well while the fluid dynamics are not closely matched between the experiments and simulations. As a measure of the flow field, a comparison was originally proposed to be made between experimental time-averaged velocity measurements near the exit of the facility and the predicted average velocity. This, however, was abandoned due to ambiguity in the meaning of the experimental results.

Model Control Parameters.

Model parameters related to discretization are tested to verify the discrete intervals assumed do not significantly influence the outcome of the test. Boundary condition variables propagate uncertainties in the experimental system through the computed domain. Physical properties of materials are also examined, which, like the boundary condition variation propagate uncertainties in the model conditions through the system. Uncertainties due to physical model assumptions are treated through appropriate variation in the model. A list of these important parameters is found in Table 2-2.

Table 2-2 Model parameters and variation

Parameter	Type*	Baseline	Variation
Fluid/PMR Mesh Refinement	Disc	500,000-650,000 nodes	1/8, 27/8
Time Step	Disc	$\Delta t=0.01$	x5, x0.2
Picard Loops**	Disc	1	3, 5
PMR Quadrature Order	Disc	4	2, 8
Inlet Turbulence Parameters	BC	20% turbulence intensity, 50 cm characteristic length	+/- 10% turbulence intensity
Unpainted Calorimeter Emissivity	BC	0.7	0.49, 0.91
Pressure Outflow** Boundary	BC	Pressure	Total Pressure
Floor/Culvert Thermal Conductivity	Prop	Best Estimate	+/- 20%
Baroclinic Vorticity Generation Model	Mod	On, using constants 0.35 and 0.0	Off
Flame Volume	Mod	9.7	+/- 30%
Flame Loading	Mod	2.43	+/- 30%

*BC = boundary condition; Prop = physical property; Disc = related to discretization; Mod = relating to physical models

** The Picard looping and pressure outflow boundary condition were found to relate to stability issues, so the way these parameters were evaluated changed from what was originally planned in the parametric variation study plan.

Validation Matrix

Given the system response measures and input parameters, a test matrix was composed. Ideally, a validation test design approach employing a Latin hyper-cube or similar type of analysis would be used. Resource limitations required an alternative approach. The computational strategy employed the combination of model parameter variables that were expected to yield respectively the maximum and minimum value for the system response measures. Scoping calculations were then used to assess the parameters in cases where the impact of the test parameter on the system response measure was not well understood. Nominal values were also tested. The comparison with experimental results was then made with the nominal predictions bracketed by the uncertainty as propagated through the

calculations. The uncertainty bounds were generated by employing a combination of test parameters that should yield the maximum and minimum variation from the baseline values.

A. Calorimeter 1.

B. The four most up-stream calorimeters

C. An isometric view at the end of a test

D. A view from the air inlet at the end of a test

Figure 2-1 Post-experiment photographs

Table 2-3 details the calculations as planned prior to starting this study. Scoping sensitivity calculations were planned to be employed to determine the impact a variable would have on the response measures in cases where the effect was unknown. These are represented in the table with a question mark. Discretization parameters were planned to be evaluated independently of the other types of model parameters in this study.

Table 2-3 Post-test simulations for comparison of system response measures

Simulation	Description	Parameter	Level	Source
1	Nominal	Turbulence Level	Nom.	Table 2-2
		Unpainted Calorimeter Emissivity	Nom.	Table 2-2
		Floor/Culvert Thermal Conductivity	Nom.	Table 2-2
		Baroclinic Vorticity Generation Model	On	Table 2-2
		Flame Volume	Nom.	Code Doc.
		Flame Loading	Nom.	Code Doc.
		Pressure Outflow Boundary Condition*		
2	Most Severe	Turbulence Level	+	Eng. Judg.
		Unpainted Calorimeter Emissivity	+	Chapter 3
		Floor/Culvert Thermal Conductivity	-	Chapter 3
		Baroclinic Vorticity Generation Model	Off	Chapter 3
		Flame Volume	+	Chapter 3
		Flame Loading	-	Chapter 3
		Pressure Outflow Boundary Condition*		
3	Least Severe	Turbulence Level	-	Eng. Judg.
		Unpainted Calorimeter Emissivity	-	Chapter 3
		Floor/Culvert Thermal Conductivity	+	Chapter 3
		Baroclinic Vorticity Generation Model	On	Chapter 3
		Flame Volume	-	Chapter 3
		Flame Loading	+	Chapter 3
		Pressure Outflow Boundary Condition*		
4	Fluid Mesh Refinement	Same as Sim. 1, except 27/8 mesh	ibid.	ibid.
5	Fluid Mesh Coarsening	Same as Sim. 1, except 1/8 mesh	ibid.	ibid.
6	Smaller Time Step	Same as Sim. 1, except $0.5\Delta t$ **	ibid.	ibid.
7	Higher Quadrature Order	Same as Sim. 1, except QO=8	ibid.	ibid.
8	Picard Loops	Same as Sim. 1, except PL=3	ibid.	ibid.

Key:
Code Doc. = values taken from code documentation
Nom. = using nominal values
Eng. Judg. = based on engineering judgement
Sim. = simulation
+ = using an incremental increase in the variable
- = using an incremental decrease in the variable
*Originally, Pressure Outflow condition was to be evaluated. It was not in the actual tests. Total pressure was used.
** Originally proposed, a time step of $0.2\Delta t$ was too costly given existing compute resource. Time step $0.5\Delta t$ was used instead.

While it would be desirable to define a quantitative success criteria for the comparisons, in reality there is only a preliminary sense for the type of agreement that would be considered acceptable versus unacceptable. Table 2-4 suggests various potential observed states of agreement with respect to both experimental and computational uncertainties, and categorizes them according to the quality of the agreement. Implicit in the formation of this table is the assumption that the experimental uncertainties will be much smaller than those of the model.

Table 2-4 Description of the success criteria or quality of agreement

Observation	Agreement
The nominal prediction is within one standard deviation of the nominal experimental value.	Excellent
The nominal prediction is within two standard deviations of the nominal experimental value.	Very Good
The nominal prediction is outside two standard deviations of the nominal experimental value, but the nominal experimental value is within one standard deviation of the nominal predicted value.	Good
The nominal prediction is outside two standard deviations of the nominal experimental value, but the nominal experimental value is within two standard deviations of the nominal predicted value.	Acceptable
None of the above cases apply, but there is common space between two standard deviation error bars extended from the nominal prediction and experiment.	Poor
None of the above cases apply, but there is common space between three standard deviation error bars extended from the nominal prediction and experiment.	Very Poor
None of the above apply.	Terrible

2-2. Mesh and Geometry

A very critical aspect to this problem is the generation of the computational mesh. Calculation time and disk space requirements tend to scale linearly with the number of elements required to solve and save information. A trade-off is inherently necessary between the level of complexity included in a calculation mesh for a problem of this magnitude, and the ability to perform simulations given the magnitude of detail included.

Fuego is currently verified for hex element topologies, although tetrahedron element topologies will also run. Meshing a complex system in tetrahedrons is comparatively simple to meshing with hexes. To run with a verified code, it was important to use hex meshes since tetrahedron geometries have not been as rigorously verified. A basic geometry for the scenario was composed in SolidWorks, and engineering solid modeling package. The geometry was exported to an ACIS format, and read into cubit. Within cubit, modifications were made to the basic geometry, and the domain was decomposed and meshed. Generation of the meshes was an iterative process at several levels. **Figure 2-2** represents a schematic of the process employed.

The meshes used for this study were developed iteratively as suggested in **Figure 2-2**. The process for generating meshes required numerous iterations. For complex geometry, step 1 (build geometry) is challenging. For hex meshes and complex geometry, step 2 (mesh geometry) is a difficult step, often requiring several times more effort than step 1. Level 1 revisions (step 3) generally were not difficult, as the mesh generation command history files could be re-used to re-build a mesh with the minor changes. Level II revisions (step 4) required geometry changes, and these typically required starting over from step 1. As

geometry changes, so does the internal numbering of elements. This means that the command history files could not be re-used, and that the process must begin again from step 1.

| 1. Build Geometry | 3. Test if it works

Level I Revisions Required:
• Mesh is incorrect (won't run)
• Sidesets revision needed
• Trying to locally refine or coarsen the mesh
• Trying to improve mesh quality in regions of interest | 4. In the process of active simulations

Level II Revisions Required:
• Geometry ignored needs to be added
• Changing boundaries improves simulation output
• Modeling methods require a modification |
| 2. Mesh Geometry | | |

Figure 2-2 Mesh design process

A determination was made to involve five principal meshes for these calculations. Each of these meshes was developed iteratively, requiring several steps through the method suggested in **Figure 2-2**. Table 2-5 lists the meshes employed. The effort required is typical for step 1 and 2 combined.

Table 2-5 The meshes employed for this study

Geometry	Code	Effort Required (days)	Sidesets	Approximate Size (elements)
LFRF flow	Fuego Fluid / PMR	5	20	75 K 600 K 2000 K
Calorimeters	Fuego Conjugate Heat Transport	1	4	100 K
C/MF	Fuego Conjugate Heat Transport	1	3	100 K
Floor	Fuego Conjugate Heat Transport	1	2	100 K
Slice Plane	None—Output Plane	1	0	30 K

The LFRF flow geometry used for the fluid calculations was also used for the PMR calculations. This was not a requirement, but doing so saved time in the development of the

mesh and geometry. This problem is large, and it is very difficult to find available sufficient processors to iteratively test the problem on the nominal sized mesh. To facilitate debugging, the LFRF flow region was created initially on a very coarse mesh. Global refinement was then employed to achieve progressively refined meshes. The sizes listed in Table 2-5 come from a 2x hex refinement (2^3 = 8, which is the scaling factor from the initial/coarse size) and a 3x hex refinement (3^3 = 27, which is the scaling factor from the initial/coarse size). Cubit was used to perform this refinement. As geometry is refined in cubit using the refinement tool, curves that are approximated by straight lines are broken and the break point is shifted to the curvature of the geometry. Thus, the discretization of the coarse mesh is retained only where there is not a more refined estimate available to override the approximation made for the first mesh. Several illustrations of the baseline mesh are found in Figure 2-3.
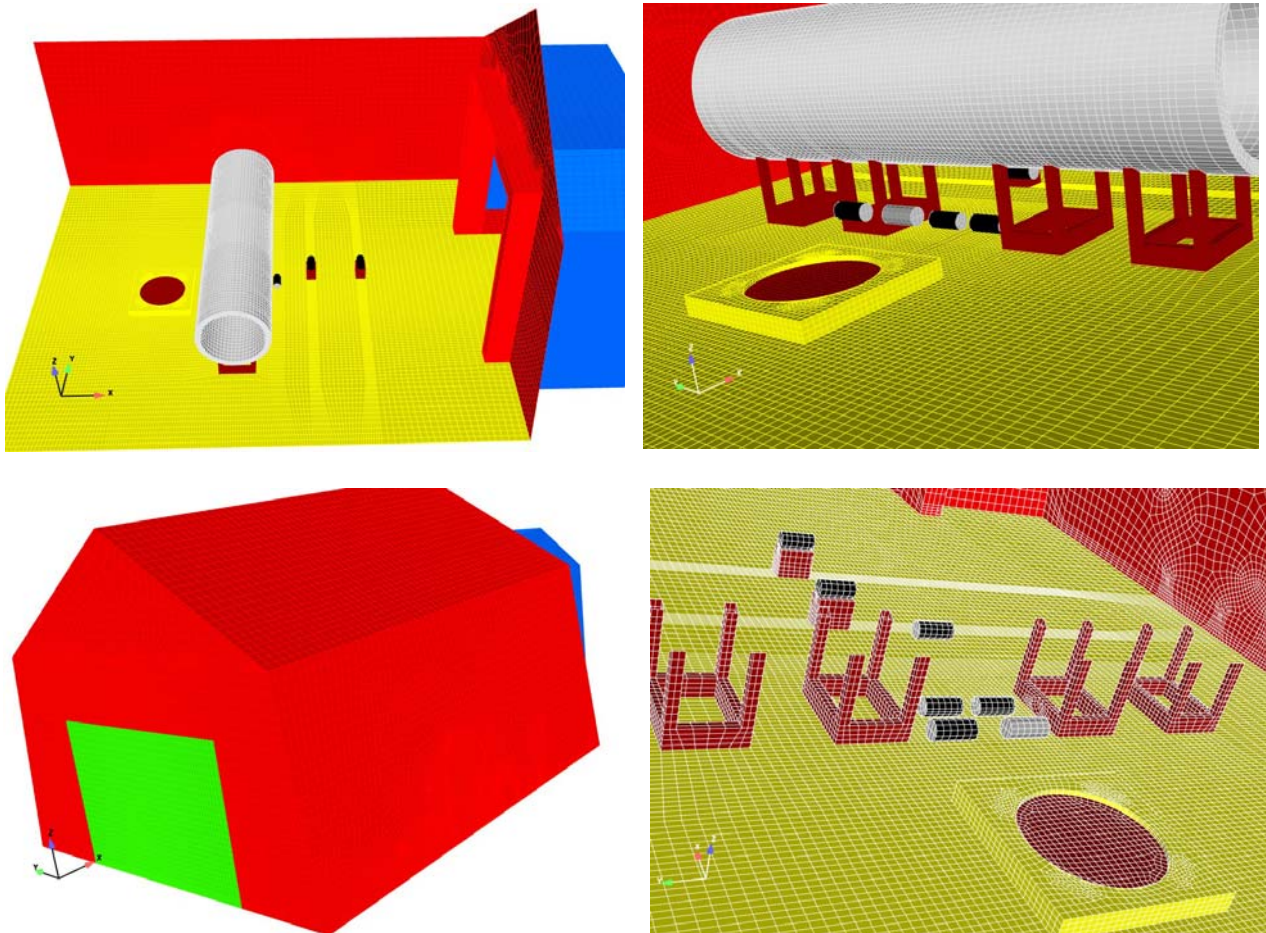
Figure 2-3 Four views of the baseline fluid mesh

Because of the meshing strategy, it was not desirable to include small geometric features. A mesh tolerance of about 6 inches was allowed to design the geometry in a way that did not result in prohibitively small mesh dimensions occurring in the simulation geometry. A consequence of this is that some small features were ignored. Also, some geometry is not exactly consistent with the experimentally measured nominal values. Small geometric

29

variations must be permitted in a simulation exercise like this; pre- and post-experiment dimensions can change because the fire causes thermal expansion, and softening of materials.

The coarse 75 K LFRF mesh was not expected to be sufficiently resolved for the problem. After refinement, the 600 K LFRF mesh was thought to involve sufficient mesh resolution to be employed as the baseline mesh. The 2000 K LFRF mesh was too large for a practical sensitivity study, so this mesh was employed to demonstrate the extent to which the solution changes as the mesh is refined. The 75 K, 600 K, and 2000 K meshes will henceforth be referred to as the coarse, baseline, and refined meshes, respectively.

The three conjugate region meshes were not refined explicitly as part of the sensitivity study. The meshes were developed iteratively, so there is a measure of confidence that the resolution employed for the sensitivity analysis was sufficient based on scoping calculations performed with earlier versions of the mesh that involved a different level of refinement. Generally, the level of grid resolution was much higher than existed on the fluid mesh (in cases several orders of magnitude more refined), but this varied depending on location. With the exception of the C/MF mesh, the solid surfaces were coincident with the fluid mesh. The conjugate region meshes are illustrated in Figure 2-4 along with a graphic of the 'slice plane' used to output time dependent prediction results along the center-plane of the facility.

The final geometry employed for these calculations was arrived at iteratively. Some cold-flow velocity comparisons with data suggested the necessity for improvements to the model, which were subsequently implemented. Examination of the first scoping results for fire calculations also suggested the need for improvements. Below is a list of most of the modifications made to the initial set of meshes for this study (many can be observed in Figure 2-3 and Figure 2-4):

- *Expanded Outflow:* Figure 2-5 shows the out-flow region of the facility before and after modification. At the exit of the facility, recirculation zones are predicted. These traversed the exit plane(s) and were thought to be the source of divergence in early calculations. To help reduce recirculation across the boundary, the out-flow boundary was extended away from the high-gradient region of the flow (also in Figure 2-5).
- *Presence and size of house:* The house located immediately down-stream of the facility was initially ignored. Early simulations suggested the outflow was grossly incorrect without the blockage. It was added, and several iterations were made on the size of the structure until the modeled blockage was within acceptable tolerance with the measured values.
- *C/MF stands:* The C/MF was initially modeled without the support structure. Cold-flow measurements suggested the blocking effect of these is seen tens of feet down-stream. The stands were approximated with rectangular geometry.

a. The Calorimeters

b. The C/MF

c. The Floor
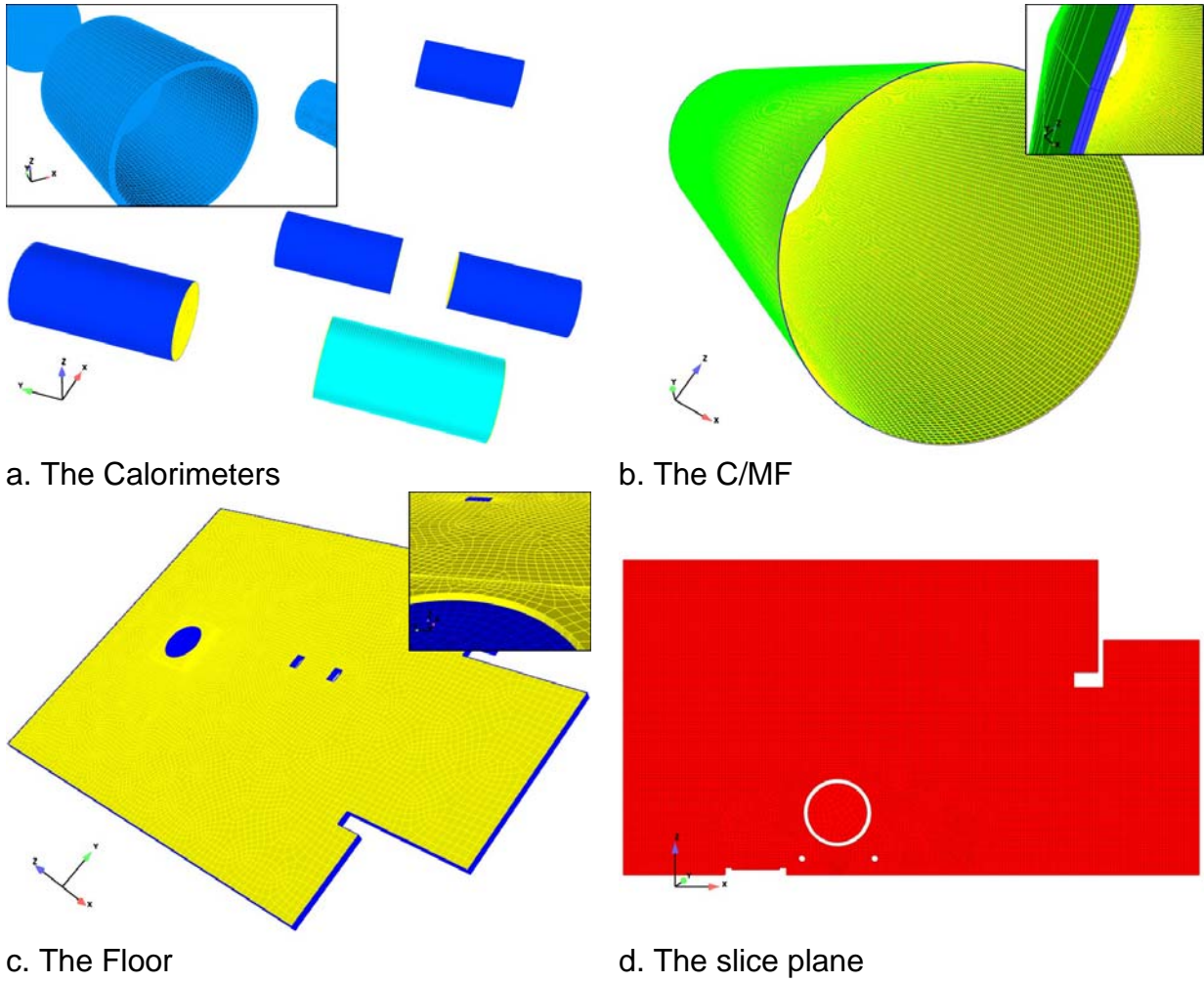
d. The slice plane

Figure 2-4 Conjugate region and slice plane meshes.

a. Before modifications

b. After modifications
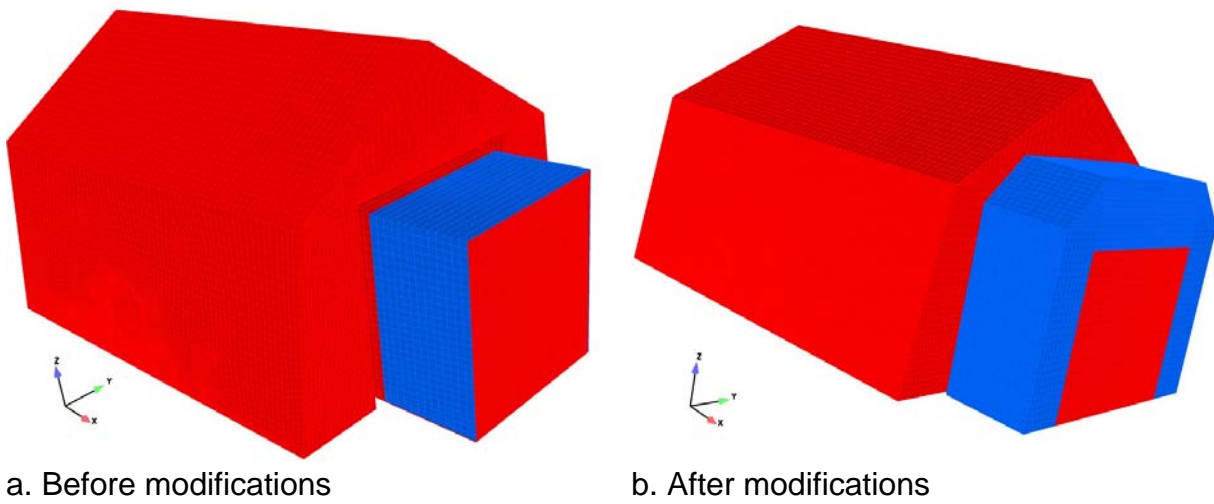
Figure 2-5 Outflow region of the LFRF

- *Pool height relative to the pan lip:* In the pre-test calculations, the fuel inlet boundary was flush with the top surface of the fuel pan pedestal. Early Fuego simulations suggested the fuel would not burn at the leading edge of the pan. In reality, the fuel surface changes during the fire relative to the pedestal surface. On average, the fuel is recessed from the top surface of the pedestal by about three inches (7.6 cm). This recession allows some flow dynamic to occur above the surface of the fuel, but below the pedestal surface. Inclusion of this feature in the model prevents a simple plate-like flow from establishing, and causes the fire to burn further up-stream as had been observed in the experiments.
- *Thickness of the C/MF:* Initially, the 3/16" (4.8 mm) C/MF was modeled as a 10 cm thick cylinder in both the fluid and CHT meshes to prevent small geometry from propagating through the fluid mesh at the interface. This was done because smaller thicknesses would create poor quality fluid mesh elements in the fluid region due to relative length scales. This required asymmetric modifications to the thermal diffusion coefficient parameters to correctly model the conjugate region, which is not possible in current versions of the code. A thin CHT mesh was composed so true thermal diffusion constants could be used. The inside of the C/MF is mapped to the 10 cm recessed surface on the fluid mesh. Flow on the inside of the C/MF is not thought to be affected significantly by this assumption. Nor is this assumption thought to significantly affect the rest of the scenario.
- *Combination of the calorimeters in a single mesh:* Calorimeters were initially modeled as separate CHT meshes. Since they are all composed of the same material, they were combined to a single mesh that is discontinuous. This significantly reduced the number of files created in the output.
- *Node biasing of the brick floor mesh:* Temperature gradients in the brick floor were examined in early simulations. The brick material is a very good insulator, and the thermal penetration into the brick is small. Mesh elements were congregated near the fluid/solid interface to better resolve this in the production calculations.

The decision was made to ignore many of the small and otherwise potentially unimportant features present in the experimental system. The impact of this decision has not been fully explored, although the process by which the omission of these features was decided is thought to be similar to the process that will be employed when evaluating scenarios in future analyses. The findings of this study relative to this process are therefore valuable. The decision to omit geometry is based on considerations of the expected impact of ignoring a feature, and the difficulty involved in including the feature. The determination is ultimately made by engineering judgment of the analyst, but is backed up in cases where possible with scoping calculations or with the analysis of results around the features from simulations that do not include the feature. The following is a selected list of these features and a description of the motivation for excluding the feature:
- *Vents:* At the top of the facility are three fans that are intended to exhaust hot air if a thermal test exceeds pre-set limits. Flaps are designed to allow flow to exit the building, but to impede flow from entering. Power to the fans was off during the tests, but the openings were not an impediment to the potential out-flow from the facility during a test. However, a significant amount of smoke was never observed emitting from these vents during a test. Including this geometry would be simple, but is not

done because of uncertainties on how to simulate the boundary. These are seen in Figure 2-6.

- *Slide-up access door:* The main equipment door is large enough for the two-story test-cell house to roll in and out of the facility (see Figure 2-7). It is a multi-panel sliding door. When open, the panels are arranged above the door. Precise measurements of this configuration were not available. Predicted air flows are low in the vicinity of these panels, and so the error in the assumed geometry is thought to be insignificant.

- *Flow under house:* The two-story test-cell house downstream of the LFRF was slightly raised off the surface of the ground to allow it to move in and out of the facility. (Figure 2-8) This gap was ignored. But pressures are fairly high at the face of the house. Flow is thought to be moderately substantial through this gap, but is ignored because the feature is smaller than the general tolerance employed for the mesh. It is assumed that the region is sufficiently down-stream of the fire and measurement devices to not affect what occurs up-stream.

- *Heater:* A space heater was mounted to one side of the inlet on the up-stream face of the facility. This is pictured in Figure 2-9. This was ignored in the facility model. Predictions without this blocking object suggest flow velocities are low in this region, so the effect of ignoring this sizable object is thought to be small. A moderate re-mesh (~2 weeks effort) would be necessary to test the effect of this feature.

- *Recessions:* Several recessions exist on the side-walls of the facility (see Figure 2-10). Two of these are to provide vertical walls for doors, and a third is for an emergency eye-wash and shower station. These are small, and the flow near them is low. A moderate re-mesh (~2 weeks effort) would be necessary to test the effect of this feature.

- *Small support structures:* Cable wire was used to retain the C/MF and the calorimeters in place. Eye-hooks and retaining bolts were used to hold these in place. Also, steel stands constructed from 2.54 cm (1 inch) wide 'L' shaped stock metal were used to hold thermocouples in the fire zone. These are show in Figure 2-11.

- *Brick floor:* The insulating brick placed over the concrete floor of the facility was between 2-3 inches high. It was placed to cover the concrete and prevent spalling as the tests were performed. Pre-test simulations performed of the fire were used to estimate coverage. Figure 2-12 shows the final lay-out of the brick. This dimension was below the geometric tolerance on the meshes, and therefore ignored. A consequence of this is that the gap between the pedestal and the floor is larger in the simulations than in the experiment. It is not clear how much this difference affects the results.

- *Small instrumentation:* Several pieces of instrumentation were included in the experiments that have not been explicitly modeled as part of this study. Heat flux gages were placed at various locations in the pan, and downstream of the pan to measure the heat flux from the fire. Some of these were non-intrusive (flush with the floor, or embedded in an object), but others were intrusive. Figure 2-13 shows some of these. Also, a linear array of bi-directional Pitot-type probes were suspended from an assembly that was not included. This assembly was down-stream of the fire, sufficient to assume it did not affect up-stream results.

- *Corrugation:* The C/MF was corrugated. These corrugations are prohibitively difficult to model in the fluid mesh due to geometric complexity. They could potentially be modeled in the solid (conjugate) mesh, but this would require more detailed knowledge than is commonly available. Whether the interface would be correctly modeled if the corrugations were only present in the conjugate mesh is not known. The corrugations generally fall below the geometric tolerance employed for this simulation exercise. The consequences of ignoring the corrugations in the C/MF are not well known. The internal walls of the LFRF were also corrugated. These are not close to any measurements, and thought to be sufficiently removed to have little effect on the fire.
- *Tarpaulin covered wall:* On the control-room side of the facility on the down-stream end, there is a thermal environments side-lab. Pre-test predictions suggested the impact of this on the flow was small. To minimize the effect of it on the experiment, a large tarpaulin was placed over the opening to create a more symmetric flow-space for the fire tests. This is illustrated in Figure 2-14.
- *Instrument cable bundles:* Cable bundles with thermocouple leads come out of each calorimeter. These were wrapped with fiber insulation, and conducted to a data-acquisition board that was insulated from the fire in the floor of the facility. A photograph of some of these is found in Figure 2-13. These bundles are on the order of about 3-5 inches in diameter after being wrapped. These have been ignored since the dimensions are below the typical geometry tolerance.
- *Miscellaneous objects mounted on walls:* The walls of the facility have numerous objects mounted thereon (Figure 2-10). Lighted exit signs are over each door (foil wrapped for the tests). Lights are fixed in the ceiling and protrude out from the surface of the ceiling. Some piping is found in the corner near the ceiling. And some fire extinguishers are mounted at several locations in the facility. These are mostly away from the regions of interest where facility flows are low in magnitude.

In examination of the two lists previously detailed, it is not obvious what must be included and what might be excluded from a model. Including all details is prohibitive to practical modeling endeavors. It is not apparent that any of the above described experimental features omitted from the model might have an effect of low enough order that they can be excluded. Nor is it apparent that they must been included. This is an important observation relative to this comparison exercise. The ability of a simulation code to model scenarios is dependent on the ability to include all features of significant effect in the model geometry. Exclusion of geometric features represents an uncertainty that is not well understood. In this controlled case, these geometry details were known. In a hypothetical scenario without data, it might be difficult to analyze the spectrum of potential outcomes without considering some of the potential minor features if detail is found to be an important factor. Being able to *a priori* identify critical features is a useful capability that is not presently mature for the Fuego code analysis team relative to scenarios that are under consideration.

Figure 2-6 A view from the south of the LFRF during a fire test

Figure 2-7 The top-north corner of the large door in the 'up' position

Figure 2-8 A view of the blocking object out the large door

Figure 2-9 The heater mounted on the upstream wall during construction

Figure 2-10 A view of the south side of the LFRF looking upwind with the house test cell installed

a. Around the upstream calorimeters

b. Eyehooks mounted to the C/MF

Figure 2-11 A close-up of some of the mounting assemblies

a. Looking down-wind
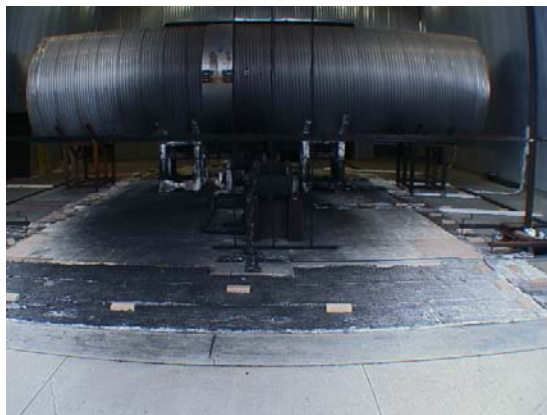
b. Looking up-wind

Figure 2-12 Two views of the brick portion of the floor

Figure 2-13 A close-up view of the pan and the instrumentation

Figure 2-14 The tarpaulin covering the side-room

2-3. Modeling Methodology

With a mesh composed, it is required to compose an input file that instructs the code how to perform the calculation. Numerical algorithms, physical properties, calculation methodologies, and boundary conditions are all specified in an input file. A sample input file is found in the Appendix in A-1. As is clear from the length of the input file, a detailed expression of the assumptions is not feasible here, but details can be uncovered by parsing the sample input file. Highlights are presented below. The mesh has been peer reviewed by multiple Fuego users for errors, and had been tested with scoping calculations prior to beginning the simulation matrix.

Boundary condition and physical parameters have been assumed from the best available data. Table 2-6 summarizes the physical properties of the conjugate regions. Table 2-7 summarizes the boundary conditions on the fluid mesh.

Table 2-6 Solid material properties assumed for the model

Parameter	Units	Calorimeters	Floor	C/MF
Thermal Conductivity	W/mK	43	0.2	43
Density	kg/m^3	7800	497	7800
Specific Heat	J/kgK	476	840	476
Emissivity	-	0.96	0.9	0.9
Initial Temperature	K	273	273	273
Reference		Holman, 1990 (steel)	Manufacturer documentation	Holman, 1990 (steel)

Table 2-7 Some boundary conditions assumed for the model

Variable	Units	Air Inlet	Fuel Inlet	Outflow	Initial Conditions
x-velocity	m/s	13	0	0	13
y-velocity	m/s	0	0	0	0
z-velocity	m/s	0	0.0161	0	0
Temperature	K	273	488	273	273
Turb. Kin. Energy	J/kg	10.14	8.748×10^{-4}	*	**
Turb. Diss.	J/kgs	10.61	2.12×10^{-6}	*	**

* Outflow turbulence parameters were usually low (1x10-10), but were varied for some cases because stability was found to relate to these parameters.
** Generally the initial turbulence parameters were the same as the air inlet parameters, but stability was functionally dependent on these parameters for some cases, and they were varied if this dependency was found.

Chemistry input files were constructed from Chemkin for use in the EDC combustion model. The fuel used in these tests was Jet-A, which is a kerosene based jet fuel. Detailed thermodynamic data for this compound were not available, so an input file was constructed

based on existing data for similar compounds to approximate the fuel using the hydrocarbon species $C_{12}H_{23}$. The Chemkin input file, chem.inp, and the ascii linking files for thermodynamic and transport properties of the species are found in the appendix in Section A-2. The transport properties of $C_{12}H_{23}$ were determined in Chemkin from kinetic theory expressions using molecular property data taken from octane.

A large suite of solution algorithms are available for cases. Details for the baseline case are found in the appendix (A-1). Transfers were set up between the various meshes as was appropriate to the case. The Aztec solver was used for all cases with symmetric Gauss-Seidel preconditioning for each variable. Upwinding was used with a first order upwind factor of 0.5. Momentum and pressure were not under-relaxed, and the other variables were under-relaxed with an under-relaxation factor of 0.5.

3. Scoping Calculations

At the time the validation plan was written, it was unclear what effect the chosen modeling parameters would have on the resulting thermal environment at the comparison points. This is clear in Table 2-3, which in the test plan suggested the necessity of determining quantified response for the various parameters. The motivation for lumping the parameters for this study into a limited number of simulations was to create a simulation test matrix that was feasible. Performing individual tests with the baseline scenario to determine the effect of the sensitivity parameter was not possible due to the scale of the problem. To circumvent this difficulty, an assumption was made that the parametric sensitivity could be estimated on the coarse mesh and that the sensitivity would be similar on the baseline mesh. The coarse mesh simulation results could then be used to formulate the basis for the parametric offset calculations described in Table 2-3.

Additional work to that initially proposed was performed. Table 3-1 outlines the calculations that were performed. Notably, the inlet velocity distribution was tested which is a parameter that was not proposed as part of the study. This involved either a plug flow assumption, or a profile assumption that was generated based on interpolation from measured cold-flow velocity data. This addition was aimed at determining the sensitivity of the results to the uncertainties in the inlet conditions. Four days and 14 processors were required to simulate 500 seconds of the baseline case using the ICC Shasta and Liberty machines.

Table 3-1 Scoping parameters tested

Parameter	Baseline	Variation
Time Step	0.01s	0.03s, 0.002s
Picard Loops	1	3
PMR Quadrature Order	4	2, 8
Inlet Turbulence Intensity (L = 5cm)	25%	20%, 30%
Unpainted Calorimeter Emissivity	0.7	0.4, 1.0
Floor/Culvert Thermal Conductivity	0.4, 43 W/m-K	+/-20%
Baroclinic Vorticity Generation	On, CBVG = 0.35, CEPS_3 = 0	Off
Flame Volume Coefficient	2.13267	+/-30%
Flame Loading Coefficient	0.41	+/-30%
Pressure Outflow Boundary	Pressure	Total Pressure
Inlet Velocity Distribution	Uniform Inlet (Plug)	Nonuniform (Profile)

3.1 Time Step Size

The influence of time stepping on the simulation results was evaluated by running simulations with time steps of 0.03 seconds and 0.002 seconds in addition to the baseline case, which used a time step of 0.01 seconds. Figure 3-1 illustrates the time-evolution of the radiation flux that is incident on the bottom of the C/MF for these cases. Smaller time steps appear to produce the largest incident radiation flux to the bottom of the culvert. This is also the case for other locations on the bottom half of the C/MF. Consequently, a higher temperature distribution on the bottom of the C/MF is produced when smaller time steps are used, as shown in Figure 3-2. The direction of rotation (CCW) used in all distribution plots is based viewing the set-up from the control room. Object temperatures are sampled at outer surfaces and near the middle of cylinder length. Calorimeters 1 and 3 also exhibit a similar trend with respect to the time step

41

as shown in Figure 3-3 and Figure 3-4 respectively. It is concluded that the simulation exhibits a time step sensitivity, in which smaller time steps increase the severity of the heat transfer to the solid objects. Additional informal simulations have been performed to further explore this dependence. This trend appears to continue at least to a time step of 0.0005s.
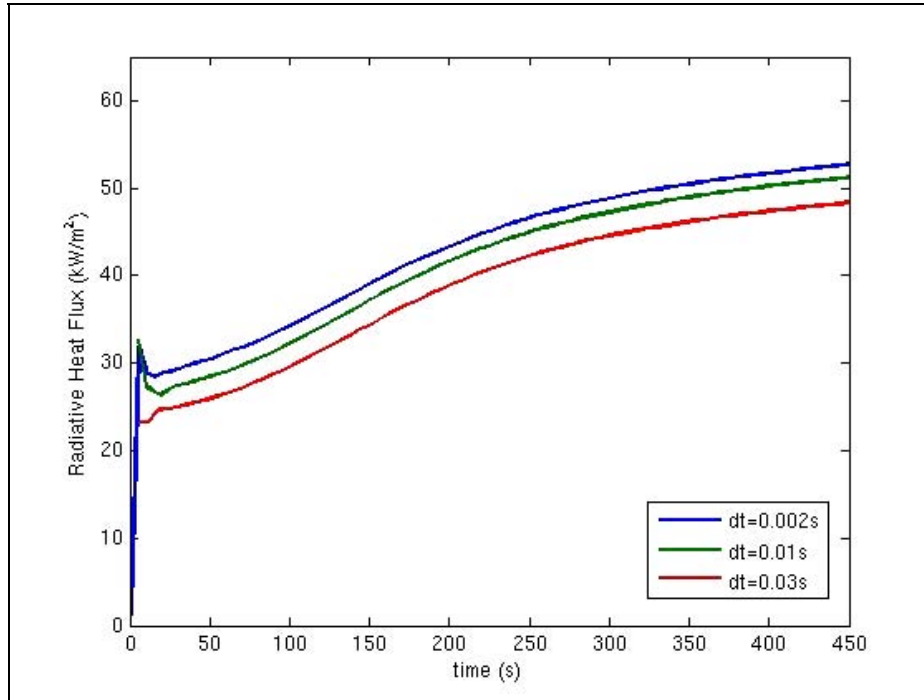
Figure 3-1 Time stepping influence on incident radiation flux to bottom of C/MF
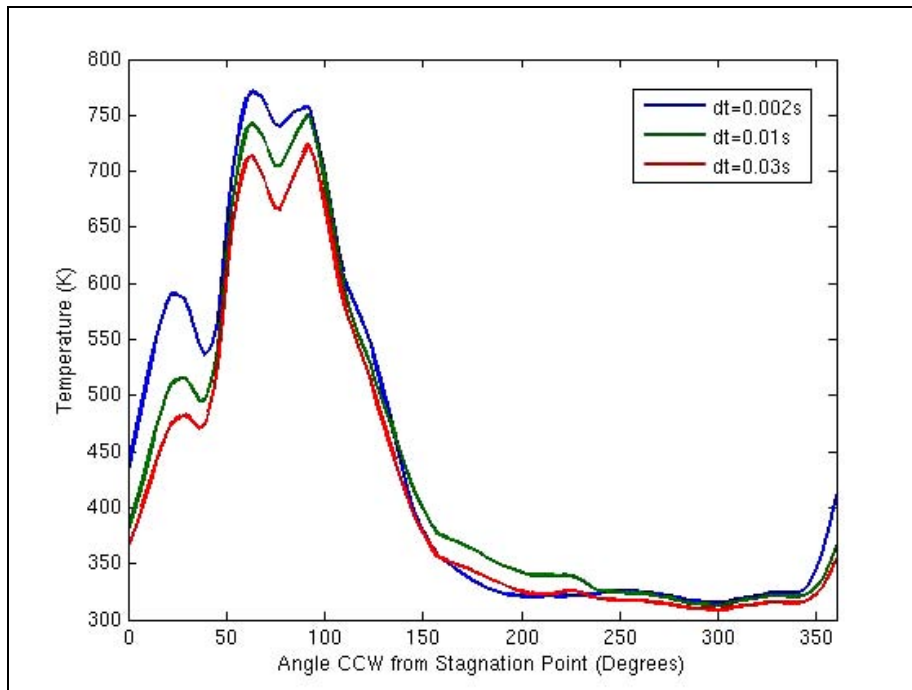
Figure 3-2 Time stepping influence on culvert temperature distribution at 450 seconds
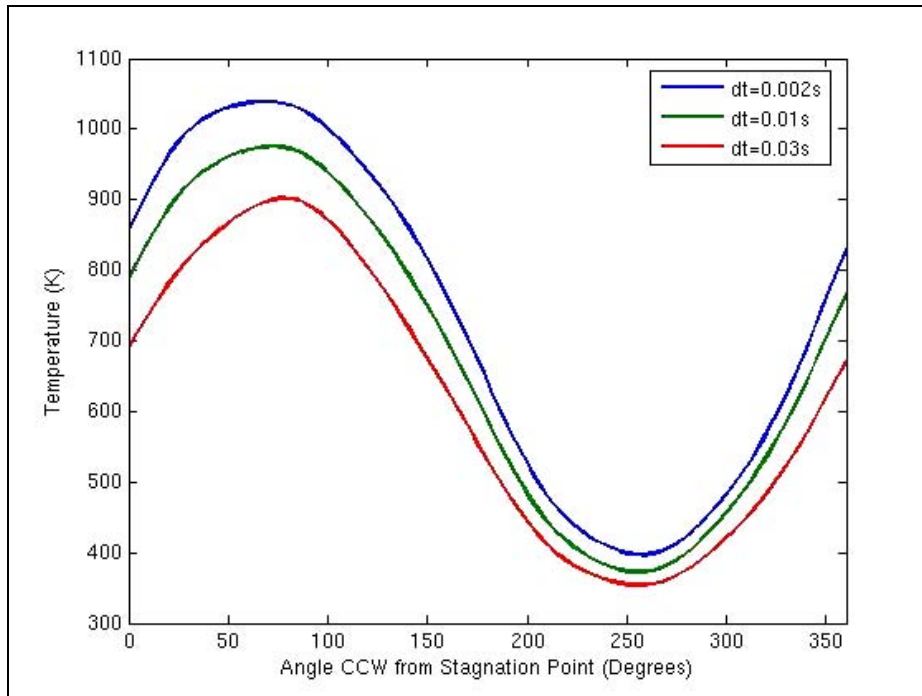
Figure 3-3 Time stepping influence on Calorimeter 1 temperature distribution at 450 s.
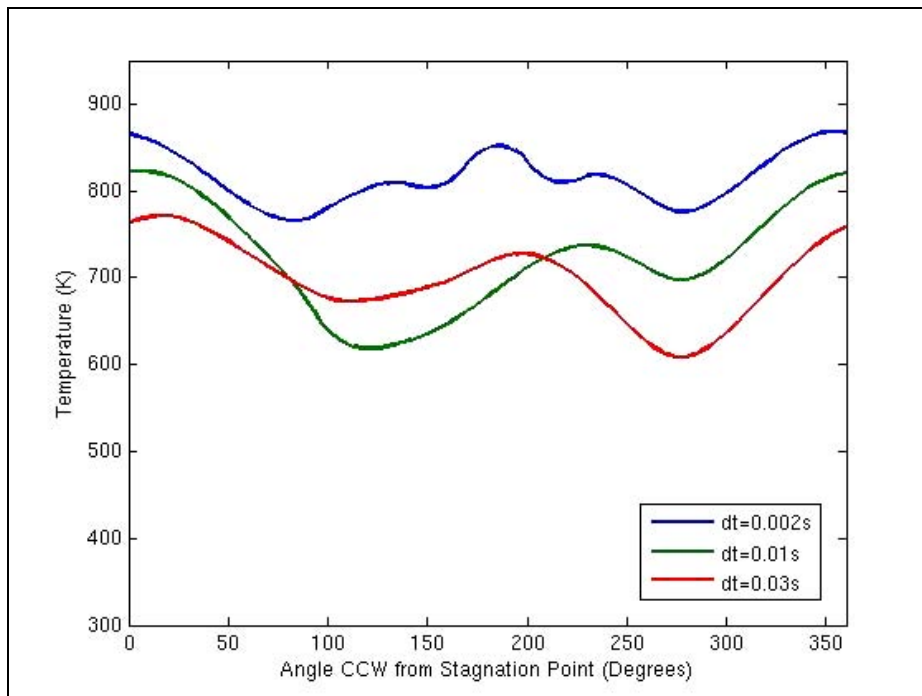
Figure 3-4 Time stepping influence on Calorimeter 3 temperature distribution at 450 s.

3.2 Picard Loops

The sensitivity of the simulation to Picard looping (number of iterations performed within a time step) was assessed by running a simulation that used 3 Picard loops. This simulation was compared to the baseline case, which used only 1 Picard loop. Under-relaxation factors of 0.5 were used in the Fuego fluid region of all simulations. Figure 3-5 illustrates the time-evolution of the radiation flux that is incident on the bottom of the culvert during the first 100 seconds. This plot demonstrates that the different Picard looping alters the solution only during the first 30 seconds of the simulation, while the fire is setting up. This discrepancy is no surprise, considering that under-relaxation factors of 0.5 were used in all of the transport equations of the Fuego fluid region.
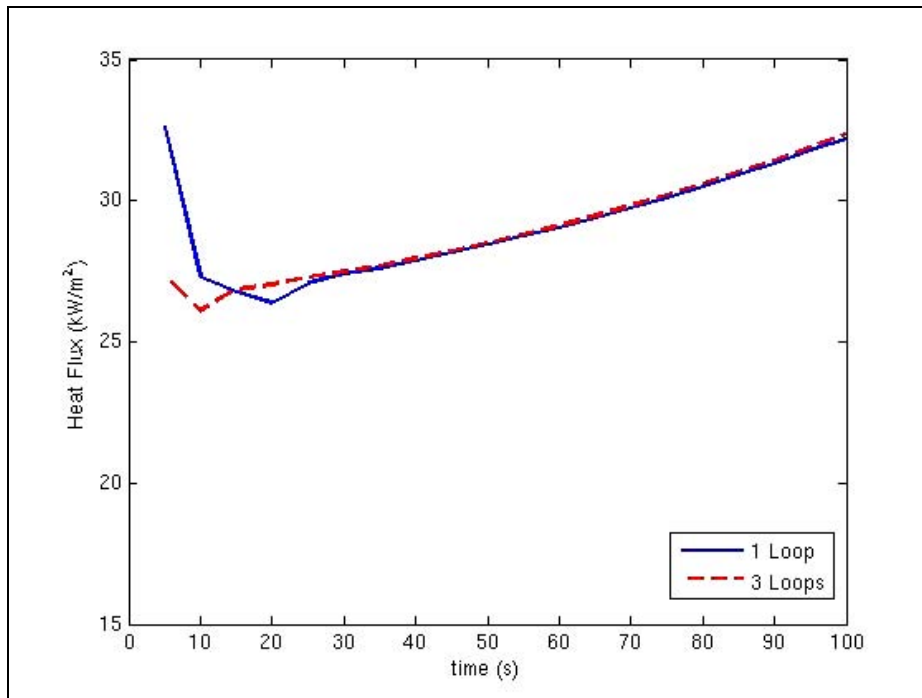
Figure 3-5 Picard looping influence on radiation flux incident on the bottom of the C/MF

After the fire sets up, modifications to the radiation field result from the re-radiation of the solid objects as they gradually heat up. These processes are controlled by the Fuego conduction and Syrinx regions, which are not under-relaxed. Consequently, the Picard looping of Fuego fluid region no longer produces disparate transient solutions after the fire sets up (after $t = 30s$). This result is further illustrated by Figure 3-6, which shows the temperature distribution around the calorimeter 1 at $t = 350$ seconds. Therefore, Picard looping does not influence the severity of the heat transfer after the fire sets up if the conduction regions are not under-relaxed.

44
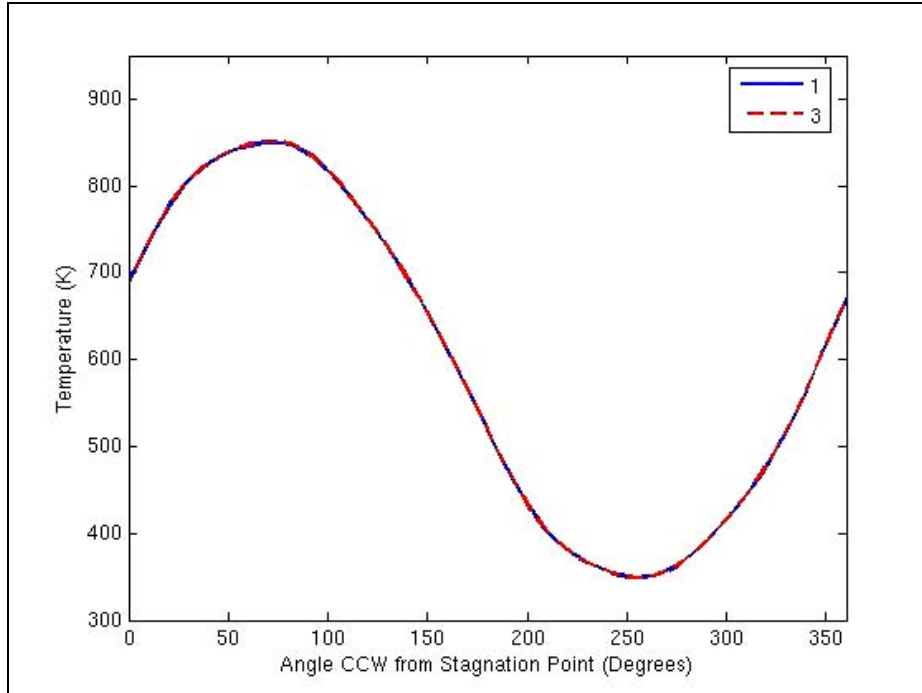
Figure 3-6 Picard looping influence on Calorimeter 1 temperature distribution at 350 s

3.3 Quadrature Order

The quadrature order is a discretization parameter for the discrete ordinates method, which Syrinx uses to solve the participating media radiation. Simulations using quadrature orders of 2 and 8 were performed in addition to the baseline case of order 4. Figure 3-7 shows the time-evolution of the net heat flux to the bottom of the C/MF for these three cases. Figure 3-8 illustrates the influence of the quadrature order on the culvert temperature distribution at t = 350 seconds. Figure 3-9 and Figure 3-10 illustrate the temperature distributions of Calorimeters 1 and 3 respectively, at 350s.

Higher quadrature orders act to smooth out the distribution of radiation intensities (and consequently temperature distributions) by utilizing a larger number of directions for transport. This trend is well illustrated in Figure 3-8. However, the quadrature order does not significantly affect the severity of the heat transfer as a whole. Rather, it controls the smoothness of the distribution, because the ability to accurately capture the angular and spatial dependencies of radiation transport is limited by the quadrature order.
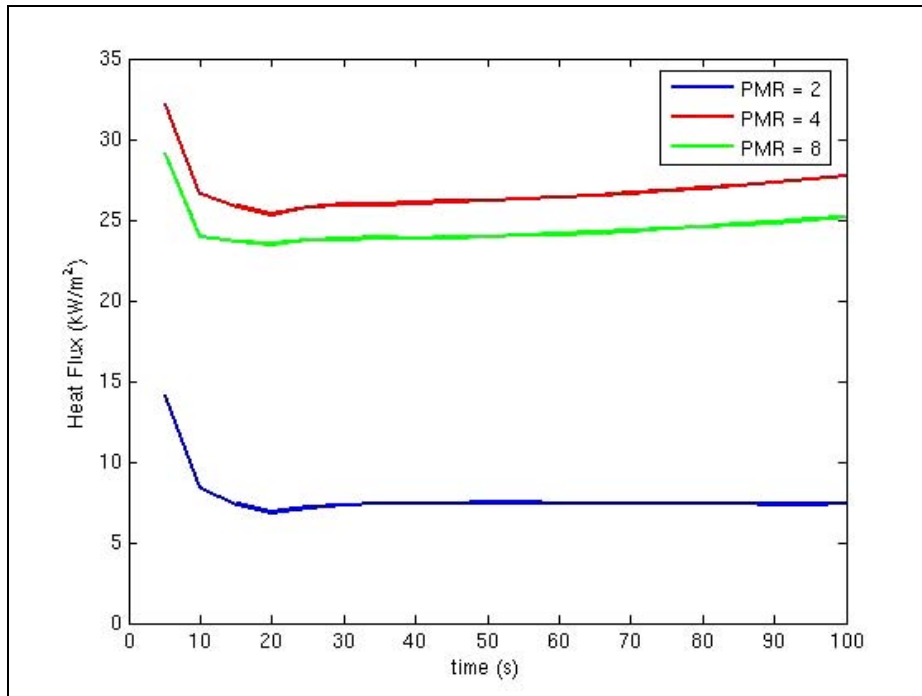
Figure 3-7 Quadrature order influence on net eat flux to bottom of C/MF
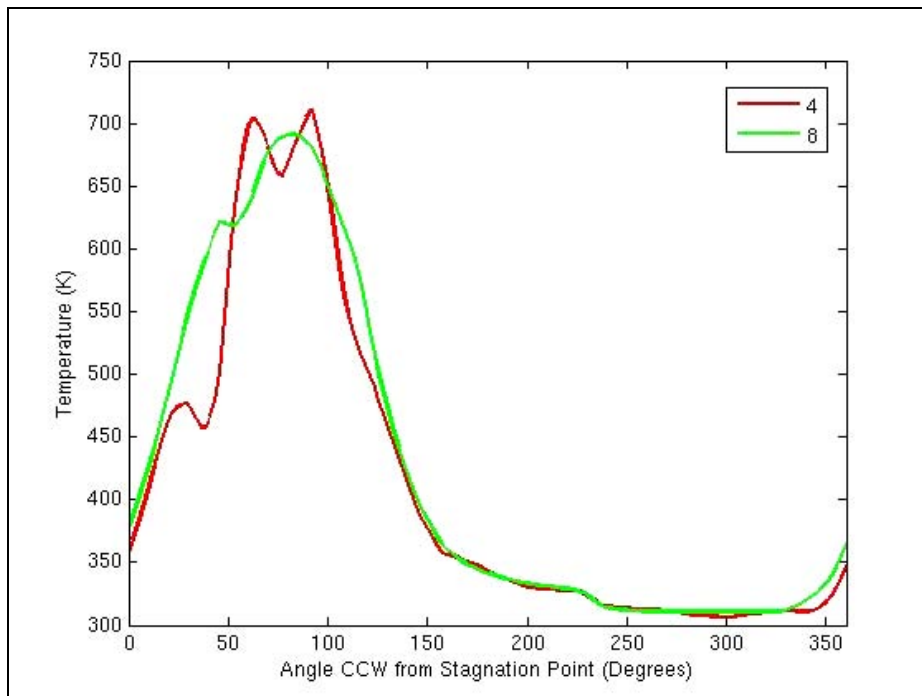
Figure 3-8 Quadrature order influence on C/MF temperature distribution at 350 s
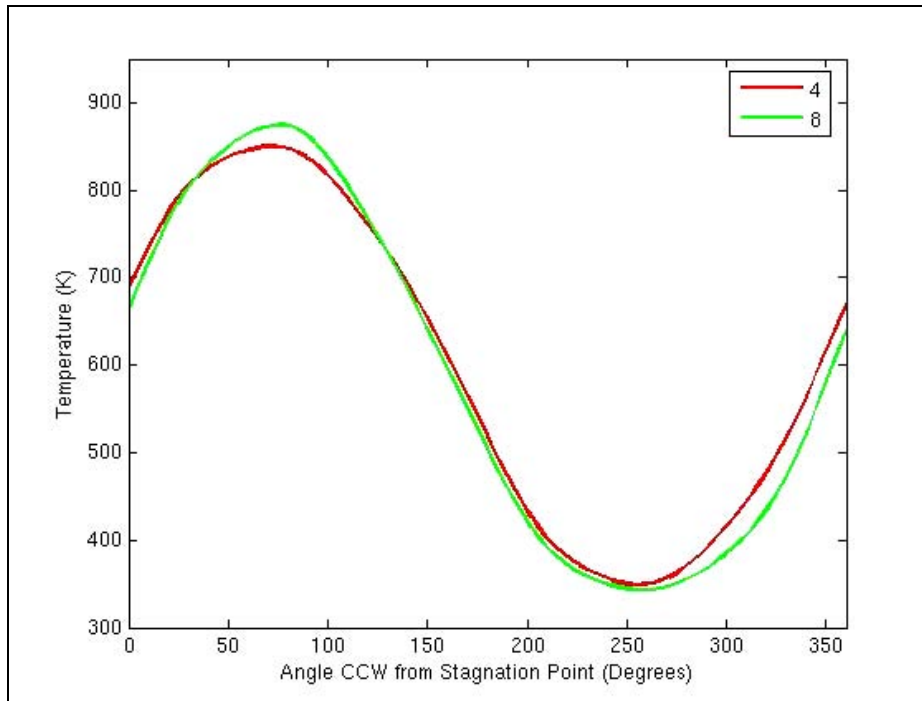
Figure 3-9 Quadrature order influence on Calorimeter 1 temperature distribution at 350 s
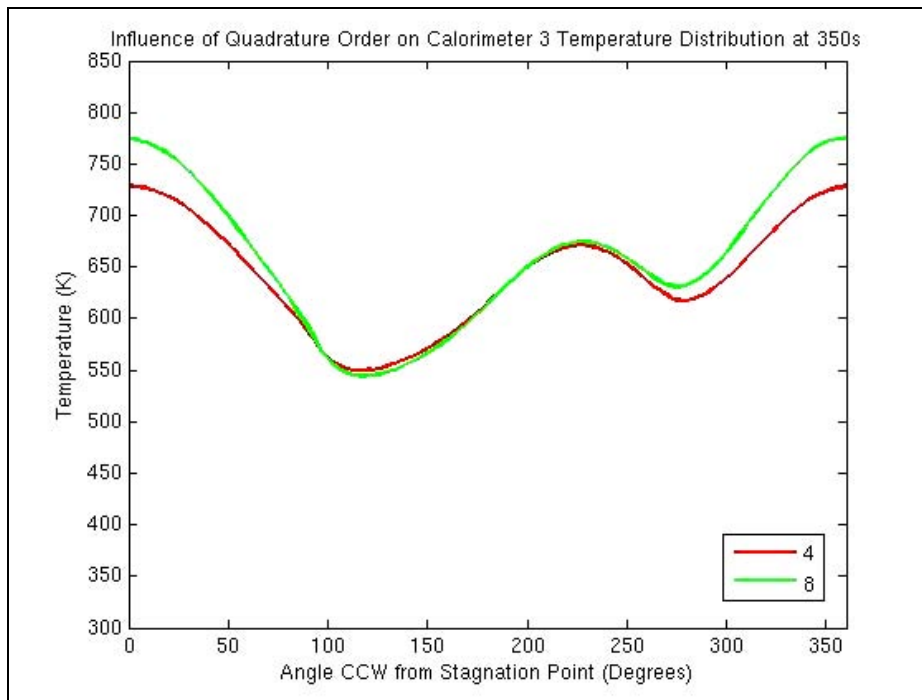
Figure 3-10 Quadrature order influence on Calorimeter 3 temperature distribution at 350 s

3.4 Inlet Turbulence Intensity (TI)

The influence of the inlet turbulence intensity (TI) on the severity of the heat transfer to the solid objects was determined by comparing the baseline inlet TI of 25% to simulations run

with turbulence intensities of 20% and 30%. Figure 3-11 illustrates the influence of the inlet TI on the radiation flux that is incident to the bottom of the culvert. Figure 3-12 shows the time-evolution of the peak temperature on calorimeter 1 for these three cases. The inlet TI does not appear to significantly affect the conjugate heat transfer to the solid objects.
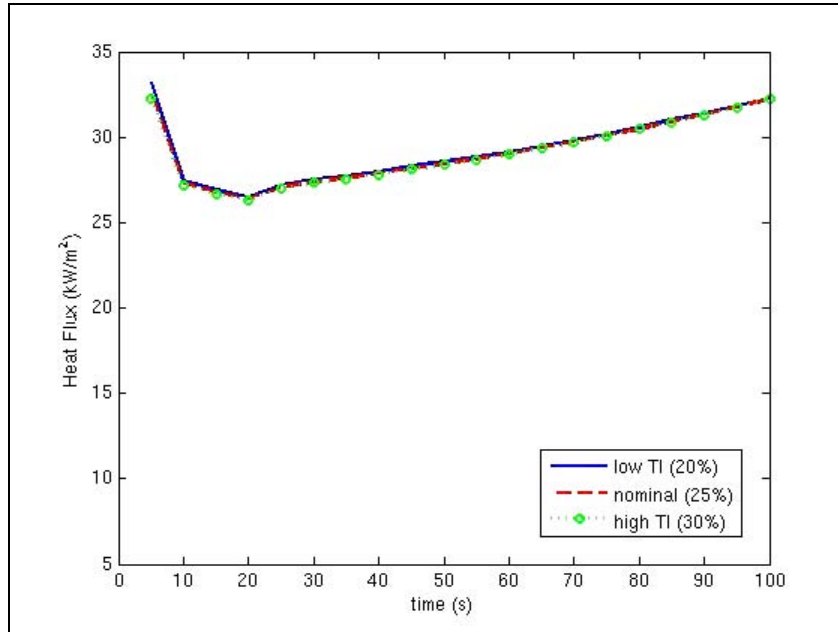
Figure 3-11 Inlet turbulelnce influence on radiation flux incident on bottom of C/MF
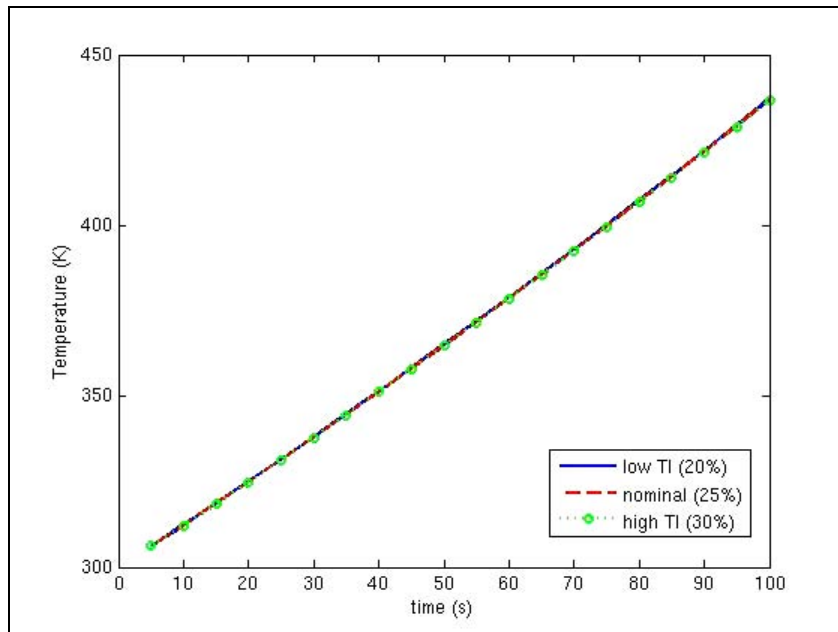
Figure 3-12 Inlet turbulence influence on Calorimeter 1 peak temperature history

3.5 Calorimeter 1 Emissivity

Calorimeter 1 in the Waterloo test facility was not painted black (all other calorimeters were painted black), giving it a lower emissivity than the other calorimeters. The influence of the calorimeter 1 emissivity was assessed by running simulations with a low (e = 0.4) and high (e = 1.0) calorimeter 1 emissivity in addition to the baseline case (e = 0.7). One expects to see a dependence of the calorimeter 1 thermal response on this parameter when considering the dominant role of radiation as a heat transfer mechanism in a sooty pool fire environment. Figure 3-13 demonstrates this dependence.

When considering the re-radiation of calorimeter 1 to other solid objects, one might expect to see that the rapid heat up of calorimeter 1 in the e = 1.0 case results in higher re-radiation to surrounding objects. However, this influence was not exhibited, as illustrated in Figure 3-14. An emissivity error that was discovered in the input file may be the source of this failure. Consequently, this emissivity sensitivity study is being performed again with corrected input files. However, the results obtained were convincing enough to substantiate the conclusion that the severity of the heat transfer is amplified by a larger calorimeter 1 emissivity.
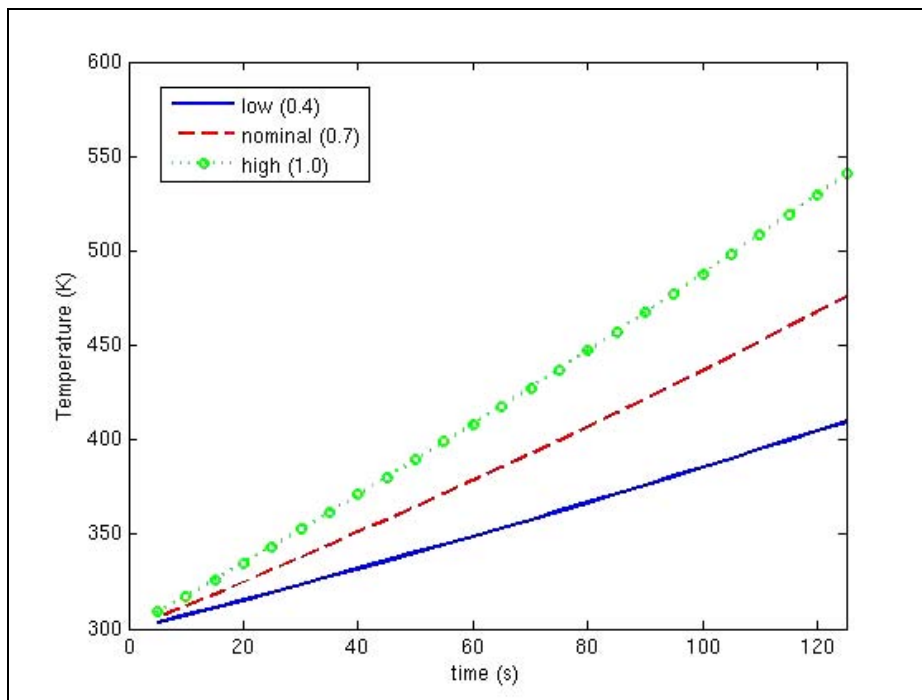
Figure 3-13 Calorimeter 1 emissivity influence on calorimeter 1 peak temperature history
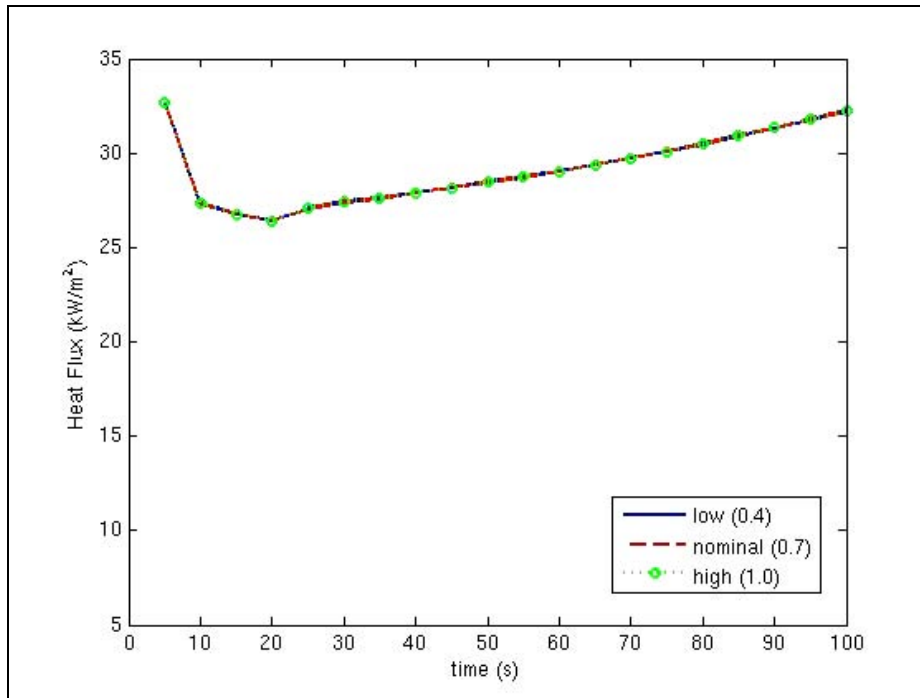
Figure 3-14 Calorimeter 1 emissivity influence on the radiation flux incident on the bottom of the C/MF

3.6 Floor and C/MF Thermal Conductivity

The influence of the floor and culvert thermal conductivities was assessed by comparing the baseline simulation with two additional simulations, in which these conductivities were increased and decreased by 20%. The nominal floor conductivity was 0.4 W/m-K and the nominal culvert conductivity was 4.3 W/m-K. Figure 3-15 shows the time-evolution of the net heat flux to the bottom of the culvert for these three cases. Figure 3-16 shows the temperature distribution on the culvert at t = 350 seconds. Figure 3-17 and Figure 3-18 illustrate the temperature distributions on calorimeters 1 and 3 respectively, at 350 seconds.

In general, simulation results do not appear to be significantly affected by the alterations in these conductivities. However, a small increase in the severity of the heat transfer is consistently produced by decreasing these conductivities.
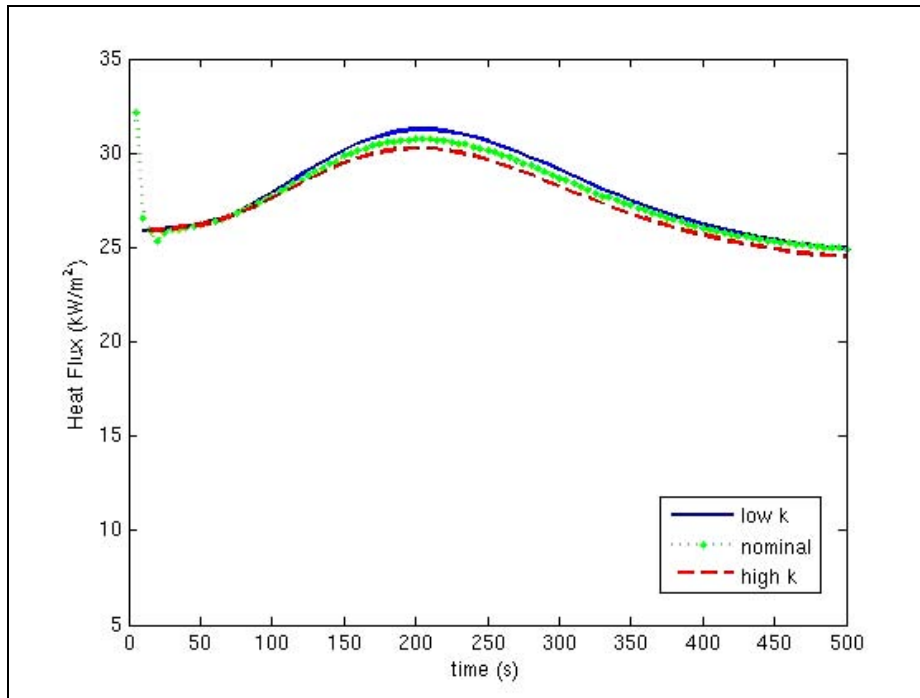
Figure 3-15 Floor & C/MF conductivity influence on net heat flux to bottom of C/MF
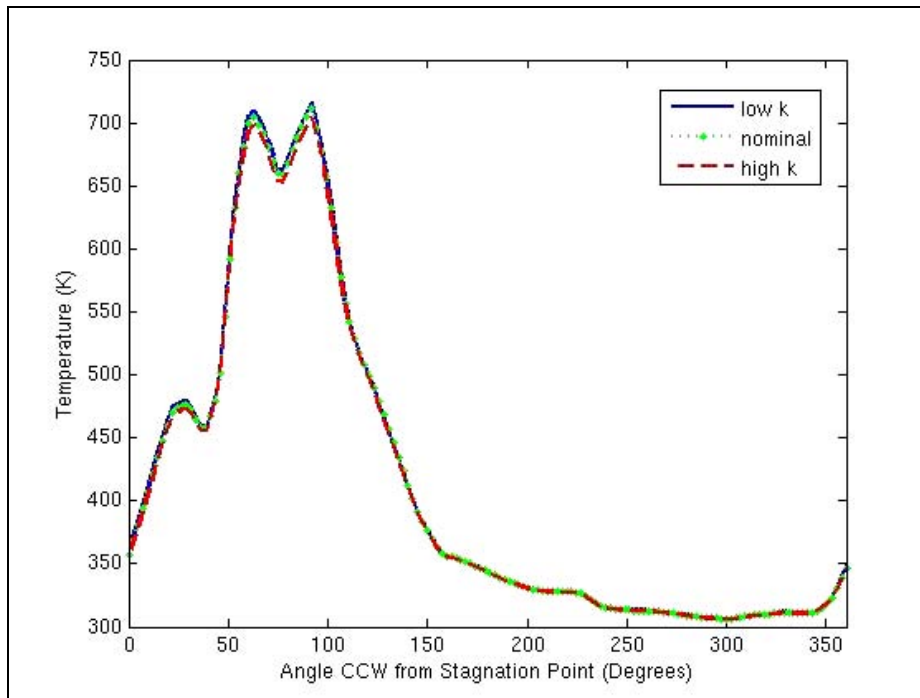
Figure 3-16 Floor & C/MF conductivity influence on C/MF temperature distribution at 350 s
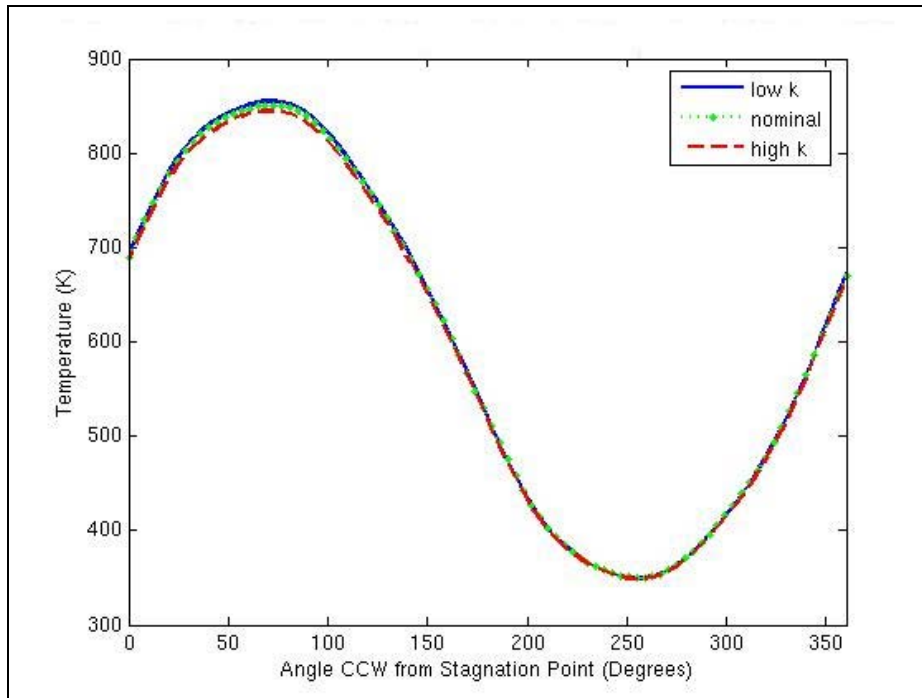
Figure 3-17 Floor & C/MF conductivity influence on Calorimeter 1 temperature distribution at 350 s
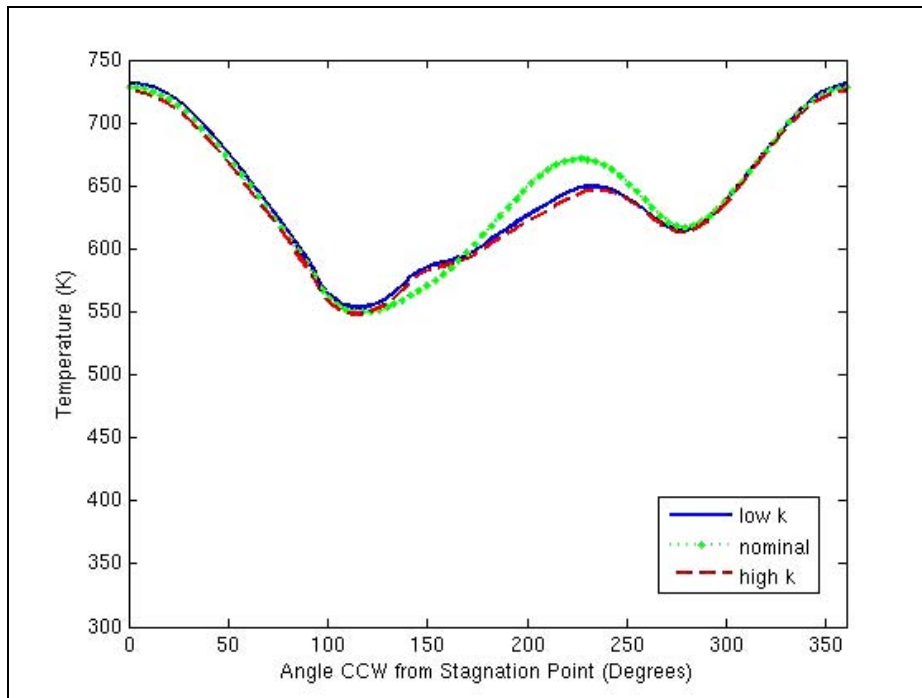
Figure 3-18 Floor & C/MF conductivity influence on Calorimeter 3 temperature distribution at 350 s

3.7 Baroclinic Vorticity Generation (BVG)

The influence of the baroclinic vorticity generation (BVG) model was assessed by comparing simulations that were run with and without the inclusion of this model. The baseline case included the BVG model. Figure 3-19 shows the time evolution of the net heat flux on the bottom of the C/MF for these two cases. Figure 3-20 shows the temperature distribution on the C/MF at t = 350 seconds. Figure 3-21 and Figure 3-22 illustrate the temperature distributions on calorimeters 1 and 3 respectively, at 350 seconds.

Although total heat transfer to the bottom of the C/MF is slightly less severe with BVG included (shown in Figure 3-19), the temperature distribution around the C/MF does not appear to be affected as illustrated in Figure 3-20. Figure 3-21 indicates that the thermal response of calorimeter 1 is not significantly affected either. The only convincing evidence of BVG sensitivity is found on calorimeter 3 as illustrated in Figure 3-22. The inclusion of the Baroclinic Vorticity Generation model increases the severity of the heat transfer, although this increase is not significant on the culvert and calorimeter 1. Due to the obscure evidence defining this weak relationship, the inclusion of BVG was not a manipulated parameter in the severity analysis to follow.
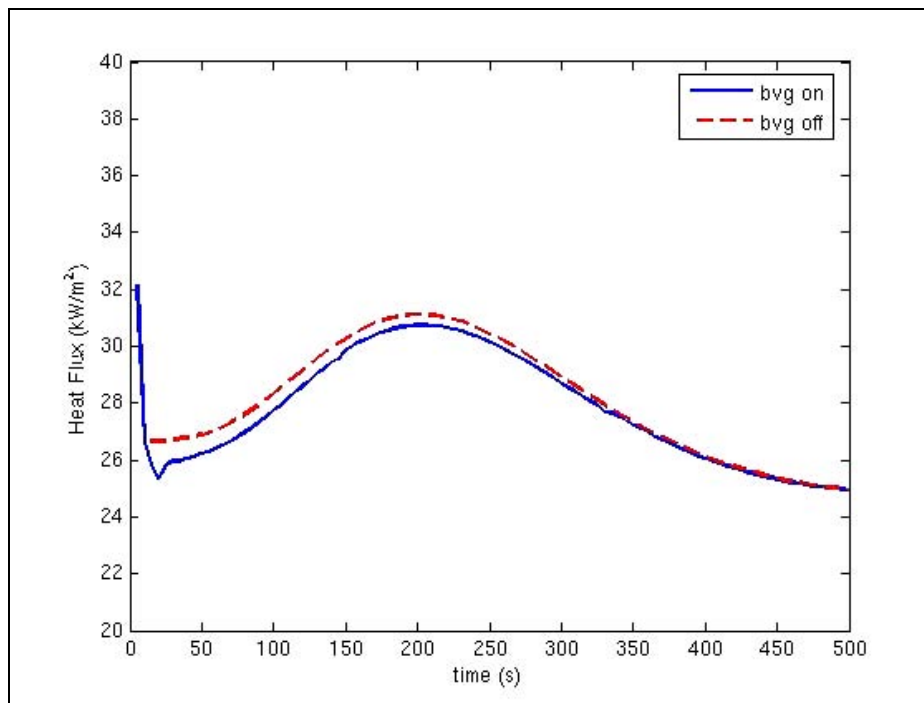
Figure 3-19 BVG influence on net heat flux to bottom of C/MF
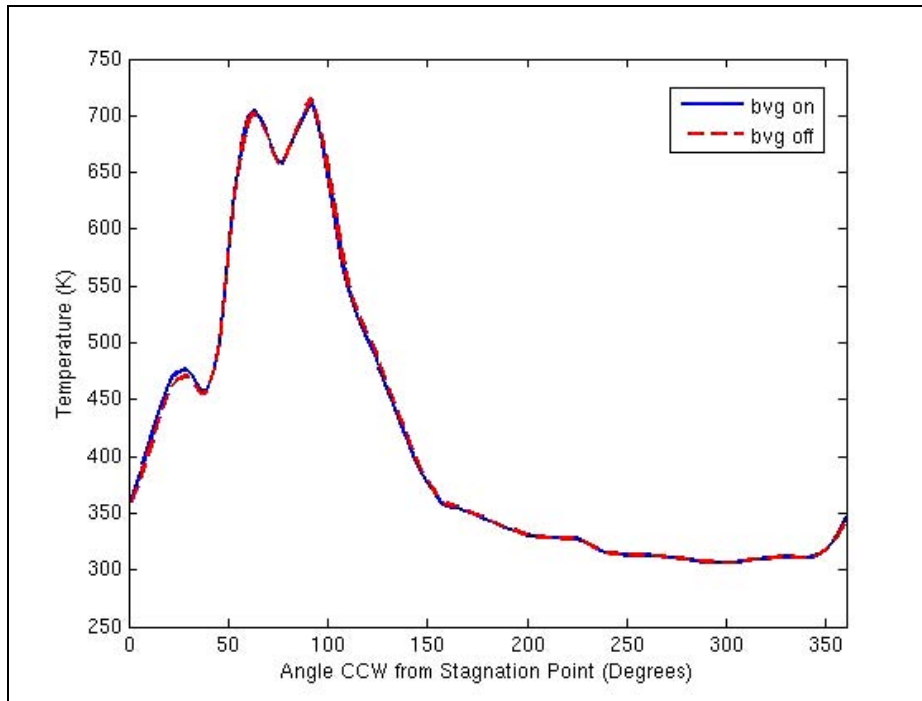
Figure 3-20 BVG influence on C/MF temperature distribution at 350 s
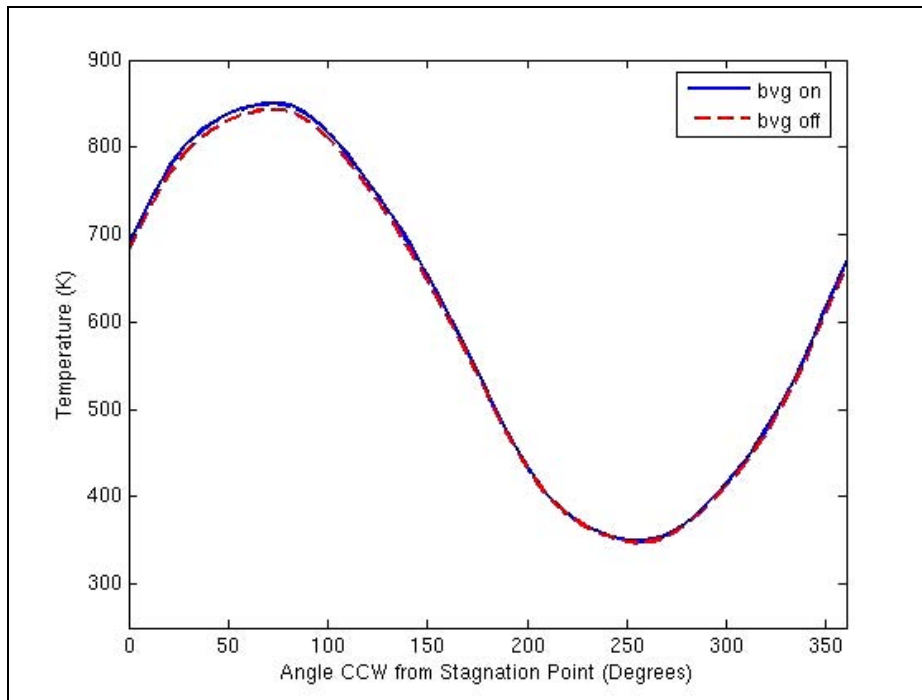
Figure 3-21 BVG influence on Calorimeter 1 temperature distribution at 350 s
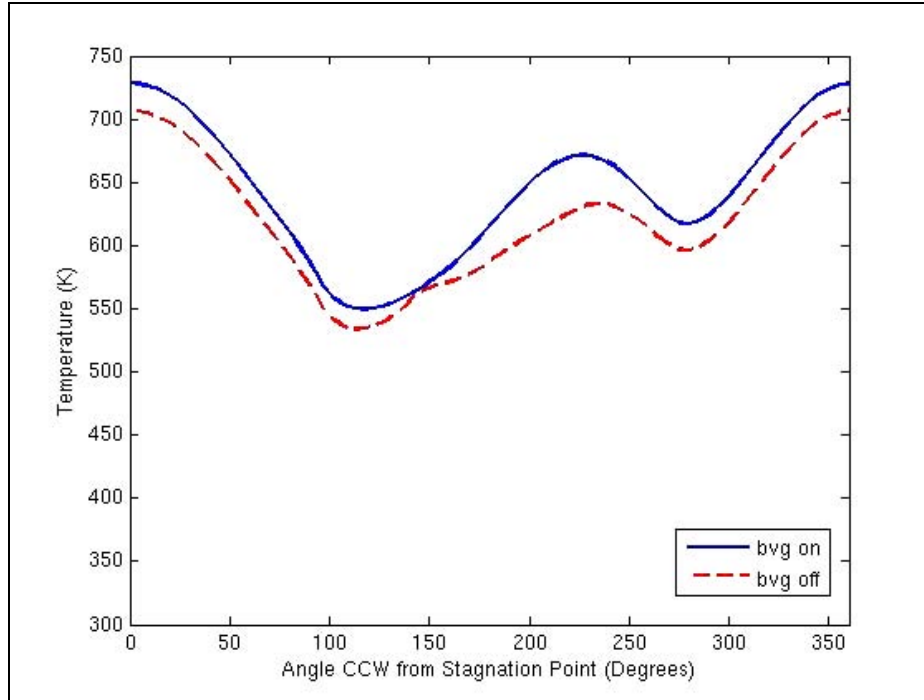
Figure 3-22 BVG influence on Calorimeter 3 temperature distribution at 350 s

3.8 Flame Volume Coefficient (FVC)

The flame volume coefficient (FVC) plays a significant role in the EDC combustion model. It represents the volume fraction of the flow possessing turbulent fine structures where mixing and combustion primarily occurs. This variable is calculated as:

$$\gamma = 9.7\left(\frac{\upsilon\varepsilon}{k^2}\right)^{\!3/4}$$

In Fuego, $\gamma^{1/3}$ is initially calculated using the expression:

$$\gamma^{1/3} = 2.13267\left(\frac{\upsilon\varepsilon}{k^2}\right)^{\!1/4}$$

The coefficient of the latter equation (2.13267) has been taken as the FVC for the sensitivity study. The 9.7 in the former equation is the true FVC. This discrepancy is not critical, since the intent of this portion of the study is to estimate sensitivity. The sensitivity of the simulation to variations in the flame volume coefficient was determined by comparing the baseline simulation with two additional simulations, which were run with a 30% increase and 30% decrease in the coefficient from the latter equation. Consequently, this manipulation of the flame volume coefficient results in a 120% increase and a 66% decrease in the FVC.

55

Figure 3-23 shows the time-evolution of the net heat flux to the bottom of the C/MF for these three cases. Figure 3-24 shows the temperature distribution on the C/MF at t = 350 seconds.
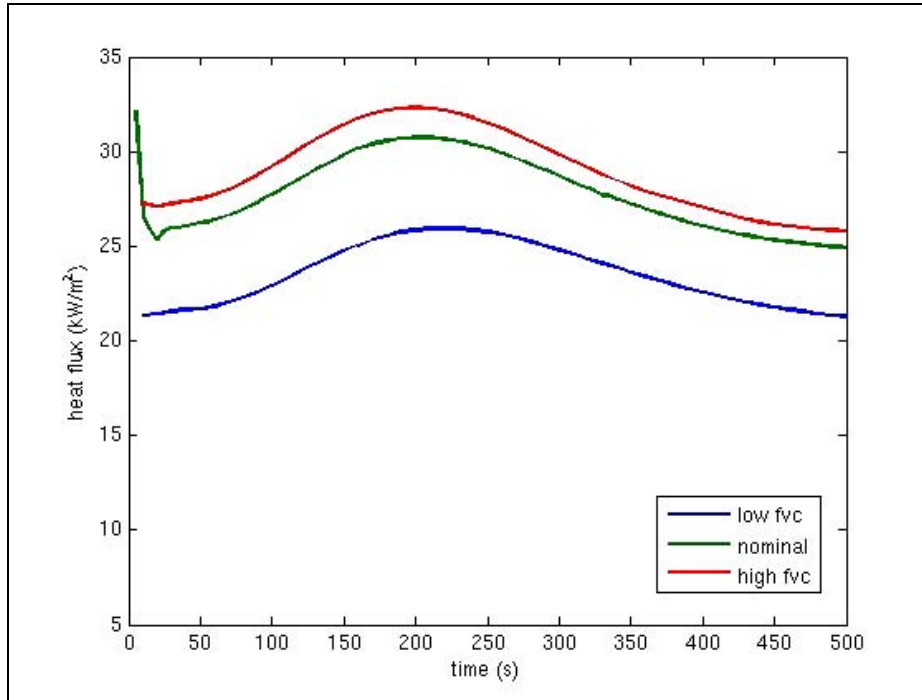
Figure 3-23 FVC influence on net heat flux to the bottom of the C/MF
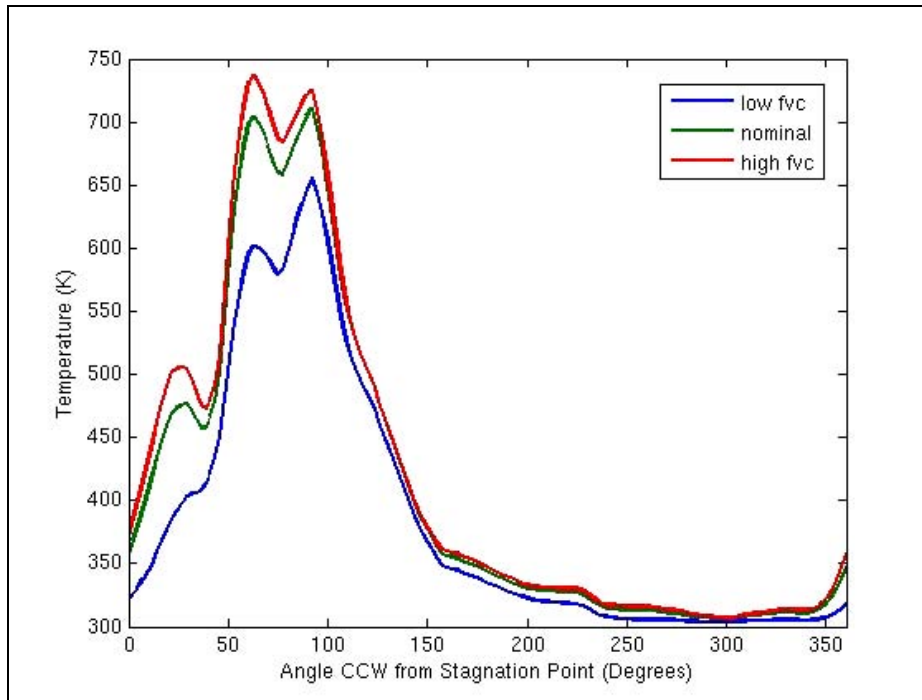
Figure 3-24 FVC influence on C/MF temperature distribution at 350 s

These plots show that an increase in the flame volume coefficient acts to increase the net heat transfer to the C/MF. Figure 3-25 and Figure 3-26 show similar dependencies on calorimeters 1 and 3 respectively.
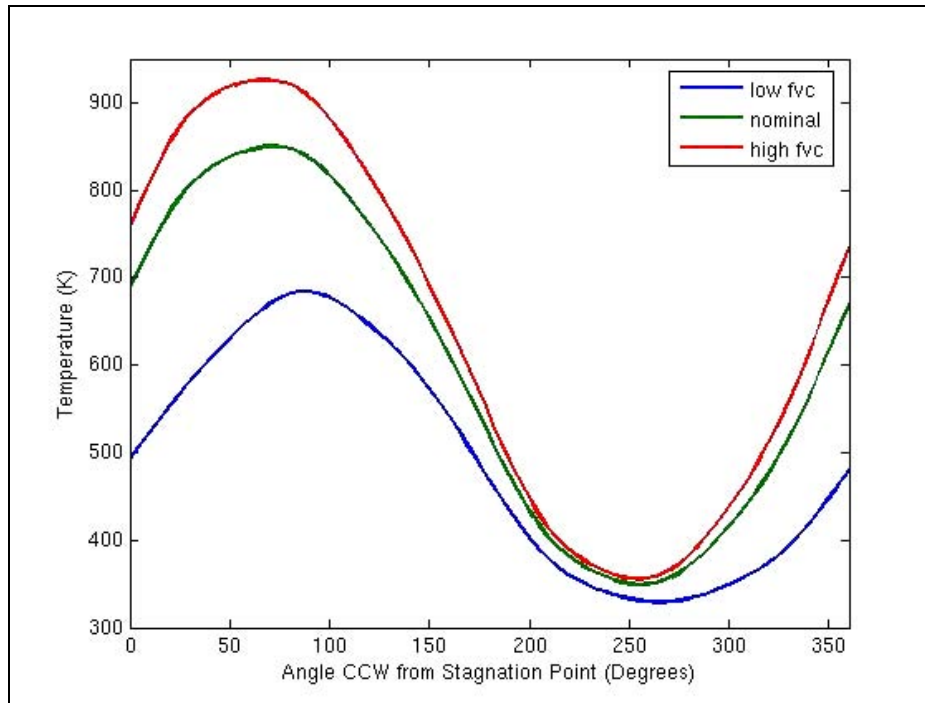
Figure 3-25 FVC influence on Calorimeter 1 temperature distribution at 350 s
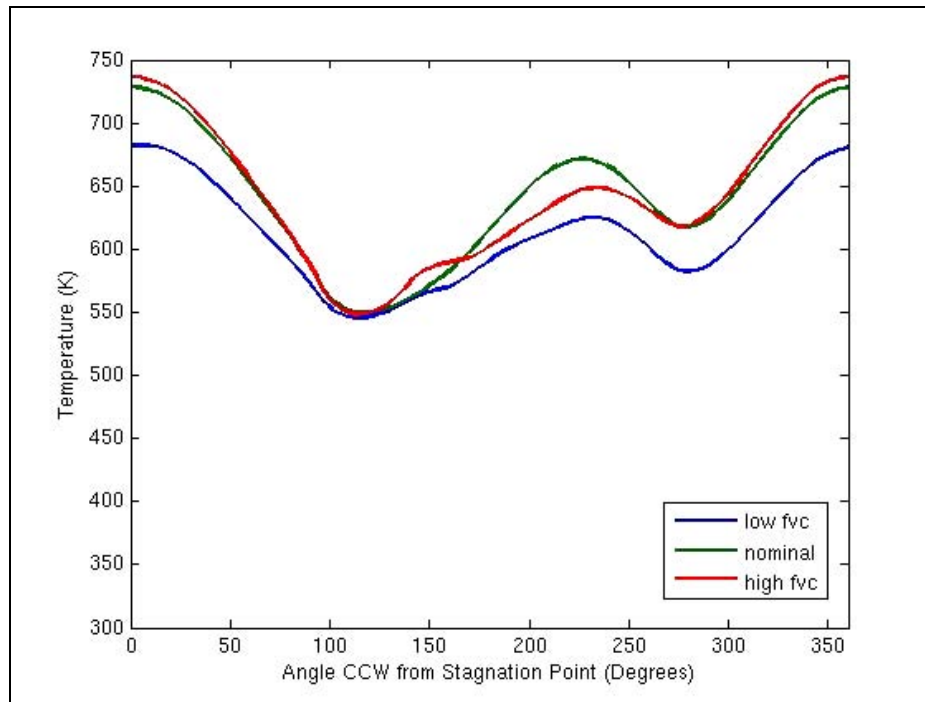
Figure 3-26 FVC influence on Calorimeter 3 temperature distribution at 350 s

3.9 Flame Loading Coefficient (FLC)

The time scale of the mass transfer between the fine structure and surrounding regions of EDC combustion model is calculated as:

$$\tau_{res} = \frac{1}{2.43}\left(\frac{\upsilon}{\varepsilon}\right)^{\frac{1}{2}}$$

where the constant 2.43 is referred to as the flame loading coefficient (FLC). The inverse (1/2.43) was taken as the flame loading coefficient for the sensitivity study. This again creates no problems except that an increase in the inverse parameter (shown in the plots) is a decrease in the true parameter, and vice versa. The sensitivity of the simulation to variations in the flame loading coefficient was determined by comparing the baseline simulation with two additional simulations, which were run with a 30% increase and 30% decrease in the flame loading coefficient. Figure 3-27 shows the time-evolution of the net heat flux to the bottom of the C/MF for these three cases. Figure 3-28 shows the temperature distribution on the C/MF at t = 350 seconds.
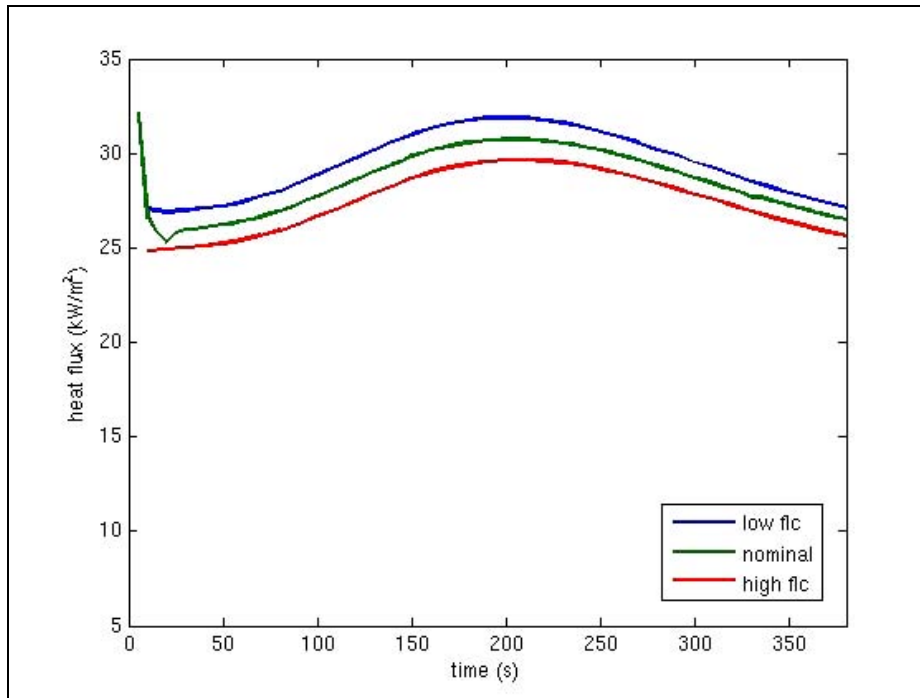
Figure 3-27 Inverse FLC influence on net heat flux to the bottom of the C/MF
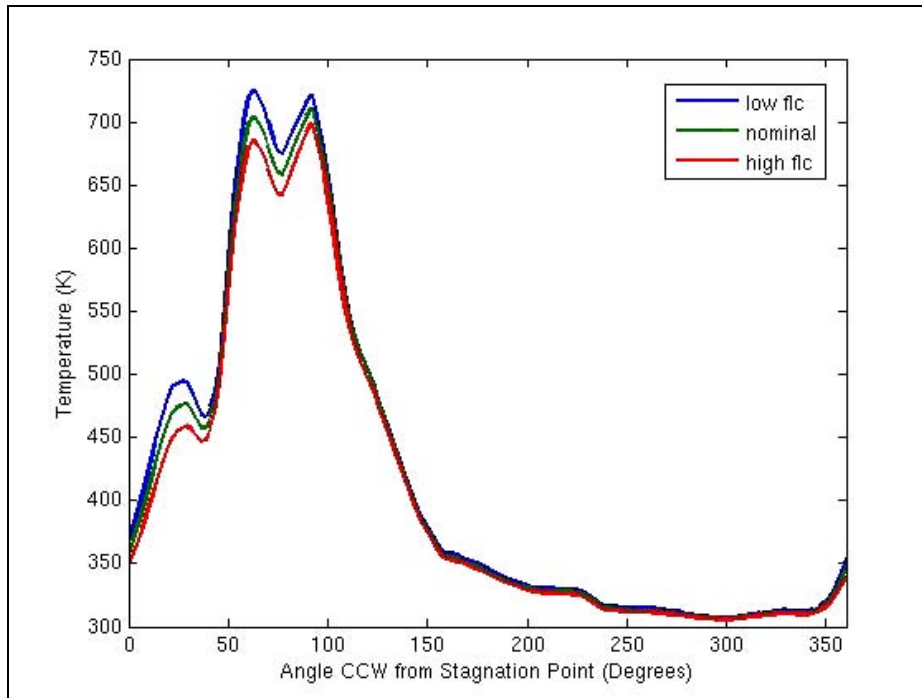
Figure 3-28 Inverse FLC influence on C/MF temperature distribution at 350 s
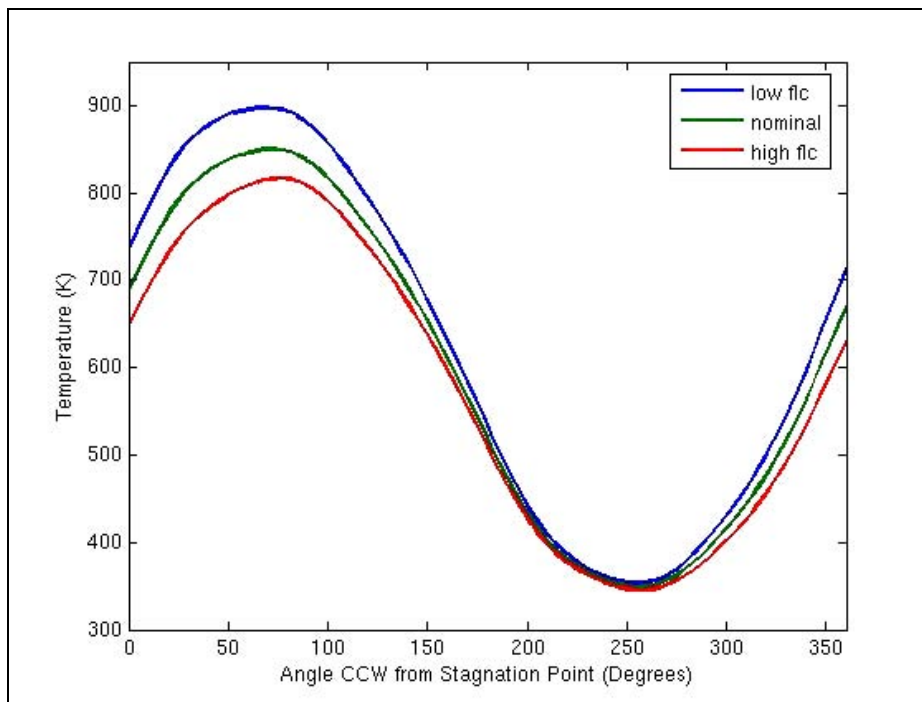
Figure 3-29 Inverse FLC influence on Calorimeter 1 temperature distribution at 350 s
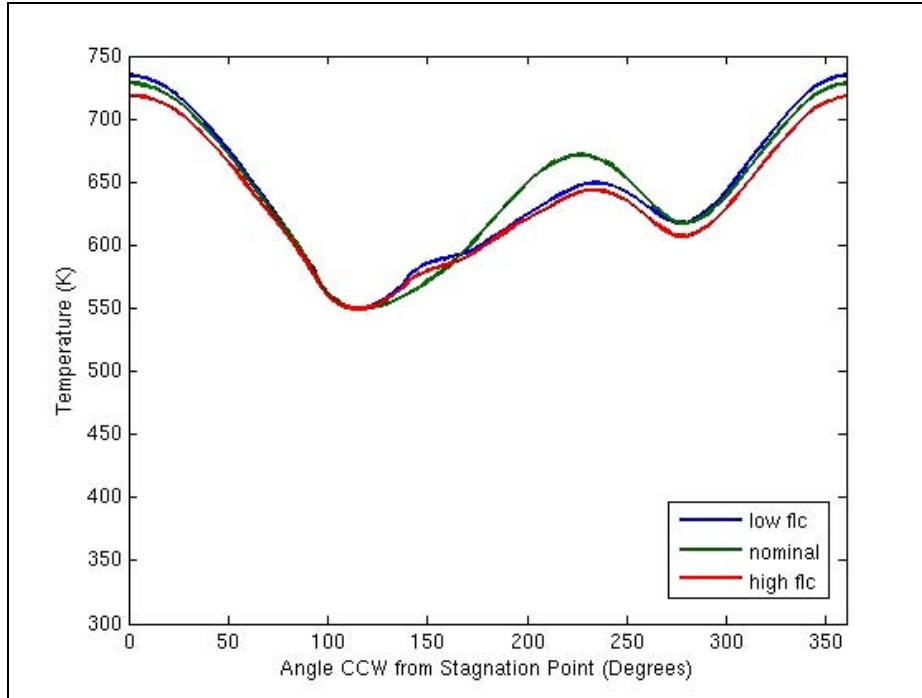
Figure 3-30 Inverse FLC influence on Calorimeter 3 temperature distribution at 350 s

Together, these plots indicate that an increase in the flame loading coefficient increases the heat transfer to the C/MF. Figure 3-29 and Figure 3-30 show similar dependencies for the calorimeter thermal responses.

3.10 Pressure Outlet Specification

Two simulations using different pressure outlet boundary conditions were performed. In one simulation (baseline case), the static pressure at the outlet was fixed to zero. In the second simulation, the total pressure at the outlet was fixed to zero. Figure 3-31 shows the time-evolution of the net heat flux on the bottom of the C/MF. Figure 3-32 shows the time-evolution of the peak temperature on calorimeter 1. No significant differences between the two sets of results are evident. In general, the alternative methods of pressure outlet specification produce results that are nearly identical.
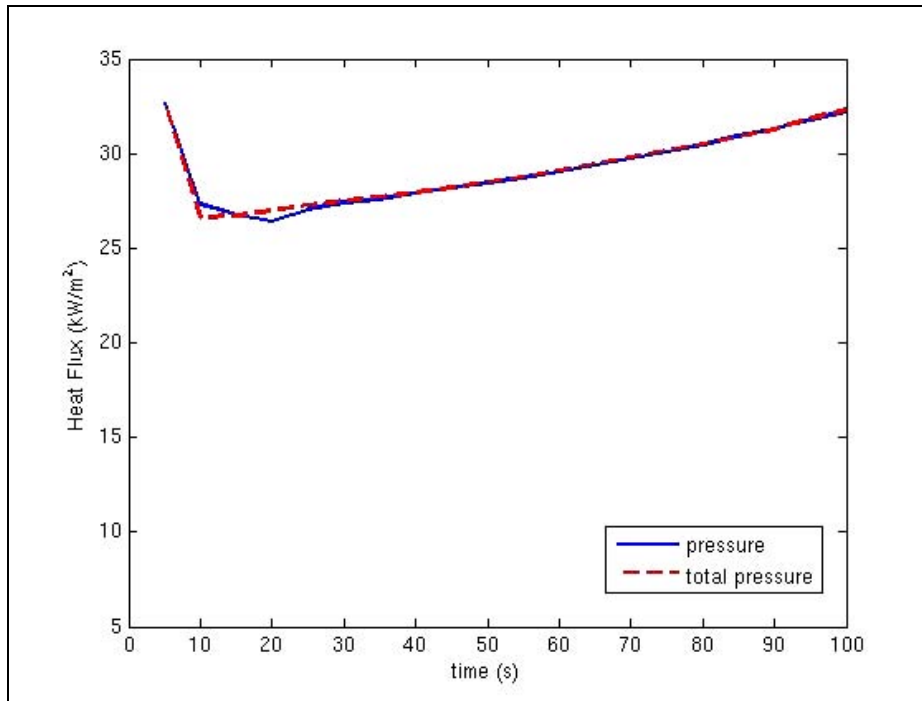
Figure 3-31 Pressure outlet influence on net heat flux to the bottom of the C/MF
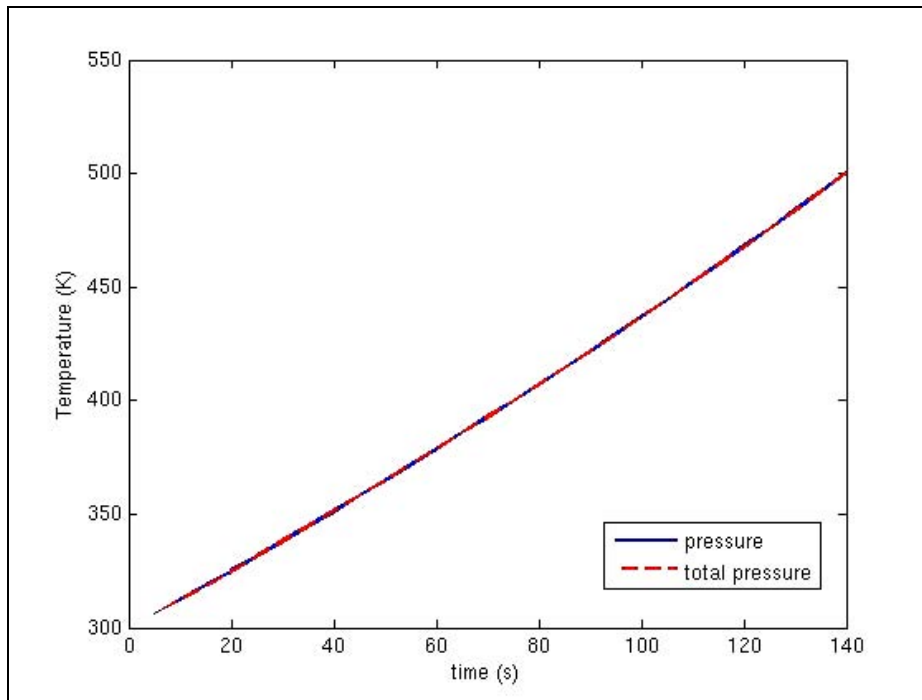
Figure 3-32 Pressure outlet influence on Calorimeter 1 peak temperature

61

3.11 Inlet Velocity Specification

Measurements of the velocity field in the Waterloo test facility have been made under isothermal conditions (Weisinger and Weckman, 2003). Figure 3-33 illustrates the nonuniform velocity distribution generated near the inlet by the plenum fans. These structures persist downstream and can be seen in the contour plot at x = 5m, near the pool fire region.
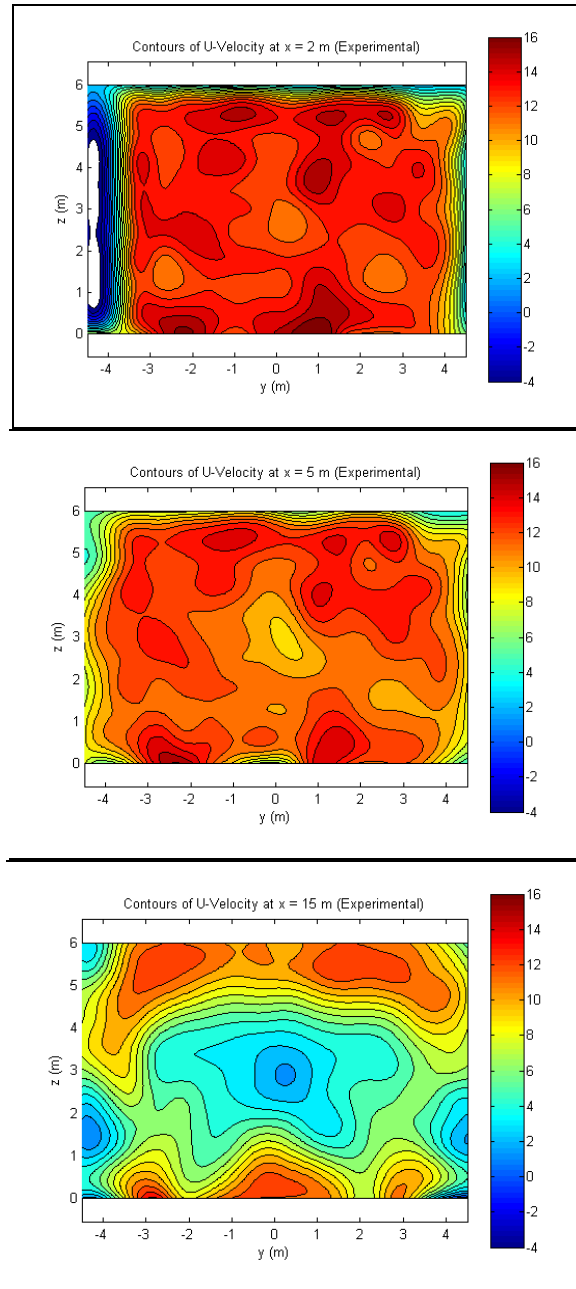
Figure 3-33 Contours of u-velocity from velocity measurements at x = 2, 5, and 15 m.

The influence of the selection of the inlet velocity specification method was assessed by running a simulation with a non-uniform velocity inlet in addition to the baseline case that

used a uniform inlet velocity. The non-uniform velocity distribution was specified on inlet nodes by interpolating within the x = 2m data, based on node locations. The contour plot of Figure 3-34 illustrates the resulting inlet velocity distribution. Figure 3-35 contains contour plots of stream-wise velocity at x = 2, 5, and 15 meters for each isothermal simulation.
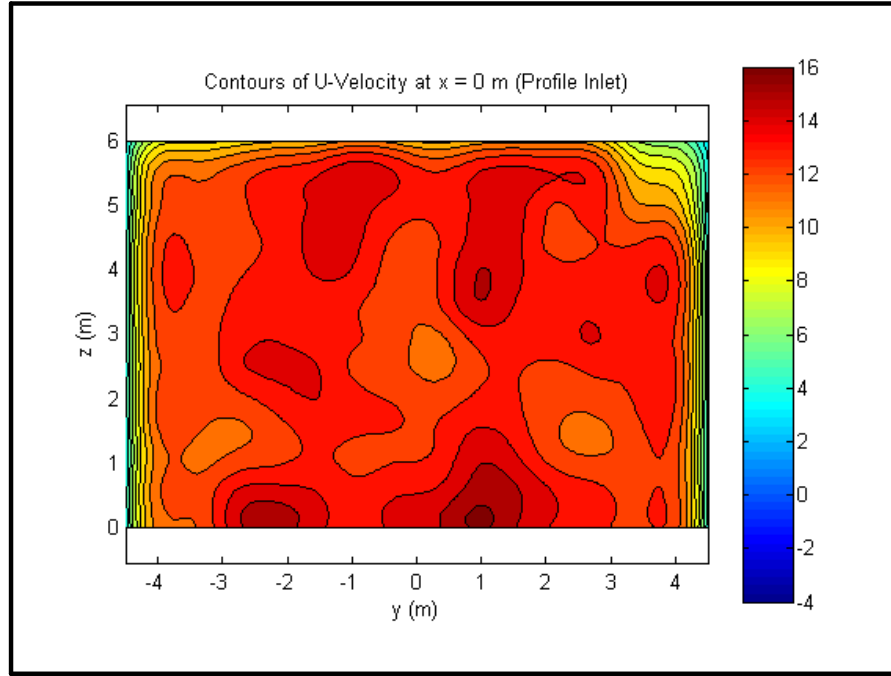
Figure 3-34 Contours of u-velocity at x = 0 m (profile inlet)

Comparison of Figure 3-33 and Figure 3-35 reveals that the non-uniform flow structures that are specified on the inlet in the profile inlet simulation persist to the pan (x = 5m) as seen in experimental results. However, these structures seem to dissipate too quickly as they are convected in the simulation. Both simulations fail to capture the wake structures after the solid objects at x = 15 meters. The similarity of the x = 15 m simulation results indicates that the structure of the flow at this location is not significantly influenced by the inlet structures, but is primarily affected by the culvert and calorimeters that redirect the flow.

The two inlet conditions were implemented into the pool fire (non-isothermal) simulations in order to evaluate the sensitivity of the simulation to the inlet velocity specification. Figure 3-36 illustrates the time evolution of the radiation heat flux incident on the bottom of the culvert for both cases. At this location, the inlet condition appears to significantly affect the heat transfer. Figure 3-37 illustrates the temperature distribution around the culvert for each case. The different inlet conditions appear to be responsible for a maximum temperature difference of only 4% on the culvert. Little sensitivity is exhibited on calorimeters 1 and 3, as illustrated in Figure 3-38 and Figure 3-39 respectively.

Profile Inlet

Plug Flow

2 m

5 m

15 m
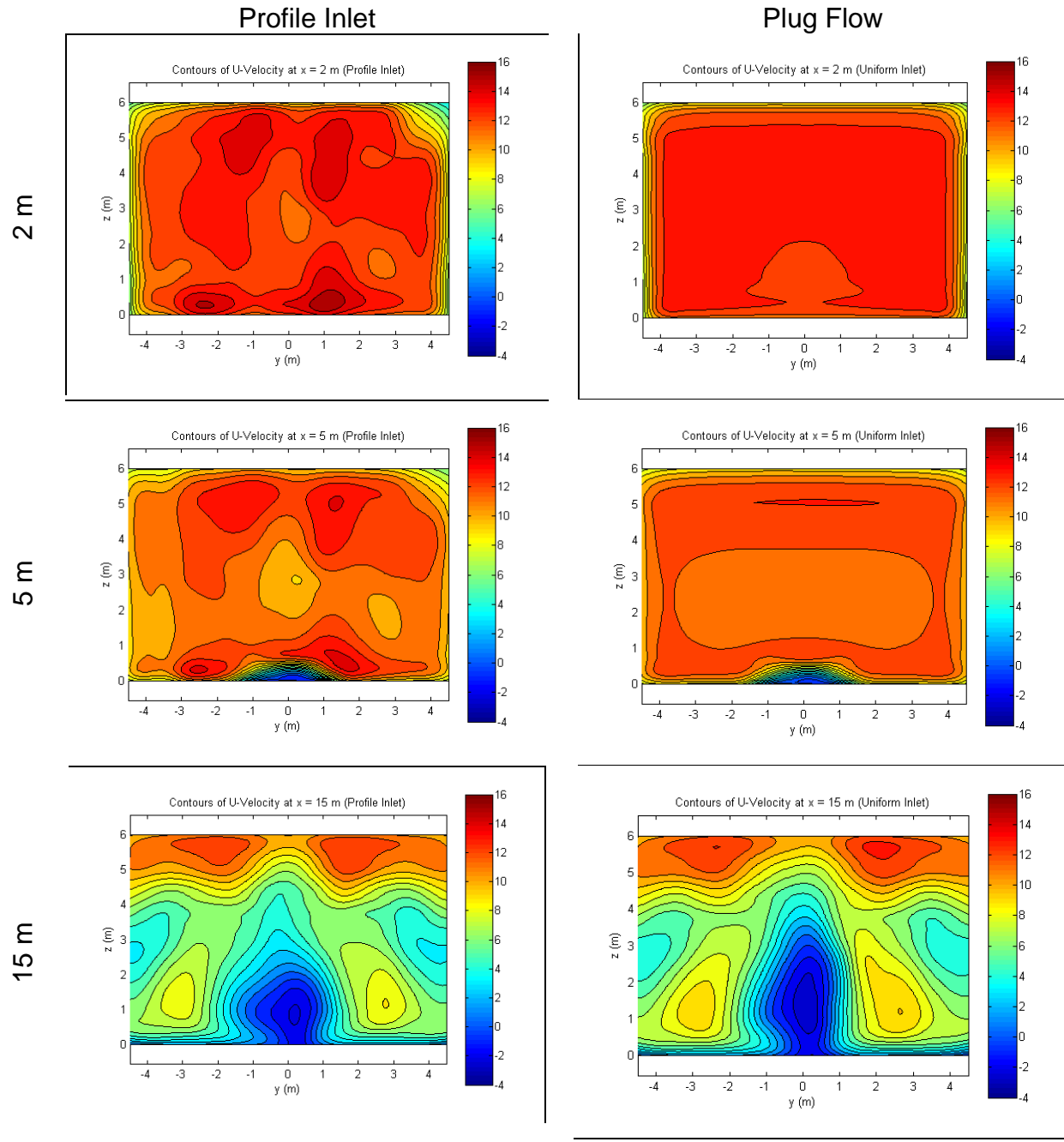
Figure 3-35 Contours of u-velocity from isothermal simulations
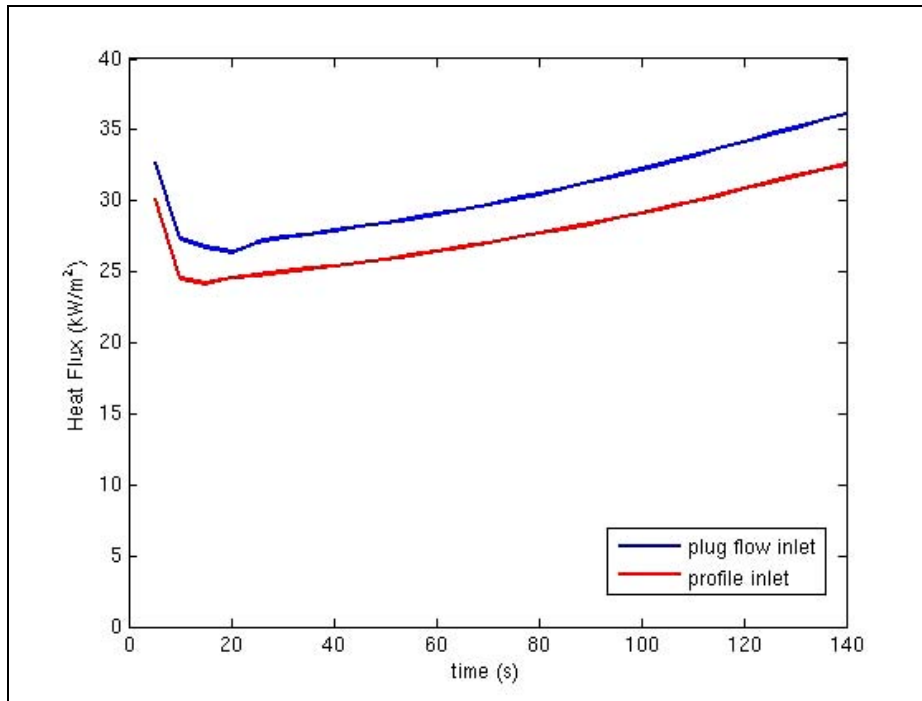
Figure 3-36 Velocity inlet condition influence on radiation flux incident to the bottom of the C/MF
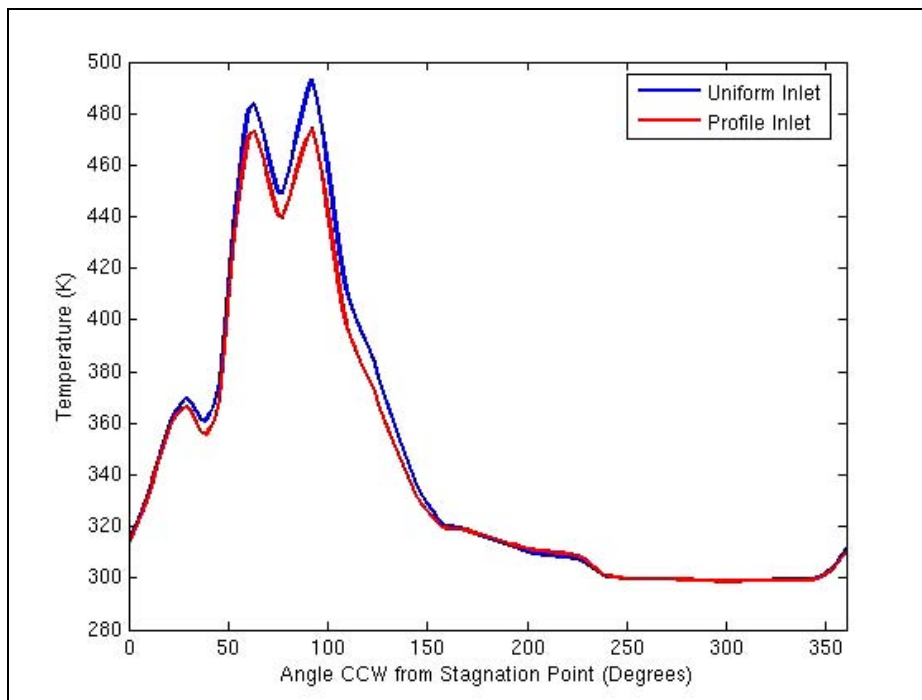
Figure 3-37 Velocity inlet condition influence on C/MF temperature distribution at 140 s
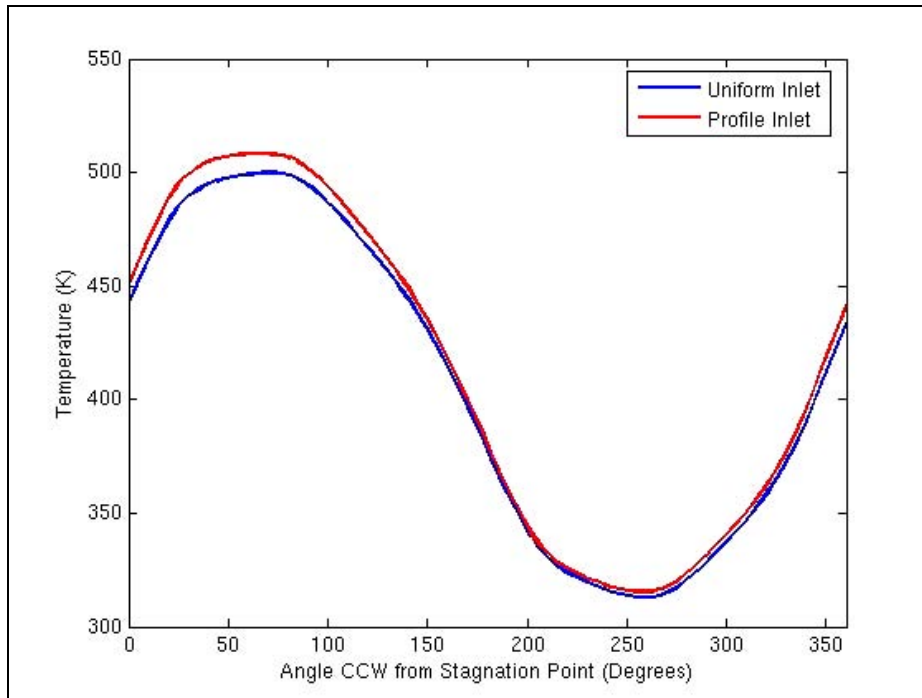
Figure 3-38 Velocity inlet condition influence on Calorimeter 1 temperature distribution at 140 s
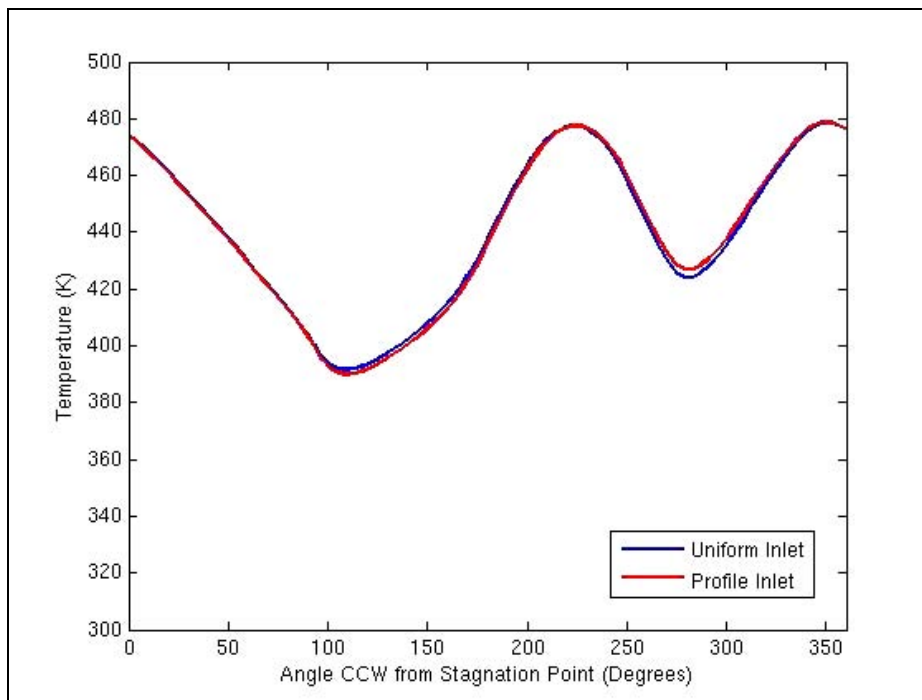
Figure 3-39 Velocity inlet condition influence on Calorimeter 3 temperature distribution at 140 s

The slight sensitivities exhibited on these three objects are not consistent. The uniform inlet simulation appears slightly more severe on the C/MF while the profile inlet simulation appears slightly more severe on calorimeter 1.

3.12 Sensitivity Analysis Conclusions

Sensitivities of various modeling uncertainties have been assessed on a small, under-resolved mesh to determine settings for the more refined study. The sensitivities discovered in this analysis are summarized in Table 3-2. Most parameters were found to have a small effect on the severity of the predicted environment at the bottom of the C/MF and at the thermocouple measurement points on the calorimeters.

Table 3-2 Sensitivity Analysis Conclusions

Parameter	Influence on Severity
Time Step	Inverse Relation
Picard Loops	Small Effect
PMR Quadrature Order	Small Effect
Inlet Turbulence Intensity	Small Effect
Unpainted Calorimeter Emissivity	Direct on Cal. 1, Small Elsewhere
Floor& C/MF Thermal Conductivity	Inverse Relation
BVG	BVG Inclusion is Mildly More Severe
FVC	Direct Relation
FLC	Direct Relation
Pressure Outflow Boundary	Small Effect
Inlet Velocity Distribution	Small Effect

4. Baseline Simulation

This section is intended to acquaint the reader with some basic and common features of the simulations by presenting detailed prediction results from the baseline simulation. The baseline simulation is simulation #1 from Table 2-3. Simulation off-sets (the other simulations from the same table) resulted in varying degrees of change in observation. Many of the general observations are applicable to all cases. For this reason, the results obtained from this case are documented in detail in this section.

The output from the simulations is extensive, and would require extensive effort to document in entirety.

4.1 Flow Predictions

Velocities have been plotted at three vertical planes. These are found in Figure 4-1, Figure 4-2, and Figure 4-3. Velocities have been plotted at three horizontal planes. These plots are found in Figure 4-4, Figure 4-5, and Figure 4-6. A consistent color scale has been used for each of these plots for the velocity magnitude, and velocity vectors are overlaid on the contours in black. Vectors have been plotted uniformly across the mesh. Portions of the plots where no vectors are present are because they are behind the contour plane.
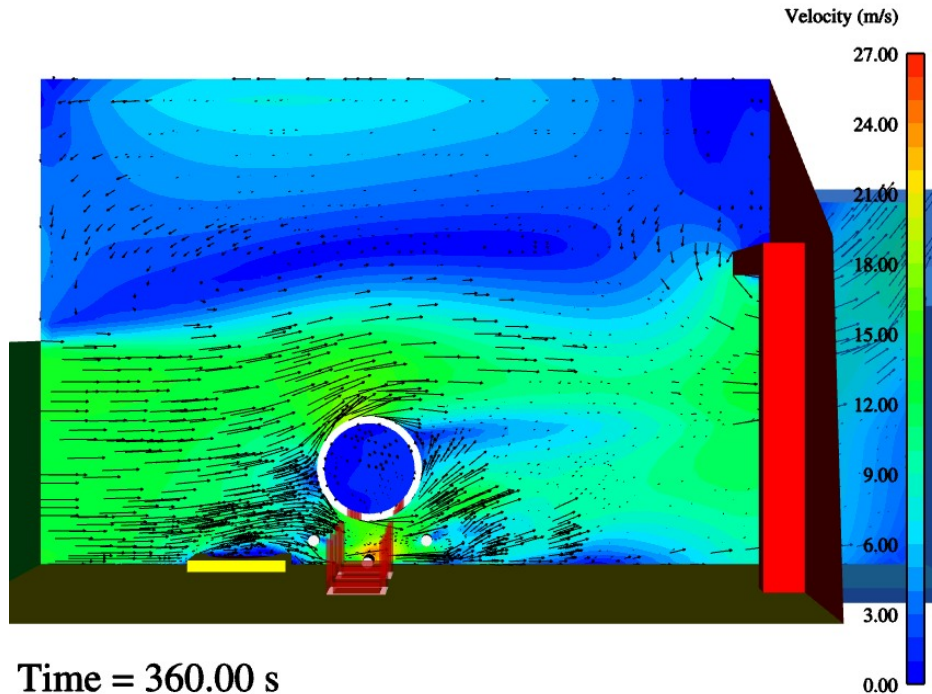
Figure 4-1 Velocity predictions at y = 8.3 m (the centerplane)

Time = 360.00 s
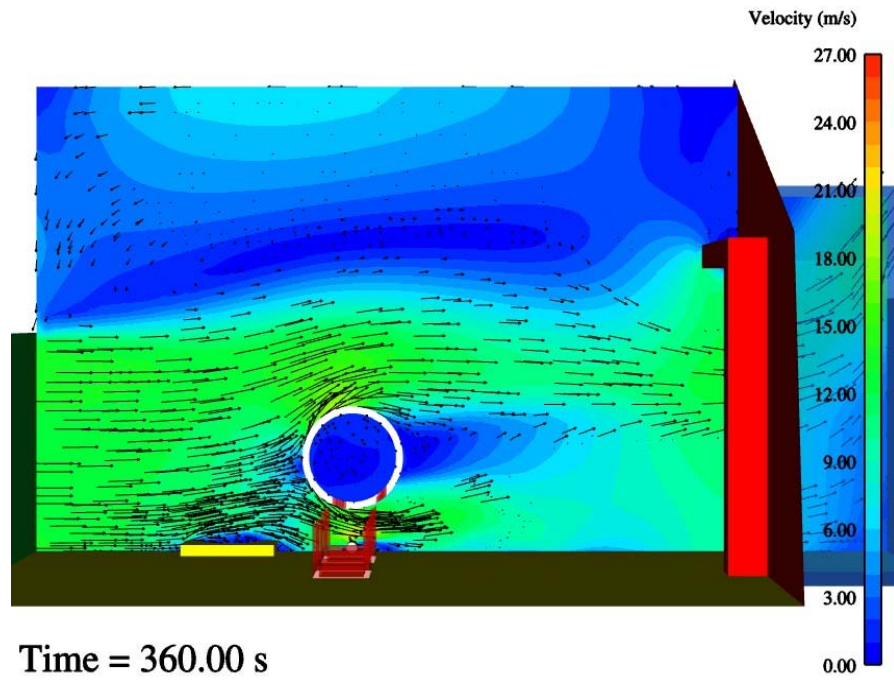
Figure 4-2 Velocity predictions at y = 7.53 m (center of Calorimeter 3)

Time = 360.00 s
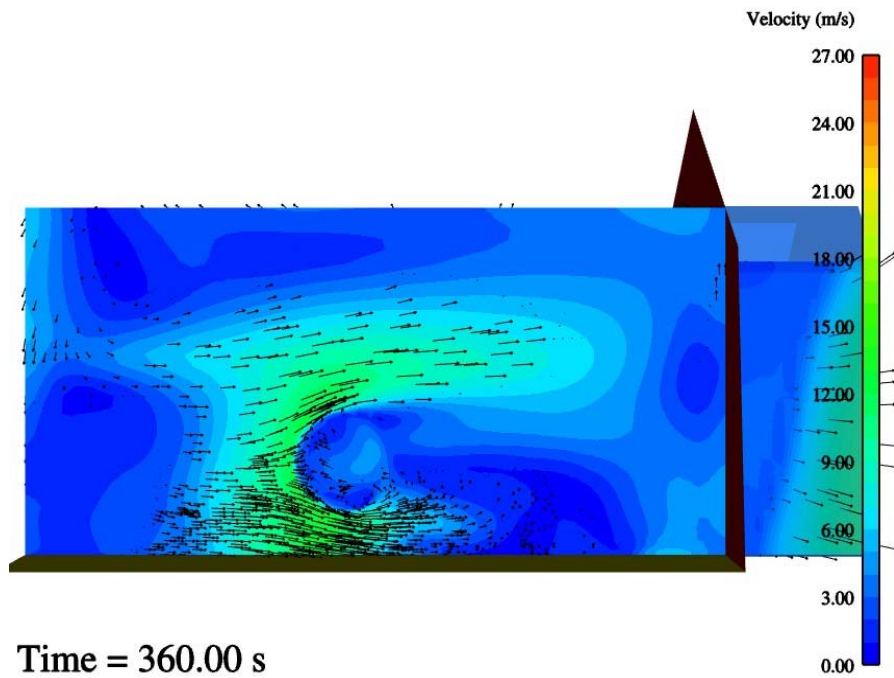
Figure 4-3 Velocity predictions at y = 2.31 m (end of C/MF)

Time = 360.00 s
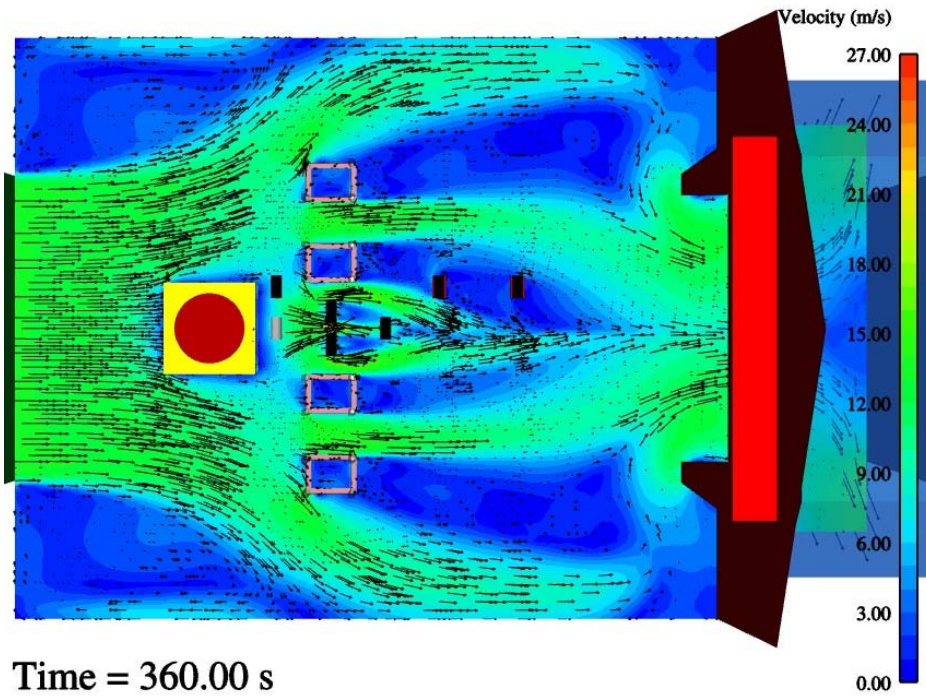
Figure 4-4 Velocity predictions at z = 0.15 m (center of ground calorimeters)

Time = 360.00 s
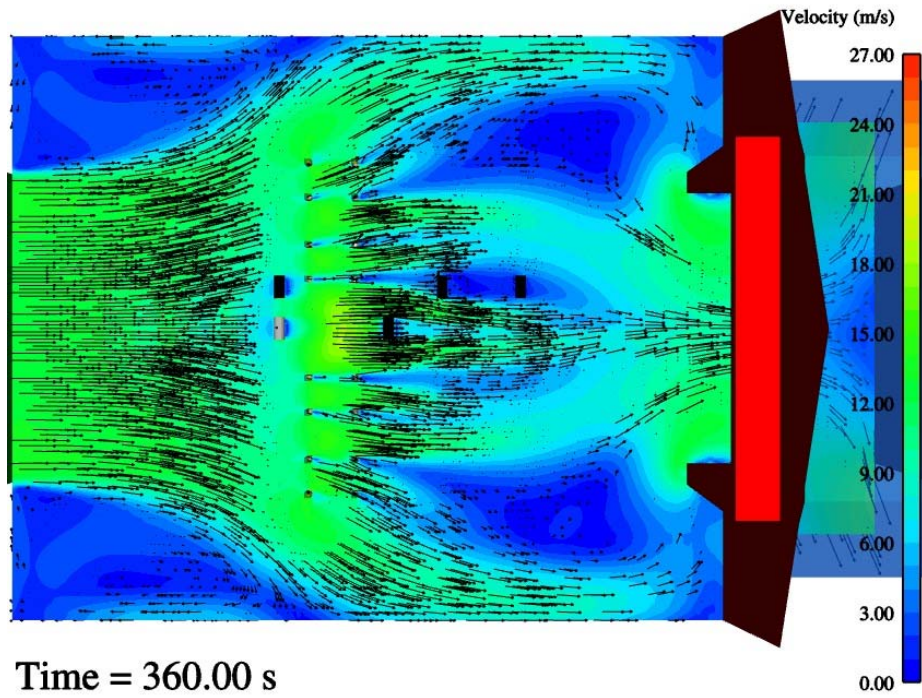
Figure 4-5 Velocity predictions at z = 0.68 m (center of elevated calorimeters)
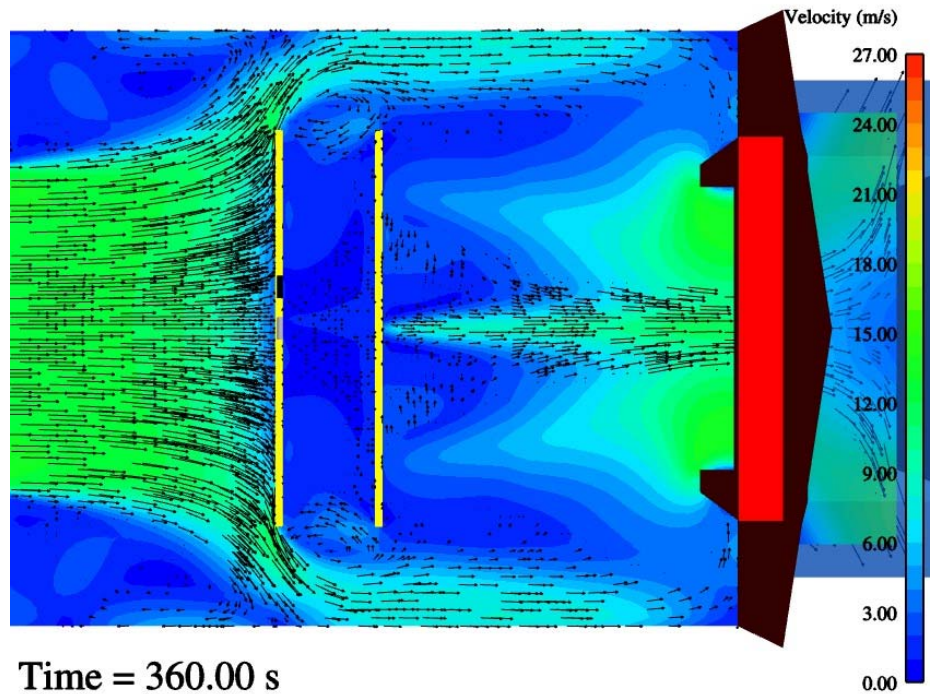
Figure 4-6 Velocity predictions at z = 2.60 m (center of C/MF)

Figure 4-1 through Figure 4-6 illustrate the complexity of the predicted flow-field in the facility at 360 seconds. The predicted extent of the C/MF wake is evident in Figure 4-1, Figure 4-2, and Figure 4-6. The predicted wake of other smaller objects in the flow is evident in Figure 4-4 and Figure 4-5. The green of the color scale suggests velocity magnitudes that are on the order of 13 m/s (the inlet velocity). The inlet velocity persists through the main section of the flow from the inlet to the outflow region with the exception of the wake regions. In the extremities and corners of the facility, complicated recirculation patterns are present in the predictions.

A final plot of the predicted flow is found in Figure 4-7. This figure shows an isometric view of velocity streamlines emitted from a vertical (green) and a horizontal (purple) linear array near the inlet of the facility. The horizontal array was positioned 0.3 m above the floor, and the vertical array is positioned along the center-plane of the facility.
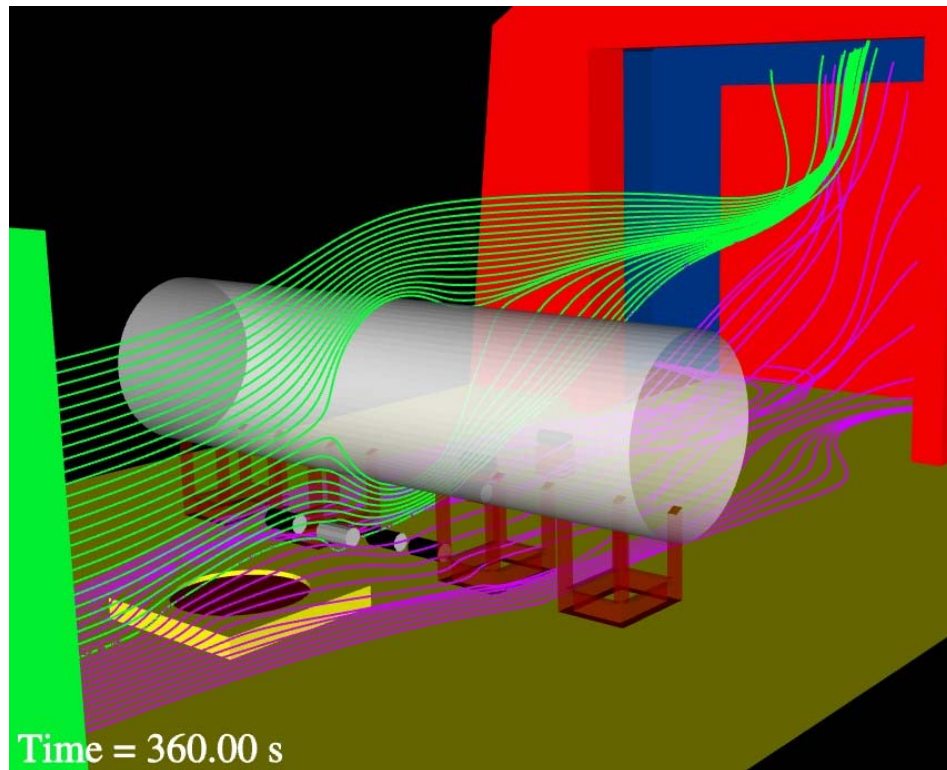
Figure 4-7 Predicted streamlines at 360 s

4.2 Gas Temperatures

Plots of predicted temperature that correspond to the same cut-planes on which velocities were plotted have been generated. Figure 4-8 through Figure 4-10 show the vertical plane plots of temperature at x = 8.3, 7.53, and 2.31 m respectively. Figure 4-11 through Figure 4-13 show the horizontal plane plots of temperature at z = 0.15, 0.68, and 2.60 m respectively. All temperature plots are plotted on the same scale with the exception of the x = 2.31 m plot, which employs a narrower scale to better illustrate the range of predicted values.

Iso-contour plots of temperature give a better sense of the 3-dimensional space of the predicted temperature. Figure 4-14 shows plots of the 900 K iso-contours of temperature from two different angles. The iso-contour of temperature is white.
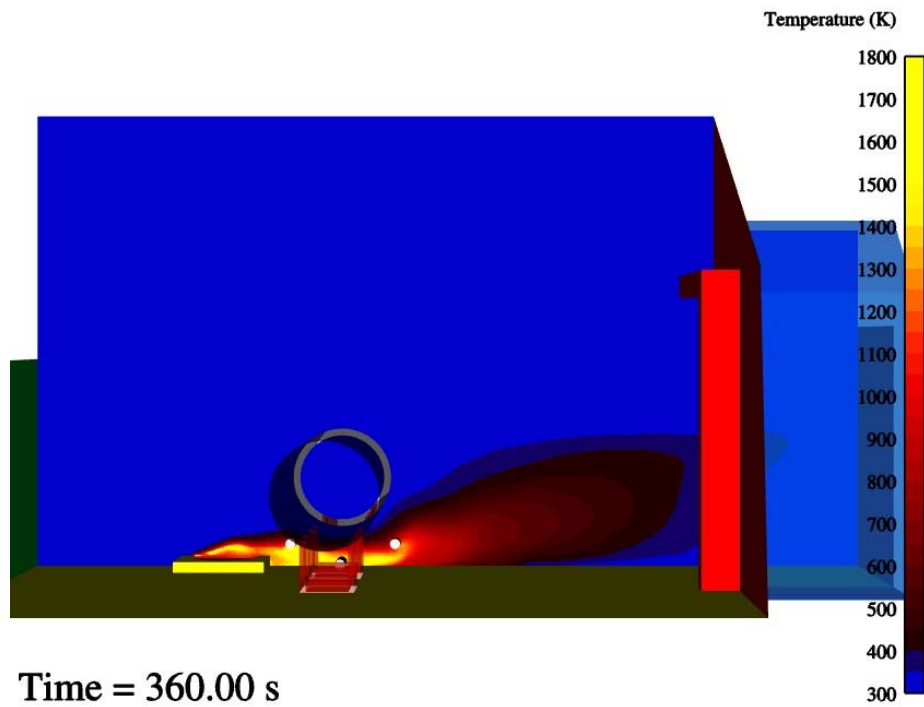
Figure 4-8 Temperature predictions at y = 8.3 m (the centerplane)
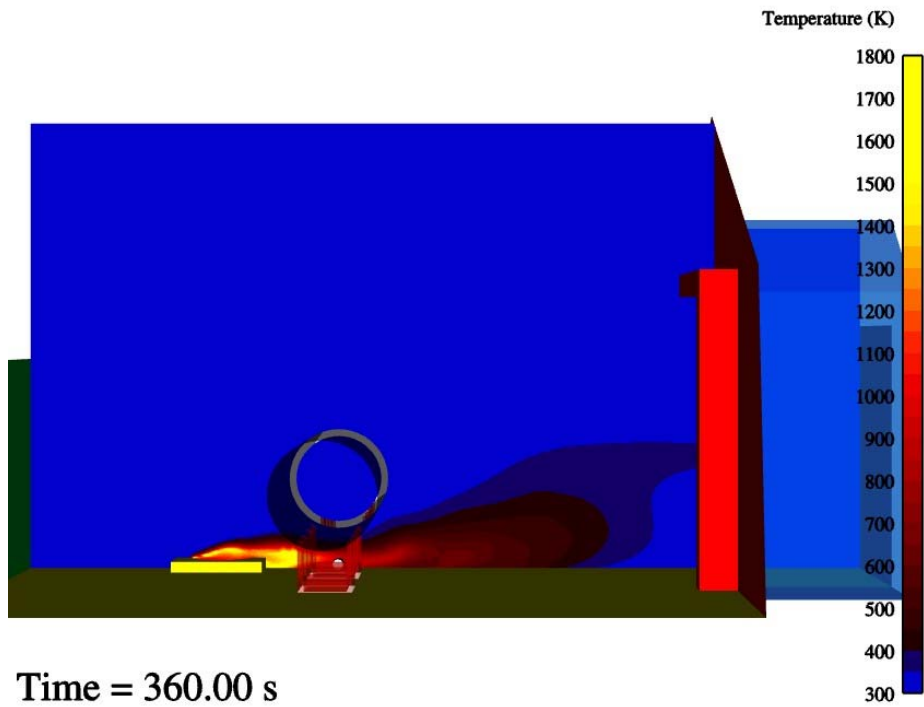
Figure 4-9 Temperature predictions at y = 7.53 m (center of Calorimeter 3)
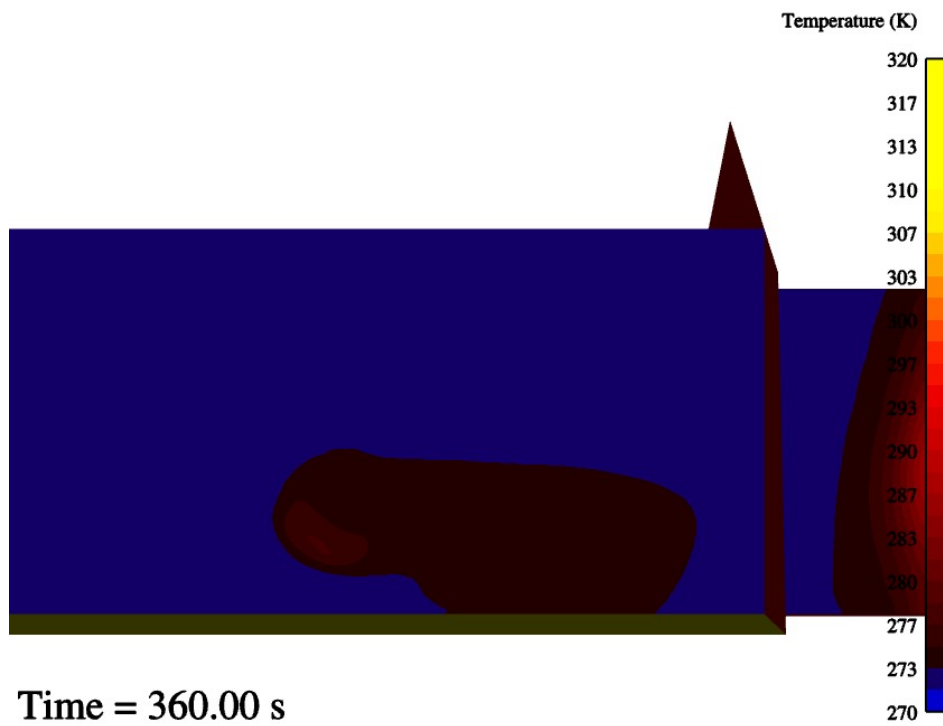
Figure 4-10 Temperature predictions at y = 2.31 m (end of C/MF)
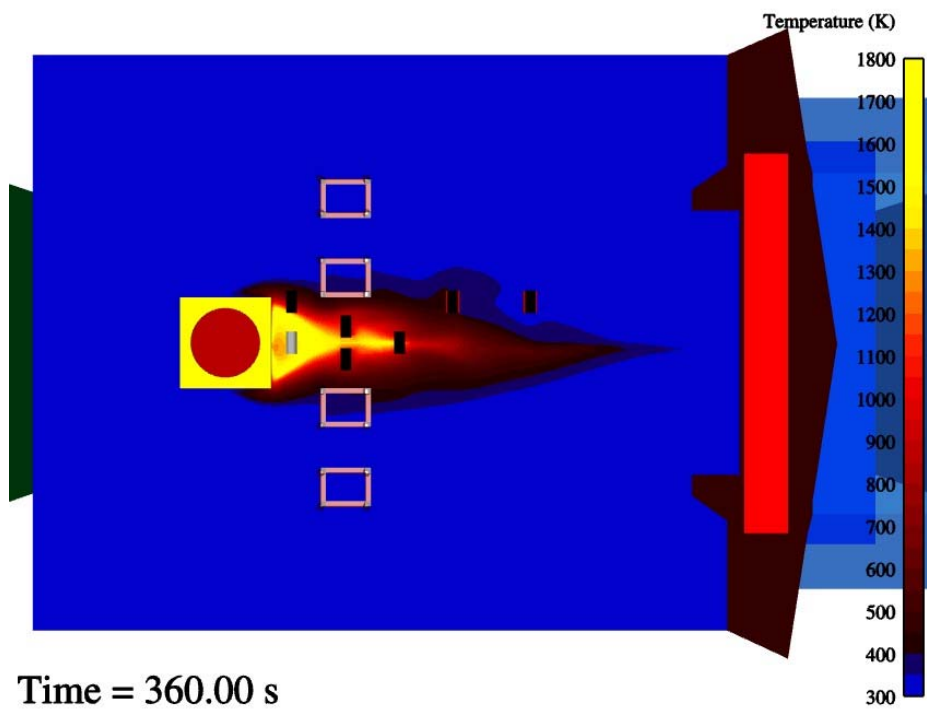
Figure 4-11 Temperature predictions at z = 0.15 m (center of ground calorimeters)

Time = 360.00 s
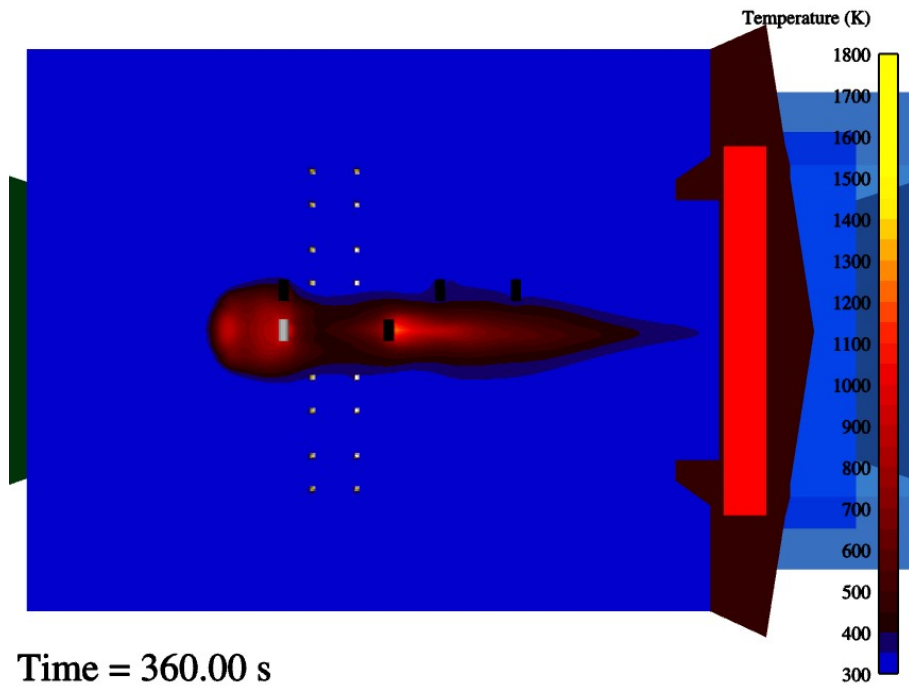
Figure 4-12 Temperature predictions at z = 0.68 m (center of elevated calorimeters)

Time = 360.00 s
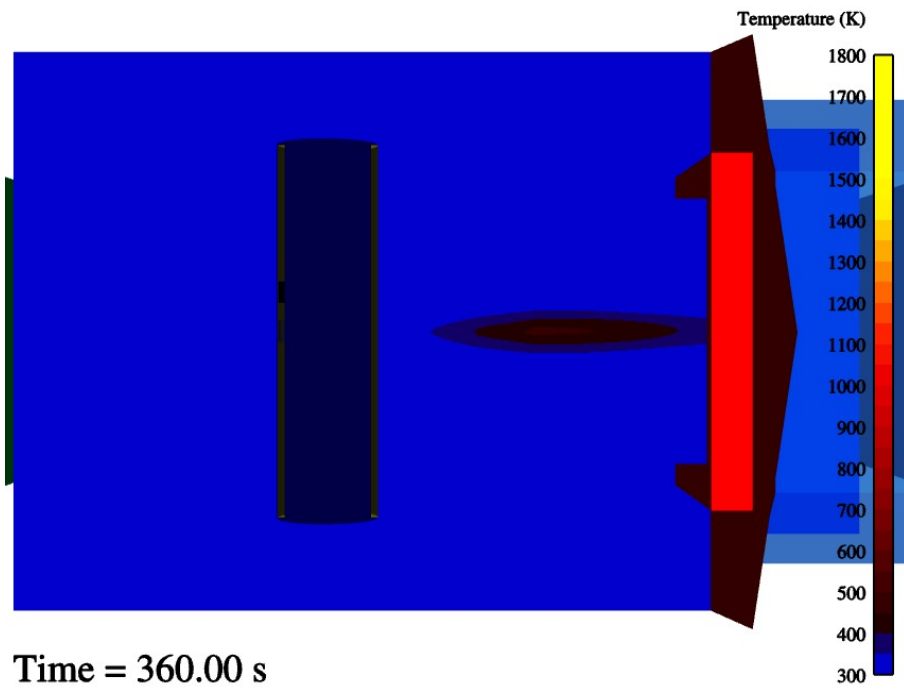
Figure 4-13 Temperature predictions at z = 2.60 m (center of C/MF)

Time = 360.00 s

a. Front View

Time = 360.00 s
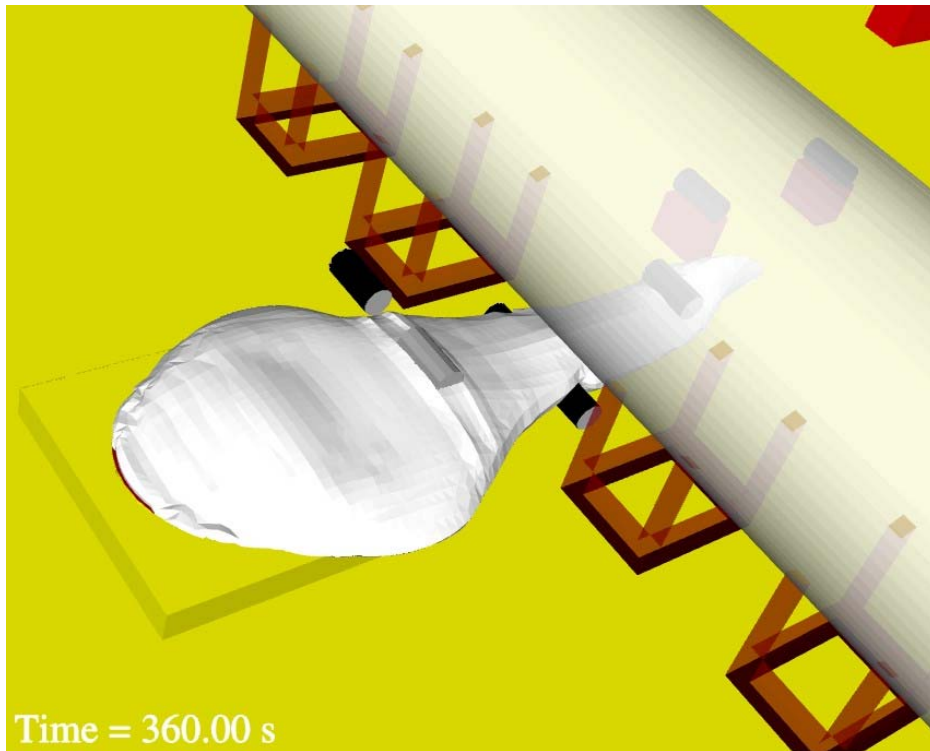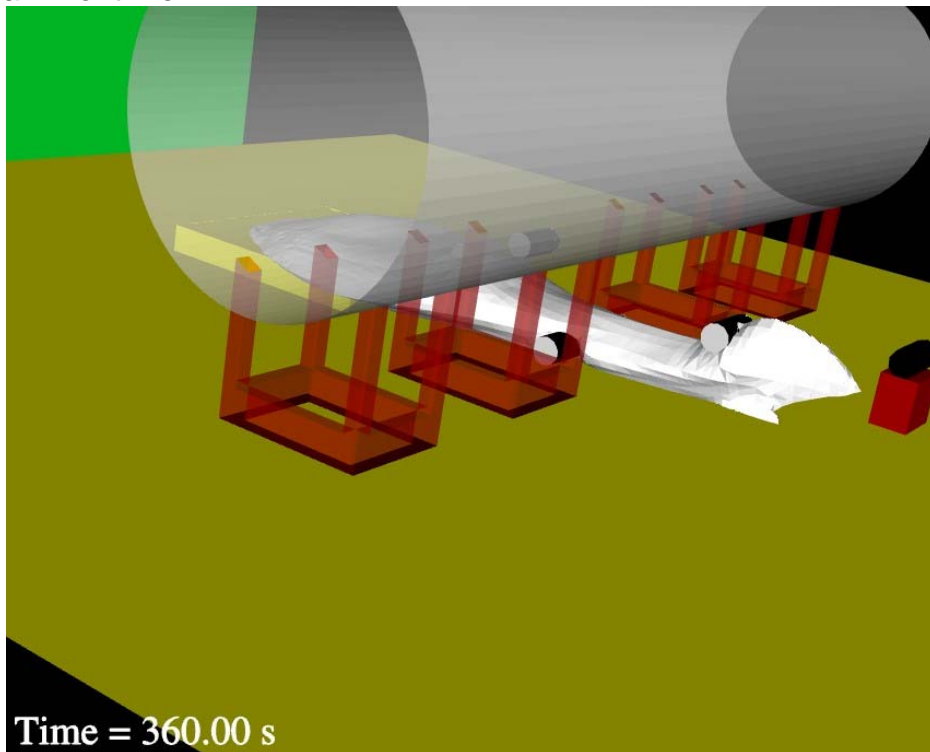
b. Back View

Figure 4-14 Temperature iso-contour predictions from two views

4.3 Other Variables

Radiation flux is monitored in the flow-field through the flux vector. The magnitude of the flux vector suggests the radiative energy present at a given location. Figure 4-15 shows the magnitude of the flux vector at the y = 8.3 m vertical plane.   Figure 4-16 through Figure 4-18 show contour plots of the magnitude of the flux vector at horizontal planes at z = 0.15, 0.68, and 2.60 m respectively. Please note the scale differences between the legends of each plot. In Figure 4-18, the non-uniform distribution of the flux magnitude in the far-field is a consequence of the algorithm employed for the radiation solve. The discrete ordinates method is known to produce such errors when low quadrature numbers are employed for predictions.

The magnitude of the predicted turbulent kinetic energy is a reflection of the intensity of the turbulence at a given location. Much can also be inferred about the flow from the predicted value of the turbulent kinetic energy. Figure 4-19 shows predictions at y = 8.3 m. Figure 4-20 and Figure 4-21 show predictions at z = 0.15 and 2.60 m respectively. Inlet turbulence is seen to dissipate in each figure progressively downstream. Figure 4-19 shows a large increase in turbulence above the C/MF where the ceiling recirculation region encounters strong sheer with the outflow. Figure 4-20 helps illustrate the importance of smaller blocking objects (the C/MF stands and calorimeters) in the generation of turbulence energy from the interaction with the flow. The units on all the turbulence plots are $[cm^2/s^2]$.
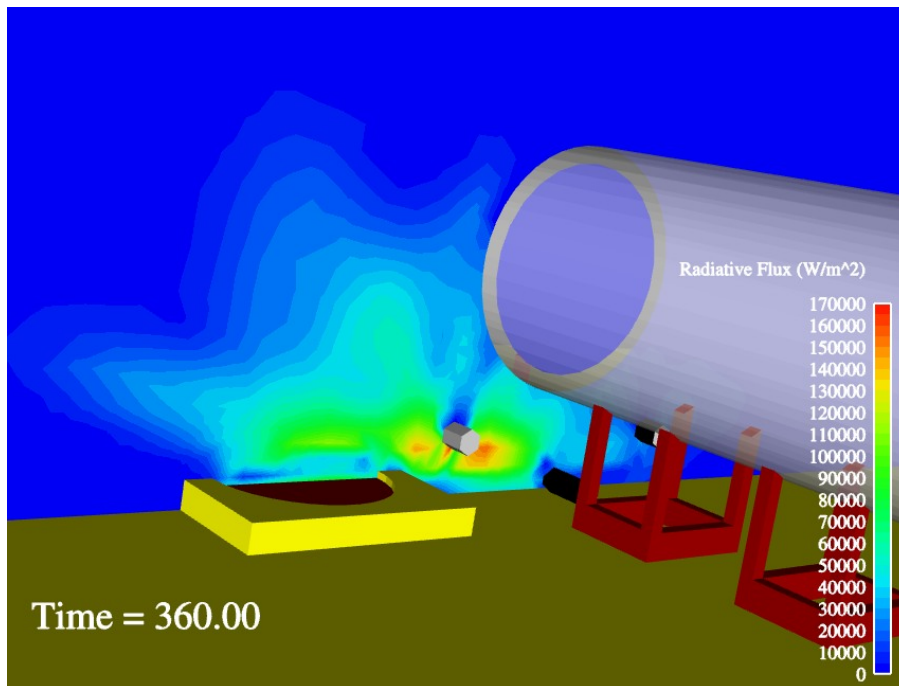
Figure 4-15 Radiative flux predictions at y = 8.3 m (the centerplane)
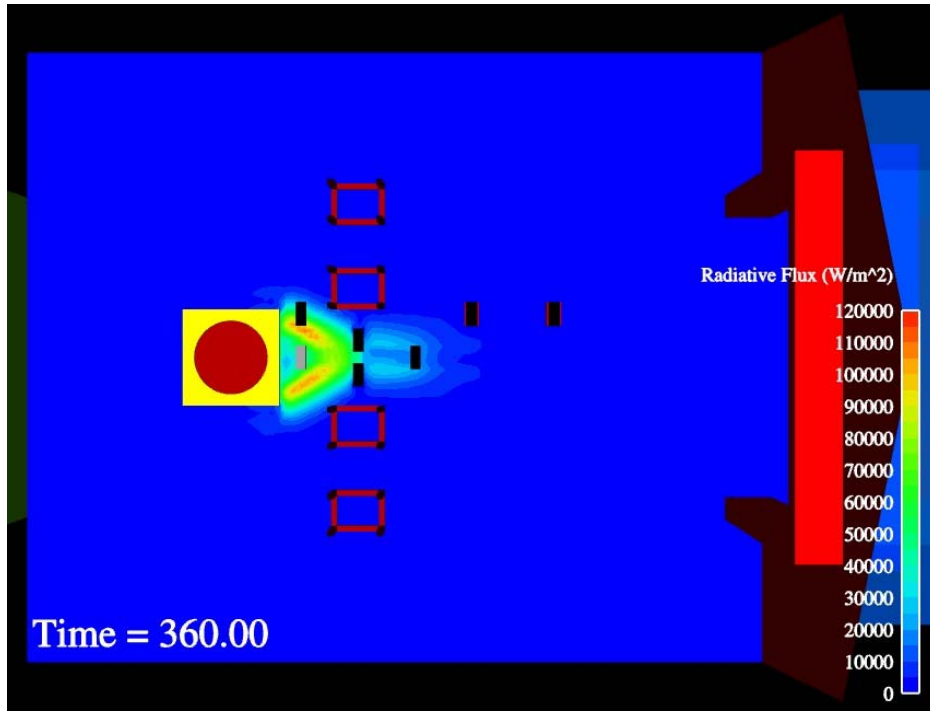
Figure 4-16 Radiative flux predictions at z = 0.15 m (center of ground calorimeters)
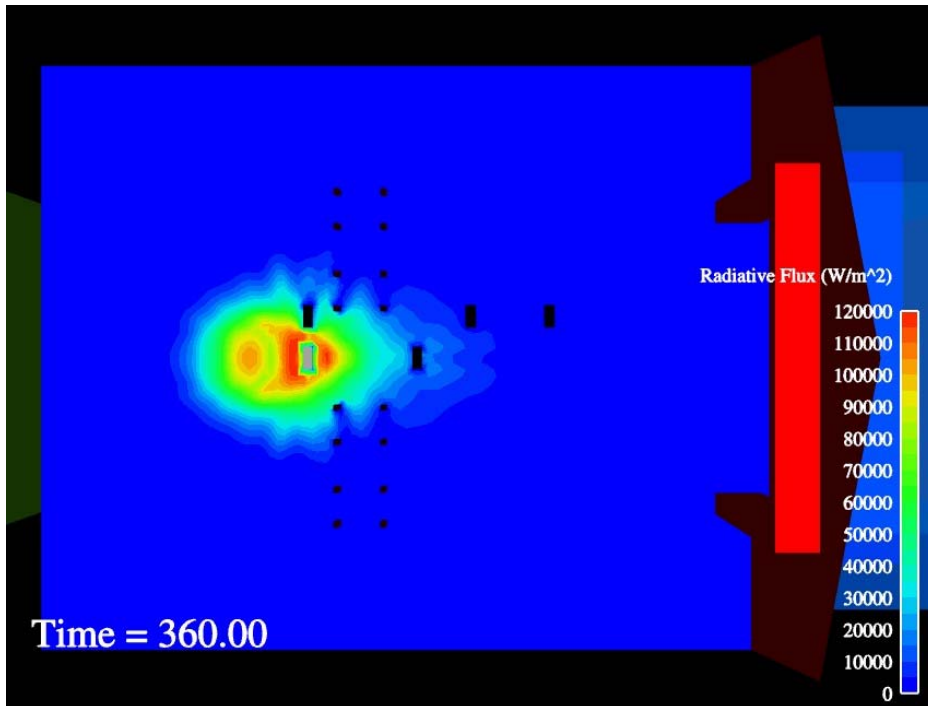
Figure 4-17 Radiative flux predictions at z = 0.68 m (center of elevated calorimeters)
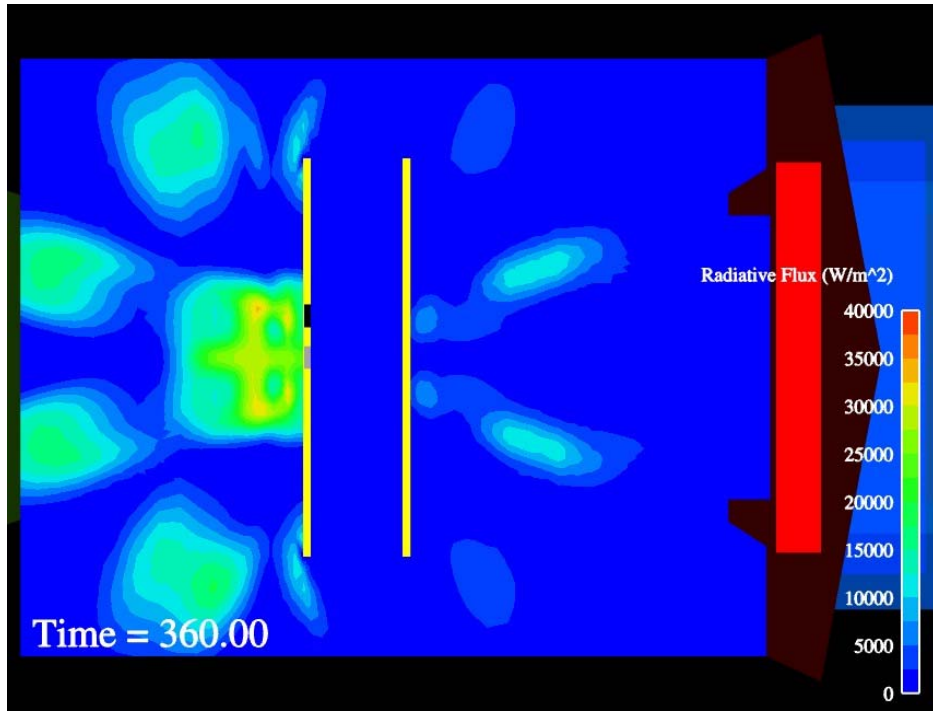
Figure 4-18 Radiative flux predictions at z = 2.60 m (center of C/MF)
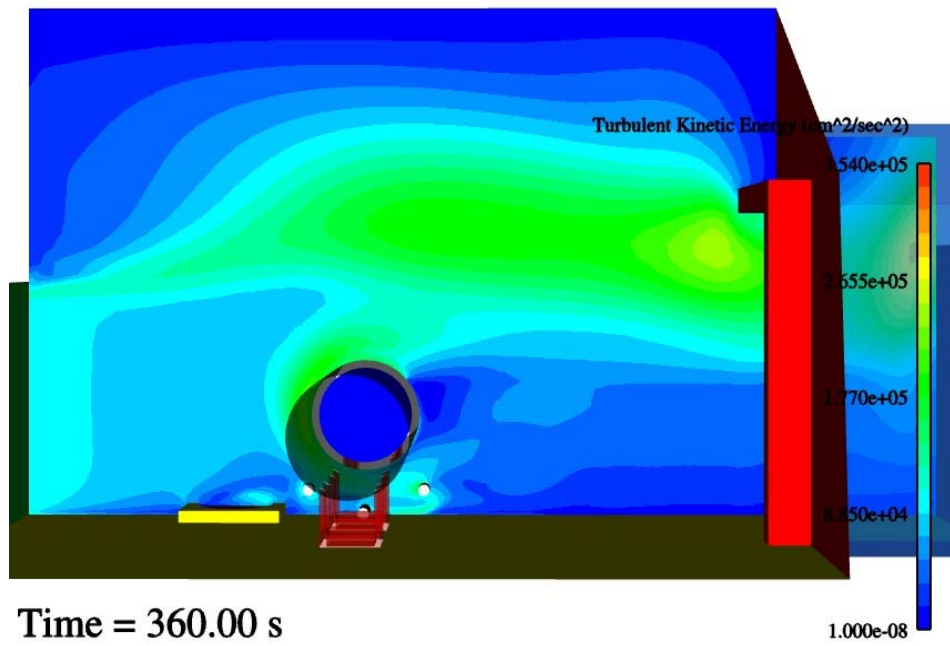
Figure 4-19 Turbulent kinetic energy predictions at y = 8.3 m (the centerplane)
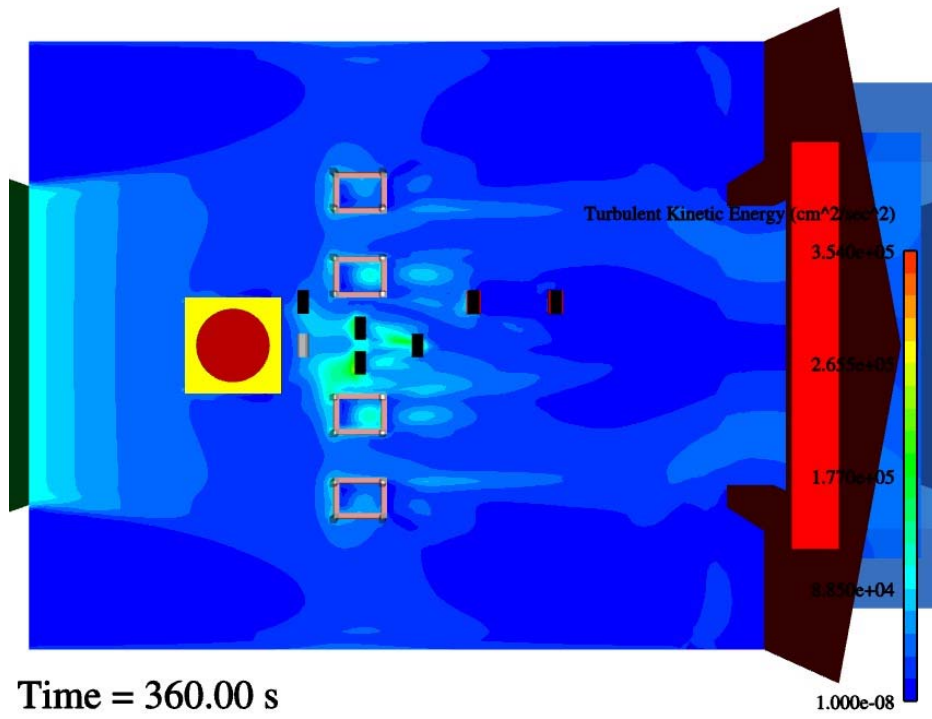
Figure 4-20 Turbulent kinetic energy predictions at z = 0.15 m (center of ground calorimeters)
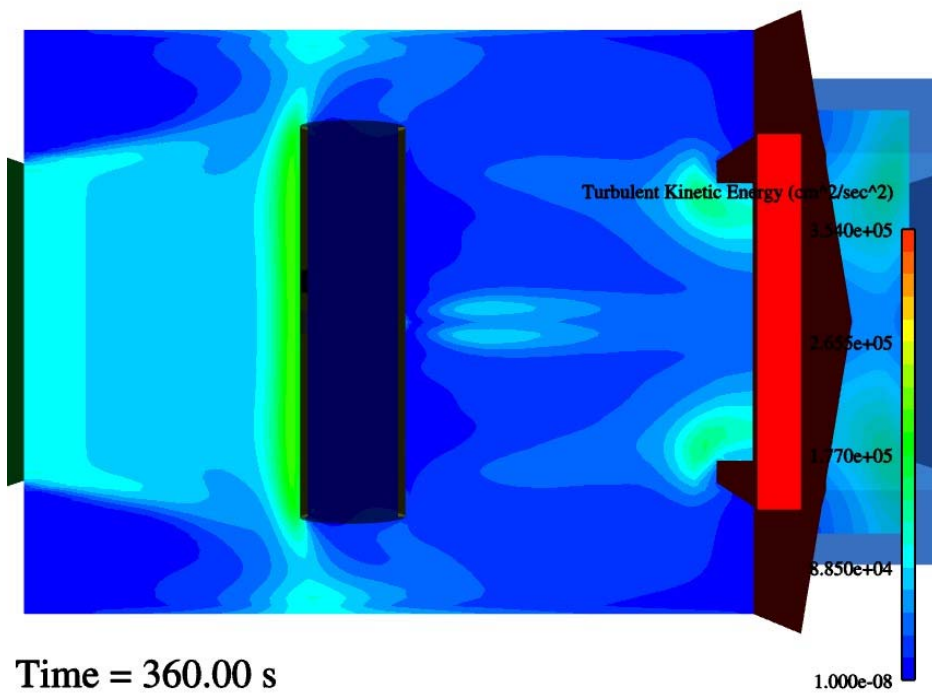
Figure 4-21 Turbulent kinetic energy predictions at z = 2.60 m (center of C/MF)

The pressure predictions from Fuego are relative pressures, not absolute. Pressures are plotted in the CGS native barye (ba) units, one of which is equivalent to 0.1 Pascal. Figure 4-22 shows predictions at the center of the facility (y = 8.3 m). Figure 4-23 through Figure 4-25 show predictions at the standard elevations (z = 0.15, 0.68, and 2.6 m). The legend scale is identical for each of the four pressure plots. It can be seen that the most substantial pressure exists just upstream of the C/MF. It can also be seen that the C/MF stands, the fuel pool pedestal, and the calorimeters contribute to an increased pressure upstream of each object.
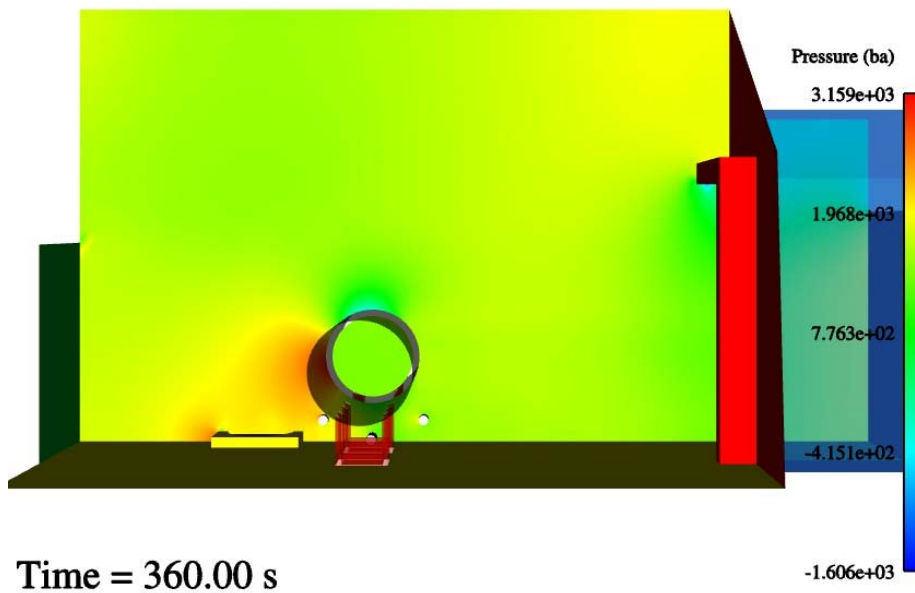
Figure 4-22 Pressure predictions at y = 8.3 m (the centerplane)

Time = 360.00 s
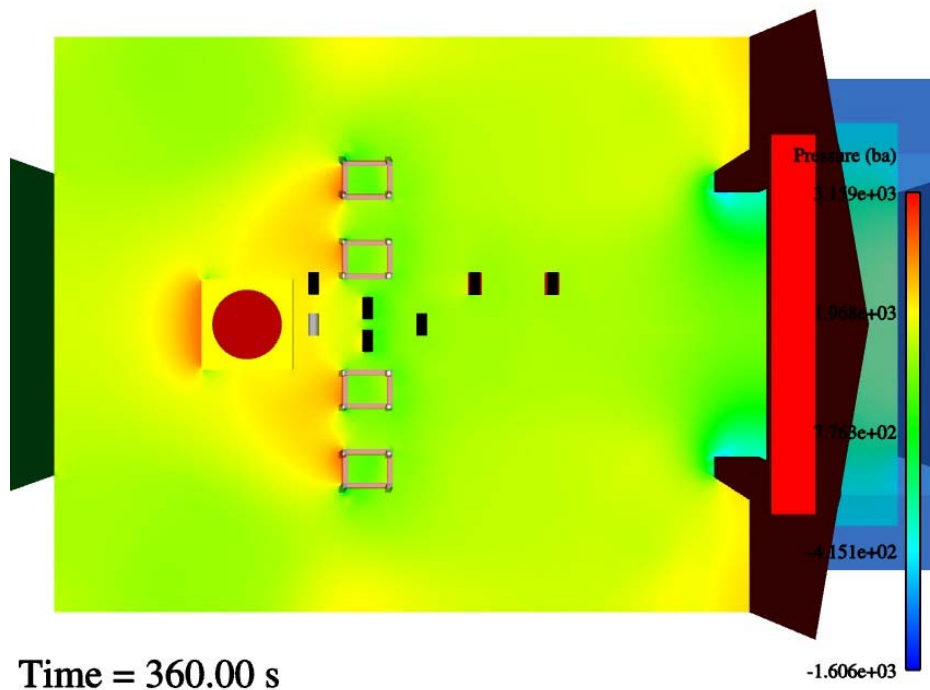
Figure 4-23 Pressure predictions at z = 0.15 m (center of ground calorimeters)

Time = 360.00 s
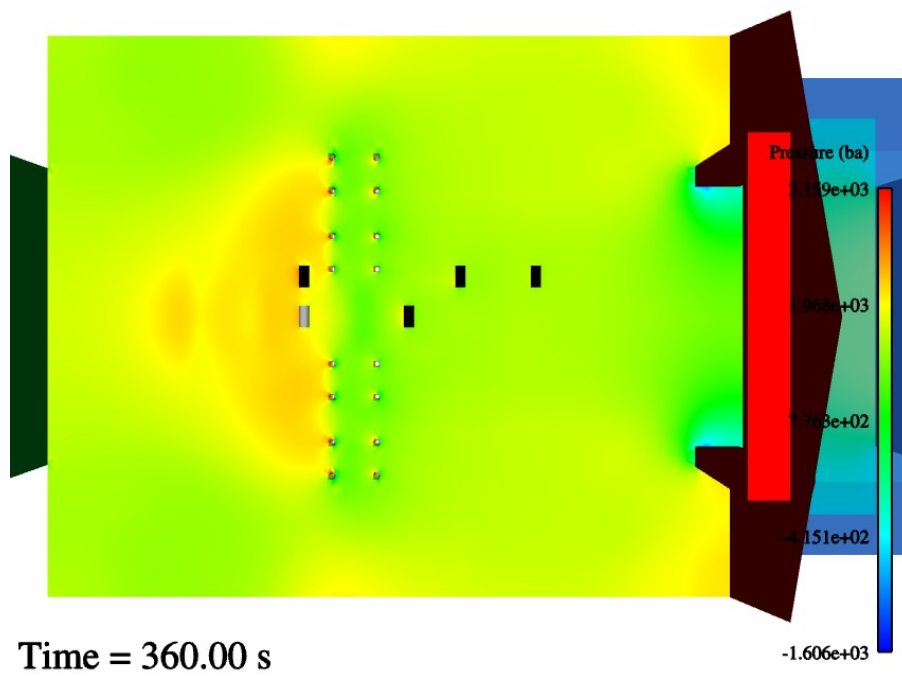
Figure 4-24 Pressure predictions at z = 0.68 m (center of elevated calorimeters)

Time = 360.00 s
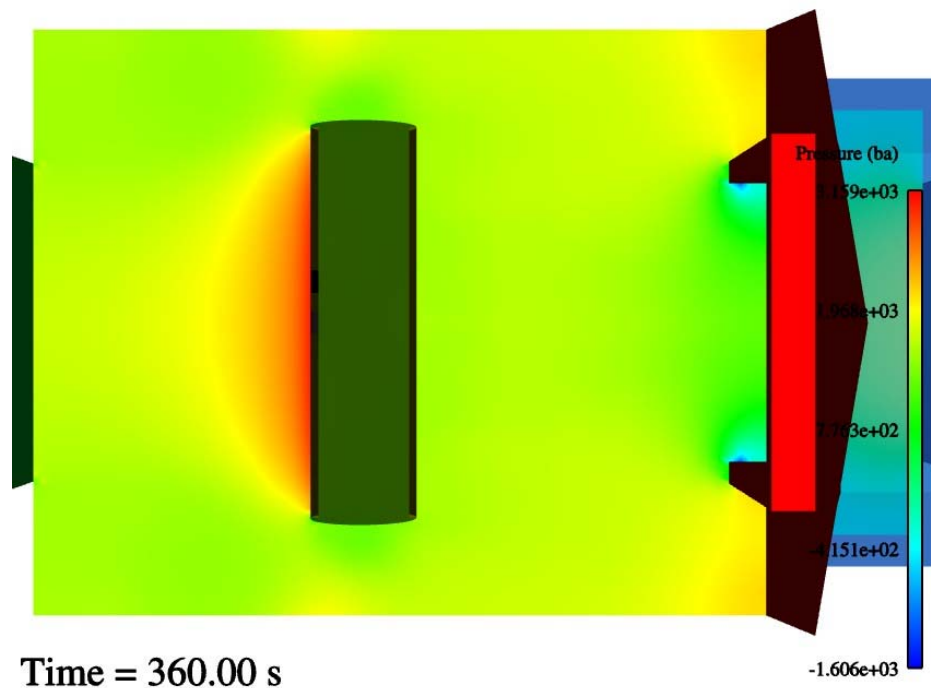
Figure 4-25 Pressure predictions at z = 2.60 m (center of C/MF)

4.4 Solid Object Temperatures and Fluxes

In addition to the gas phase predictions, solid object response is also calculated for selected objects. Temperature predictions are a function of the heat transport calculated from the gas phase predictions and an interchange with the solid objects. Figure 4-26 shows the predicted temperature of the floor and five calorimeters at 50 seconds. Figure 4-27 shows the same variable and parts at 360 seconds. Comparing these two plots, the predicted effect of the objects being immersed in a fire for nearly 5 minutes is evident. In Figure 4-27, there is a moderately large spike in temperature on the down-wind face of the pedestal. In other regions, the temperature is a bit below the mean values. This thought to be due to the inadequate mesh resolution in the region in the proximity of the face. Figure 4-28 shows the same predicted values except with the surface mesh overlaid in black. The mesh on the horizontal surface of the pedestal is projected downward into the pedestal. It is seen that the mesh spacing is narrower in the region of the temperature spike, and larger in regions where temperatures are lower. In general, the mesh resolution on exposed surfaces was kept high, so this problem is not thought to be substantial in other regions. This is apparent in the overlay on the pedestal vertical surfaces. The pedestal side surfaces were knowingly kept with a resolution that was under-resolved because of difficulties in achieving a compact mesh in these regions without resorting to prohibitively high resolution elsewhere.

It is evident from examination of the incident radiative heat flux on these same surfaces that the temperature observations in the previously described figures are not due to gradients in the

83

radiative heat flux. Figure 4-29 shows incident flux predictions at 360 seconds. As expected with the discrete ordinates method in the fire region, the predicted flux contours are relatively smooth across the face of the pedestal.
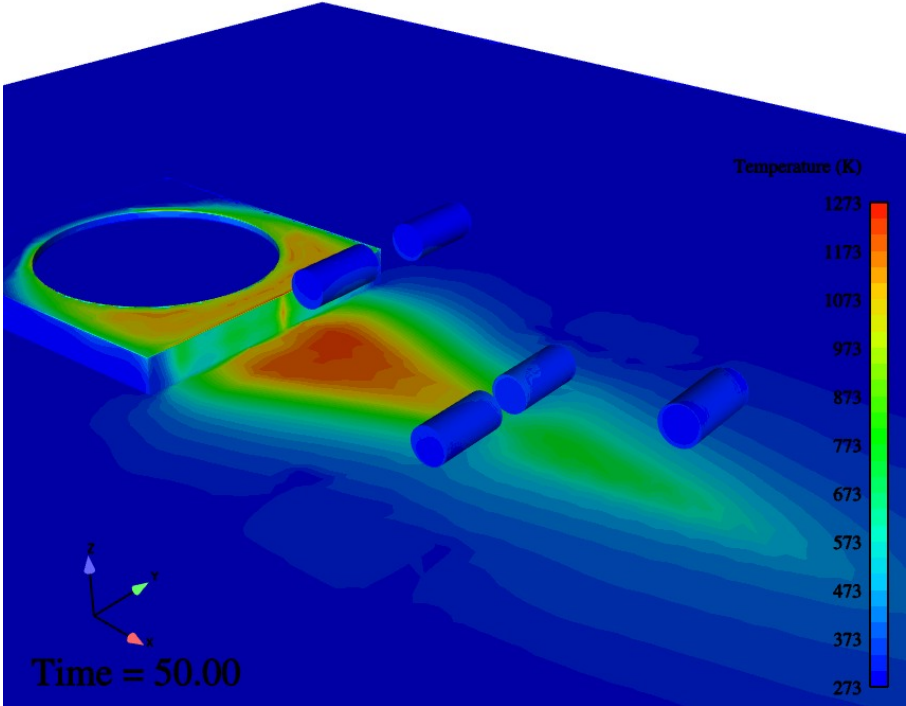
Figure 4-26 Floor and calorimeter solid surface temperatures at 50 seconds
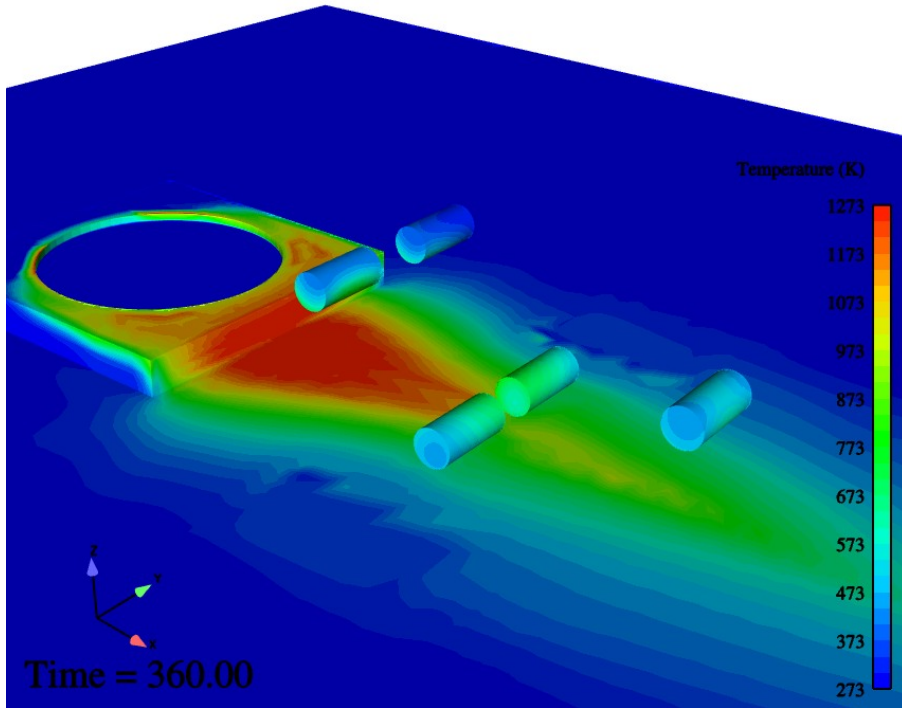
Figure 4-27 Floor and calorimeter solid surface temperatures at 360 seconds
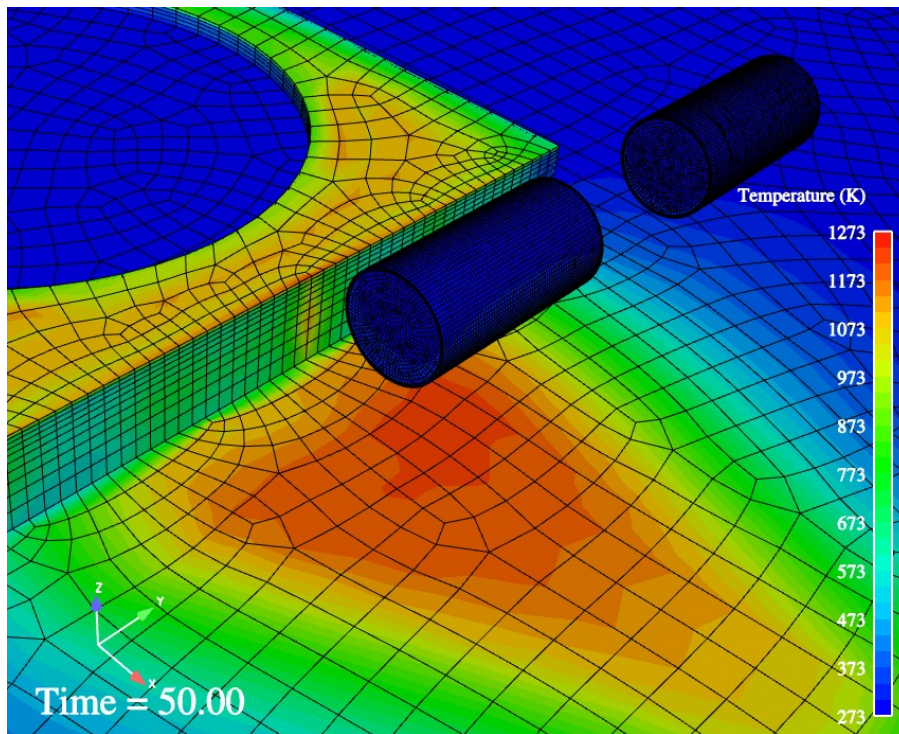
Figure 4-28 Floor and calorimeter solid surface temperatures at 50 seconds with mesh overlay
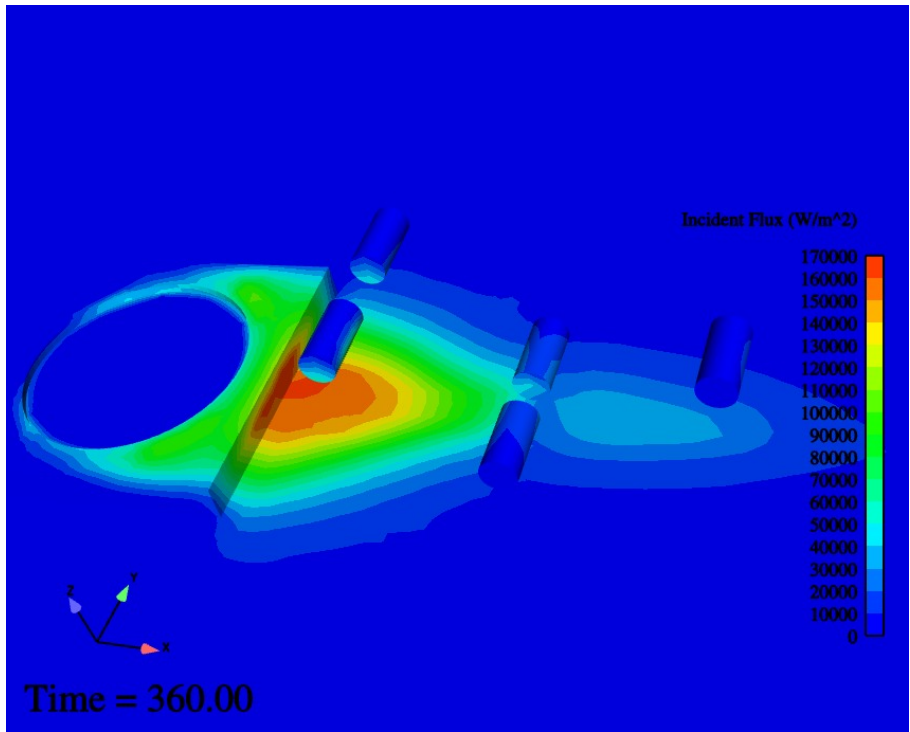
Figure 4-29 Floor and calorimeter solid surface incident flux at 360 seconds

Predictions of heat flux and temperature on the bottom of the C/MF are also shown in Figure 4-30 and Figure 4-31 respectively.
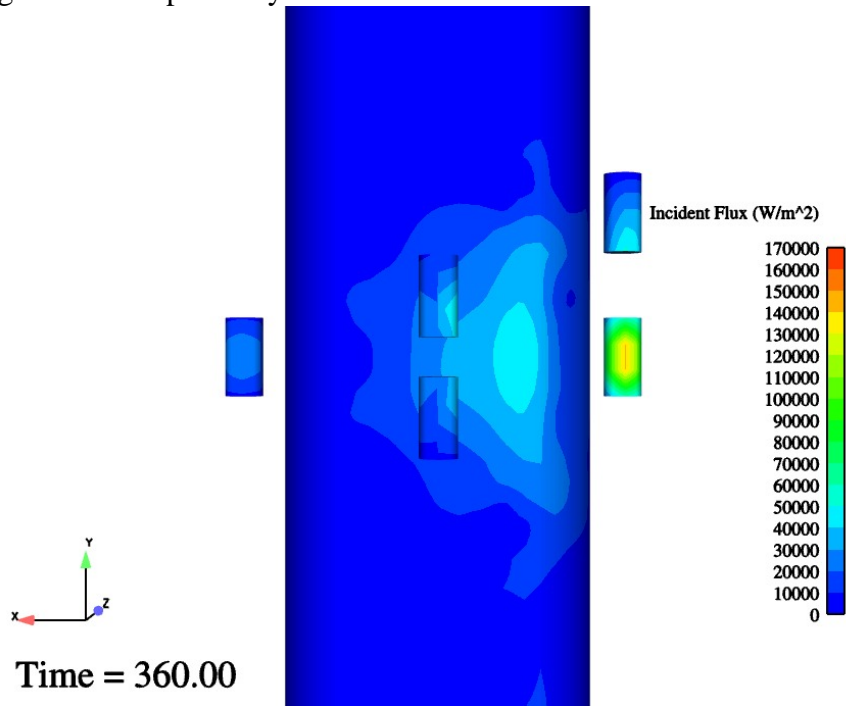
Figure 4-30 C/MF and calorimeter solid surface incident flux at 360 seconds
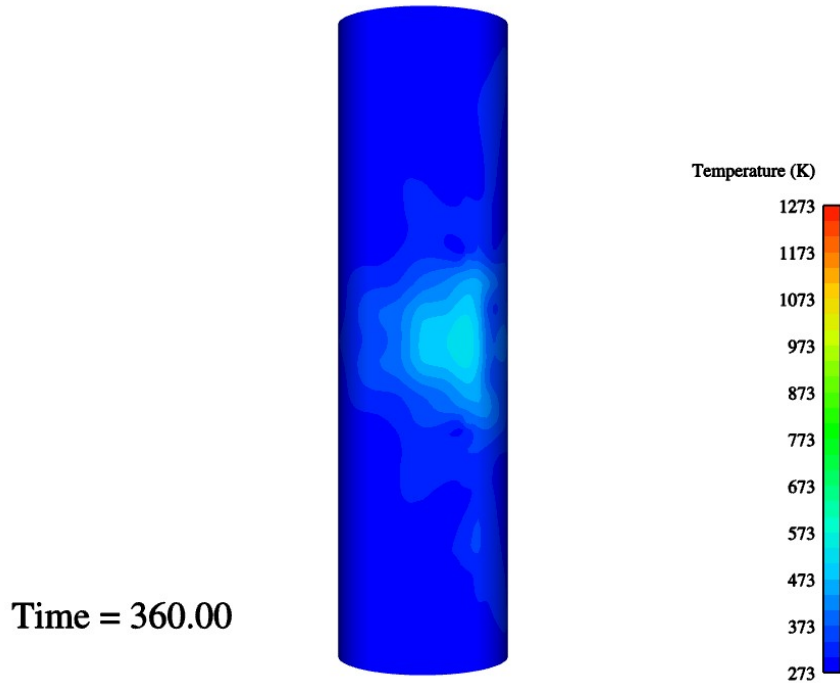
Figure 4-31 C/MF and calorimeter surface incident flux at 360 seconds

4.5 Variables at Comparison Points

Table 2-1 lists the locations at which comparisons are made to data-points. 'Heartbeat' output was employed to extract various scalars at these measurement points at regular intervals. Predicted temperatures at the calorimeters are plotted in the subsequent chapter. At the C/MF, the free-stream and object temperature, nodal velocity, and convective heat transport coefficient, and incident radiative flux are found in Figure 4-32 and Figure 4-33.

In Figure 4-32, the predicted values for T_{inf} do not increase much above 300 K, which is very close to the ambient input temperatures. Object temperatures, however, are considerably higher, reaching nearly 500 K by 360 seconds.

In Figure 4-33, the node u-velocity at the bottom center of the C/MF is seen on average to be between 15 and 16 m/s, which is about 20% higher than the nominal 13 m/s inlet velocity. The predicted convective flux is calculated based on the three parameters in Figure 4-32. As the object heats up, the convective flux approaches 20 kW/m^2 at 360 seconds. The radiative heat flux is less of a function of time, but still exhibits some time dependency as the objects below the C/MF continue to increase in temperature. Peak predicted radiative flux is between 30 and 40 kW/m^2 at 360 seconds.
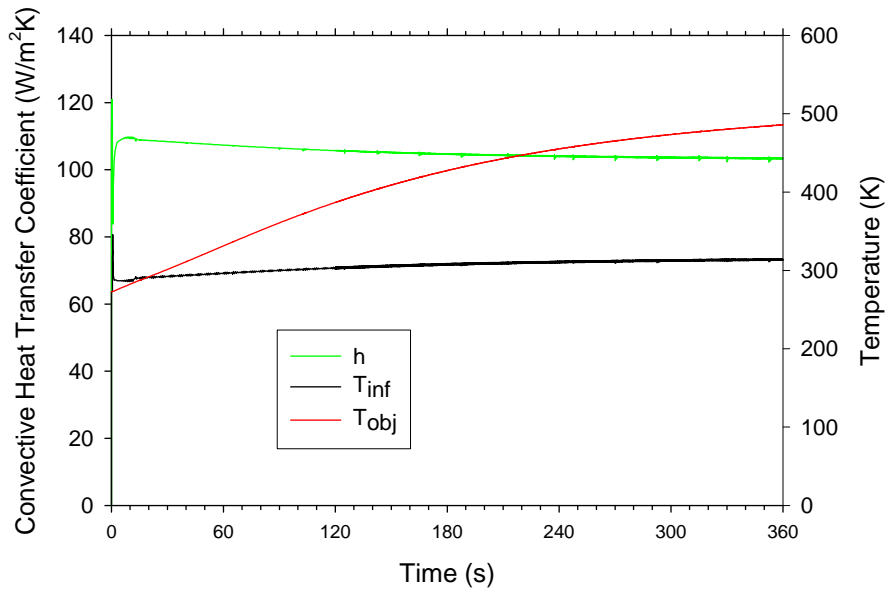
Figure 4-32 C/MF predicted convective heat transfer coefficient and temperatures
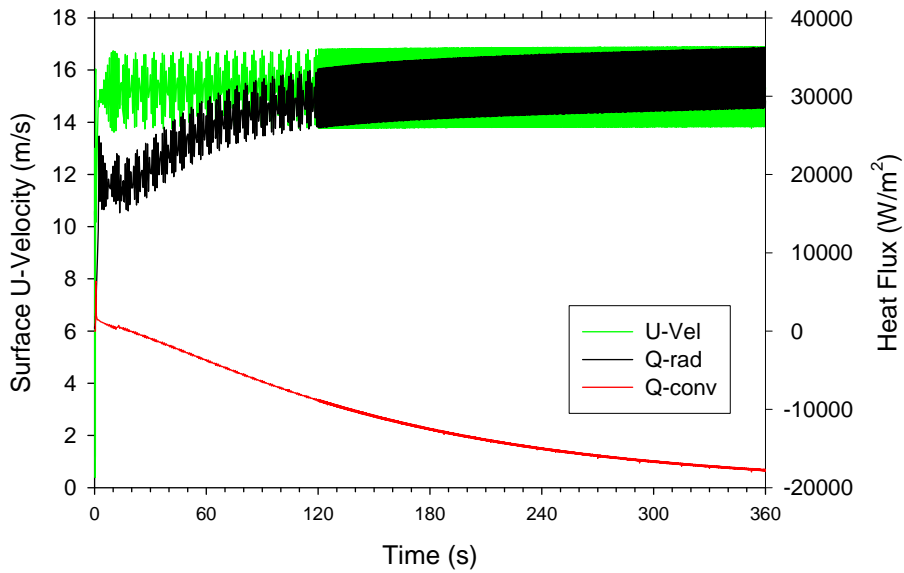
Figure 4-33 C/MF predicted convective and radiative heat flux and u-velocity

4.6 Residuals

Non-linear residuals as reported in Fuego are un-scaled. Their magnitude suggests the degree to which the equations that are being solved have been satisfied by the solution iterations.

Figure 4-34 plots the nonlinear residuals from the baseline simulation. The baseline simulation involved two nonlinear iterations per time step. Since a constant time step of 0.005 seconds was used, the numbers on the abscissa correspond to approximately 200 steps per second of simulation time. At early times, only one nonlinear iteration is taken, so step numbers do not correspond perfectly to times unless the duration of the single non-linear step phase is known.
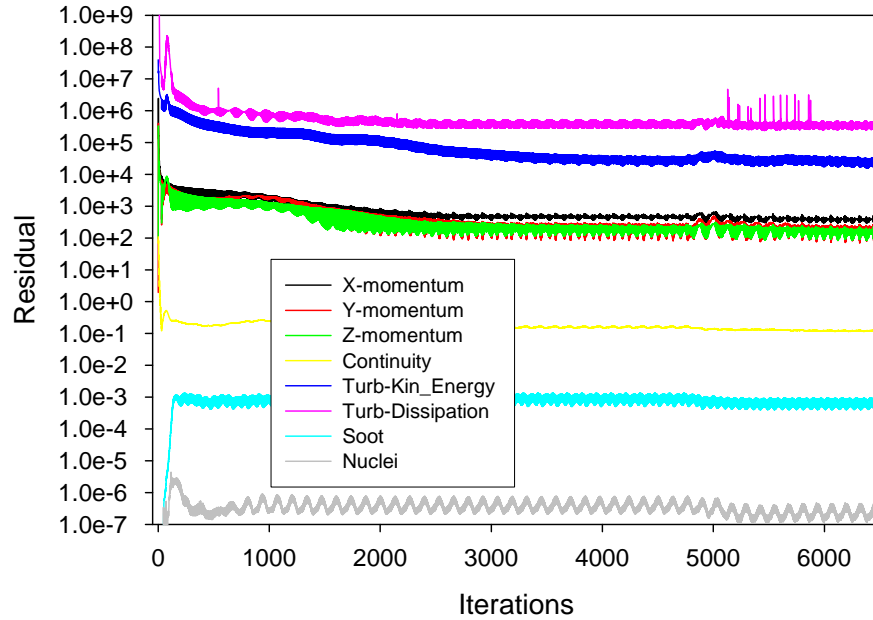
a.
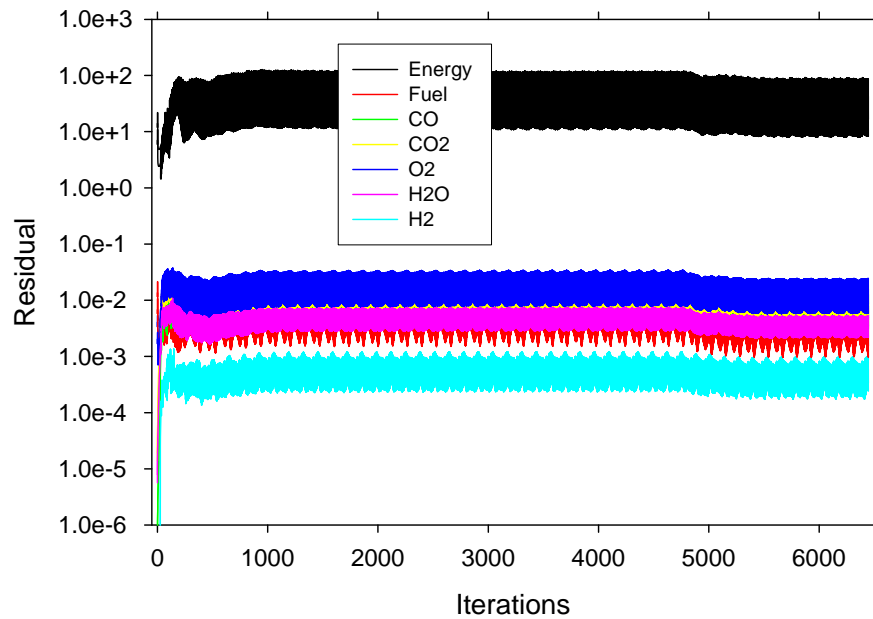
b.

Figure 4-34 Non-linear residuals for selected variables plotted on a log scale

Residuals of the velocities, turbulence parameters, and continuity start several orders of magnitude above the point they converge to beyond several hundred iterations in this simulation. Energy and species equations, soot and soot nuclei start low because the initial domain is isothermal with only air and has a trivial solution. They increase as the fire begins to evolve. The minor change in trend at about 4800 iterations corresponds to the BVG model activating at 12 seconds. As opposed to the other variables, the continuity equation shows very little added convergence due to the second nonlinear iteration.

Part of this study was designed to examine the role of the number of nonlinear steps in the convergence and result of a calculation. This will be elaborated on later in this document.

5. Validation Comparisons

In January of 2005, the predictions and data were brought together for the first time. The experimental results included time-temperature histories from the calorimeters, heat flux gauge readings, temperatures from thermocouples in the flow, and fuel consumption rate data. Calorimeter 1 and 3 thermocouple temperatures have been selected for comparison to predicted temperatures from the simulations. Heat flux to the bottom of the C/MF is examined as a comparison point as well.

Comparisons are made assuming the model uncertainties expressed through the parametric study. Because this was a blind comparison, there was little indication before the simulation and experimental results were brought together, of any quantitative discrepancies. Following validation principles, the modeling team was represented in the design and performance of the experiments through calculation of pre-test predictions to aid in the experimental design and attendance during the tests. Some qualitative knowledge was had by the simulation team regarding the experiments, but quantitative measurements were not examined by the simulation team until complete experimental and predictive results were brought together as detailed in this report. Similarly, the experimental team had no quantitative knowledge of the simulation results prior to the comparison. The exception to this rule was with respect to boundary conditions, for which quantitative experimental results were provided to the simulation team.

In Trucano et al. (2002), a hierarchy of validation comparison methods is presented (Figure 7.1). The highest quality comparison involves nondeterministic analysis of the simulation predictions (i.e. a PDF cloud). This type of analysis exceeds current computing capabilities for a problem of this magnitude. The next highest quality comparison involves overlaying deterministic experimental and computational results with estimates of uncertainties included on both the experiment and the prediction. This class of comparison is feasible, and is the standard that is maintained in the comparisons presented herein.

5.1. Data Reduction

To make comparisons with simulations, the data required interpretation. Several complicating factors challenged the interpretation of the data.

- Data were all taken on the same day. Objects with large thermal time constants require significant time to thermally equilibrate to the ambient temperatures. Even though approximately 2 hours were allowed to elapse between experiments, some temperatures had not returned to the ambient value of 0 °C. The initial condition of some of the measurement points was a function of the time elapsed from the preceeding test. Interpreting the data on the basis of the magnitude of the temperature resulted in large error bounds. It was found that for example if a thermocouple read 20 °C at time zero for test 2 compared to 0 °C for test 1, that the thermocouple reading would typically be 20 °C different at 6 minutes as well. These differences contributed significantly to the experimental uncertainties. To circumvent this issue in interpreting the data, the experimental team decided to use the change in temperature as the reported data at the comparison times of 2 and 6 minutes. By doing this, the

experimental uncertainties of the calorimeter thermocouple readings were significantly reduced.

- The data acquisition system inserted an extra step each second that skewed the interpretation of the time variable relative to the rest of the measurements. Data required post-processing to remove the extra step.

- Heat flux data are inferred through an inverse heat flux calculation using measured temperatures from thermocouples embedded in the gauge assembly and a gauge thermal model. Uncertainties in this measurement arise from physical properties of the gauge that may vary dynamically during the course of a fire, missing physics in the gauge model, and simplifying assumptions. These uncertainties have been quantified and are part of the output of the gauge reading (Blanchat et al, 2002)

- Thermocouple temperature uncertainties presented in the remainder of this document reflect the simple test-to-test variation in the measured temperature. It has been well documented that the uncertainty in the thermocouple readings is dominated by factors in the installation of the thermocouple such as contact resistance, presence of spatial thermal gradients, etc. (Nakos, 2004). In the calorimeter installations here, these factors are minimized, leaving the test-to-test variation being the only important contributor to the uncertainty. Therefore, unless otherwise stated, the experimental uncertainty bounds are a test-to-test single standard deviation.

The calorimeters (0.3 m OD x 0.6 m long x 9.5 mm wall SS304 tubes) contained 8 thermocouples spaced at equal distance around the perimeter of the inside metal surface of the calorimeter at the center-plane. As a convention for reporting results in this document, the lowest thermocouple is at 0º, with the angle of the thermocouple increasing clock-wise when viewing the calorimeter from the side of the facility where the control room is (the east, or from the negative-y direction).

The heat flux gauges consisting of two 100 X 100 by 9mm thick Inconel plates sandwiching a 100 X 100 X 13 mm thick stainless felt metal block were instrumented with thermocouples welded to the inner surfaces of the Inconel plates. The assembly was installed on the C/MF so that one Inconel plate faced the fire. The thermocouple response was subjected to an inverse analysis to determine the net heat flux absorbed by the gauge (Blanchat, et al, 2002)

5.2. Calorimeter 1 Temperatures

Calorimeter 1 was suspended by cables from the up-stream side of the C/MF and was oriented with the thermocouples along the center-plane of the facility. The temperature difference predictions for this calorimeter were good compared with the measurements. Figure 5-1 shows the baseline simulation predicted time-evolving temperature as solid lines. The dashed lines are the results of the two cases that were called 'most severe' and 'least severe' and were intended to provide an estimate of the model uncertainty based on the simultaneous change of various uncertainty parameters. For the purposes of this comparison, these are the estimated parametric uncertainty for this case.

The magnitude of the difference between the baseline simulation and the simulations where the parametric uncertainties were considered is smaller than is generally expected for

simulations when comprehensive uncertainties are assessed. Uncertainties in the models are thought to be typically much larger than experimental uncertainties. Noticeably missing from the parameter list in Table 2-2 and Table 2-1 are any uncertainty parameters related to the fuel. This omission was by design. The boundary condition for the fuel was probably the best characterized boundary condition for these tests (see Randsalu et al., 2004). Assumed properties for the fuel were taken as true nominal values. Based on findings from Nakos et al. (2005), the omission of a parameter related to the fuel is likely the top reason the magnitude of the simulation uncertainties are below what is expected for this class of problems. Noticeably absent from Figure 5-1 are uncertainty bars on the time axis. There is a high degree of subjectivity in the determination methods for this value, and consultation with the experimental team suggests an appropriate value is on the order of 11 seconds.
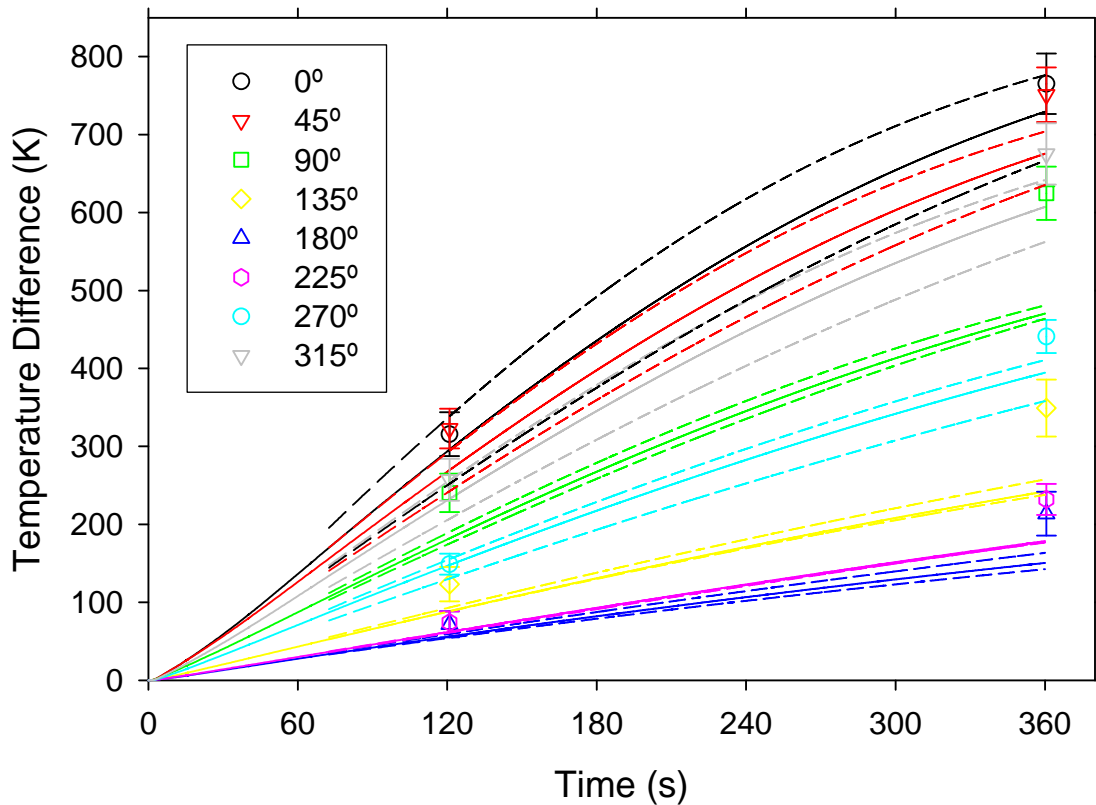
Figure 5-1 Predicted Calorimeter 1 temperatures

Figure 5-2 and Figure 5-3 show the same data as found in Figure 5-1, except the temperature differences are plotted versus the angular position of the thermocouple on the calorimeter. Figure 5-2 shows the comparison at 120 seconds, and Figure 5-3 shows the comparison at 360 seconds. In these figures, the spatial dependency of the results is more apparent. Baseline predictions are within a standard deviation of the measurement for five of the eight thermocouples at 120 seconds. At 360 seconds, only one prediction is so close. The

predictions are closest to the experiments at 0º, the bottom of the calorimeter. The predictions are the furthest from the experiments at from the experiments at 90º, or the point on the calorimeter that is furthest upstream.

Perhaps the most noticeable feature of the temperature comparison plots that are shown versus the angle is that the general trends found in the experiments are accurately represented by the model. The simulation predictions consistently fall below the measured temperature values. This sort of an error can result from a misalignment of the extraction of the experimental time. This is likely not the case for this problem.
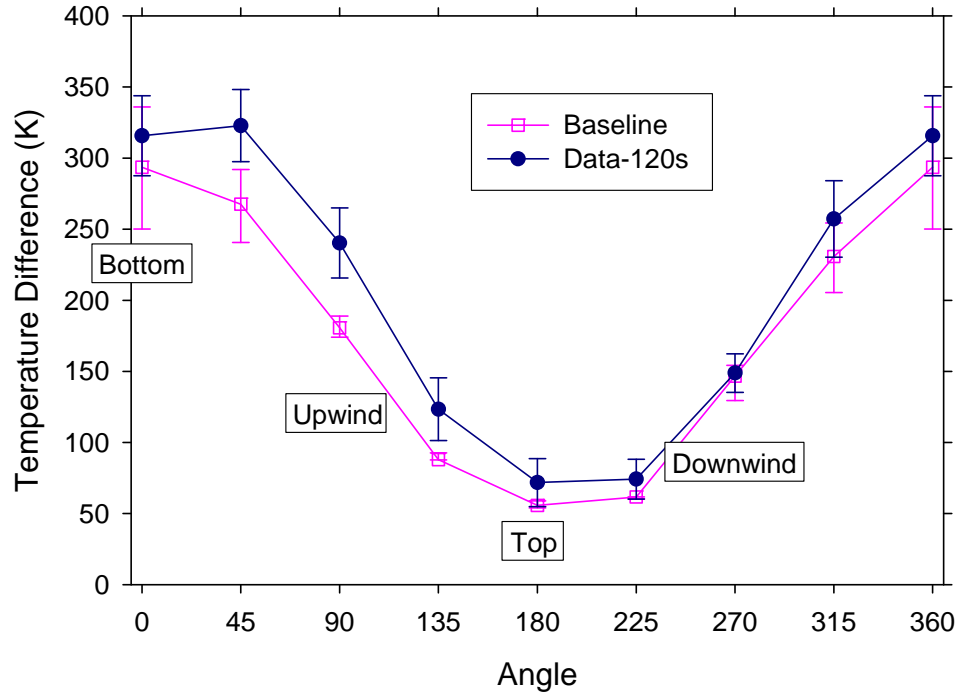
Figure 5-2 Calorimeter 1 temperatures at 120 seconds
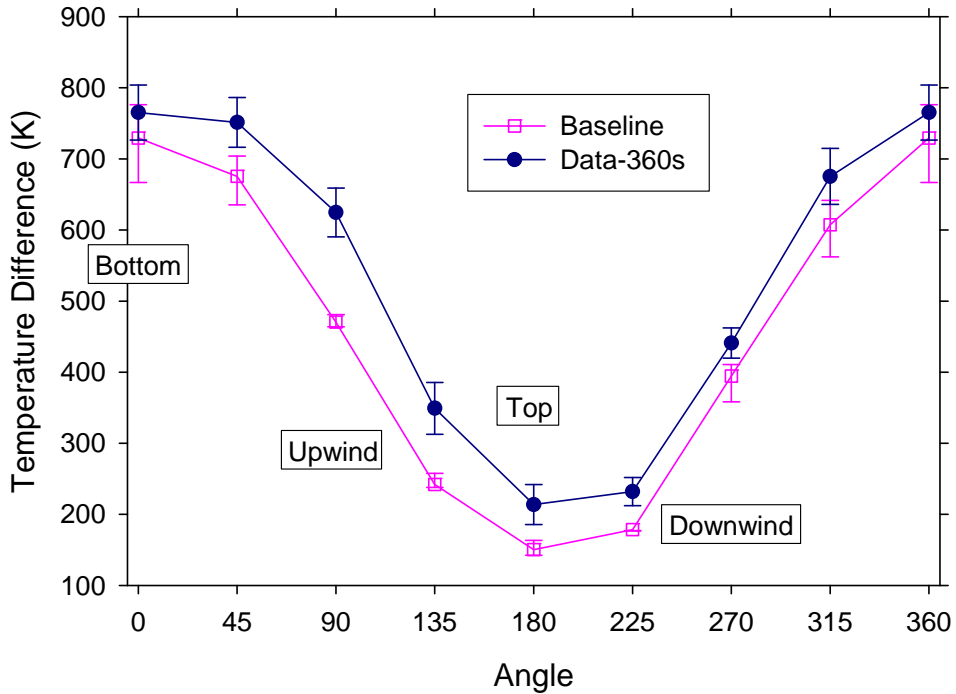
Figure 5-3 Calorimeter 1 temperatures at 360 seconds

In Table 2-1, two system response measures were proposed for calorimeter 1. The first was the maximum calorimeter temperature difference, which is calculated by taking T_{max} - T_{min} where T_{max} is the largest measured or predicted temperature and T_{min} is the smallest. This comparison can be found plotted in Figure 5-1 through Figure 5-3. T_{max} was found at the 0º location for both the predictions and measurements at both 120 and 360 s. T_{min} was likewise found at 180º for the predictions and measurements at each time.

When two statistically determined quantities are added or subtracted, some knowledge regarding the interrelationship between the two quantities is useful in determining how to assess the uncertainty for the resulting sum or difference. If the two are considered independent uncertainties, they may be considered geometrically orthogonal. This being the case, the cumulative magnitude would best be represented by the following relationship for the combination of standard deviations:

$$\sigma_{diff} = \sqrt{\left(\sigma_{T\max}^2 + \sigma_{T\min}^2\right)}$$

The resulting uncertainty is then greater than the uncertainty of either of the single measured uncertainties. This methodology is standard in engineering analysis, but the accuracy of the assumption is subject to the assumption that the uncertainties are independent (see Coleman and Steele, 1999). An alternative method for assessing the uncertainty is to calculate the temperature difference for each test, and calculate the standard deviation from the uncertainty in the difference. This methodology is applied to the simulation uncertainty bounds as found in Figure 5-4. The data and predictions are in very close agreement. If the above equation is

used, the data uncertainty is nearly 3 times greater at 120 seconds and about twice as large at 360 seconds.
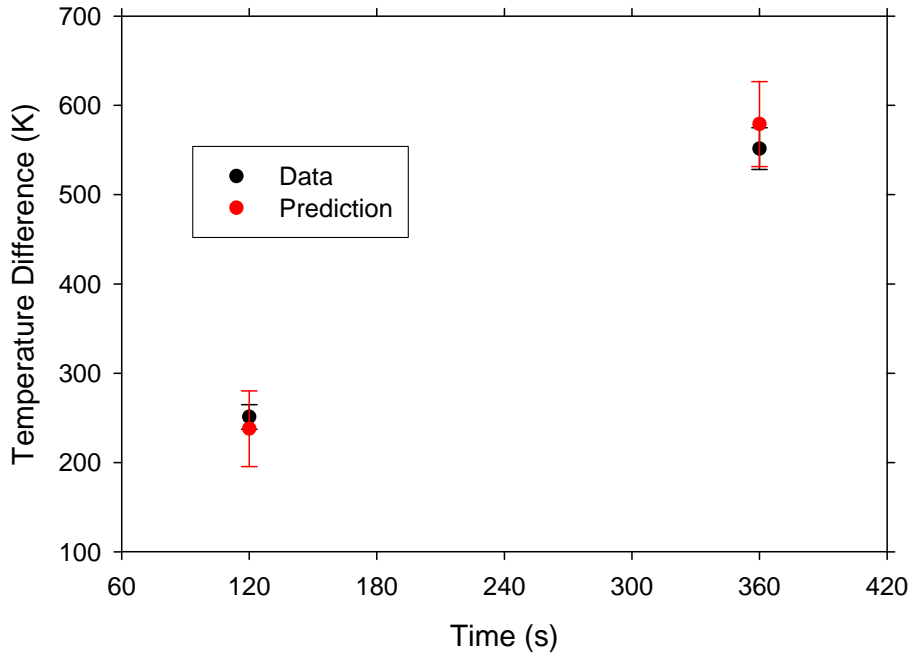
Figure 5-4 Calorimeter 1 temperature differences

The second system response measure from Table 2-1 is the maximum calorimeter temperature. The maximum temperature comparison is plotted in Figure 5-1 through Figure 5-3 at 0°. The baseline prediction falls within one standard deviation of the measured value at both 120 and 360 seconds.

5.3. Calorimeter 3 Temperatures

Calorimeter 3 was located on the floor of the facility directly beneath the C/MF. The calorimeter was not located along the center-plane of the facility. Rather, it was offset from the center-plane by about 16" towards the control room side of the facility. Another calorimeter was located symmetrically away from the control room on the other side of the center-plane. Figure 5-5 shows the baseline simulation predicted time-evolving temperature as solid lines. As with the calorimeter 1 results, the dashed lines are the results of the two cases that were called 'most severe' and 'least severe' and were intended to provide an estimate of the model uncertainty based on the simultaneous change of various uncertainty parameters.
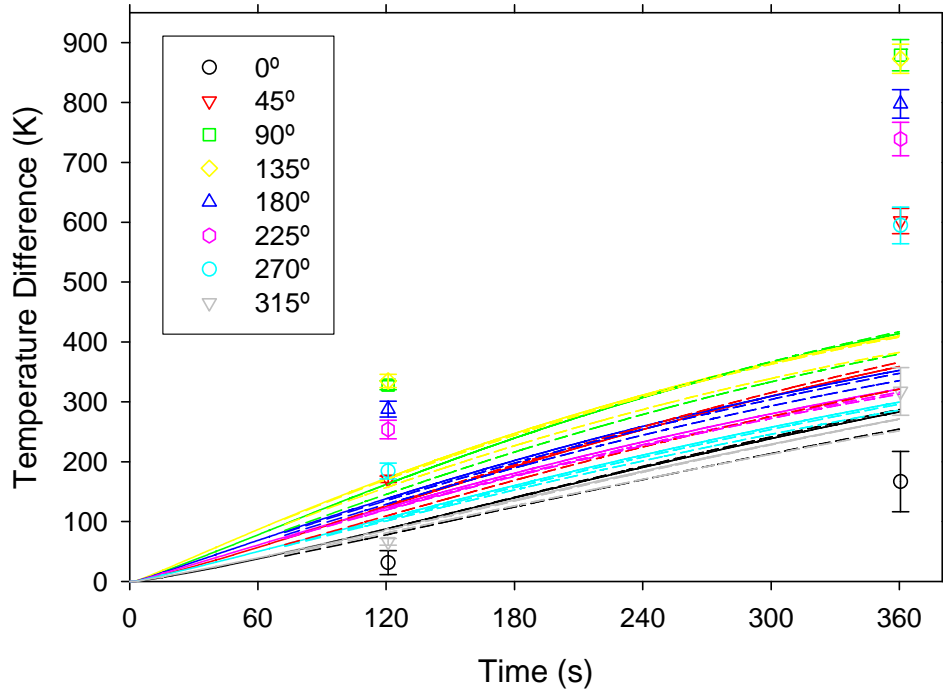
Figure 5-5 Predicted Calorimeter 3 temperatures

The differences between the simulations and the predictions are remarkable. Hundreds of degrees difference is found at most angles between the simulation results and the experimental results. The experiment suggests significant gradients exist, with the 90-135º region being the hottest. The simulations suggest these are the hottest locations, but large gradients do not exist. Simulations and experiments agree the best at 315º, but predictions are still not within experimental uncertainty. Neither the experimental uncertainties nor the parametric model uncertainties demonstrate sufficient range to explain the discrepancy. The reason for the discrepancy is likely related to a feature not accounted for in the parametric study. Quantitatively, the model uncertainties are even smaller for calorimeter 3 than they were for calorimeter 1. Similar to the calorimeter 1 results, the experimental uncertainties are much larger than the uncertainties due to the modeling parameters.

Figure 5-6 and Figure 5-7 show comparisons at 120 and 360 seconds respectively plotted versus angle. Simulation and experiment suggest peak temperatures at either 90º or 135º. They also suggest the lowest temperatures are found at 360º (experiment) and nearby at 315º (simulation). While the general trends are mostly predicted, the magnitudes are significantly different.

The system response measures (see row 3 and 4 of Table 2-1) also suggest poor agreement. The temperature difference comparison is plotted in Figure 5-8. Similar methods were employed to create this figure. Maximum temperatures are found in Figure 5-5 through Figure 5-7. Experiments and predictions differ by over 150 ºC at 120 seconds, and by over 500 ºC at 360 seconds.
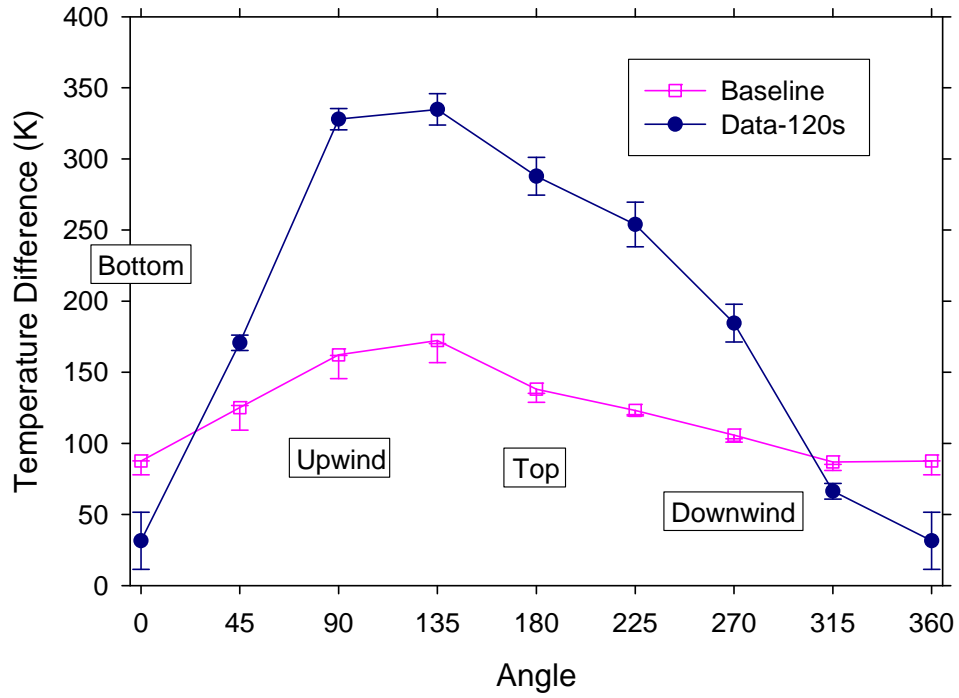
Figure 5-6 Calorimeter 3 temperatures at 120 seconds
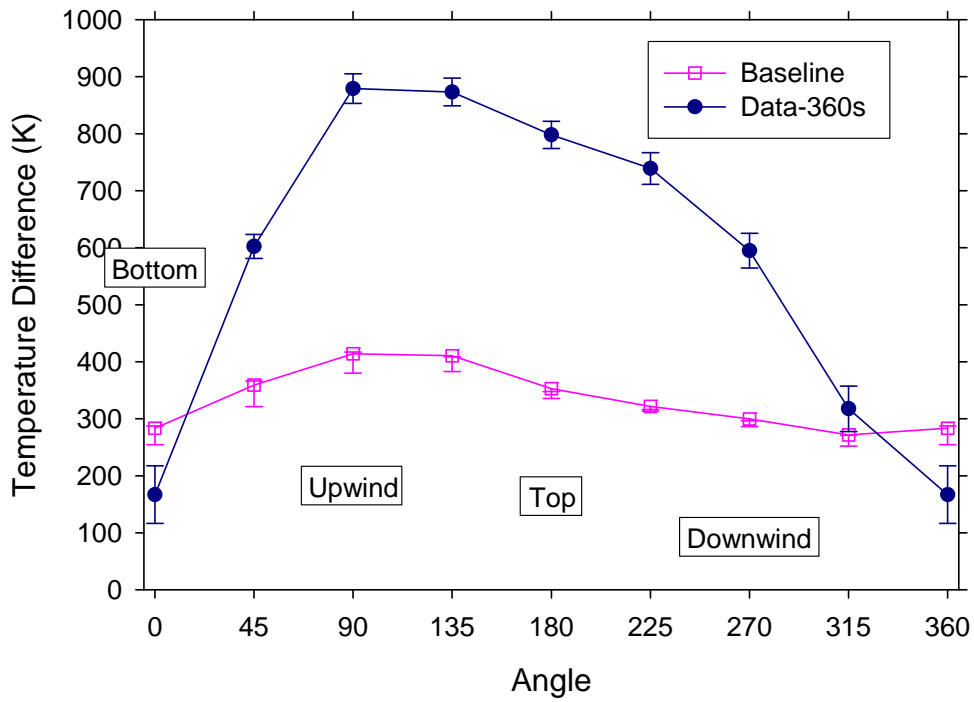
Figure 5-7 Calorimeter 3 temperatures at 360 seconds
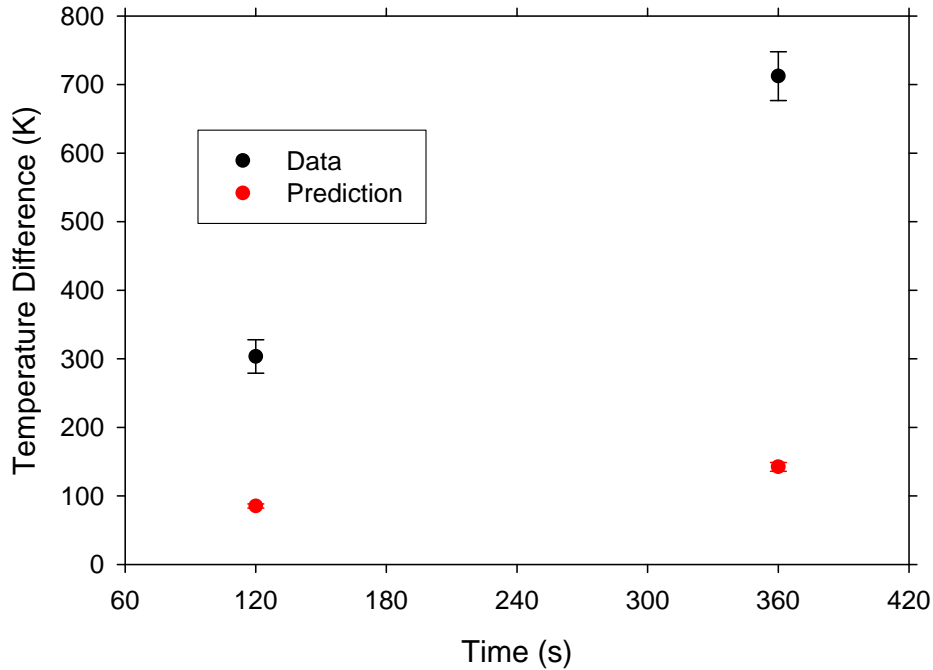
Figure 5-8 Calorimeter 3 temperature differences

5.4. C/MF Total Heat Flux

The final two system response measures relate to the total heat flux to the bottom of the C/MF. The measurement was inferred from the response of a thermocouple embedded in a radiative flux gauge (see Lam et al., 2004). This instrument involves two well characterized metal plates between which an insulating material of known properties is placed. Thermocouples monitor the temperature at the insulation/metal interface, and the total heat flux may be inferred through an inverse heat transfer calculation. Total heat flux was selected as the metric because it was measured and it could also be predicted in the model. In retrospect, this was not the best comparison measure. Because of the insulation in the gage, the gage was able to heat to a much higher temperature than the C/MF. Conduction through the substrate and convection on the back-side of the C/MF are added thermal sinks that were present in the simulation, but not in the experiment. The temperature of the gage appears functionally in the calculation of the total heat flux in the radiation and convection terms. Because the gage participates in the problem, it must be modeled correctly to correctly compare experimental total heat flux with predicted total heat flux. The model as calculated did not have a heat flux gage response model. Rather, the total heat flux to the culvert was monitored. The virtual heat flux gage model is a feature currently unavailable in Fuego, but on a list of code requirements to be developed in the future.

The gage response can be estimated by post-processing the simulation results. The free-stream temperature, incident radiative flux, and the convective heat transport coefficient were extracted from the calculation. These variables are mostly independent functionally from the temperature of the surface on which they are incident. Assuming the gage to be wide enough

99

that the response is one-dimensional, the gage response can be calculated. Table 5-1 contains the thermal properties of the materials from reference material. Response is fairly independent of the properties in range found in Table 5-1, so for the model the properties were taken as constant at the value found in the second row of the table. In addition to the properties in Table 5-1, an emissivity of the gage surface is assumed to be 0.85.

Using these data, a calculation was made in a spreadsheet with an adiabatic boundary condition on the back side of the gage. Figure 5-9 shows a plot of the predicted C/MF temperature and the predicted temperature of the heat flux gage plate. By the 360 second point (6 minutes), the surface temperatures differ by over 50ºC. As a reference, Figure 4-32 and Figure 4-33 show a plot of the components of the total predicted heat flux for the baseline case based on the Fuego predicted C/MF temperature. Because the thermal response of the measuring instrument is a significant component in the determination of total heat flux, original plan to make quantitative comparisons at this location have been abandoned.

Table 5-1 Thermophysical properties of the heat flux gage materials

Inconel			
T (C)	k (W/mC)	T (C)	ρC_p(J/m³C)
-17	14	25	3740000
200	17.5	204	4080000
427	20.8	650	4880000
870	28.8		
Metal Felt			
T (C)	k (W/mC)	T (C)	ρC_p(J/m³C)
20	0.07	25	305560
300	0.2	330	383570
650	0.31	730	585110
910	1.2		
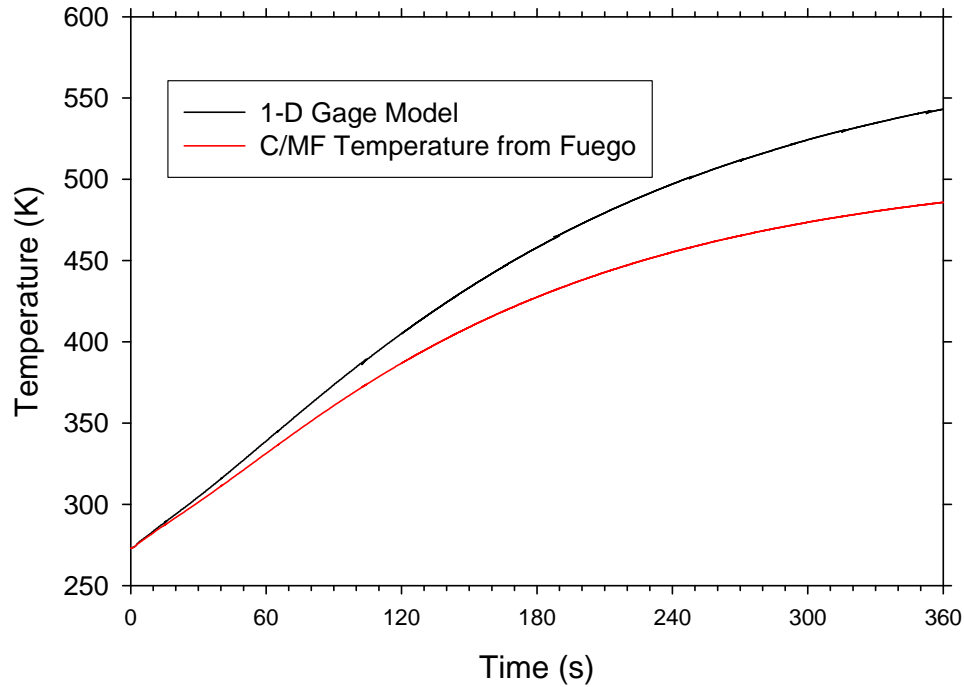
Figure 5-9 Surface temperatures for two predictive methods

Predicted and measured total heat flux for the baseline calculation are plotted in Figure 5-10 versus time. It is seen that the total heat flux is under-predicted by over half at early times. Nearing 360 seconds, the predicted and total heat flux are closer in magnitude. Corresponding temperatures are also plotted.

Figure 5-11 shows the total heat flux plotted versus temperature for the prediction and measurement. As the surface temperature approaches the convection temperature, the convection term drops out of the energy balance at the surface, and the total heat flux linearly approaches the radiative heat flux for a problem of constant average heat flux. Neglecting the low-temperature results from the start-up, the experimental absorbed radiative heat flux can be estimated to be around 50 kW/m^2. Predicted incident flux is around 30 kW/m^2, as found in Figure 4-33 in the previous chapter. For the simulations, the peak total heat flux is approximately 25 kW/m^2, whereas for the experiments the value is about 50 kW/m^2. It is evident that the simulations are under-predicting the radiative flux at this location by about ½.
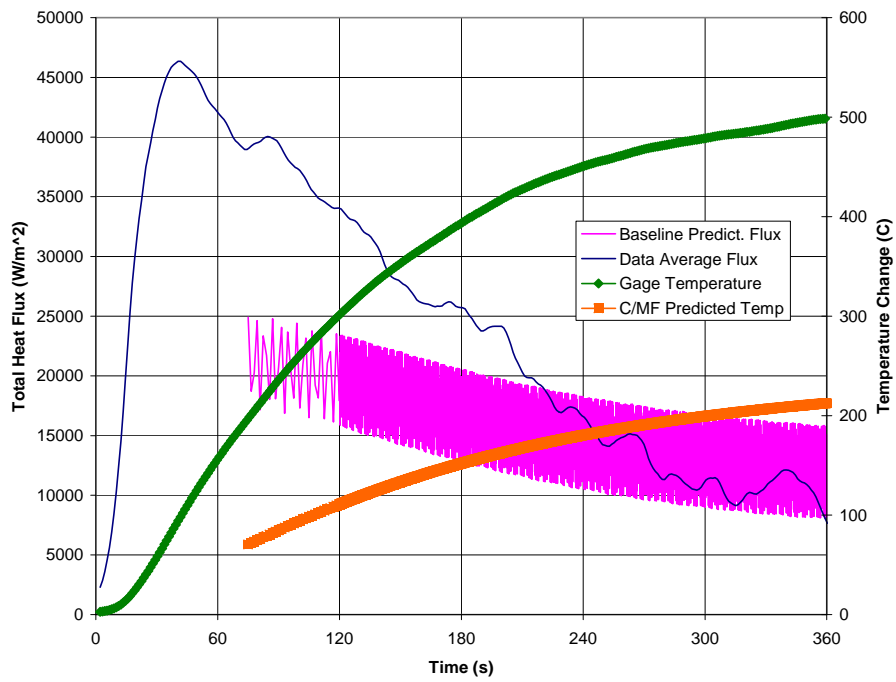
Figure 5-10 Total heat flux and surface temperature
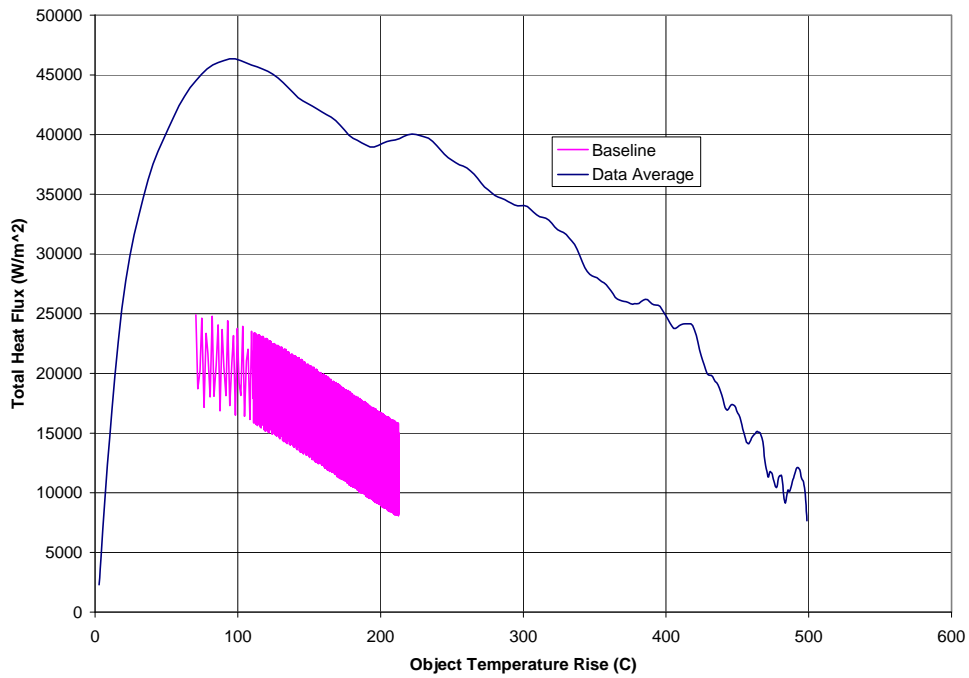
Figure 5-11 Total heat flux versus surface temperature

102

As with the results for Calorimeter 3, the comparison between the predicted and measured total heat flux suggests significant discrepancies. Figure 5-12 shows the comparison of the predicted and measured total heat flux. Simulation prediction error bars are not present in the comparison plot. This is because the information required to post-process the two simulations used to assess the parametric uncertainty was not recorded for the duration of the simulation required to perform this analysis. The capability (heartbeat output) had never previously been tested in Fuego at the time these two simulations were initiated. It was during the course of the calculations that the capability was acquired and employed. The magnitude of the parametric uncertainty bounds is thought to be small. The most and least severe calculated radiative flux differed from the baseline radiative flux by about 0.5 kW/m^2. Based on the radiative flux estimates, the discrepancy in the radiation heat flux is thought to be the source of the error. Figure 5-13 shows the comparison of the slope determined from point values at 120 seconds and 360 seconds.

Because of the difficulties with the analysis of the total heat flux comparison metric, subsequent sections will abandon this metric and look at the radiative heat flux. Total heat flux can only be estimated from the experiments. With predictions for the baseline simulations substantially low (about ½ the value), it will be apparent what off-set parameters cause predictions to begin to align more closely with the experiments as baseline simulation off-sets are analyzed.
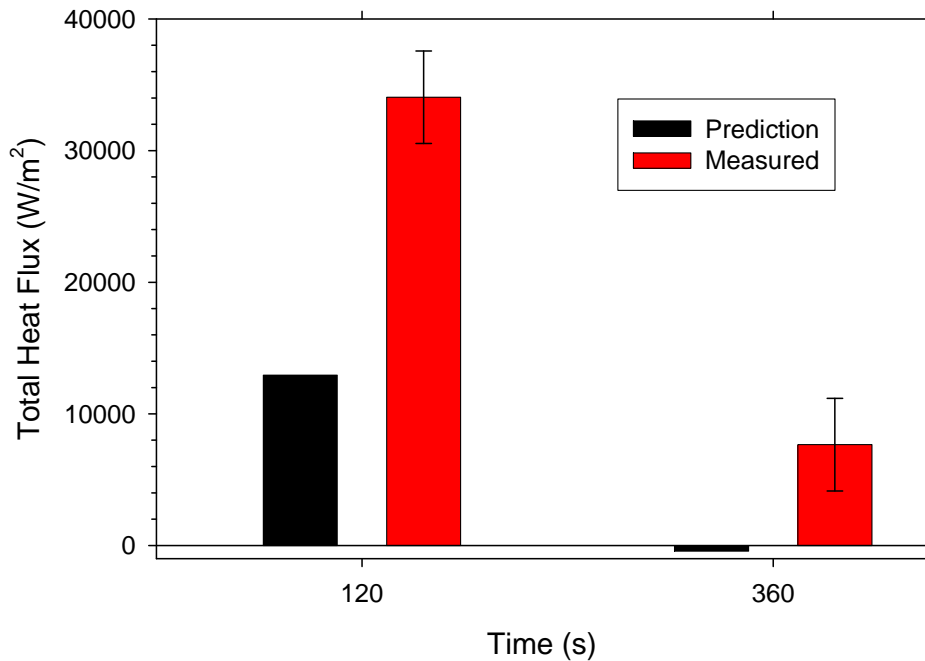
Figure 5-12 Total heat flux comparison
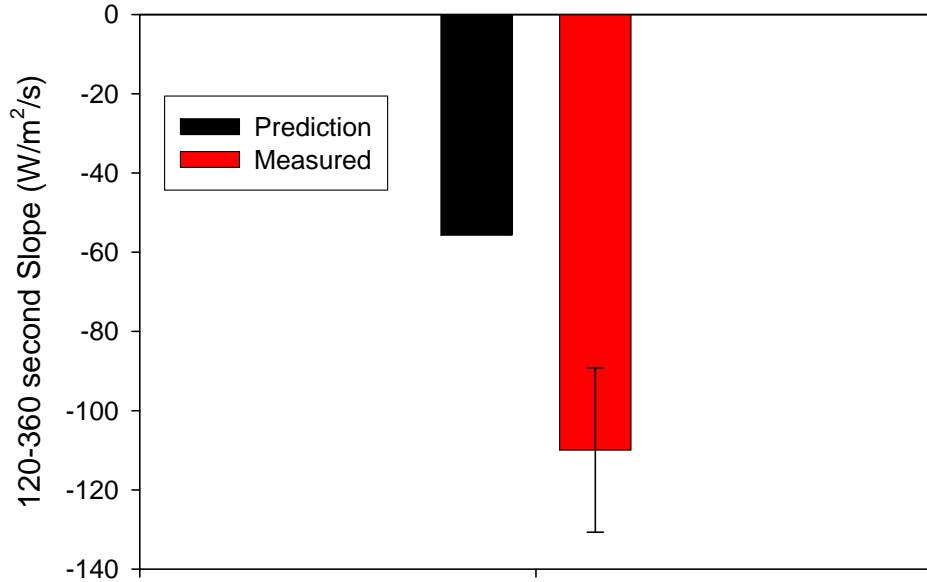
Figure 5-13 Total heat flux slope comparison

5.5. Discussion and Summary

Looking at the validation comparison results as a whole, there are significant discrepancies between the simulation and the experiment. Calorimeter 1 predictions agreed with the experiments within one standard deviation of the experimental uncertainty due to random error for each comparison. This finding suggests the model is correctly predicting the dynamics of the fire around Calorimeter 1. But the Calorimeter 3 predictions were not close to the experimental results. Nor were the heat flux results to the bottom of the C/MF.

Calculated uncertainties based on the 'most' and 'least' severe calculations were surprisingly small. Because binary offsets were not employed in this study, it is impossible to deduce the interaction between the parameters that resulted in such a low simulation error estimate. It is possible that none of the variables nor their magnitude contribute substantially to the uncertainties in the predicted outcome of the simulations. Other neglected parameters might be more significant to this case. The fuel source has been found to be a significant source of uncertainty in other studies (Nakos et al., 2005). This source was intentionally neglected since four independent measurements were taken of the fuel regression rate, and the relative magnitude of the uncertainty was thought to be comparatively small (Randsalu et al., 2004; single digit percent compared with double-digit percent). This omission is probably more substantial than the combined effect of all the parameters found in Table 2-2.

The discrepancies between the predictions and measurements are of particular concern. They suggest significant inadequacies in the predictions. The full nature of the inadequacies is not

apparent from what has thus far been presented. This will be further explored in forthcoming chapters.

Part of the reason for the discrepancy can be understood by examining the figures in the previous sections. Figure 4-11 shows gas temperatures plotted at a plane that goes through the centerline of the calorimeters on the floor at 15 cm above the floor. Large gradients in the predicted gas temperature are observed from the center-plane of the facility to the comparison plane at the middle of Calorimeter 3. A slight change in the location of the calorimeter or the predicted temperature field would expect to yield a large change in the predicted temperatures. Also, the predicted temperature field appears fairly symmetric about the center-plane of the facility around the calorimeters. Figure 4-8 and Figure 4-9 also suggest the degree to which temperature gradients exist in the predicted gas temperature directly underneath the C/MF. At the y=8.30 m center-plane, the predicted gas temperatures are between 1500 and 1800 K, whereas 47 cm away the temperatures are greater than 500 K lower. Figure 2-1 shows the post-test condition of the facility. Calorimeter 3 and 1 are clearly glowing in the post-test still images. The calorimeter that is symmetrically opposite to Calorimeter 3 is not glowing. This suggests that there is a strong experimental gradient, but that there is an asymmetric off-set in the gradient away from the center-plane and towards Calorimeter 3. Based on these observations, it is clear that the simulations are predicting a more symmetric fire than was observed in the experiments. If the predicted temperature field in Figure 4-8 and Figure 4-11 were displaced by 47 cm, the hot gases that were predicted low and between the two calorimeters would have to rise closer to the C/MF to transport over Calorimeter 3 instead of between the two calorimeters located on the ground.

6. Discretization Sensitivities

In addition to the parametric sensitivities that are documented in the previous section, various discretization sensitivities have been evaluated as part of the experimental plan. The motivation for including these sensitivities as part of the study was to attempt to quantify the level of discretization required to adequately represent the system with the calculations. It was clear from the start of the calculation plan that simplifying assumptions would be required to make the calculation of the test matrix feasible given finite compute resource. Simulations 4, 5, 6, 7, and 8 from the test matrix (Table 2-3) test simulation sensitivity to mesh, time, convergence, and radiation solve discretization. Because of difficulties with the radiation solve, the matrix was solved with the coarse mesh used for the Syrinx region. Difficulties were resolved as the simulations were in progress. Since calculations were in progress, the base simulation was re-defined to include the coarse Syrinx region, and two additional cases were added that were essentially Simulation 1 and 4 repeated except with the same mesh used in the Syrinx region as for the Fuego (fluids) region to assess the impact of the Syrinx mesh on the prediction.

With the exception of the coarse mesh simulation, the simulation results presented in this section do not extend to 360 seconds. Rather, they terminate at 125 seconds. The decision was made to limit the extent of these calculations to make the results more easily obtainable. The baseline simulation required greater than a month of CPU time on the rogue cluster using 60 processors. When comparing the 360 second results and the 120 second results in the previous section, it was found that for this case there were not significant changes in trends from what was found at 120 seconds to what was found at 360 seconds (see Figure 5-1 through Figure 5-8). This suggests the ability project to what a result would be at 360 seconds based on 120 seconds of calculation results is quite good. The coarse mesh was sufficiently small that the impact of solving the problem to 360 seconds was minimal.

6.1. Mesh Refinement-Calorimeters

As has been previously described in more detail in the mesh Chapter 2 (see **Table 2-5**), three fluid meshes existed. The coarsest was developed to test the input files before running larger cases and to make inferences without the costly additional elements. The next two were created by a strict refinement of the coarse mesh. They involved splitting one hexahedron into 8 (2^3-baseline) and 27 (3^3-refined) hexahedrons of similar shape. Consequently, the length scale resolved by a case with the baseline case is 100% greater than the length scale for the coarse mesh. The subsequent step from the baseline to the refined mesh is only a 33% increase. Comparison of results obtained on each of these indicates the degree to which the mesh refinement, or spatial discretiztion, affects simulation results.

Figure 6-1 and Figure 6-2 show prediction results for Calorimeter 1 from the coarse and fine mesh at 120 seconds and from the coarse mesh at 360 seconds. Figure 6-3 and Figure 6-4 show similar predictions for Calorimeter 3. Differences between predictions with the 600 K and 2000 K mesh were small, as were the simulation uncertainty bars (on the same order). Differences between the 75 K and 600 K mesh were surprisingly small, but larger than the uncertainty from the parametric offsets.
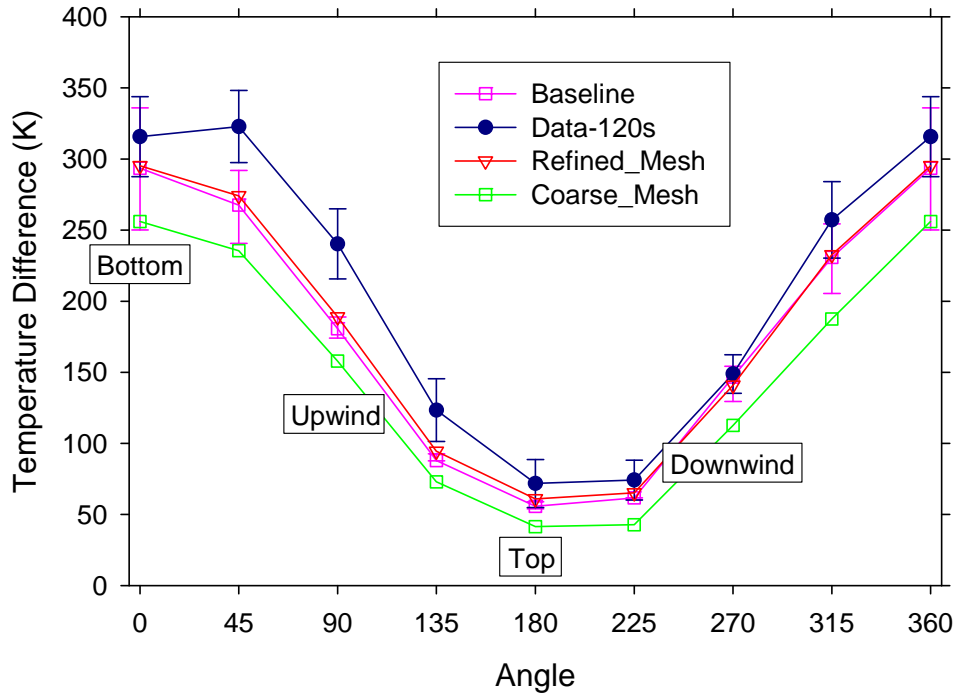
Figure 6-1 Mesh refinement for Calorimeter 1 tempereatures at 120 s
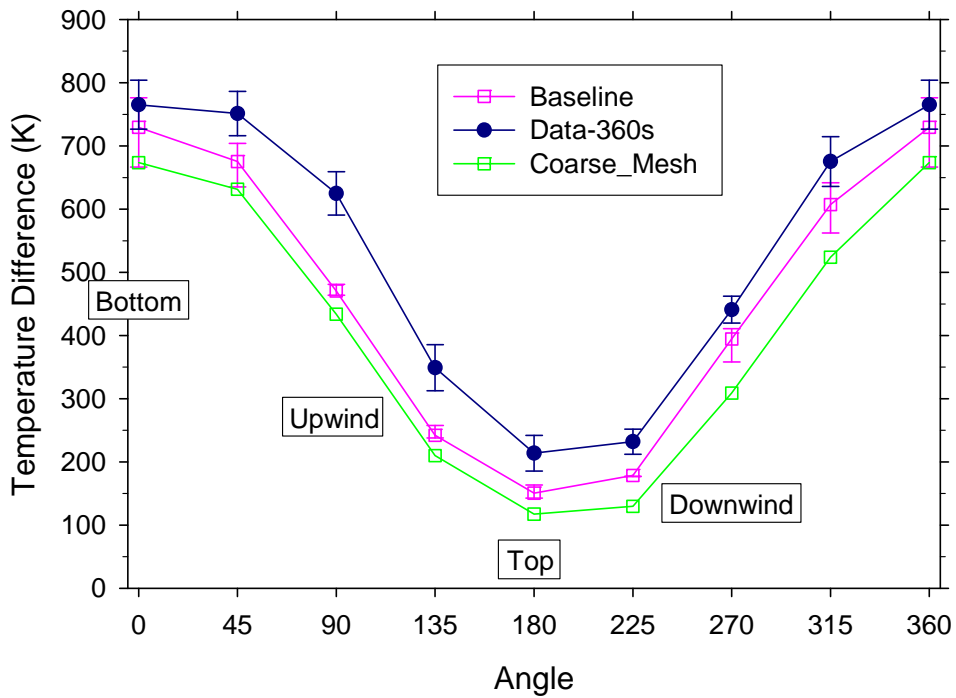
Figure 6-2 Mesh refinement for Calorimeter 1 tempereatures at 360 s
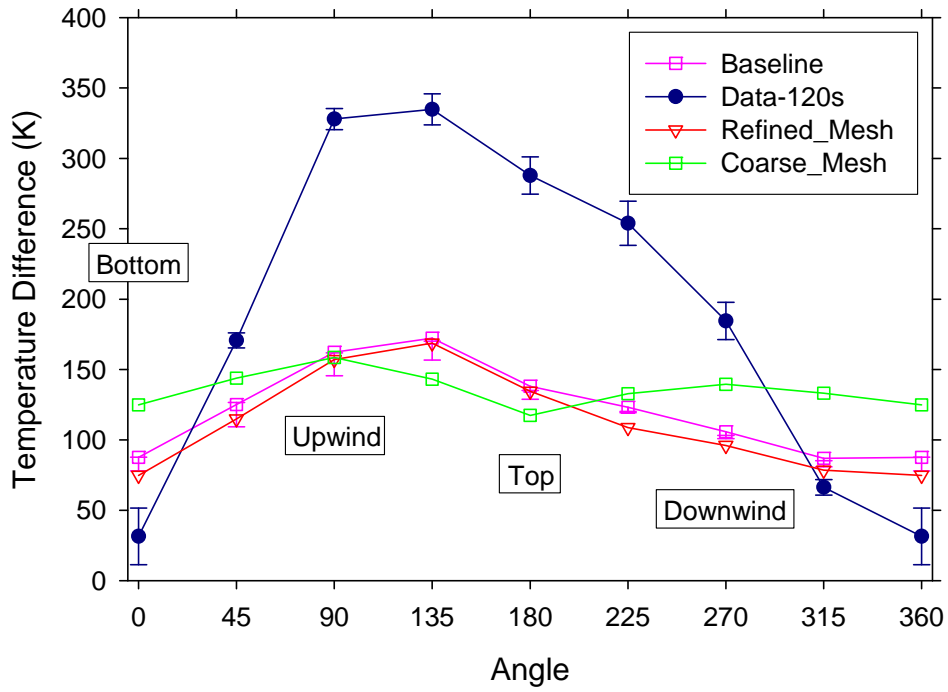
Figure 6-3 Mesh refinement for Calorimeter 3 tempereatures at 120 s
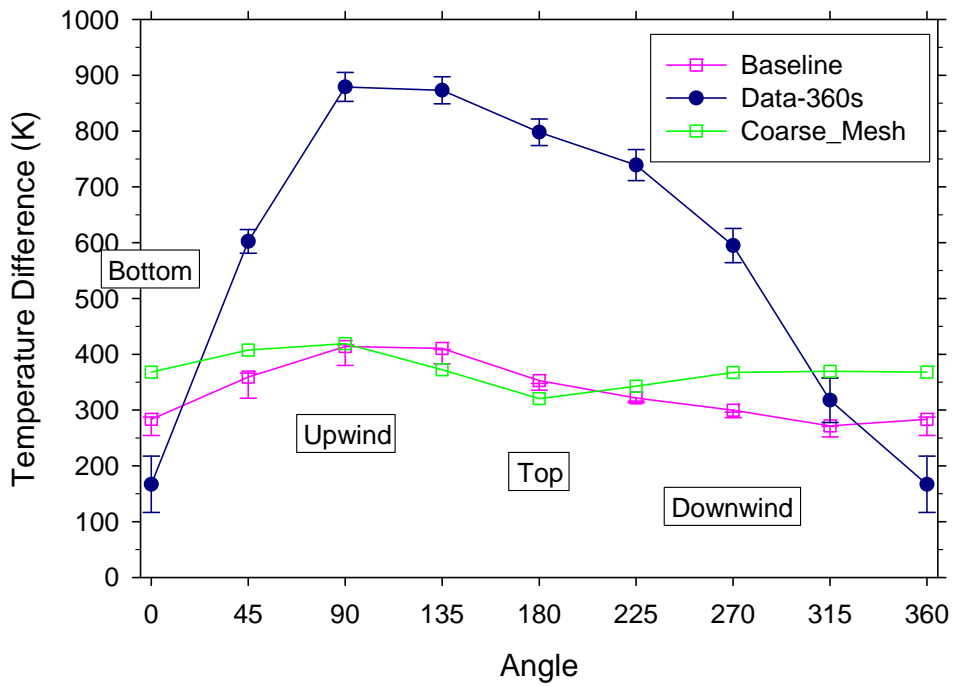
Figure 6-4 Mesh refinement for Calorimeter 3 tempereatures at 360 s

6.2. Other Discretization-Calorimeters

Besides the mesh, there are several additional sources of discretization error that are evaluated in this study. The time step and the quadrature order (radiation solve discretization) are evaluated as discretization parameters.

Also, the number of nonlinear iterations allowed for the fluid region calculation per time step has been evaluated within the construct of the study. This isn't a true numeric discretization like the others evaluated. This parameter is used to stop the non-linear equation solver from iterating on a problem by employing the assumption that the solution obtained is sufficiently converged to proceed to the subsequent time-step. Since computing resources are seldom available to perform practical problems while converging every step to numeric convergence, fire simulations are often performed with a limited number non-linear iterations. Good practice involves estimating the impact of this assumption, much like making predictions on a coarse mesh and refining the mesh to demonstrate the adequacy of the coarse mesh.

Figure 6-5 shows the temperature predictions for Calorimeter 1 at 120 seconds. Figure 6-6 shows the temperature predictions for Calorimeter 3 at the same point in time. Calorimeter 1 predictions appear most sensitive to the time-step compared to the other two parameters. Calorimeter 3 temperature predictions appear more sensitive to the time step and the number of nonlinear steps. In these figures, the number of nonlinear iterations is abbreviated #PL, with PL being short for 'Picard Loop', which is a name given to the nonlinear step.
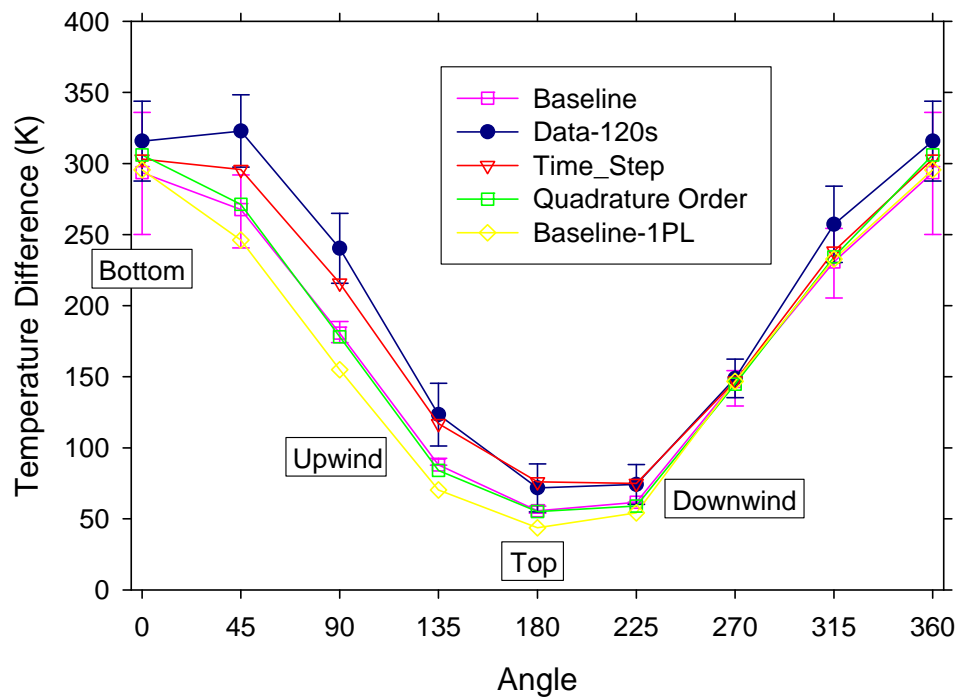
Figure 6-5 Discretization parameters for Calorimeter 1
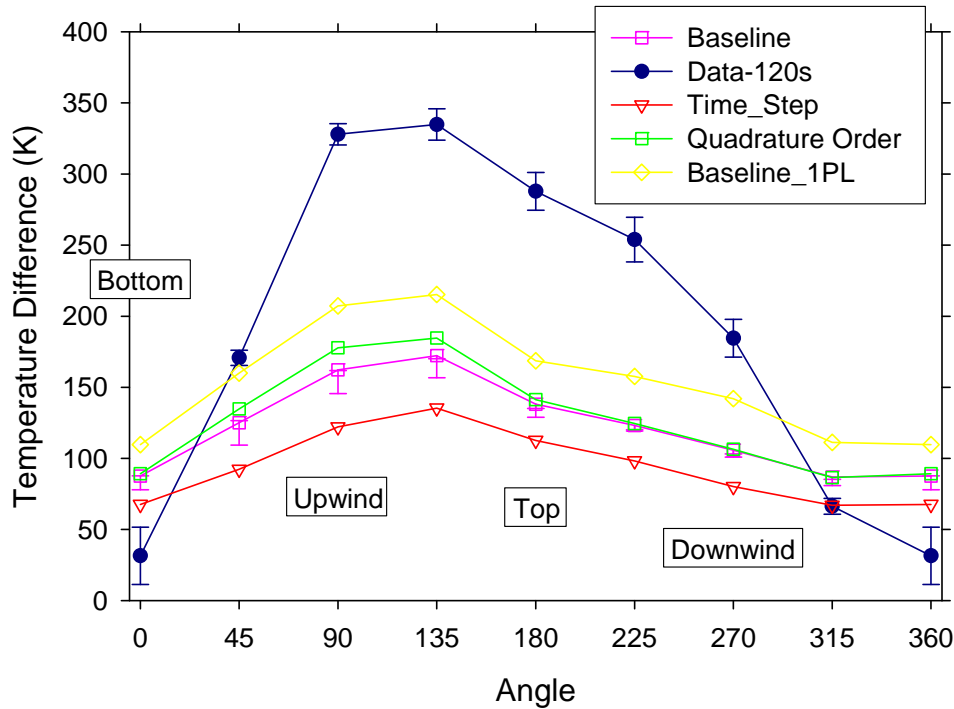
Figure 6-6 Discretization parameters for Calorimeter 3

Outside the scope of the initial study proposed, the importance of the nonlinear iterations assumed for the fluid region has been explored. This was motivated by discussion among users of the code who suggested that the 2nd nonlinear step yields results that are non-intuitive. The intent was to discover the extent to which the assumption of 2 nonlinear steps impacts the calculation results. Figure 6-7 and Figure 6-8 show the temperature predictions for Calorimeter 1 and 3 with the coarse mesh predictions using different numbers of nonlinear steps. Most simulation results are identical to each other to three significant figures except for the case with two nonlinear iterations. The case with two nonlinear iterations is close to the other results for Calorimeter 1 predictions, but not to three significant figures. For Calorimeter 3, the one, three, four, and nine nonlinear step predictions are also accurate to three significant figures. The two nonlinear step predictions vary more substantially (20.0 ℃ different on average) from the other predictions. Figure 6-9 and Figure 6-10 show the temperature predictions for Calorimeter 1 and 3 with the baseline mesh predictions using 1, 2, and 3 nonlinear steps. Results with 1 and 3 nonlinear steps are identical to 2 significant figures for each calorimeter, with the maximum difference being 1.4 ℃. This maximum value was the same for both calorimeters. Calorimeter 3 temperature predictions appear more sensitive to the selection of 2 nonlinear steps than Calorimeter 1 temperature predictions as judged by the differences with respect to angle in the temperature predictions for the two calorimeters.
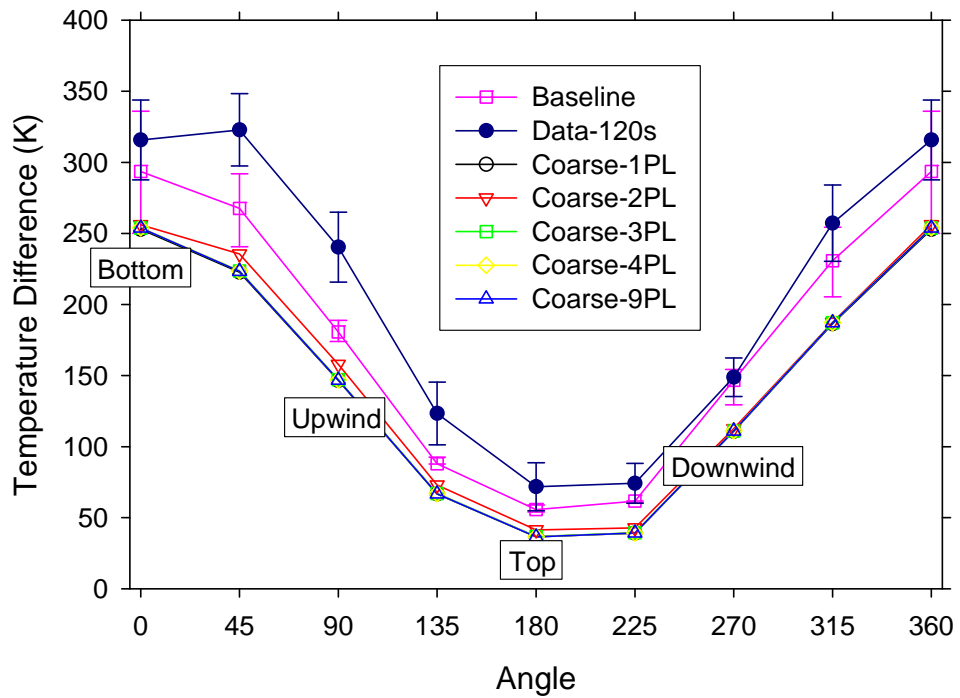
Figure 6-7 Coarse mesh non-linear iteration study results for Calorimeter 1
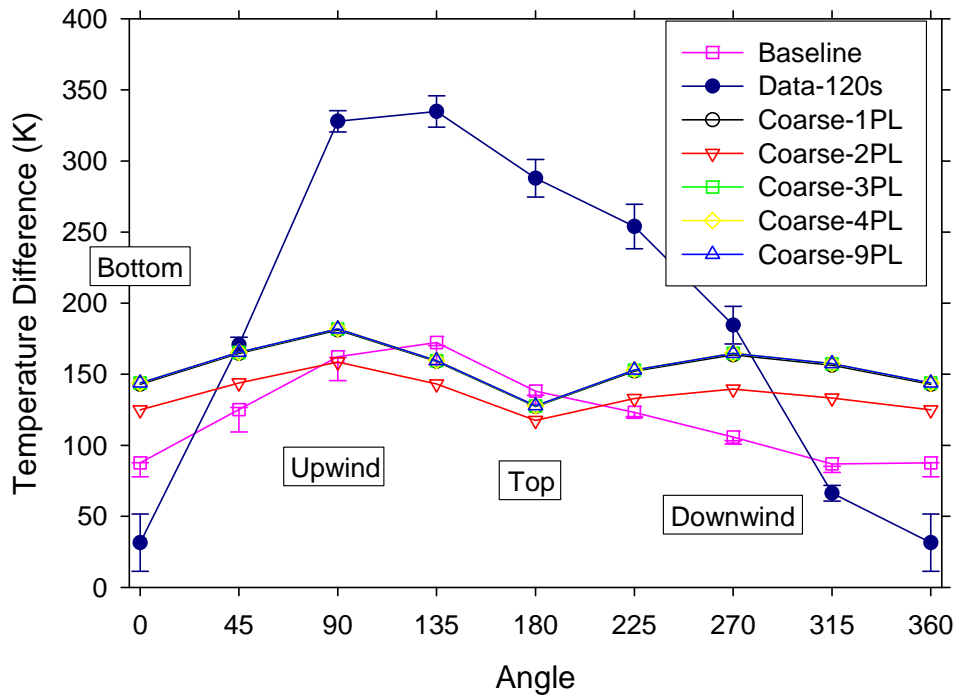
Figure 6-8 Coarse mesh non-linear iteration study results for Calorimeter 3
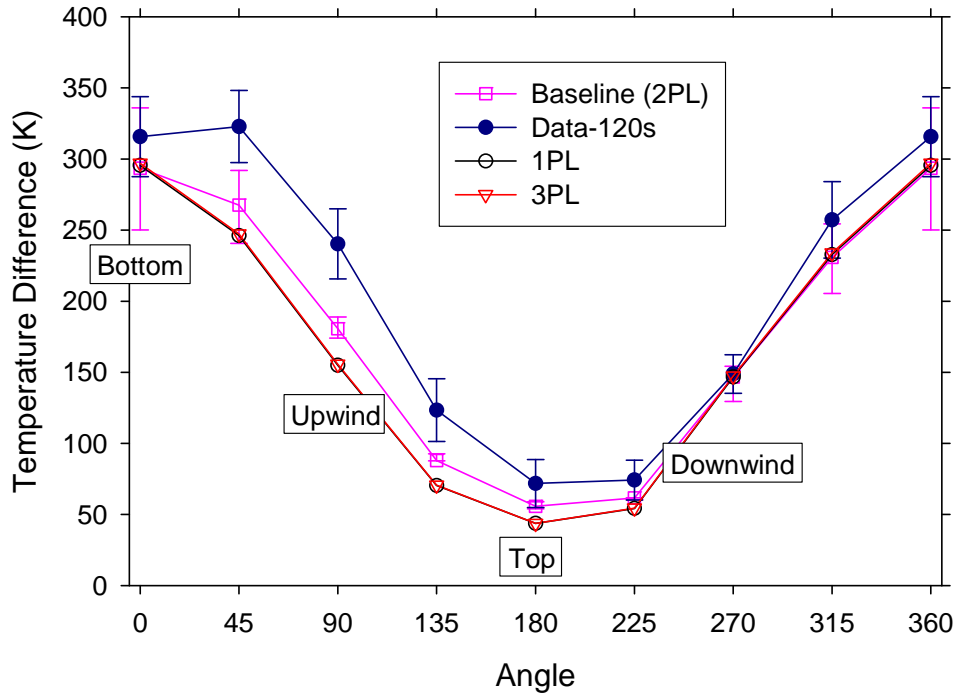
Figure 6-9 Baseline mesh non-linear iteration study results for Calorimeter 1
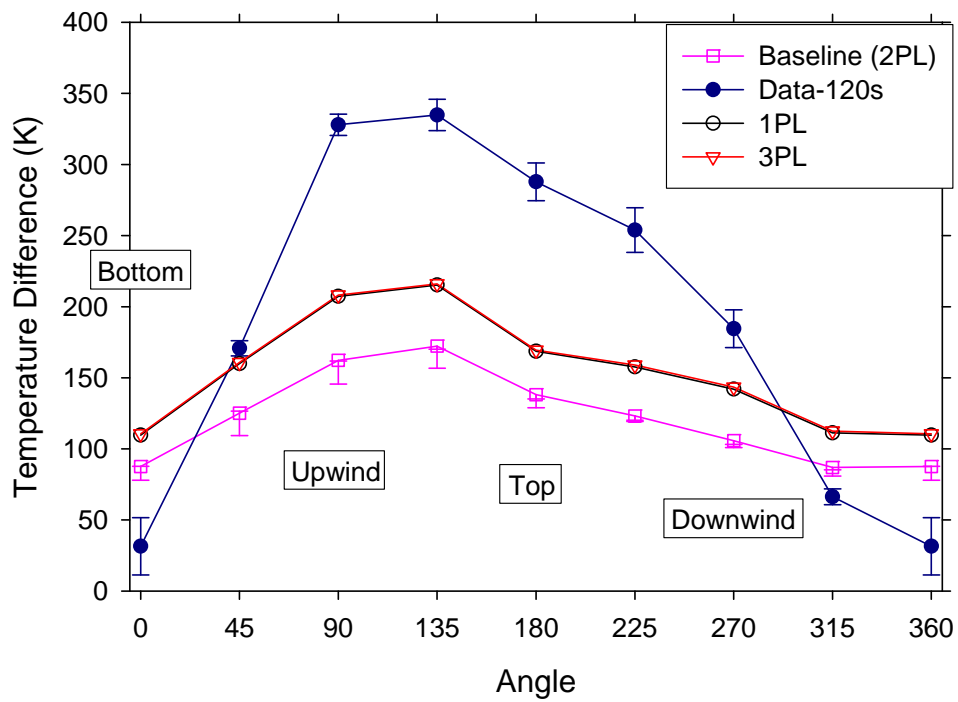
Figure 6-10 Baseline mesh non-linear iteration study results for Calorimeter 3

Residuals for the baseline case except with one non-linear iteration are found in Figure 6-11. When compared with Figure 4-34, the single non-linear iteration case exhibits lower residuals.
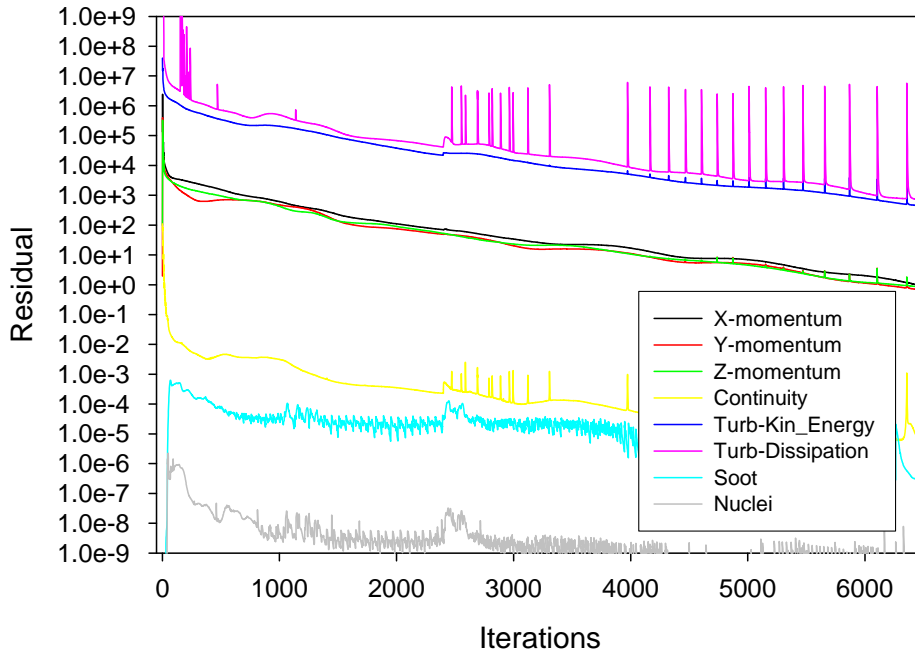
a.
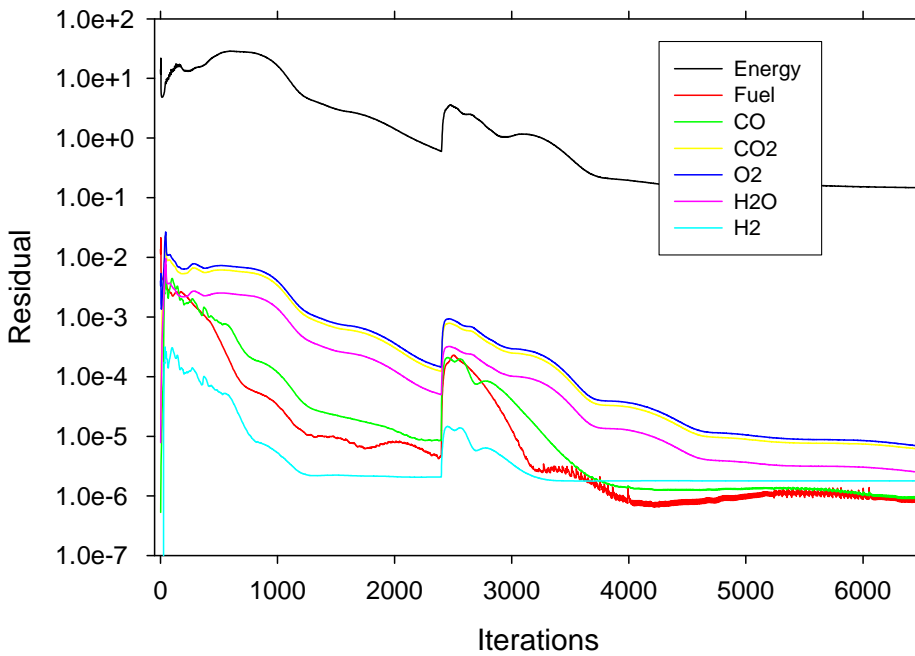
b.

Figure 6-11 Residuals for the baseline case with one non-linear iteration

6.3. Syrinx Mesh-Calorimeters

As previously described, the baseline calculations were performed with the coarse mesh for the Syrinx region. The baseline and refined mesh calculations were re-run employing the same mesh for the radiation calculation as was used for the fluid calculation to assess the consequences of this assumption. Figure 6-12 and Figure 6-13 show the predicted temperatures for Calorimeter 1 and 3 using the same Syrinx mesh as was used for the fluid region. Plots labeled 'Syrinx_Mesh' were performed with the 600 K mesh for both the Fuego and Syrinx regions. Plots labeled 'Refined_Syrinx_Mesh' were performed with the 2000 K mesh for both the Fuego and Syrinx regions. The more refined Syrinx mesh predictions are very close to the predictions with the coarse Syrinx mesh at most points, with the exception of predictions at the location of highest temperature. For Calorimeter 1, the peak temperature differences at the maximum temperature location are around 100 ºC.
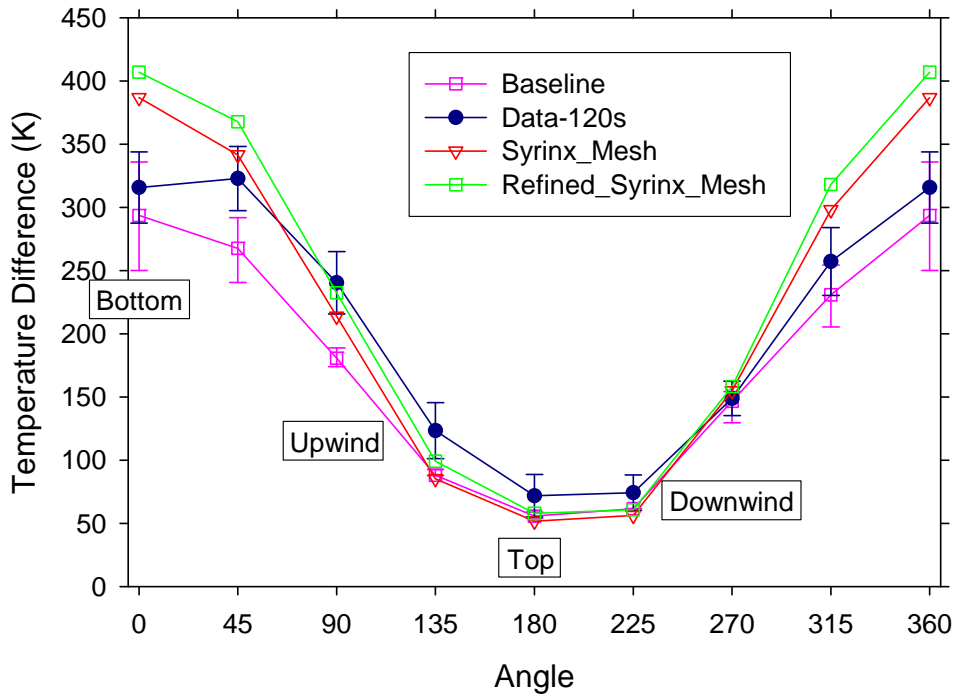
Figure 6-12 Calorimeter 1 predictions using identical Syrinx and Fuego region meshes
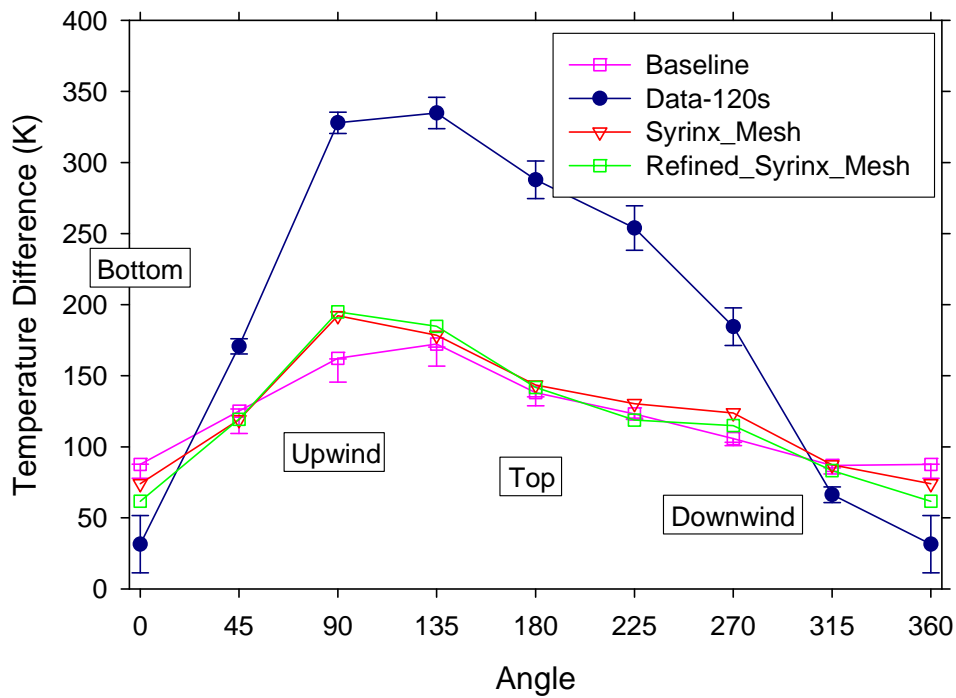
Figure 6-13 Calorimeter 3 predictions using identical Syrinx and Fuego region meshes

6.4. C/MF Radiative Flux

The C/MF radiative flux results for the discretization study are found in Figure 6-14. Of note, the magnitude of the predicted radiative flux for the baseline case with one and three nonlinear iterations were substantially higher than any other of the predictions, and much closer in magnitude to the ~50 kW/m^2 from the experiment. Predictions are still about 20% lower than the data.
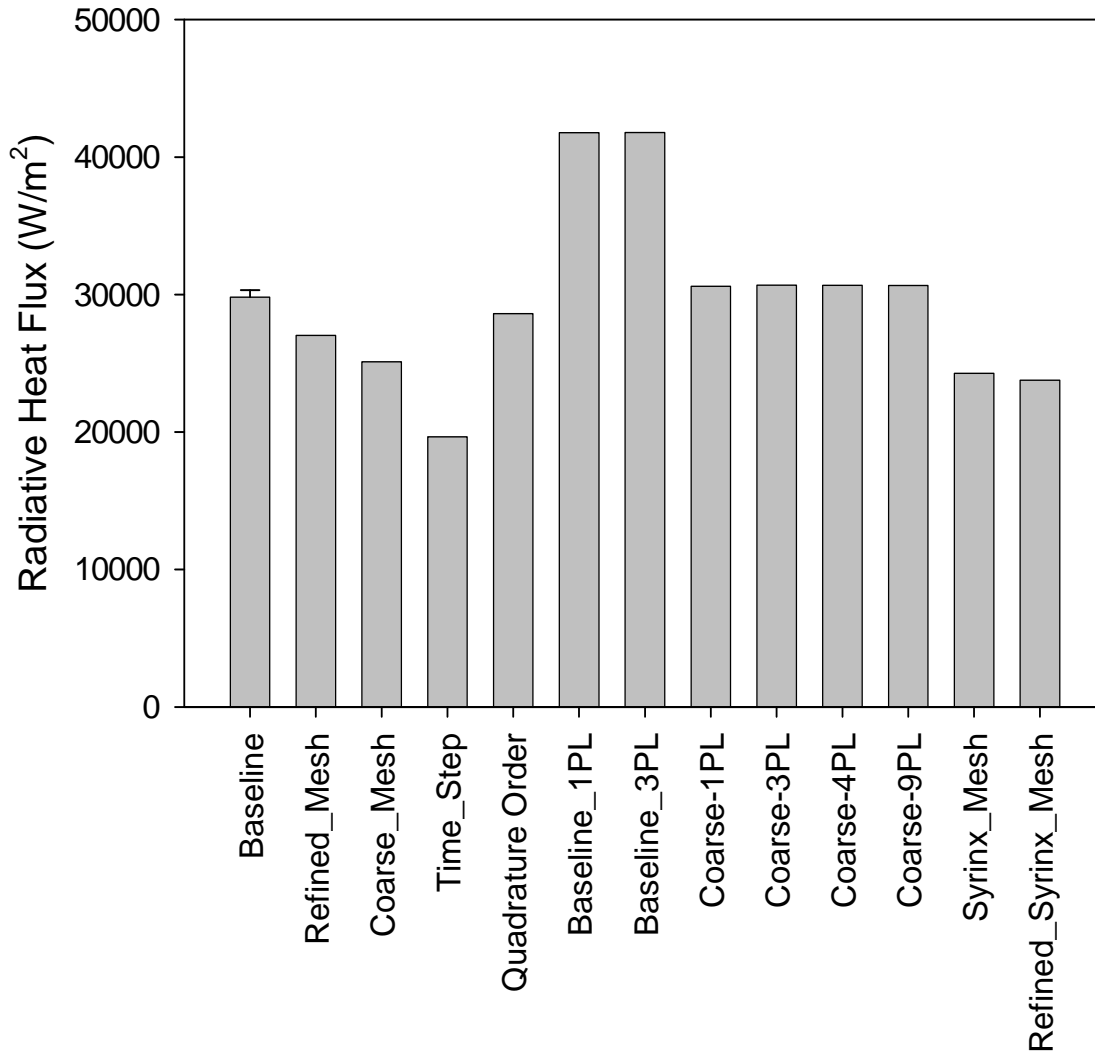
Figure 6-14 Predicted radiative heat flux to the bottom of the C/MF

6.5. Discussion and Summary

A survey of the majority of the results presented in this chapter suggest that the magnitude of the differences induced by the discrete quantities varied is generally greater than the magnitude from the parametric cases used to construct the error bars placed on the simulations. It would be appropriate to reconstruct the simulation uncertainties based on the variability found in the cases in this chapter. Doing this would not address a larger problem. It is clear that even with expanded uncertainty bounds that the disagreements between the simulations and experiments for the C/MF and Calorimeter 3 are not explained. It follows that either the simulation test matrix was inadequate to encompass the true range of uncertainty in the simulation, that the physical assumptions in the model are inadequate for this class of problems, or something was completely wrong or not understood with respect to the problem.

The relative magnitude of error due to grid refinement as suggested by the three grid refinement cases is surprisingly small. The coarse grid predictions for Calorimeter 1 were within 50 ºC of the baseline and refined mesh predictions for all angles at 120 seconds, and the trends were similar. Calorimeter 3 trends for the baseline and refined grid were similar and magnitudes were close. The coarse grid temperature prediction trends for Calorimeter 3 were different than the baseline and refined predictions, but the magnitudes were mostly within 50 ºC. If grid refinement is viewed as independent of all other parameters and discretizations, the solution provided by the baseline case is probably acceptably refined given the differences observed with the refined grid predictions and the compared magnitude that other parameters and discretizations incur on the problem.

The time step was probably too large for this case. The smaller time step resulted in one of the larger differences in results for Calorimeter 1, 3, and C/MF flux results compared with other sensitivities looked at in this chapter. It is unknown how this observation might change if a different number of nonlinear iterations were taken for this case.

The number of nonlinear steps taken for this study was not ideal. Oddly, it appears from results that the study would have been better had one nonlinear step been the base case. Results for the coarse and baseline mesh for 1, 2, and 3 nonlinear steps suggest that 1 is sufficient to provide 3+ digits of accuracy to the temperature and heat flux predictions compared with the case with 3 nonlinear steps. The results with 2 nonlinear steps are indicative of a potential bug that is isolated to the second nonlinear step. In future studies, terminating a time-step after 2 nonlinear iterations should be avoided until this problem is corrected or adequately explained. The coarse mesh results suggest that for 1, 3, 4, and 9 nonlinear steps that the results are nearly identical. The fact that the baseline case with 1 and 3 nonlinear iterations yielded very similar solutions suggests a similar trend as the mesh is refined. For future calculations of this type for this code, it may be an advisable practice to start with 1 nonlinear step (a quick calculation) and verify the accuracy of this assumption by making comparisons to a progressively increasing number of nonlinear iterations (skipping 2). This is particularly advisable for calculations of the magnitude and scope of these.

The quadrature order had an effect on the results of the calculations, but not a highly significant effect. The objects for this study were all close to the fire, limiting the uncertainty induced by the assumption of a low quadrature order. If the objects were not close to the fire, this assumption might be much worse. Given the impact of the quadrature order on the calorimeter temperature predictions (~10 ºC difference at the worst) and the sensitivity to other model assumptions, the assumed value for the quadrature order is probably acceptable for this calculation.

The extra calculations performed with the refined Syrinx mesh suggest the importance of the radiation to the calculations. Refining the Syrinx mesh for a better approximation resulted in substantially different results at one of the critical comparison points.

7. Follow-up Investigation

7-1. Modeling small features

Simulation uncertainties evaluated in the previous sections could not adequately explain the reason the prediction results for Calorimeter 3 differed substantially from the experimental results. Visual observations during the tests suggested Calorimeter 1 and 3 were glowing as the fire died down. The calorimeter symmetrically adjacent to Calorimeter 3 was not glowing. This suggests that the experimental results were asymmetric with respect to the centerplane of the facility, while the simulation results were mostly symmetric (see Figure 4-8, Figure 4-9, and Figure 4-11). An asymmetric inflow condition has been evaluated in simulations presented in Chapter 3, and this condition was not found to make a large difference. This lead to the assumption that the missing geometry detailed in Chapter 2 contributed at some level to the discrepancies between the model and the simulation.

Since Calorimeter 1 results were acceptably close to the data for most cases, it was hypothesized that the discrepancy might be due to something in-between or in the vicinity of Calorimeter 1 and Calorimeter 3. The cable bundles from the two up-stream calorimeters descended from near ends to the floor of the facility and under the fire brick to the data acquisition system. Also, several heat flux gages were located in the up-stream of Calorimeter 3. Most of these were neglected in the design of the test because they fell below the tolerance employed for generating the mesh. Also, there were several 1-inch (2.54 cm) metal poles that were used to support thermocouples in the fire region.

Part of the reason the geometric tolerance was chosen because it was difficult to generate a mesh that was much more refined and obtain an answer to the problem given a limited time scope. The limitation is related both to compute resources (processor availability, disk space) and mesh design (the ability to describe the problem on a mesh given existing mesh software). As a follow-up activity, it was desirable to explore the possibility of these small features as the source of the discrepancies. Assuming these small features are the reason for the discrepancy, it is not clear how to best model them in Fuego. There is currently a model development task underway for modeling sub-grid clutter. The model is not available in current versions of Fuego. The next best method for modeling these is to generate them on the grid. A recently released version of the cubit mesh generation tool allows the user to select certain hexes and change their assigned block. This allows for mesh-conformal adaptation of the mesh without having to exhaust several days re-meshing the system following a geometry change. An alpha version of cubit was secured and employed to generate a mesh with the cable bundles. In a scoping calculation, this did little to change the symmetry of the fire. It also did little to the pressure and velocity fields. Because Fuego is a CVFEM code, missing a node does not result in a stagnation node like with a more typical control volume code. Appendix B details the results of a grid refinement test performed to assess the necessary mesh resolution to model a small blocking object. The results suggest that an object that is a single node wide will behave like a much smaller object (depending on the shape of the object). The study also suggests the need to have 2 or more nodes representing an object to begin to approach a mesh resolved solution to the case. The mesh was locally refined around the cables, and re-run in a scoping calculation. The early solution suggested the fire was still fairly symmetric. It was then assumed that the five 2.54 cm wide

poles could be represented on the baseline grid with a single node wide at the width of the baseline mesh at that location. Typical spacing was approximately 15 cm (6 inches, or about 6x the actual width of the objects).   Based on the scoping calculations detailed in Appendix B, this assumption might be expected to result in a moderately good representation of the objects that are actually much smaller than they are represented on the mesh.

7-2. New meshes with clutter

Two new meshes were generated that were based on the baseline mesh used for this study. The first included the cable bundles descending from the two upstream calorimeters. Nodes were removed from the calculation with a feature new to Cubit version 10 (in Cubit Alpha at the time). The mesh was then refined locally around this modification so the objects would behave in a way that approaches the refined grid solution as per the study described in the previous section. The bundles were modeled as rectangular objects that were three nodes wide. Because the mesh modification capability only allows mesh conformal modifications and the mesh was not perfectly rectangular, the bundles were not perfectly rectangular.

A scoping calculation was performed with this mesh using the baseline case conditions, and it was found that the predicted fire was still somewhat symmetric about the center-plane with the bundles in place. No further results from this scoping calculation are documented here.

The mesh was then further modified to include two heat flux gages and five instrument poles. A graphic of this mesh is seen in Figure 7-1. The instrument poles in the mesh (~10-15 cm) were much larger than the actual poles were (~2.5 cm) for the tests. Based on the discussion in the previous section, the one node wide poles are expected to behave much like an object of much smaller dimension. So, even though the mesh objects are significantly larger than the actual objects, they are thought to represent the small objects better than might be expected given the size discrepancy. Based on code capability existing at the time of this study (version 1.3), this is probably the best approximation that can be made of the system without meshing the geometry to prohibitive detail. As with the cable bundles, the poles are not perfect rectangles. They are mesh conformal, and slightly skewed. This is not thought to be a significant departure from the geometry in the actual case. In the actual tests, these poles were not rigid. During a test, they would become sufficiently hot and pliable that the gas flow around the objects deformed the poles. By the end of the 4th test, several of the poles were bent and offset in some cases by more than 30 cm in the down-wind direction.
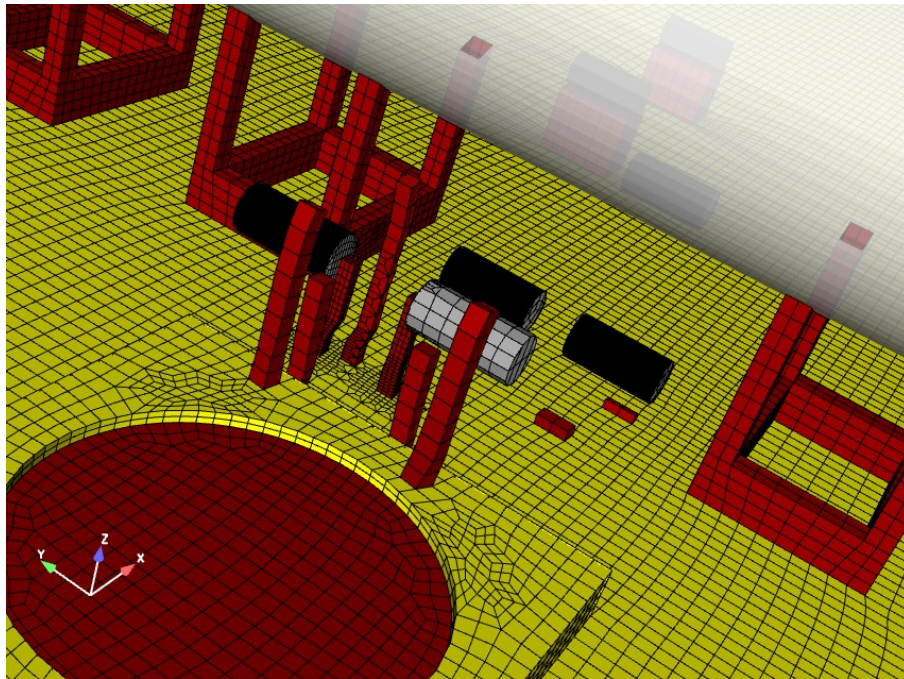
Figure 7-1 A rendering of the surface mesh of the second baseline modified mesh

The baseline case with this second new mesh was evaluated in a scoping calculation. It was found that the results were more asymmetric than in any case previously calculated. This case was subsequently run to 120 seconds.

7-3. K-epsilon and TFNS simulation results

Using the new mesh with the calorimeter cable bundles, the five thermocouple poles, and the two heat flux gages, two new calculations were performed. This mesh (the second one) will henceforth be referred to as the mesh with clutter. One of the simulations was with the baseline input deck and included the new mesh. The other included the new mesh and a turbulence model modification that involved the temporal filtering of the Navier-Stokes equations, or the TFNS model (Tieszen et al., 2005). This model is like a LES turbulence model. A time scale filter is used to filter the turbulence, and the k-epsilon model is used for sub-grid turbulence. A consequence of using the TFNS model is that the time varying fluctuations are more prone to be present in the solution. The time filter chosen was two times the magnitude of the simulation time step (0.01 second filter).

Other studies have suggested that the mesh resolution required to adequately resolve a quiescent pool fire using the TFNS model involves about 70 nodes across the diameter of the pan. This is much higher resolution than is required for the k-epsilon model simulations. The mesh employed for this case is approximately 25 nodes across the pan diameter. The results as a consequence may be somewhat under-resolved. The refined grid (2000 K) might be used for this case, but a uniform refinement of this mesh would result in multiple nodes across the thermocouple poles, and a substantial over-prediction of the importance of the geometry.

Localized refinement is not currently feasible in the mesh package employed for this case due to bugs (that have been reported and are under evaluation) in the Cubit mesh refinement tool.

An aspect of TFNS that requires modification is that the turbulence is expressed at the temporal scale of the filter. Simply specifying a velocity and turbulence intensity is not sufficient as was the case for the k-epsilon model. Details of the inflow turbulence are forthcoming, so it was impossible to map data to the inlet or to generate detailed statistics. An inflow profile has been assumed based on the best available measurements that suggest a mean flow of 13 m/s and turbulence levels of approximately 20 %. The details of the temporally varying input are found in the Appendix in Section C-1.

The new mesh simulations were run to 120 seconds, and the calorimeter temperature prediction results are plotted in Figure 7-2 and Figure 7-3. Calorimeter 1 results for the k-epsilon model and the mesh with clutter suggest a much higher peak temperature than was predicted for any of the other parametric and discretization parameters examined. The low temperature prediction was similar to those predicted with the baseline mesh. Qualitatively, the agreement is good. Calorimeter 3 results with the clutter mesh suggest improved quantitative agreement when compared to the baseline and other perturbation cases. The peak predicted temperature is lower than the data, but 50 degrees higher than the baseline simulation.
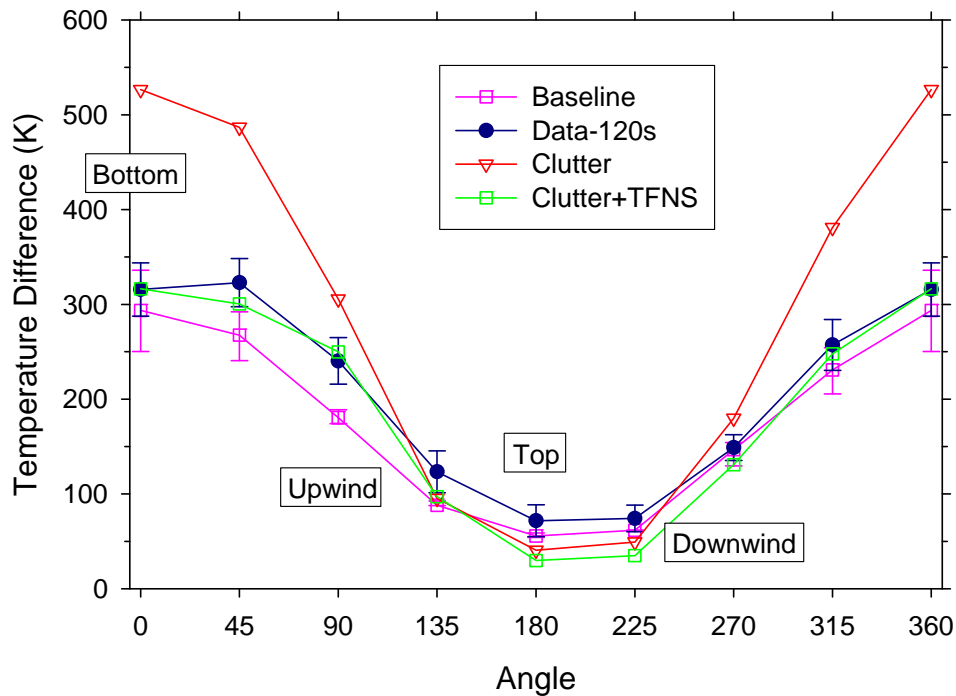
Figure 7-2 Calormeter 1 predictions for the clutter mesh
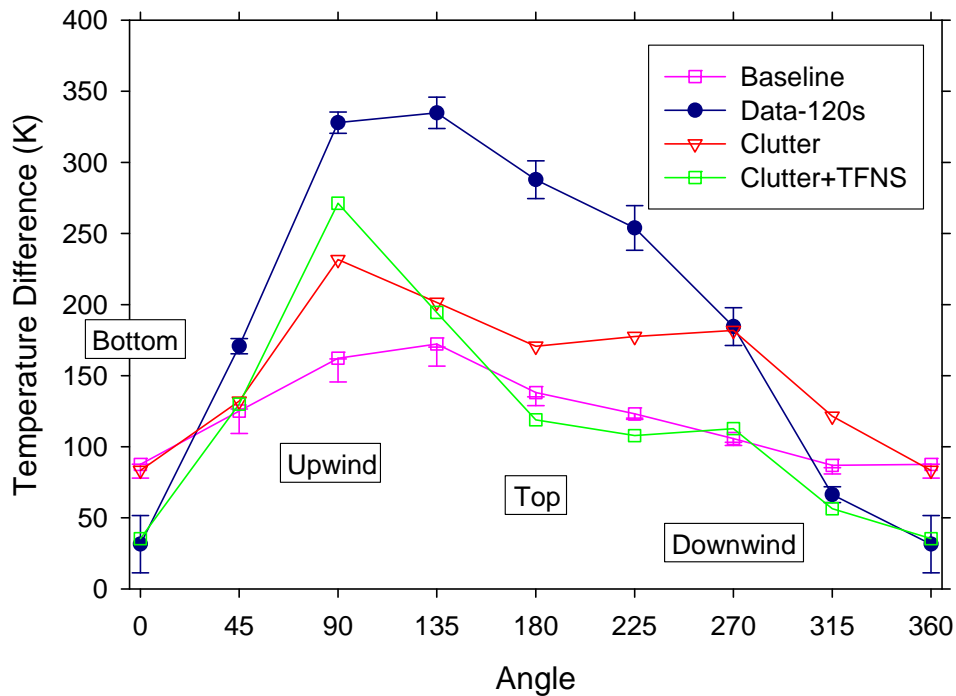
Figure 7-3 Calorimeter 3 predictions for the clutter mesh

The TFNS results with the mesh that includes the clutter for Calorimeter 1 and 3 are also plotted on Figure 7-2 and Figure 7-3. While the standard k-epsilon resulted in worse predictions than the baseline case for Calorimeter 1, the TFNS model predictions compared very well with the data. Further, Calorimeter 3 results appear to approach the measured data much better than any of the formerly presented predictions. The peak temperature is still under-predicted by ~60 degrees, but the low temperature prediction is very good. The qualitative agreement is moderately good, with low and high temperatures predicted at the correct position on the calorimeter, but the quantitative results still differ by several hundred degrees at some locations.

Examining the predicted radiative flux for these cases at the measurement location on the C/MF, the predictions with the modified mesh are in improved agreement with the measurements. Figure 7-4 shows the predicted radiative flux for the k-epsilon and TFNS simulations on the mesh with clutter. The magnitude of the radiative flux is much closer to the value estimated for this parameter from the measurements.
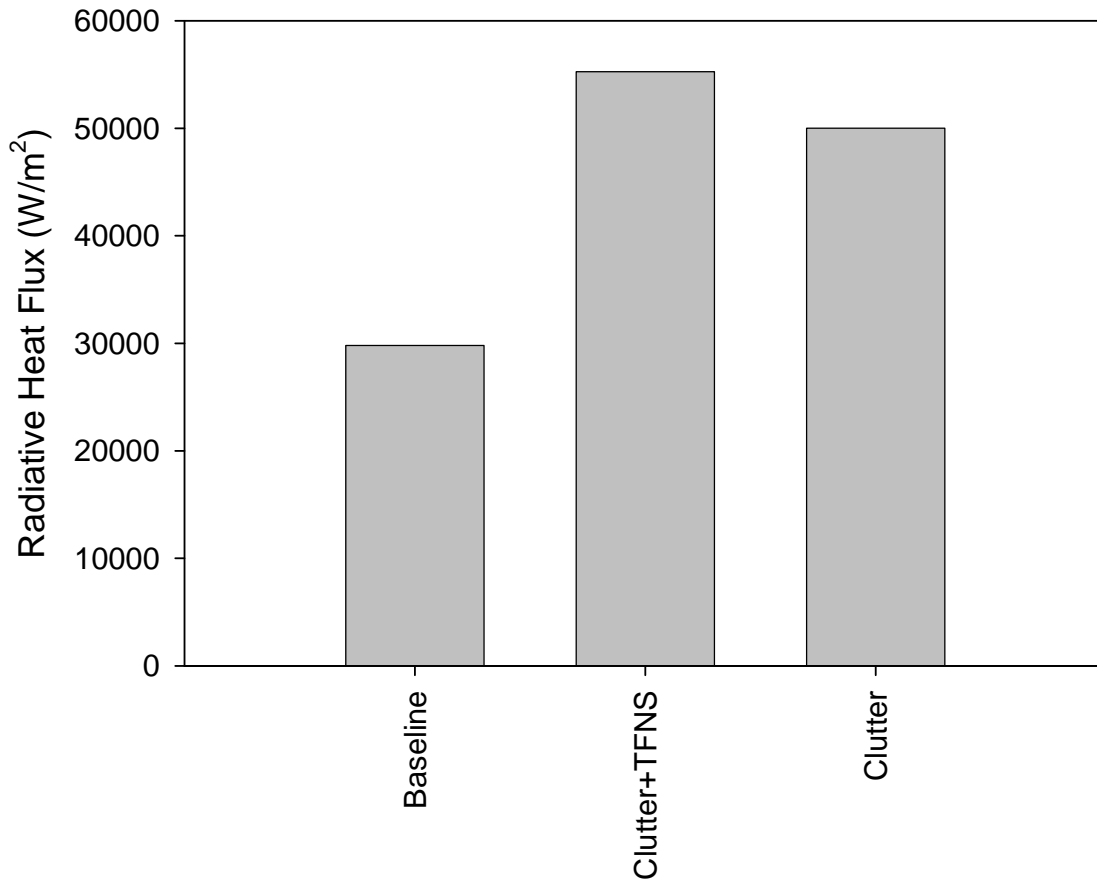
Figure 7-4 Predicted heat flux to the bottom of the C/MF

Close examination of the C/MF predictions for the TFNS case resulted in an interesting observation. The predicted convective heat transfer coefficient is plotted in Figure 7-5 for the TFNS case. The coefficient is more than an order of magnitude below that predicted for the baseline case (as found in Figure 4-32). Consulting a heat transfer reference table (Holman, 1990), a value of 5 W/m^2K is that typical of a free convection problem. Clearly this is an under-prediction of the convective heat transfer coefficient. The listed reference value from the same table for forced convection at 35 m/s over a flat plate is 75 W/m^2K. Based on these values, it appears that the k-epsilon model tends to over-predict the convection (maybe 2-3 times) at this point. The TFNS model results in convective heat transfer coefficients that are about an order of magnitude below the expected values. This discrepancy is curious, since the equations for predicting the coefficient are identical for each turbulence model. Predicted velocities, densities, and temperatures at this location are approximately the same. The difference therefore is attributable to the dramatic difference in the predicted turbulence parameters at that location. It seems that the treatment of the wall boundaries in the TFNS model neglects some important physics that need to be included before this model is used for scenarios of this type for which convection is important. This point has been raised, and will

be addressed in future versions of the TFNS model. Since this mesh was likely under-resolved, this could be an aggravating factor.
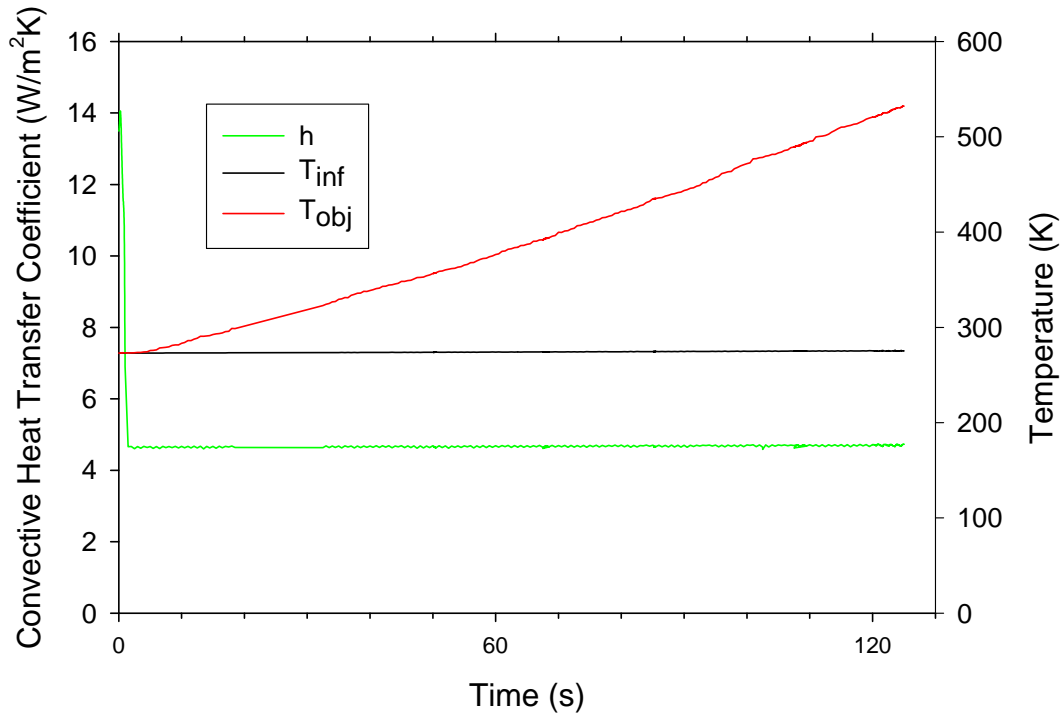
Figure 7-5 Predicted C/MF convection coefficient for the TFNS simulation

7-4. Summary and Discussion

A principal finding from this follow-up investigation is that the assumptions that were originally employed to model this particular scenario were a major contributor to the lack of agreement between the model and the experiment. Ignoring the many small objects that were placed in the vicinity of the fuel pool in these tests has been shown to be a very significant assumption. Although many factors contribute to the decision to ignore these features, the most significant reason is because there is insufficient compute resource to practically model a scenario with peak dimensions on the order of 10^2-10^3 m and resolve features on a 10^{-1}-10^{-3} m scale using a mesh based approach. It may never be practical to explicitly model scale differences as large as are found in this problem. The mesh refinement study detailed in Appendix B suggests that an object must be modeled with several nodes to approach the refined solution to the pressure drop and the velocity field. Other small time scale and length scale physical phenomena that occur in fires are modeled by employing sub-mesh assumptions, like the flame sheet, small scale turbulence, wall roughness, and chemical reactions. No current model presently exists that will allow a sub-model to predict the effect of minor geometry that cannot be modeled on the grid. The results of this study seem to suggest the importance of developing and including such a model in future versions of the code.

A challenge in this case was having to re-mesh the geometry to include some minor geometric changes. Employing an alpha version of cubit was required to do this to avoid having to throw away the original mesh. The feature that was used is an advanced feature. Without it, several weeks might have been expended making the mesh changes for the new geometry. With the advanced feature, the effort was reduced to several days worth of work. Future work will likely require parametrically varying geometry to understand sensitivities. Even the 2-day effort per variation is prohibitive to working such a problem with on the order of a dozen variations. Clearly, there are advances that can be made in the way the geometry is decomposed to a mesh that will enhance the ability to solve these problems in the future.

Resolving small features on a mesh might not be the only solution to this problem. The features modeled were experimental measurement devices. The thermocouple poles were not required to be in the fire as part of the test. Development of less invasive measurement methods might provide improved data while not impacting the experiment. Design of future tests should consider the invasive potential of the measurement device relative to the significance of the expected data when determining whether to include the instrumentation. Calculation tools like fuego might be helpful in defining this relationship if pre-test simulations are employed to design a test.

The follow-up work reported in this chapter helps explain the discrepancies found between the model and the experiment in the original study. While not completely resolving the differences, it is clear that the minor geometry ignored in the original study was a major reason behind the poor comparisons. It is not clear that the findings are universal for all wind velocities. The tests that were compared involved nominally 13 m/s wind speed (~29 mph), which is a very fast wind. It is possible for lower wind speeds that the objects that have been found to be significant might be less so.

The results using the standard k-epsilon model with the modified grid show a clear improvement in predictions for Calorimeter 3. This is at the expense of the excellent predictions on Calorimeter 1. Peak temperatures are increased on both Calorimeter 1 and 3. While predictions using the original geometry with Calorimeter 1 were good, they became poor as the peak temperature was significantly over-predicted. Calorimeter 3 predictions were substantially improved. The temperature difference between the maximum and minimum for Calorimeter 3 was closer to the measured value by nearly 100 ºC. The radiative flux prediction to the bottom of the culvert was clearly improved with the geometric modification to the mesh.

The comparisons between data and simulation were clearly improved when the TFNS was employed with the modified geometry. Calorimeter 1 predictions were slightly closer to the data than they were for the excellent predictions given in the original baseline case. Calorimeter 3 predictions still exhibited substantial differences, but the peak predicted temperature was within 100 ºC of the measurement, and the low predicted temperature was almost identical to the measurement. This was not the case for any of the previous simulations. The radiative heat flux prediction to the bottom of the culvert was also very close to the value extracted from the measurements.

While evidence presented herein may suggest the resounding success of the TFNS model compared to the standard k-epsilon model, the enthusiasm for this model must be tempered by several considerations. The resolution required to resolve a case with this type of turbulence model is much higher than for the standard k-epsilon model. This case was under-resolved based on rules of thumb employed by the calculation team. It is not understood how the results would change if improved resolution were possible for this case. Also, the transient nature of the predictions is expected to necessitate increased attention to the convergence of the equations between time steps. In this case, three picard loops were employed for the TFNS case without studying the convergence with respect to this assumption. Future work would benefit from more detailed investigation of this relationship between convergence, the TFNS model and the number of non-linear iterations take per time step. It is also known that the convection heat transport is significantly underestimated in this case. Inputting the turbulence at the inlet boundary condition is more involved for the TFNS model than for the standard k-epsilon model. In this case, there was insufficient information in this regard such that each model may have been equally bad in this respect. This merits future investigation.

8. Conclusions

The most significant results of this study are related to the knowledge gained related to how simulations should be performed for the class of problem that is being examined. This case is a practical case that is difficult to assess experimentally due to the size, cost, and scope. Results related to the uncertainties in the simulations for this class of problems have also been presented. This work has also elucidated several properties of the code, both in functionality and in capability, that were observed that may require improvement as development efforts continue. As with proper validation efforts, the results of this study also address confidence in the simulation tool. Some of the more significant conclusions are summarized in the bullet list below:

- Small geometry can be very difficult to model and very significant to fire code predictions. Increased development effort to support this class of problem would be beneficial to an analyst attempting to understand a problem with similar features. Helpful development to resolving this difficulty could occur in mesh generation, subgrid models, and experimental investigations.
- Solving this class of problems is resource intensive.
- It is difficult to estimate the importance of modeling parameters without parametric evaluations. Improved test matrices could provide improved understanding of parametric uncertainties.
- The predictions with the k-epsilon model were demonstrated to be only modestly sensitive to the mesh resolution employed in this study.
- The set of parameters considered for this study omitted geometric uncertainties and fuel source (regression rate) term uncertainties. Each of these is probably more important than the combined importance of all the other parameters that were included. Other studies suggest a greater degree of importance of these parameters. The importance of a parameter may be functionally related to the nature of the scenario (e.g. the wind velocity).
- The discretization study suggests the cases were neither grid resolved, nor time step resolved. Improved resolution did not result in substantial changes in trends, rather it affected the quantitative results by a moderate amount. Resource was not available to test at higher resolutions. It may not be possible or pragmatic to fully resolve many practical cases.
- The discrete ordinates quadrature order assumed for this case was adequate for this scenario based on the magnitude of the change induced in thermocouple temperature predictions employing a higher quadrature order. For cases with points of interest removed from the fire region, it may be necessary to increase the quadrature order to resolve the fluxes correctly.
- Picard looping with two global loops per time step should be avoided in present versions of Fuego. Results from this case were otherwise quite insensitive the number of non-linear sub-iterations taken per time step. The qualitative effect of using 2 picard loops was minimal, and the quantitative effect was on the order of the effect of the discretization uncertainties.

- The simulation that resulted in the best comparison with the data is the case with the TFNS turbulence model and the clutter. The mesh was under-resolved for doing quantitative TFNS calculations based on experience with other cases.
- The TFNS turbulence model shows promise for modeling fire scenarios. Mesh resolution requirements will probably necessitate continued use of the k-epsilon model for many practical cases. The predicted convective heat transfer coefficient for the TFNS case requires further investigation.
- When designing tests and simulating cases, it is important to consider all details of the geometry of the test.
- Calorimetry is a reliable way of assessing a fire environment. Of the hundreds of data channels employed, the embedded thermocouple readings were the most reliable and the easiest to compare to calculation. The ability to make the comparisons is enhanced due to the new conjugate transport coupling capabilities present in the code.
- Data exist at other velocities. A similar detailed comparison with these data should be an interesting companion study to this one that was focused on the 13 m/s velocity condition.
- The development of integral scale validation data requires a strong synergistic effort between modelers and experimentalists. Meaningful comparison between the computational and experimental results requires careful characterization, interpretation and control of the experimental features or parameters used as inputs into the computational model.
- Formal methodologies for the validation of computational models have been developed at SNL and are being followed here. Employing these practices should lead to a quality level of validation here-to-for unavailable in the fire modeling community.

9. References

Blanchat, T.K., and Humphries, L.L., Gill, W., "Sandia Heat Flux Gauge Thermal Response and Uncertainty Models," *Thermal Measurements: The Foundation of Fire Standards, ASTM STP 1427*, L. A. Gritzo and N. J. Alvarez, Eds., American Society for Testing and Materials, West Conshohocken, PA, 2002.

Coleman, H.W., and Steele, W.G., Experimentation and Uncertainty Analysis for Engineers Second Edition, John Wiley & Sons, Inc., 1999.

Holman, J.P., Heat Transfer, Seventh Edition, McGraw Hill, Inc., 1990.

Lam, C.S., Thermal Characterization of a Pool Fire in Crosswind with a Large Adjacent Cylindrical Object: Experimental Design, M.S. thesis, University of Waterloo, Ontario, Canada, Dpt. of Mechanical Engineering, 2003.

Lam, C.S., E.J. Weckman, A.L. Brown, W. Gill, "Measurement of heat flux from fires," HT-FED2004-56896, 2004 ASME Heat Transfer/Fluids Engineering Summer Conference, July 11–15, 2004, Charlotte, North Carolina USA.

Nakos, J. T., "Uncertainty Analysis of Thermocouple Measurements Used in Normal and Abnormal Thermal Environment Experiments at Sandia's Radiant Heat Facility and Lurance Canyon Burn Site", SAND2004-1023, Sandia National Laboratories, Albuquerque, NM 87185-1135, 2004

Nakos, J.T., A.L. Brown, W.D. Sundberg, S.R. Tieszen, "Experimental Data and Model Predictions from a Series of Storage Igloo Fire Experiments," SAND report in progress, 2005.

Randsalu, E.J., C.S. Lam, E.J. Weckman, A.L. Brown, W. Gill, "Measurement of fuel regression rates in a jet fuel pool fire in crosswind," HT-FED2004-56888, 2004 ASME Heat Transfer/Fluids Engineering Summer Conference, July 11–15, 2004, Charlotte, North Carolina USA

Theory Manual: SIERRA/Fuego Theory Manual-Version 2.0, December 10, 2002, Sandia National Laboratories.

Tieszen, S.R., S.P. Domino, A.R. Black, "Validation of a Simple Turbulence Model Suitable for Closure of Temporally-Filtered Navier-Stokes Equations Using a Helium Plume," Sandia National Laboratories, Albuquerque, NM, SAND2005-3210, 2005.

Trucano, T.G., Pilch, M., and Oberkampf, W.L., "General Concepts for Experimental Validation of ASCI Code Applications," SAND2002-0341, March, 2002.

Users Manual: SIERRA/Fuego Users Manual-Version 2.0, September 1, 2004, Sandia National Laboratories.

Verification Manual: SIERRA/Fuego Verification Documentation, May 15, 2003, Sandia National Laboratories[2].

Weisinger, J.E.; E.J. Weckman "Characterization of Wind Generation System at the University of Waterloo Live Fire Research Facility," University of Waterloo, December, 2003.

Weisinger, J.E., S.A.Sc. Thesis, University of Waterloo, Waterloo, Ontario, Canada, 2004.

Zepper, J., Aragon, K., Ellis, M., Byle, K., and Eaton, D., "ASCI Applications Software Quality Engineering Practices," SAND2002-0121, Sandia National Laboratories, Albuquerque, NM, 2005

---

[2] At the time of publication the living document that is the verification manual was available on a web site internal to Sandia National Laboratories:
http://scico.sandia.gov/fuego/votd/votdFuegoSyrinxVerificationManual.pdf

10.   Appendix

Appendix A. A listing of the baseline calculation input files

The input File:

```
BEGIN SIERRA FUEGO


  TITLE Waterloo problem with calorimeters, fire, pmr, conjugate HT.

$=================================================================
$
$  Assign material properties to element blocks here.
$
$=================================================================

  BEGIN FINITE ELEMENT MODEL calorim
    Database Name = 0l/wtl_cals_New_hollow_3-04.par
    Database Type = EXODUSII

    BEGIN PARAMETERS FOR BLOCK block_1
      MATERIAL stainless_fiber
    END    PARAMETERS FOR BLOCK block_1
  END   FINITE ELEMENT MODEL calorim

  BEGIN FINITE ELEMENT MODEL culvert
    Database Name = 0l/culvert_6_3css_thin.par
    Database Type = EXODUSII

    BEGIN PARAMETERS FOR BLOCK block_1
      MATERIAL steel_mod
    END    PARAMETERS FOR BLOCK block_1
  END   FINITE ELEMENT MODEL culvert

  BEGIN FINITE ELEMENT MODEL floor
    Database Name = 0l/wtl_Floor_New_Pan_3-04.par
    Database Type = EXODUSII

    BEGIN PARAMETERS FOR BLOCK block_1
      MATERIAL brick
    END    PARAMETERS FOR BLOCK block_1
  END   FINITE ELEMENT MODEL floor


  BEGIN FINITE ELEMENT MODEL radiation
    Database Name = 0l/waterloo_stands_75k_expand.par
    Database Type = EXODUSII

    BEGIN PARAMETERS FOR BLOCK block_1
      MATERIAL radiation_material
    END    PARAMETERS FOR BLOCK block_1
  END   FINITE ELEMENT MODEL radiation

  BEGIN FINITE ELEMENT MODEL fluid
    Database Name = 0l/waterloo_stands_605k_expand.par
    Database Type = EXODUSII

    BEGIN PARAMETERS FOR BLOCK block_1
      MATERIAL gas
    END    PARAMETERS FOR BLOCK block_1
  END   FINITE ELEMENT MODEL fluid

  BEGIN FINITE ELEMENT MODEL output_plane
    Database Name = 0l/average_plane.par
    Database Type = EXODUSII

    BEGIN PARAMETERS FOR BLOCK block_1
      MATERIAL gas
    END    PARAMETERS FOR BLOCK block_1
  END   FINITE ELEMENT MODEL output_plane



$=================================================================
$
$  Define a material property set here.
$  Constant values must still be entered as functions.
$
$=================================================================
  BEGIN PROPERTY SPECIFICATION FOR MATERIAL radiation_material
    ABSORPTIVITY COEFFICIENT FUNCTION = abs_fun
    SCATTERING COEFFICIENT FUNCTION = scat_fun
  END    PROPERTY SPECIFICATION FOR MATERIAL radiation_material

  BEGIN PROPERTY SPECIFICATION FOR MATERIAL steel_mod
    DENSITY       = 7.801   $gm/cm^3 = 7801 kg/m^3
    SPECIFIC HEAT = 4.73e6  $erg/g-k = 476 J/kg-k
    CONDUCTIVITY  = 4.3e6 $erg/s-cm-K = 43 W/m-k
  END    PROPERTY SPECIFICATION FOR MATERIAL steel_mod

  BEGIN PROPERTY SPECIFICATION FOR MATERIAL stainless_fiber
    DENSITY       = 7.801   $gm/cm^3 = 7801 kg/m^3
    SPECIFIC HEAT = 4730.e3  $erg/g-k = 476 J/kg-k
    CONDUCTIVITY  = 4.3e6 $erg/s-cm-K = 43 W/m-k
  END    PROPERTY SPECIFICATION FOR MATERIAL stainless_fiber

  BEGIN PROPERTY SPECIFICATION FOR MATERIAL brick    $<--Im still working
to verify these
    DENSITY       = 0.497   $gm/cm^3 = 497 kg/m^3
    SPECIFIC HEAT = 8.4e6  $erg/g-k = 840 J/kg-k
    CONDUCTIVITY  = 2.e4 $erg/s-cm-K = 0.2 W/m-k
```

```
  END    PROPERTY SPECIFICATION FOR MATERIAL brick

  BEGIN PROPERTY SPECIFICATION FOR MATERIAL gas
    CHEMKIN INPUT FILE = chem.inp
    REFERENCE PRESSURE = 1.0          $ atmosphere
    REFERENCE TEMPERATURE = 298.0       $ Kelvin
    REFERENCE MASS FRACTION C12H23 = 0.0  $ this defines the ordering
    REFERENCE MASS FRACTION CO    = 0.0   $ for everywhere else
    REFERENCE MASS FRACTION CO2   = 0.0   $ this defines the ordering
    REFERENCE MASS FRACTION O2    = 0.233 $
    REFERENCE MASS FRACTION H2O   = 0.0   $
    REFERENCE MASS FRACTION H2    = 0.0   $
    REFERENCE MASS FRACTION N2    = 0.767 $

    SCHMIDT NUMBER         = 0.9
    PRANDTL NUMBER         = 0.9
  END    PROPERTY SPECIFICATION FOR MATERIAL gas

  begin definition for function abs_fun
    type is Constant
    begin values
      0.0
    end values
  end   definition for function abs_fun

  begin definition for function scat_fun
    type is Constant
    begin values
      0.0
    end values
  end   definition for function scat_fun

$---------------------------------------------

  begin definition for function emis_fcn_free1
    type is Constant
    begin values
      1.0
    end values
  end   definition for function emis_fcn_free1

  begin definition for function emis_fcn_free.9
    type is Constant
    begin values
      0.9
    end values
  end   definition for function emis_fcn_free.9

  begin definition for function emis_fcn_free.96
    type is Constant
    begin values
      0.96
    end values
  end   definition for function emis_fcn_free.96

  begin definition for function emis_fcn_free.7
    type is Constant
    begin values
      0.7
    end values
  end   definition for function emis_fcn_free.7

  begin definition for function emis_fcn_free.1
    type is Constant
    begin values
      0.1
    end values
  end   definition for function emis_fcn_free.1

  begin definition for function tran_fcn_free0
    type is Constant
    begin values
      0.0
    end values
  end   definition for function tran_fcn_free0

  begin definition for function tran_fcn_free.1
    type is Constant
    begin values
      0.1
    end values
  end   definition for function tran_fcn_free.1

  begin definition for function tran_fcn_free.04
    type is Constant
    begin values
      0.04
    end values
  end   definition for function tran_fcn_free.04

  begin definition for function tran_fcn_free.3
    type is Constant
    begin values
      0.3
    end values
  end   definition for function tran_fcn_free.3
```

```
    begin definition for function tran_fcn_free.9
      type is Constant
      begin values
         0.9
      end values
    end  definition for function tran_fcn_free.9

    begin definition for function tran_fcn_pool
      type is Constant
      begin values
         1.0
      end values
    end  definition for function tran_fcn_pool

    begin definition for function emis_fcn_pool
      type is Constant
      begin values
         0.0
      end values
    end  definition for function emis_fcn_pool

$====================================================================
$
$  Define the global constansts here
$
$====================================================================

    BEGIN GLOBAL CONSTANTS all
      GRAVITY VECTOR = 0.0, 0.0, -980.67 $ cgs units = -9.8067 m/s^2
      K-E TURBULENCE MODEL PARAMETER CMU = 0.09
      K-E TURBULENCE MODEL PARAMETER SIGMA_K = 1.0
      K-E TURBULENCE MODEL PARAMETER SIGMA_E = 1.3
      K-E TURBULENCE MODEL PARAMETER CEPS_1  = 1.45
      K-E TURBULENCE MODEL PARAMETER CEPS_2  = 1.92
      K-E TURBULENCE MODEL PARAMETER CBVG    = 0.35
      K-E TURBULENCE MODEL PARAMETER CEPS_3  = 0.0
$     K-E TURBULENCE MODEL PARAMETER CBVG    = 5.00
$     K-E TURBULENCE MODEL PARAMETER CEPS_3  = 1.3
      TURBULENCE MODEL PRANDTL NUMBER = 0.9
      TURBULENCE MODEL SCHMIDT NUMBER = 0.9
      STEFAN BOLTZMANN CONSTANT = 5.67040e-5 $ erg/(cm^2 s K^4) = 5.6704e-8
W/m^2-K^4
    END  GLOBAL CONSTANTS all


$====================================================================
$
$  Define the linear solver parameters here.
$
$====================================================================

    BEGIN aztec EQUATION SOLVER continuity
      SOLUTION METHOD = gmres
      PRECONDITIONING METHOD =  symmetric-gauss-seidel
      PRECONDITIONING STEPS = 2
      RESTART ITERATIONS = 100
      MAXIMUM ITERATIONS = 250
      RESIDUAL NORM TOLERANCE = 1.0e-4
      RESIDUAL NORM SCALING = R0
    END   aztec EQUATION SOLVER continuity

    BEGIN aztec EQUATION SOLVER scalar
      SOLUTION METHOD = gmres
      PRECONDITIONING METHOD = symmetric-gauss-seidel
      PRECONDITIONING STEPS = 1
      RESTART ITERATIONS = 100
      MAXIMUM ITERATIONS = 250
      RESIDUAL NORM TOLERANCE = 1.0e-4
      RESIDUAL NORM SCALING = R0
$     DEBUG OUTPUT LEVEL = 1
      BC ENFORCEMENT = exact
    END   aztec EQUATION SOLVER scalar

    BEGIN aztec EQUATION SOLVER heat
      SOLUTION METHOD = gmres
      PRECONDITIONING METHOD = symmetric-gauss-seidel
      PRECONDITIONING STEPS = 1
      RESTART ITERATIONS = 100
      MAXIMUM ITERATIONS = 100
      RESIDUAL NORM TOLERANCE = 1.0e-4
      RESIDUAL NORM SCALING = R0
$     DEBUG OUTPUT LEVEL = 1
    END   aztec EQUATION SOLVER heat

    BEGIN aztec EQUATION SOLVER pmr
      SOLUTION METHOD = bicgstab
      PRECONDITIONING METHOD = symmetric-gauss-seidel
      PRECONDITIONING STEPS = 2
      MAXIMUM ITERATIONS = 250
      RESIDUAL NORM TOLERANCE = 1.0e-8
      RESIDUAL NORM SCALING = R0
      DEBUG OUTPUT LEVEL = 0
    END aztec EQUATION SOLVER pmr

    user subroutine file = Afgo_Usub_Template.F

$ Restart Time

      RESTART = automatic

$====================================================================
$
$  Begin the Fuego procedure (integration of equations).
$
$====================================================================

    BEGIN FUEGO PROCEDURE fuego_procedure

$====================================================================
$
$  Define the parameters for time integration over an interval here.
$
$====================================================================
```

```
    begin time control
        BEGIN TIME STEPPING BLOCK  time_block

            START TIME IS   0.0
            TIME STEP = 0.005
            BEGIN PARAMETERS FOR FUEGO REGION fluid_region
              TRANSIENT STEP TYPE IS fixed
$              TRANSIENT STEP TYPE IS automatic
$              CFL LIMIT = 10.0
$              TIME STEP CHANGE FACTOR = 1.5
            END    PARAMETERS FOR FUEGO REGION fluid_region

            BEGIN PARAMETERS FOR FUEGO REGION object_calorim_region
              TRANSIENT STEP TYPE IS fixed
            END    PARAMETERS FOR FUEGO REGION object_calorim_region

            BEGIN PARAMETERS FOR FUEGO REGION object_culvert_region
              TRANSIENT STEP TYPE IS fixed
            END    PARAMETERS FOR FUEGO REGION object_culvert_region

            BEGIN PARAMETERS FOR FUEGO REGION object_floor_region
              TRANSIENT STEP TYPE IS fixed
            END    PARAMETERS FOR FUEGO REGION object_floor_region

        END   TIME STEPPING BLOCK time_block

        TERMINATION TIME IS   0.2e6
    end time control


    VERSION 1.3.0

    TIME START = 0.0, STOP = 365.0, STATUS INTERVAL = 50

$====================================================================
$ define pmr skip variable, i.e., the frequency of each syrinx call
$====================================================================

    SKIP STEPS FOR PMR = 10

$====================================================================
$
$  Set up a transfer
$
$====================================================================
$
$ unpainted calorimeter

    BEGIN TRANSFER Fluid_Object1
      TRANSFER BETWEEN FUEGO FLUID REGION fluid_region SURFACE surface_11
\$
                AND  FUEGO  CONDUCTION  REGION  object_calorim_region  SURFACE
surface_1  \$
                USING interp
      SURFACE GAP TOLERANCE = 25.0
      TRANSFER PROBLEM DEFINITION = CONJUGATE HEAT TRANSFER
    END   TRANSFER Fluid_Object1

$ painted calorimeters

    BEGIN TRANSFER Fluid_Object2
      TRANSFER BETWEEN FUEGO FLUID REGION fluid_region SURFACE surface_12
\$
                AND  FUEGO  CONDUCTION  REGION  object_calorim_region  SURFACE
surface_2  \$
                USING interp
      SURFACE GAP TOLERANCE = 25.0
      TRANSFER PROBLEM DEFINITION = CONJUGATE HEAT TRANSFER
    END   TRANSFER Fluid_Object2

$ calorimeter ends

    BEGIN TRANSFER Fluid_Object3
      TRANSFER BETWEEN FUEGO FLUID REGION fluid_region SURFACE surface_13
\$
                AND  FUEGO  CONDUCTION  REGION  object_calorim_region  SURFACE
surface_3  \$
                USING interp
      SURFACE GAP TOLERANCE = 25.0
      TRANSFER PROBLEM DEFINITION = CONJUGATE HEAT TRANSFER
    END   TRANSFER Fluid_Object3

$ culvert (outer surface)

    BEGIN TRANSFER Fluid_Object5a
      TRANSFER BETWEEN FUEGO FLUID REGION fluid_region SURFACE surface_3
\$
                AND  FUEGO  CONDUCTION  REGION  object_culvert_region  SURFACE
surface_1  \$
                USING interp
      SURFACE GAP TOLERANCE = 25.0
      TRANSFER PROBLEM DEFINITION = CONJUGATE HEAT TRANSFER
    END   TRANSFER Fluid_Object5a

$ culvert ends

    BEGIN TRANSFER Fluid_Object5b
      TRANSFER BETWEEN FUEGO FLUID REGION fluid_region SURFACE surface_21
\$
                AND  FUEGO  CONDUCTION  REGION  object_culvert_region  SURFACE
surface_2  \$
                USING interp
      SURFACE GAP TOLERANCE = 25.0
      TRANSFER PROBLEM DEFINITION = CONJUGATE HEAT TRANSFER
    END   TRANSFER Fluid_Object5b

$ culvert (inner surface)

    BEGIN TRANSFER Fluid_Object5c
      TRANSFER BETWEEN FUEGO FLUID REGION fluid_region SURFACE surface_22
\$
                AND  FUEGO  CONDUCTION  REGION  object_culvert_region  SURFACE
surface_3  \$
```

```
        USING interp
    SURFACE GAP TOLERANCE = 50.0
    TRANSFER PROBLEM DEFINITION = CONJUGATE HEAT TRANSFER
  END    TRANSFER Fluid_Object5c


$ floor

   BEGIN TRANSFER Fluid_Object6
    TRANSFER BETWEEN FUEGO FLUID REGION fluid_region SURFACE surface_10
\$
           AND  FUEGO  CONDUCTION  REGION  object_floor_region  SURFACE
surface_1  \$
           USING interp
    SURFACE GAP TOLERANCE = 25.0
    TRANSFER PROBLEM DEFINITION = CONJUGATE HEAT TRANSFER
  END    TRANSFER Fluid_Object6

   BEGIN TRANSFER Fluid_PMR
     TRANSFER BETWEEN REGION fluid_region  VOLUME block_1     \$
              AND  REGION pmr_region VOLUME block_1     \$
              USING interp
$              USING copy
      TRANSFER PROBLEM DEFINITION = FIRE
   END    TRANSFER Fluid_PMR

   BEGIN TRANSFER PMR_Object1
    TRANSFER BETWEEN REGION object_calorim_region      SURFACE surface_1
\$
           AND       REGION pmr_region    SURFACE surface_11 \$
           USING interp
    SURFACE GAP TOLERANCE = 25.0
    TRANSFER PROBLEM DEFINITION = CONDUCTION RADIATION
  END    TRANSFER PMR_Object1

   BEGIN TRANSFER PMR_Object2
    TRANSFER BETWEEN REGION object_calorim_region      SURFACE surface_2
\$
           AND       REGION pmr_region    SURFACE surface_12 \$
           USING interp
    SURFACE GAP TOLERANCE = 25.0
    TRANSFER PROBLEM DEFINITION = CONDUCTION RADIATION
  END    TRANSFER PMR_Object2

   BEGIN TRANSFER PMR_Object3
    TRANSFER BETWEEN REGION object_calorim_region      SURFACE surface_3
\$
           AND       REGION pmr_region    SURFACE surface_13 \$
           USING interp
    SURFACE GAP TOLERANCE = 25.0
    TRANSFER PROBLEM DEFINITION = CONDUCTION RADIATION
  END    TRANSFER PMR_Object3

   BEGIN TRANSFER PMR_Object5a
    TRANSFER BETWEEN REGION object_culvert_region      SURFACE surface_1
\$
           AND       REGION pmr_region    SURFACE surface_3 \$
           USING interp
    SURFACE GAP TOLERANCE = 25.0
    TRANSFER PROBLEM DEFINITION = CONDUCTION RADIATION
  END    TRANSFER PMR_Object5a

   BEGIN TRANSFER PMR_Object5b
    TRANSFER BETWEEN REGION object_culvert_region      SURFACE surface_2
\$
           AND       REGION pmr_region    SURFACE surface_21 \$
           USING interp
    SURFACE GAP TOLERANCE = 25.0
    TRANSFER PROBLEM DEFINITION = CONDUCTION RADIATION
  END    TRANSFER PMR_Object5b

   BEGIN TRANSFER PMR_Object5c
    TRANSFER BETWEEN REGION object_culvert_region      SURFACE surface_3
\$
           AND       REGION pmr_region    SURFACE surface_22 \$
           USING interp
    SURFACE GAP TOLERANCE = 50.0
    TRANSFER PROBLEM DEFINITION = CONDUCTION RADIATION
  END    TRANSFER PMR_Object5c

   BEGIN TRANSFER PMR_Object6
    TRANSFER BETWEEN REGION object_floor_region      SURFACE surface_1  \$
           AND       REGION pmr_region    SURFACE surface_10 \$
           USING interp
    SURFACE GAP TOLERANCE = 25.0
    TRANSFER PROBLEM DEFINITION = CONDUCTION RADIATION
  END    TRANSFER PMR_Object6

   BEGIN TRANSFER average1
     TRANSFER BETWEEN REGION fluid_region VOLUME block_1      \$
              AND REGION average_region VOLUME block_1  \$
              USING interp
     TRANSFER PROBLEM DEFINITION = AVERAGE
  END    TRANSFER average1

$   BEGIN TRANSFER average2
$     TRANSFER BETWEEN REGION pmr_region VOLUME block_1      \$
$              AND REGION average_region VOLUME block_1  \$
$              USING interp
$
$     TRANSFER PROBLEM DEFINITION = AVERAGE
$     TRANSFER TIMERS ON
$   END    TRANSFER average2


   BEGIN FUEGO REGION object_calorim_region

$====================================================================
$
$ Select the math model configuration for this run.
$
$====================================================================

     OPTIONS ARE heat conduction
```

```
$====================================================================
$
$  Select the mesh, defined at the Domain level.
$
$====================================================================

         USE FINITE ELEMENT MODEL calorim

$====================================================================
$
$  Select the linear solvers for the different equation sets.
$
$====================================================================

         USE EQUATION SOLVER heat FOR EQUATION SET t

$====================================================================
$
$  Define the nonlinear solver parameters.
$
$====================================================================

         NONLINEAR RESIDUAL PLOTFILE = calorim.res

         MINIMUM NUMBER OF NONLINEAR ITERATIONS = 1
         MAXIMUM NUMBER OF NONLINEAR ITERATIONS = 2

         FIND MAXIMUM RESIDUALS

$====================================================================
$
$  Begin the definition of the contents of the plot file
$  for this region.
$
$====================================================================

         Begin Results Output Label output
            DATABASE Name = calorim.e
            At Step 0,  Increment = 1000
            TITLE Conduction in a solid block
            NODAL Variables = temperature AS TObjnd
            NODAL Variables = incident_flux AS G
         End   Results Output Label output

$====================================================================
$
$  Begin the heartbeat output for this region
$
$====================================================================
$ Calorim1
         Begin Heartbeat Output out_2
            Stream Name is calorim1.txt
            Variable is Global time as Time
            Variable is Node Temperature at Node 35969 as T1
            Variable is Node Temperature at Node 35957 as T2
            Variable is Node Temperature at Node 33246 as T3
            Variable is Node Temperature at Node 36025 as T4
            Variable is Node Temperature at Node 36014 as T5
            Variable is Node Temperature at Node 36002 as T6
            Variable is Node Temperature at Node 35991 as T7
            Variable is Node Temperature at Node 35980 as T8
            At Time 0.0 Interval is 0.01
            At Time 1.0 Interval is 0.5
            At Time 120.0 Interval is 0.005
            Termination Time is 360.0
         End Heartbeat Output out_2
$ Calorim2
         Begin Heartbeat Output out_3
            Stream Name is calorim2.txt
            Variable is Global time as Time
            Variable is Node Temperature at Node 80609 as T1
            Variable is Node Temperature at Node 80597 as T2
            Variable is Node Temperature at Node 77886 as T3
            Variable is Node Temperature at Node 80665 as T4
            Variable is Node Temperature at Node 80654 as T5
            Variable is Node Temperature at Node 80642 as T6
            Variable is Node Temperature at Node 80631 as T7
            Variable is Node Temperature at Node 80620 as T8
            At Time 0.0 Interval is 0.01
            At Time 1.0 Interval is 0.5
            At Time 120.0 Interval is 0.005
            Termination Time is 360.0
         End Heartbeat Output out_3

$====================================================================
$
$  Begin the definition of the restart file
$  for this region.
$
$====================================================================

         Begin Restart Data restart
            Input Database Name = calorim.rsout-s0002
            Output Database Name = calorim.rsout
            At Step 500 Increment = 500
         End Restart Data restart

$====================================================================
$
$  Set the initial condition for this region.
$
$====================================================================

         Begin Initial Condition Block Calorimeter
            volume is block_1
            temperature = 273.0
         End   Initial Condition Block Calorimeter

$====================================================================
$
```

```
$  Define the boundary conditions for this region.                                    At Step 500 Increment = 500
$                                                                                   End Restart Data restart
$==================================================================
                                                                         $==================================================================
      $ Calorimeter surface1 - unpainted calorimeter                     $
      begin interface boundary condition on surface surface_1            $  Set the initial condition for this region.
        emissivity = 0.7                                                 $
        $                                                                $==================================================================
        $  this is the boundary where conjugate heat transfer occurs
        $                                                                      Begin Initial Condition Block Culvert
      end   interface boundary condition on surface surface_1                   volume is block_1
                                                                                temperature = 273.0
      $ Calorimeter surface2 - painted calorimeters                            End   Initial Condition Block Culvert
      begin interface boundary condition on surface surface_2
        emissivity = 0.96                                               $==================================================================
        $                                                                $
        $  this is the boundary where conjugate heat transfer occurs     $  Define the boundary conditions for this region.
        $                                                                $
      end   interface boundary condition on surface surface_2            $==================================================================

      $ Calorimeter surface3 - calorimeter end surfaces                       $ Culvert (Outer Surface)
      begin interface boundary condition on surface surface_3                 begin interface boundary condition on surface surface_1
        emissivity = 0.1                                                        emissivity = 0.9
        $                                                                        $
        $  this is the boundary where conjugate heat transfer occurs             $  this is the boundary where conjugate heat transfer occurs
        $                                                                        $
      end   interface boundary condition on surface surface_3                  end   interface boundary condition on surface surface_1

   END    FUEGO REGION object_calorim_region                                  $ Culvert Ends
                                                                              begin interface boundary condition on surface surface_2
                                                                                emissivity = 0.9
   BEGIN FUEGO REGION object_culvert_region                                     $
                                                                                $  this is the boundary where conjugate heat transfer occurs
$==================================================================              $
$                                                                              end   interface boundary condition on surface surface_2
$  Select the math model configuration for this run.
$                                                                              $ Culvert (Inner Surface)
$==================================================================            begin interface boundary condition on surface surface_3
                                                                                emissivity = 0.9
      OPTIONS ARE heat conduction                                               $
                                                                                $  this is the boundary where conjugate heat transfer occurs
                                                                                $
$==================================================================            end   interface boundary condition on surface surface_3
$                                                                         END    FUEGO REGION object_culvert_region
$  Select the mesh, defined at the Domain level.
$
$==================================================================         BEGIN FUEGO REGION object_floor_region

      USE FINITE ELEMENT MODEL culvert                                  $==================================================================
                                                                         $
$==================================================================      $  Select the math model configuration for this run.
$                                                                         $
$  Select the linear solvers for the different equation sets.            $==================================================================
$
$==================================================================            OPTIONS ARE heat conduction

      USE EQUATION SOLVER heat FOR EQUATION SET t
                                                                         $==================================================================
                                                                         $
$==================================================================      $  Select the mesh, defined at the Domain level.
$                                                                         $
$  Define the nonlinear solver parameters.                               $==================================================================
$
$==================================================================            USE FINITE ELEMENT MODEL floor

      NONLINEAR RESIDUAL PLOTFILE = culvert.res                         $==================================================================
                                                                         $
      MINIMUM NUMBER OF NONLINEAR ITERATIONS = 1                         $  Select the linear solvers for the different equation sets.
      MAXIMUM NUMBER OF NONLINEAR ITERATIONS = 2                         $
                                                                         $==================================================================
      FIND MAXIMUM RESIDUALS
                                                                               USE EQUATION SOLVER heat FOR EQUATION SET t

$==================================================================
$                                                                         $==================================================================
$  Begin the definition of the contents of the plot file                 $
$  for this region.                                                       $  Define the nonlinear solver parameters.
$                                                                         $
$==================================================================      $==================================================================

      Begin Results Output Label output                                        NONLINEAR RESIDUAL PLOTFILE = floor.res
        DATABASE Name = culvert.e
        At Step 0, Increment = 1000                                            MINIMUM NUMBER OF NONLINEAR ITERATIONS = 1
        TITLE Conduction in a solid block                                      MAXIMUM NUMBER OF NONLINEAR ITERATIONS = 2
        NODAL Variables = temperature AS TObjnd
        NODAL Variables = incident_flux AS G                                   FIND MAXIMUM RESIDUALS
      End   Results Output Label output

$ Output for culvert                                                     $==================================================================
    Begin Heartbeat Output out_culv                                      $
      Stream Name is solid.txt                                           $  Begin the definition of the contents of the plot file
      Variable is Global time as Time                                    $  for this region.
      Variable is Node Temperature at Node 1405 as T                     $
      Variable is Node incident_flux at Node 1405 as G                   $==================================================================
      Variable is Node convection_coefficient at node 1405 as hcon
      Variable is Node convection_temperature at Node 1405 as Tinf             Begin Results Output Label output
      At Time 0.0 Interval is 0.01                                              DATABASE Name = floor.e
      At Time 1.0 Interval is 0.5                                               At Step 0, Increment = 1000
      At Time 120.0 Interval is 0.005                                          TITLE Conduction in a solid block
      Termination Time is 360.0                                                NODAL Variables = temperature AS TObjnd
    End Heartbeat Output out_culv                                             NODAL Variables = incident_flux AS G
                                                                             End   Results Output Label output

$==================================================================
$                                                                         $==================================================================
$  Begin the definition of the restart file                              $
$  for this region.                                                       $  Begin the definition of the restart file
$                                                                         $  for this region.
$==================================================================      $
                                                                         $==================================================================
      Begin Restart Data restart
        Input Database Name = culvert.rsout-s0002                              Begin Restart Data restart
        Output Database Name = culvert.rsout                                    Input Database Name = floor.rsout-s0002
                                                                                Output Database Name = floor.rsout
                                                                                At Step 500 Increment = 500
```

134

```
      End Restart Data restart

$=================================================================
$
$  Set the initial condition for this region.
$
$=================================================================

      Begin Initial Condition Block Floor
         volume is block_1
         temperature = 273.0
      End    Initial Condition Block Floor

$=================================================================
$
$  Define the boundary conditions for this region.
$
$=================================================================

      $ Floor
      begin interface boundary condition on surface surface_1
         emissivity = 0.9
         $
         $  this is the boundary where conjugate heat transfer occurs
         $
      end    interface boundary condition on surface surface_1

      $ Interface of floor conduction region with environment, consisting
      $ of sides and bottom of fuel pan, floor contact with earth below,
      $ and on edges around perimeter of facility.

      begin fixed boundary condition on surface surface_2

         temperature = 273.0

      end    fixed boundary condition on surface surface_2

    END    FUEGO REGION object_floor_region


    BEGIN AVERAGE REGION average_region
$=================================================================
$
$  Select the math model configuration for this run.
$
$=================================================================

      OPTIONS ARE fluid flow, turbulent, thermal, \$
                  enthalpy form, nonuniform, Fire
      NUMBER OF SPECIES IS 7

$=================================================================
$
$  Select the mesh, defined at the Domain level.
$
$=================================================================

      USE FINITE ELEMENT MODEL output_plane

$=================================================================
$
$  Begin the definition of the contents of the plot file
$  for this region.
$
$=================================================================

      USE RADIATION SOURCE FROM EXTERNAL REGION
      Begin Results Output Label output
        DATABASE Name = average.e
        At Step 0, Increment = 20
        At Step 12000, Increment = 200
        TITLE WaterlooFacilityCutplane
        NODAL Variables = pressure       AS Press_nd
        NODAL Variables = x_velocity     AS U_nd
        NODAL Variables = y_velocity     AS V_nd
        NODAL Variables = z_velocity     AS W_nd
        NODAL Variables = turbulent_ke   AS TKE_nd
        NODAL Variables = turbulent_diss AS Eps_nd
        NODAL Variables = enthalpy       AS Enth_nd
        NODAL Variables = temperature    AS Temp_nd
        NODAL Variables = mass_fraction  AS Y_nd
        NODAL Variables = soot           AS Soot_nd
        NODAL Variables = nucleate       AS Nuc_nd
        NODAL Variables = edc_rate       AS EDC
        NODAL Variables = absorption     AS Abs_nd
        NODAL Variables = density_nd     As Den_nd
$        NODAL Variables = radiative_flux AS qrad-nd
        NODAL Variables = turb_visc_nd AS TVisc
        End    Results Output Label output


$=================================================================
$
$  Begin the definition of the restart file
$  for this region.
$
$=================================================================

      Begin Restart Data restart_fuego
        Input Database Name = avg_output.rsout-s0002
        Output Database Name = avg_output.rsout
        At Step  500 Increment = 500
      End Restart Data restart_fuego

    END    AVERAGE REGION average_region


    BEGIN SYRINX REGION pmr_region

$=================================================================
$
$  Select the math model configuration for this run.
$
```

```
$=================================================================

      OPTIONS ARE SUPG, ROTATE, DELTA, FIRE, NOLIN

      QUADRATURE ORDER IS 4
      QUADRATURE TYPE  IS  LC_lwemsq

      THIN  LIMIT IS 1.0
      MASS LUMPING COEFFICIENT IS 0.0

      MAXIMUM SOURCE ITERATION = 3
      SOURCE ITERATION CONVERGENCE CRITERIA = 1.0e-7

$=================================================================
$
$  Define the output file
$
$=================================================================

      Begin Results Output Label fire output
        DATABASE Name = waterloo_syrinx.e
        At Step 0, Increment = 1000
$        At Time 0.0, Increment = 0.0
        Title Waterloo Test Facility JP8 Fire With Crosswind and Obstacle

        NODAL Variables = rad_source AS EMSnd
        NODAL Variables = absorption AS ABSnd
        NODAL Variables = radiative_flux AS QRADnd
        NODAL Variables = scalar_flux AS Gnd
        NODAL Variables = incident_flux AS IncFlux
      End Results Output Label fire output


$=================================================================
$
$  Begin the definition of the restart file
$  for this region.
$
$=================================================================

      Begin Restart Data restart
        Input Database Name = waterloo_syrinx.rsout-s0002
        Output Database Name = waterloo_syrinx.rsout
        At Step 500 Increment = 500
      End Restart Data restart

$=================================================================
$
$  Set the mesh and solver
$
$=================================================================

      use finite element model radiation
      use linear solver pmr

$=================================================================
$
$  Set the boundary conditions
$
$=================================================================

      $entrainment
      begin gray diffuse boundary condition on surface surface_1
         emissivity function   = emis_fcn_free1
         transmittance function = tran_fcn_free0
      end    gray diffuse boundary condition on surface surface_1

      $outflow
      begin gray diffuse boundary condition on surface surface_5
         emissivity function   = emis_fcn_free1
         transmittance function = tran_fcn_free0
      end    gray diffuse boundary condition on surface surface_5

      $upstream wall
      begin gray diffuse boundary condition on surface surface_4
         emissivity function   = emis_fcn_free.9
         transmittance function = tran_fcn_free.1
      end    gray diffuse boundary condition on surface surface_4

      $downstream wall
      begin gray diffuse boundary condition on surface surface_2
         emissivity function   = emis_fcn_free.9
         transmittance function = tran_fcn_free.1
      end    gray diffuse boundary condition on surface surface_2

      $pool
      begin gray diffuse boundary condition on surface surface_6
         emissivity function   = emis_fcn_pool
         transmittance function = tran_fcn_pool
         environment temperature = 488.0
      end    gray diffuse boundary condition on surface surface_6

      $floor - CHT region
      begin gray diffuse boundary condition on surface surface_10
         emissivity function   = emis_fcn_free.9
         transmittance function = tran_fcn_free.1
         environment temperature = 488.0
      end    gray diffuse boundary condition on surface surface_10

      $side wall (min y)
      begin gray diffuse boundary condition on surface surface_7
         emissivity function   = emis_fcn_free.9
         transmittance function = tran_fcn_free.1
      end    gray diffuse boundary condition on surface surface_7

      $side wall (max y)
      begin gray diffuse boundary condition on surface surface_9
         emissivity function   = emis_fcn_free.9
         transmittance function = tran_fcn_free.1
      end    gray diffuse boundary condition on surface surface_9

      $roof
      begin gray diffuse boundary condition on surface surface_8
```

```
      emissivity function    = emis_fcn_free.9
      transmittance function = tran_fcn_free.1
   end   gray diffuse boundary condition on surface surface_8

   $sideset 20 (calorimeter stand ?? is this the culvert stand??)
   begin gray diffuse boundary condition on surface surface_20
      emissivity function    = emis_fcn_free.9
      transmittance function = tran_fcn_free.1
   end   gray diffuse boundary condition on surface surface_20

   $sideset 19 (calorimeter stand)
   begin gray diffuse boundary condition on surface surface_19
      emissivity function    = emis_fcn_free.9
      transmittance function = tran_fcn_free.1
   end   gray diffuse boundary condition on surface surface_19

   $sideset 18 (calorimeter stand)
   begin gray diffuse boundary condition on surface surface_18
      emissivity function    = emis_fcn_free.9
      transmittance function = tran_fcn_free.1
   end   gray diffuse boundary condition on surface surface_18

   $sideset 17 (downstream offset calorimeter)
   begin gray diffuse boundary condition on surface surface_17
      emissivity function    = emis_fcn_free.9
      transmittance function = tran_fcn_free.1
   end   gray diffuse boundary condition on surface surface_17

   $sideset 16 (downstream offset calorimeter)
   begin gray diffuse boundary condition on surface surface_16
      emissivity function    = emis_fcn_free.9
      transmittance function = tran_fcn_free.1
   end   gray diffuse boundary condition on surface surface_16

   $culvert - CHT region (outer surface)
   begin gray diffuse boundary condition on surface surface_3
      emissivity function    = emis_fcn_free.9
      transmittance function = tran_fcn_free.1
   end   gray diffuse boundary condition on surface surface_3

   $culvert - CHT region (ends)
   begin gray diffuse boundary condition on surface surface_21
      emissivity function    = emis_fcn_free.9
      transmittance function = tran_fcn_free.1
   end   gray diffuse boundary condition on surface surface_21

   $culvert - CHT region (inner surface)
   begin gray diffuse boundary condition on surface surface_22
      emissivity function    = emis_fcn_free.9
      transmittance function = tran_fcn_free.1
   end   gray diffuse boundary condition on surface surface_22

   $calorimeter no. 1 (unpainted calorimeter) - CHT region
   begin gray diffuse boundary condition on surface surface_11
      emissivity function    = emis_fcn_free.7
      transmittance function = tran_fcn_free.3
   end   gray diffuse boundary condition on surface surface_11

   $calorimeter no. 2 (painted calorimeters) - CHT region
   begin gray diffuse boundary condition on surface surface_12
      emissivity function    = emis_fcn_free.96
      transmittance function = tran_fcn_free.04
   end   gray diffuse boundary condition on surface surface_12

   $calorimeter no. 3 (calorimeter ends) - CHT region
   begin gray diffuse boundary condition on surface surface_13
      emissivity function    = emis_fcn_free.1
      transmittance function = tran_fcn_free.9
   end   gray diffuse boundary condition on surface surface_13

   END   SYRINX REGION pmr_region


   BEGIN FUEGO REGION fluid_region

      USE SOLUTION STEERING WITH INTERVAL = 4

$=====================================================================
$
$  Select the math model configuration for this run.
$
$=====================================================================

      OPTIONS ARE fluid flow, turbulent, thermal, \$
                  enthalpy form, nonuniform, Fire

      USE RADIATION SOURCE FROM EXTERNAL REGION

      UPWIND METHOD IS UPW
      FIRST ORDER UPWIND FACTOR = 0.5
      USE ENTHALPY SCALING
      PROJECTION METHOD = smoothed WITH timestep SCALING
$      PROJECTION METHOD = stabilized

$      OMIT NEAR WALL TURBULENT KE TRANSPORT EQUATION
      INCLUDE MOLECULAR VISCOSITY IN K-E DIFFUSION COEFFICIENT
      USE BAROCLINIC VORTICITY GENERATION AT 12.0 SECONDS

$      PROJECTION METHOD = smoothed WITH timestep SCALING
$      USE BAROCLINIC VORTICITY GENERATION AT 8. SECONDS

      NUMBER OF SPECIES IS 7

      EDC FUEL NAME = C12H23
      EDC MINIMUM PRODUCT FRACTION = 1.0e-6
      EDC IGNITION TIME = 0.00
      EDC REACTION TIME SCALE = 70.0e-6   $ this is the default value, too

$      INCLUDE EDC LAMINAR LIMIT MODEL

      USE SINTEF SOOT MODEL
      MINIMUM SOOT PRODUCTION TEMPERATURE = 900.0
```

```
      BUOYANCY MODEL = DIFFERENTIAL
      BUOYANCY REFERENCE TEMPERATURE = 273.0      $ Kelvin
      BUOYANCY REFERENCE MASS FRACTION C12H23 = 0.0
      BUOYANCY REFERENCE MASS FRACTION CO    = 0.0
      BUOYANCY REFERENCE MASS FRACTION CO2   = 0.0
      BUOYANCY REFERENCE MASS FRACTION O2    = 0.233
      BUOYANCY REFERENCE MASS FRACTION H2O   = 0.0
      BUOYANCY REFERENCE MASS FRACTION H2    = 0.0
      BUOYANCY REFERENCE MASS FRACTION N2    = 0.767

$=====================================================================
$
$  Select under relaxations for this run.
$
$=====================================================================

      UNDER RELAX Turbulent Viscosity     by 0.5
      UNDER RELAX Turbulence Dissipation  by 0.5
      UNDER RELAX Turbulent Kinetic Energy by 0.5

      UNDER RELAX Momentum                by 1.0
      UNDER RELAX Pressure                by 1.0
      UNDER RELAX Enthalpy                by 0.5
      UNDER RELAX Species                 by 0.5
      UNDER RELAX Soot                    by 0.5
      UNDER RELAX Nuclei                  by 0.5


$=====================================================================
$
$  Select the mesh, defined at the Domain level.
$
$=====================================================================

      USE FINITE ELEMENT MODEL fluid


$=====================================================================
$
$  Select the linear solvers for the different equation sets.
$
$=====================================================================

      USE EQUATION SOLVER continuity FOR EQUATION SET p
      USE EQUATION SOLVER scalar FOR EQUATION SET u
      USE EQUATION SOLVER scalar FOR EQUATION SET v
      USE EQUATION SOLVER scalar FOR EQUATION SET w
      USE EQUATION SOLVER scalar FOR EQUATION SET k
      USE EQUATION SOLVER scalar FOR EQUATION SET e
      USE EQUATION SOLVER scalar FOR EQUATION SET h
      USE EQUATION SOLVER scalar FOR EQUATION SET y
      USE EQUATION SOLVER scalar FOR EQUATION SET s
      USE EQUATION SOLVER scalar FOR EQUATION SET n

$=====================================================================
$
$  Define the nonlinear solver parameters.
$
$=====================================================================

      NONLINEAR RESIDUAL PLOTFILE = waterloo.res

      MINIMUM NUMBER OF NONLINEAR ITERATIONS = 1
      MAXIMUM NUMBER OF NONLINEAR ITERATIONS = 2
      MAXIMUM NUMBER OF CONTINUITY_MOMENTUM NONLINEAR ITERATIONS = 1
      MAXIMUM NUMBER OF ENERGY NONLINEAR ITERATIONS = 1
      MAXIMUM NUMBER OF ENERGY_SPECIES NONLINEAR ITERATIONS = 2
      MAXIMUM NUMBER OF SPECIES NONLINEAR ITERATIONS = 1
      MINIMUM TEMPERATURE ALLOWED FROM TEMPERATURE EXTRACTION = 260

      FIND MAXIMUM RESIDUALS

$=====================================================================
$
$  Begin the definition of the contents of the plot file
$  for this region.
$
$=====================================================================

      Begin Results Output Label output
         DATABASE Name = waterloo.e
         At Step 0, Increment = 1000
         TITLE Waterloo Test Facility JP8 Fire With Crosswind and Obstacle
         NODAL Variables = pressure AS Press-nd
            NODAL Variables = density_nd AS Den-nd
            NODAL Variables = viscosity_nd AS MU-nd
$           NODAL Variables = conductivity_nd AS CONDnd
         NODAL Variables = x_velocity AS U-nd
         NODAL Variables = y_velocity AS V-nd
         NODAL Variables = z_velocity AS W-nd
         NODAL Variables = turbulent_ke AS TKE-nd
         NODAL Variables = turbulent_diss AS Epsi-nd
$         NODAL Variables = enthalpy AS Enth-nd
         NODAL Variables = temperature AS Temp-nd
         NODAL Variables = mass_fraction AS Y-nd
         NODAL Variables = soot AS Soot-nd
$         NODAL Variables = nucleate AS Nuc-nd
$         NODAL Variables = edc_rate AS EDC
$         NODAL Variables = turb_visc_nd AS MUTurb-nd
         NODAL Variables = radiative_flux AS qrad-nd
         NODAL Variables = absorption AS ABSCOEF-nd
         NODAL Variables = convection_coefficient AS HTCoef-nd
         NODAL Variables = convection_temperature AS cTemp-nd
         NODAL Variables = eff_wallyp_bnd AS effYp-nd
         NODAL Variables = eff_wall_area_bnd AS effArea-nd
      End   Results Output Label output

      Begin Results Output Label pputut
         DATABASE Name = waterloo_temps.e
         At Step 0, Increment = 20
         At Step 5000, Increment = 10000
         TITLE Waterloo Test Facility JP8 Fire With Crosswind and Obstacle
$         NODAL Variables = pressure AS Press-nd
$         NODAL Variables = density_nd AS Den-nd
```

```
$         NODAL Variables = viscosity_nd AS MU-nd
$$        NODAL Variables = conductivity_nd AS CONDnd
$         NODAL Variables = x_velocity AS U-nd
$         NODAL Variables = y_velocity AS V-nd
$         NODAL Variables = z_velocity AS W-nd
$         NODAL Variables = turbulent_ke AS TKE-nd
$         NODAL Variables = turbulent_diss AS Epsi-nd
$         NODAL Variables = enthalpy AS Enth-nd
          NODAL Variables = temperature AS Temp-nd
$         NODAL Variables = mass_fraction AS Y-nd
$         NODAL Variables = soot AS Soot-nd
$         NODAL Variables = nucleate AS Nuc-nd
$         NODAL Variables = edc_rate AS EDC
$         NODAL Variables = turb_visc_nd AS MUTurb-nd
$         NODAL Variables = radiative_flux AS qrad-nd
$         NODAL Variables = absorption AS ABSCOEF-nd
$          NODAL Variables = convection_coefficient AS HTCoef-nd
$          NODAL Variables = convection_temperature AS cTemp-nd
$          NODAL Variables = eff_wallyp_bnd AS effYp-nd
$          NODAL Variables = eff_wall_area_bnd AS effArea-nd
       End    Results Output Label putput

$====================================================================
$
$  Begin the heartbeat output for this region
$
$====================================================================

$ Output for culvert
$ Nodes          Case
$ ----------------------------
$ 1367 1366      75 K mesh
$ 186032         605 K mesh
$ 600489 600488  2042 K mesh
      Begin Heartbeat Output out_1
        Stream Name is flow.txt
        Variable is Global time as Time
        Variable is Node Temperature at Node 186032 as T
        Variable is Node x_velocity at Node 186032 as U
        Variable is Node density_nd at Node 186032 as rho
        Variable is Node viscosity_nd at Node 186032 as visc
$       Variable is Node Temperature at Node 1366 as T1
$       Variable is Node x_velocity at Node 1366 as U1
$       Variable is Node density_nd at Node 1366 as rho1
$       Variable is Node viscosity_nd at Node 1366 as visc1
        At Time 0.0 Interval is 0.01
        At Time 1.0 Interval is 0.5
        At Time 120.0 Interval is 0.005
        Termination Time is 360.0
      End Heartbeat Output out_1


$====================================================================
$
$  Begin the definition of the restart file
$  for this region.
$
$====================================================================

      Begin Restart Data restart
        Input Database Name = waterloo.rsout-s0002
        Output Database Name = waterloo.rsout
        At Step 500 Increment = 500
      End Restart Data restart

$====================================================================
$
$  Set the initial condition for this region.
$
$====================================================================

      Begin Initial Condition Block blah
        volume is block_1

        ignite

        pressure = 0.0
        x-velocity = 1300.0
        y-velocity = 0.0
        z-velocity = 0.0

        turbulent kinetic energy = 10.14e4    $ erg/gm = 10.14 J/kg; Tin =
20%
        turbulence dissipation   = 10.61e4 $ erg/gm-s = 10.61 J/kg-s; L =
50 cm

        temperature = 273.0

        mass fraction C12H23 = 0.0
        mass fraction CO     = 0.0
        mass fraction CO2    = 0.0
        mass fraction O2     = 0.233
        mass fraction H2O    = 0.0
        mass fraction H2     = 0.0
        mass fraction N2     = 0.767

        soot mass fraction = 0.0
        soot nuclei mass fraction =  0.0

      End Initial Condition Block blah


$====================================================================
$
$  Define the boundary conditions for this region.
$
$====================================================================

$ Inlet to test facility

      begin inflow boundary condition on surface surface_1
```

```
        x-velocity = 1300.0 $ all six fans running
$        x-velocity subroutine = VEL_INFLOW
        y-velocity = 0.0
        z-velocity = 0.0

        turbulent kinetic energy = 10.14e4    $ erg/gm = 10.14 J/kg; Tin =
20%
        turbulence dissipation    = 10.61e4 $ erg/gm-s = 10.61 J/kg-s; L =
50 cm


        temperature = 273. $ December, near 0 Kelvin

        mass fraction C12H23 = 0.0
        mass fraction CO  = 0.0
        mass fraction CO2 = 0.0
        mass fraction O2  = .233
        mass fraction H2O = 0.0
        mass fraction H2  = 0.0
        mass fraction N2  = 0.767
        soot mass fraction = 0.0
        soot nuclei mass fraction = 0.0

        use fluxes

      end   inflow boundary condition on surface surface_1

$ Upstream wall between test facility room and plenum room

      begin wall boundary condition on surface surface_4

            temperature = 273.0
            USE EQUILIBRIUM PRODUCTION MODEL

      end   wall boundary condition on surface surface_4

$ Outflow/Open at downstream end of test facility room

      begin open boundary condition on surface surface_5

        total pressure = 0.0
        temperature = 273.0    $ December tests...near zero kelvin
        turbulent kinetic energy = 1.e-6 $ low TI
        turbulence dissipation = 1.e-6  $ small length scale
        mass fraction C12H23 = 0.0
        mass fraction CO  = 0.0
        mass fraction CO2 = 0.0
        mass fraction O2  = .233
        mass fraction H2O = 0.0
        mass fraction H2  = 0.0
        mass fraction N2  = 0.767
        soot mass fraction = 0.0
        soot nuclei mass fraction = 0.0

$        FLOW MUST EXIT DOMAIN

      end   open boundary condition on surface surface_5

$ Downstream wall at outlet of test facility room

      begin wall boundary condition on surface surface_2

            temperature = 273.0
            USE EQUILIBRIUM PRODUCTION MODEL

      end   wall boundary condition on surface surface_2

$ Side wall at minimum y coordinate value

      begin wall boundary condition on surface surface_7

            temperature = 273.0
            USE EQUILIBRIUM PRODUCTION MODEL

      end   wall boundary condition on surface surface_7

$ Side wall at maximum y coordinate value

      begin wall boundary condition on surface surface_9

            temperature = 273.0
            USE EQUILIBRIUM PRODUCTION MODEL

      end   wall boundary condition on surface surface_9

$ Floor of test facility room (excluding circular fuel surface);
$ CHT object.

      begin wall boundary condition on surface surface_10

        interface boundary
        USE EQUILIBRIUM PRODUCTION MODEL

      end   wall boundary condition on surface surface_10

$ Fuel pool surface (circular region in test facility floor)

      begin inflow boundary condition on surface surface_6

        x-velocity = 0.0
        y-velocity = 0.0
        z-velocity = 1.61

        turbulent kinetic energy = 8.748    $ erg/gm = 8.748e-4 J/kg; Tin =
150%
        turbulence dissipation    = 0.0212 $ erg/gm-s = 2.12e-6 J/kg-s; L =
200 cm

        temperature = 488.0

        mass fraction C12H23 = 1.0
        mass fraction CO  = 0.0
        mass fraction CO2 = 0.0
        mass fraction O2  = 0.0
```

```
    mass fraction H2O = 0.0
    mass fraction H2  = 0.0
    mass fraction N2  = 0.0
    soot mass fraction = 0.0
    soot nuclei mass fraction = 0.0

    use fluxes

  end   inflow boundary condition on surface surface_6

$ Roof of test facility room

  begin wall boundary condition on surface surface_8

        temperature = 273.0
        USE EQUILIBRIUM PRODUCTION MODEL

  end   wall boundary condition on surface surface_8

$ Cylindrical blocking object (flow can go through interior);
$ This is the culvert - a CHT object.

    $ culvert outer surface
    begin wall boundary condition on surface surface_3

      interface boundary
      USE EQUILIBRIUM PRODUCTION MODEL

    end   wall boundary condition on surface surface_3

    $ culvert ends
    begin wall boundary condition on surface surface_21

      interface boundary
      USE EQUILIBRIUM PRODUCTION MODEL

    end   wall boundary condition on surface surface_21

      $ culvert inner surface
    begin wall boundary condition on surface surface_22

      interface boundary
      USE EQUILIBRIUM PRODUCTION MODEL

    end   wall boundary condition on surface surface_22

$ Calorimeter (unpainted) blocking object;
$ CHT object.

    begin wall boundary condition on surface surface_11

      interface boundary
      USE EQUILIBRIUM PRODUCTION MODEL

    end   wall boundary condition on surface surface_11

$ Calorimeter (painted) blocking object;
$ CHT object.

    begin wall boundary condition on surface surface_12

      interface boundary
      USE EQUILIBRIUM PRODUCTION MODEL
```

```
          end   wall boundary condition on surface surface_12

$ Calorimeter (insulated ends) blocking object;
$ CHT object.

    begin wall boundary condition on surface surface_13

      interface boundary
      USE EQUILIBRIUM PRODUCTION MODEL

    end   wall boundary condition on surface surface_13

$ Downstream offset calorimeter at min x coordinate value

    begin wall boundary condition on surface surface_16

      temperature = 273.0
      USE EQUILIBRIUM PRODUCTION MODEL

    end   wall boundary condition on surface surface_16

$ Downstream offset calorimeter at max x coordinate value

    begin wall boundary condition on surface surface_17

      temperature = 273.0
      USE EQUILIBRIUM PRODUCTION MODEL

    end   wall boundary condition on surface surface_17

$ Calorimeter stand at min x coordinate value

    begin wall boundary condition on surface surface_18

      temperature = 273.0
      USE EQUILIBRIUM PRODUCTION MODEL

    end   wall boundary condition on surface surface_18

$ Calorimeter stand at max x coordinate value

    begin wall boundary condition on surface surface_19

      temperature = 273.0
      USE EQUILIBRIUM PRODUCTION MODEL

    end   wall boundary condition on surface surface_19

$ Calorimeter stand

    begin wall boundary condition on surface surface_20

$       temperature = 273.0 %Commented to achieve insulated behavior
        USE EQUILIBRIUM PRODUCTION MODEL

    end   wall boundary condition on surface surface_20

  END   FUEGO REGION fluid_region

 END   FUEGO PROCEDURE fuego_procedure

END   SIERRA FUEGO
```

The chem.inp File:

```
ELEMENTS
C
O
H
N
END
SPECIES
C12H23
CO
CO2
O2
H2O
H2
N2
END
REACTIONS
1.0C12H23 + 6.0O2 = 12.0CO + 11.5H2 + 0.0N2  0.0 0.0 0.0
1.0CO + 1.0H2 + 1.0O2 = 1.0CO2 + 1.0H2O 0.0 0.0 0.0
END
```

The chem.asc File:

```
1.1
6.20A
DOUBLE
   F
    212       212        11
     12         0         3         5         3         2         8         9        10         4
      4         7         2         0         0         0         0         0         0         0
      0         0         0         0         0         0         0         2         0         0
      0
```

```
    1.0000000000000000E-03
C            O            H            N
  1.2011150000000001E+01  1.5999400000000000E+01  1.0079700000000000E+00  1.4006700000000000E+01
C12H23       CO           CO2          O2           H2O          H2           N2
  1.6731711000000001E+02  2.8010550000000002E+01  4.4009950000000003E+01  3.1998799999999999E+01  1.8015339999999998E+01
  2.0159400000000001E+00  2.8013400000000001E+01
         12          0         23          0          1          1          0          0          1          2
          0          0          0          2          0          0          0          1          2          0
          0          0          2          0          0          0          0          2
          0          0          0          0          0          0          0
          3          3          3          3          3          3          3
          0          0          0          0          0          0          0
  3.0000000000000000E+02  1.3960000000000000E+03  5.0000000000000000E+03  3.0000000000000000E+02  1.0000000000000000E+03
  5.0000000000000000E+03  3.0000000000000000E+02  1.0000000000000000E+03  5.0000000000000000E+03  3.0000000000000000E+02
  1.0000000000000000E+03  5.0000000000000000E+03  3.0000000000000000E+02  1.0000000000000000E+03  5.0000000000000000E+03
  3.0000000000000000E+02  1.0000000000000000E+03  5.0000000000000000E+03  3.0000000000000000E+02  1.0000000000000000E+03
  5.0000000000000000E+03
 -4.2086889300000001E+00  1.1144058100000000E-01 -7.9134658200000001E-05  2.9240624200000000E-08 -4.4374319100000000E-12
 -2.9944687500000000E+04  4.4952170099999996E+01  2.7137359000000000E+01  3.7900489000000002E-02 -1.2943735800000000E-05
  2.0076037200000000E-09 -1.1640058000000001E-13 -4.0795817700000000E+04 -1.2327749500000000E+02  3.2624510000000000E+00
  1.5119408999999999E-03 -3.8817550000000001E-06  5.5819440000000003E-09 -2.4749509999999998E-12 -1.4310539000000001E+04
  4.8488970000000000E+00  3.0250780000000002E+00  1.4426885000000001E-03 -5.6308269999999998E-07  1.0185813000000000E-10
 -6.9109509999999998E-15 -1.4268350000000000E+04  6.1082169999999998E+00  2.2757239999999999E+00  9.9220720000000005E-03
 -1.0409113000000001E-05  6.8666860000000004E-09 -2.1172800000000002E-12 -4.8373139999999999E+04  1.0188488000000000E+01
  4.4536230000000003E+00  3.1401680000000000E-03 -1.2784105000000001E-06  2.3939960000000000E-10 -1.6690332999999999E-14
 -4.8966959999999999E+04 -9.5539589999999996E-01  3.2129360000000000E+00  1.1274863999999999E-03 -5.7561500000000004E-07
  1.3138773000000000E-09 -8.7685540000000003E-13 -1.0052490000000000E+03  6.0347369999999998E+00  3.6975780000000000E+00
  6.1351970000000000E-04 -1.2588420000000000E-07  1.7752810000000000E-11 -1.1364354000000000E-15 -1.2339301000000000E+03
  3.1891650000000000E+00  3.3868420000000001E-03  3.4749820000000000E-02 -6.3546960000000002E-06  6.9685809999999998E-09
 -2.5065880000000002E-12 -3.0208110000000001E+04  2.5902319999999999E+00  2.6721450000000000E+00  3.0562929999999999E-03
 -8.7302600000000002E-07  1.2009964000000000E-10 -6.3916179999999999E-15 -2.9899209999999999E+04  6.8628169999999997E+00
  3.2981240000000001E+00  8.2494410000000002E-04 -8.1430150000000002E-07 -9.4754339999999994E-11  4.1348719999999999E-13
 -1.0125209000000000E+03 -3.2940939999999999E+00  2.9914230000000002E+00  7.0006440000000005E-04 -5.6338280000000001E-08
 -9.2315779999999998E-12  1.5827519000000000E-15 -8.3503399999999999E+02 -1.3551101000000001E+00  3.2986770000000001E+00
  1.4082404000000000E-03 -3.9632219999999999E-06  5.6415150000000000E-09 -2.4448539999999999E-12 -1.0208999000000000E+03
  3.9503720000000002E+00  2.9266399999999999E-03  1.4879768000000001E-03 -5.6847600000000001E-07  1.0097038000000000E-10
 -6.7533509999999998E-15 -9.2279769999999996E+02  5.9805279999999996E+00
          5          5
          2          3
          0          1          0          4          0          0          0          0          0          0
          0          0          0          2          0          6          0          7          0          0
          0          0          0          0          0          0          2          0          6          0
          4          0          0          0          0          0          0          0          3          0
          5          0          0          0          0          0          0          0          0          0
  0.0000000000000000E+00  0.0000000000000000E+00  0.0000000000000000E+00  0.0000000000000000E+00  0.0000000000000000E+00
  0.0000000000000000E+00
          2
          1          2
 -1.0000000000000000E+00 -6.0000000000000000E+00  0.0000000000000000E+00  0.0000000000000000E+00  0.0000000000000000E+00
  0.0000000000000000E+00  1.2000000000000000E+01  1.1500000000000000E+01  0.0000000000000000E+00  0.0000000000000000E+00
  0.0000000000000000E+00  0.0000000000000000E+00  1.6500000000000000E+01 -1.0000000000000000E+00 -1.0000000000000000E+00
 -1.0000000000000000E+00  0.0000000000000000E+00  0.0000000000000000E+00  0.0000000000000000E+00  1.0000000000000000E+00
  1.0000000000000000E+00  0.0000000000000000E+00  0.0000000000000000E+00  0.0000000000000000E+00  0.0000000000000000E+00
 -1.0000000000000000E+00
```

The tran.asc File:

```
1.1
6.20A
DOUBLE
      F
        212        212         11
         12          0          3          5          3          2          8          9         10          4
          4          7          2          0          0          0          0          0          0          0
          0          0          0          0          0          0          0          2          0          0
          0
    1.0000000000000000E-03
C            O            H            N
  1.2011150000000001E+01  1.5999400000000000E+01  1.0079700000000000E+00  1.4006700000000000E+01
C12H23       CO           CO2          O2           H2O          H2           N2
  1.6731711000000001E+02  2.8010550000000002E+01  4.4009950000000003E+01  3.1998799999999999E+01  1.8015339999999998E+01
  2.0159400000000001E+00  2.8013400000000001E+01
         12          0         23          0          1          1          0          0          1          2
          0          0          0          2          0          0          0          1          2          0
          0          0          2          0          0          0          0
          0          0          0          0          0          0          0
          3          3          3          3          3          3          3
          0          0          0          0          0          0          0
  3.0000000000000000E+02  1.3960000000000000E+03  5.0000000000000000E+03  3.0000000000000000E+02  1.0000000000000000E+03
  5.0000000000000000E+03  3.0000000000000000E+02  1.0000000000000000E+03  5.0000000000000000E+03  3.0000000000000000E+02
  1.0000000000000000E+03  5.0000000000000000E+03  3.0000000000000000E+02  1.0000000000000000E+03  5.0000000000000000E+03
  3.0000000000000000E+02  1.0000000000000000E+03  5.0000000000000000E+03  3.0000000000000000E+02  1.0000000000000000E+03
  5.0000000000000000E+03
 -4.2086889300000001E+00  1.1144058100000000E-01 -7.9134658200000001E-05  2.9240624200000000E-08 -4.4374319100000000E-12
 -2.9944687500000000E+04  4.4952170099999996E+01  2.7137359000000000E+01  3.7900489000000002E-02 -1.2943735800000000E-05
  2.0076037200000000E-09 -1.1640058000000001E-13 -4.0795817700000000E+04 -1.2327749500000000E+02  3.2624510000000000E+00
  1.5119408999999999E-03 -3.8817550000000001E-06  5.5819440000000003E-09 -2.4749509999999998E-12 -1.4310539000000001E+04
  4.8488970000000000E+00  3.0250780000000002E+00  1.4426885000000001E-03 -5.6308269999999998E-07  1.0185813000000000E-10
 -6.9109509999999998E-15 -1.4268350000000000E+04  6.1082169999999998E+00  2.2757239999999999E+00  9.9220720000000005E-03
 -1.0409113000000001E-05  6.8666860000000004E-09 -2.1172800000000002E-12 -4.8373139999999999E+04  1.0188488000000000E+01
  4.4536230000000003E+00  3.1401680000000000E-03 -1.2784105000000001E-06  2.3939960000000000E-10 -1.6690332999999999E-14
 -4.8966959999999999E+04 -9.5539589999999996E-01  3.2129360000000000E+00  1.1274863999999999E-03 -5.7561500000000004E-07
  1.3138773000000000E-09 -8.7685540000000003E-13 -1.0052490000000000E+03  6.0347369999999998E+00  3.6975780000000000E+00
  6.1351970000000000E-04 -1.2588420000000000E-07  1.7752810000000000E-11 -1.1364354000000000E-15 -1.2339301000000000E+03
```

```
     3.1891650000000000E+00    3.3868420000000001E+00    3.4749820000000002E-03   -6.3546960000000002E-06    6.9685809999999998E-09
    -2.5065880000000002E-12   -3.0208110000000001E+04    2.5902319999999999E+00    2.6721450000000000E+00    3.0562929999999999E-03
    -8.7302600000000002E-07    1.2009964000000000E-10   -6.3916179999999999E-15   -2.9899209999999999E+04    6.8628169999999997E+00
     3.2981240000000001E+00    8.2494410000000002E-04   -8.1430150000000002E-07   -9.4754339999999994E-11    4.1348719999999999E-13
    -1.0125209000000000E+03   -3.2940939999999999E+00    2.9914230000000002E+00    7.0006440000000005E-04   -5.6338280000000001E-08
    -9.2315779999999998E-12    1.5827519000000000E-15   -8.3503399999999999E+02   -1.3551101000000001E+00    3.2986770000000001E+00
     1.4082404000000000E-03   -3.9632219999999998E-06    5.6415150000000002E+00   -2.4448539999999999E-12   -1.0208999000000000E+03
     3.9503720000000002E+00    2.9266399999999999E+00    1.4879768000000001E-03   -5.6847600000000001E-07    1.0097038000000000E-10
    -6.7533509999999998E-15   -9.2279769999999996E+02    5.9805279999999996E+00
          5          5
          2          3
          0          1          0          4          0          0          0          0          0          0
          0          0          0          2          0          6          0          7          0          0
          0          0          0          0          0          0          2          0          6          0
          4          0          0          0          0          0          0          0          3          0
          5          0          0          0          0          0          0          0          0          0
     0.0000000000000000E+00    0.0000000000000000E+00    0.0000000000000000E+00    0.0000000000000000E+00    0.0000000000000000E+00
     0.0000000000000000E+00
          2
          1          2
    -1.0000000000000000E+00   -6.0000000000000000E+00    0.0000000000000000E+00    0.0000000000000000E+00    0.0000000000000000E+00
     0.0000000000000000E+00    1.2000000000000000E+01    1.1500000000000000E+01    0.0000000000000000E+00    0.0000000000000000E+00
     0.0000000000000000E+00    0.0000000000000000E+00    1.6500000000000000E+01   -1.0000000000000000E+00   -1.0000000000000000E+00
    -1.0000000000000000E+00    0.0000000000000000E+00    0.0000000000000000E+00    0.0000000000000000E+00    1.0000000000000000E+00
     1.0000000000000000E+00    0.0000000000000000E+00    0.0000000000000000E+00    0.0000000000000000E+00    0.0000000000000000E+00
    -1.0000000000000000E+00
```

Appendix B. Results from the refinement study

CFD and fire codes are more commonly written in a node centered control volume formulation. Fuego, being written in a control volume finite element formulation with a vertex centered scheme, will behave differently in some regards. When an object (assume a hex element with flow perpendicular to a face) is a single node wide with a node centered scheme, flow perpendicular to the object cannot pass in that perpendicular direction. A vertex centered scheme is different with respect to a single node wide object. A control volume is assumed around the vertex, which includes flow area that has adjoining area with a down-stream node. It is not until an object is two nodes wide that a vertex exists without adjoining area to the down-stream nodes. The impact of having a single node wide object has been further investigated.

A small test case was designed that includes a rectangular channel with a rectangular object. The channel was 5 cm x 5 cm, and the object had a 1 cm cross-section. An inlet velocity of 50 cm/sec was used. A graphic is found in Figure 10-1. This case was progressively refined from a 5 x 5 x 10 domain by dividing each hexagonal element 1x, 2x, and 3x. This results in the blocking object having 1, 2, 3, and 4 nodes across each face. The pressure, stream-wise (x) velocity, and transverse (z) velocity have been examined as a function of the mesh refinement.   These are found in Figure 10-2 through Figure 10-4 respectively. In each figure, the resolution is evident by observing the mesh that is overlaid on the mesh in subtly different colors. In the gap of the blocking object, a clearer indication is found sketched in the gap.
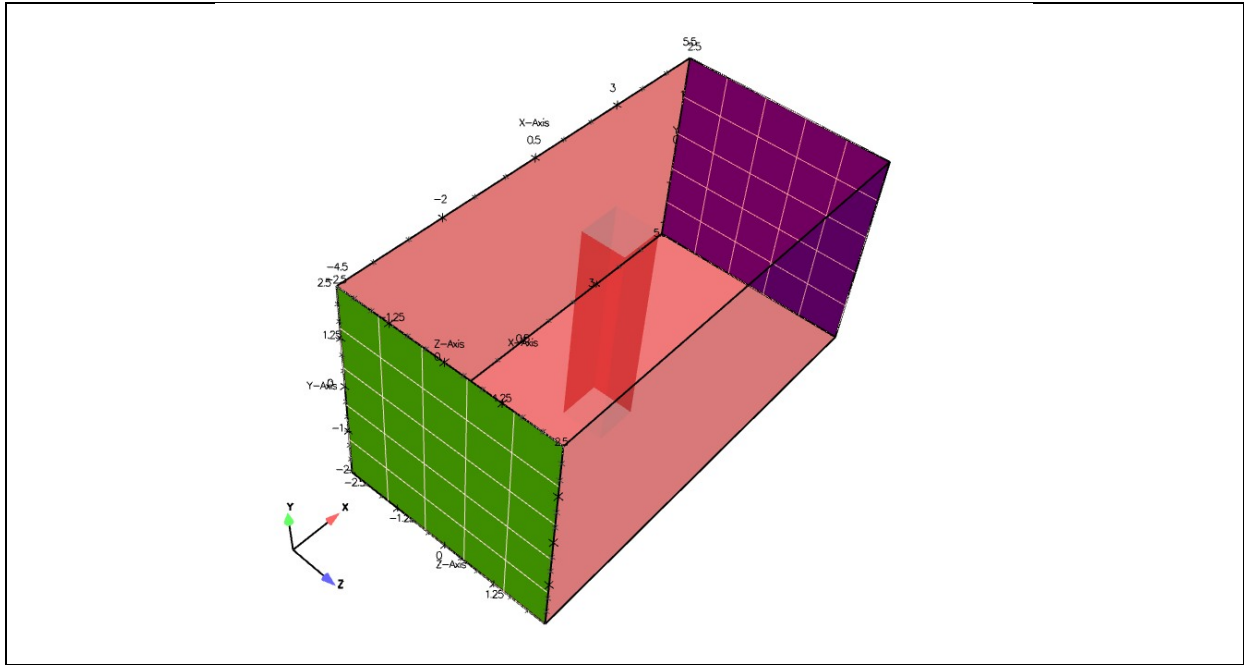
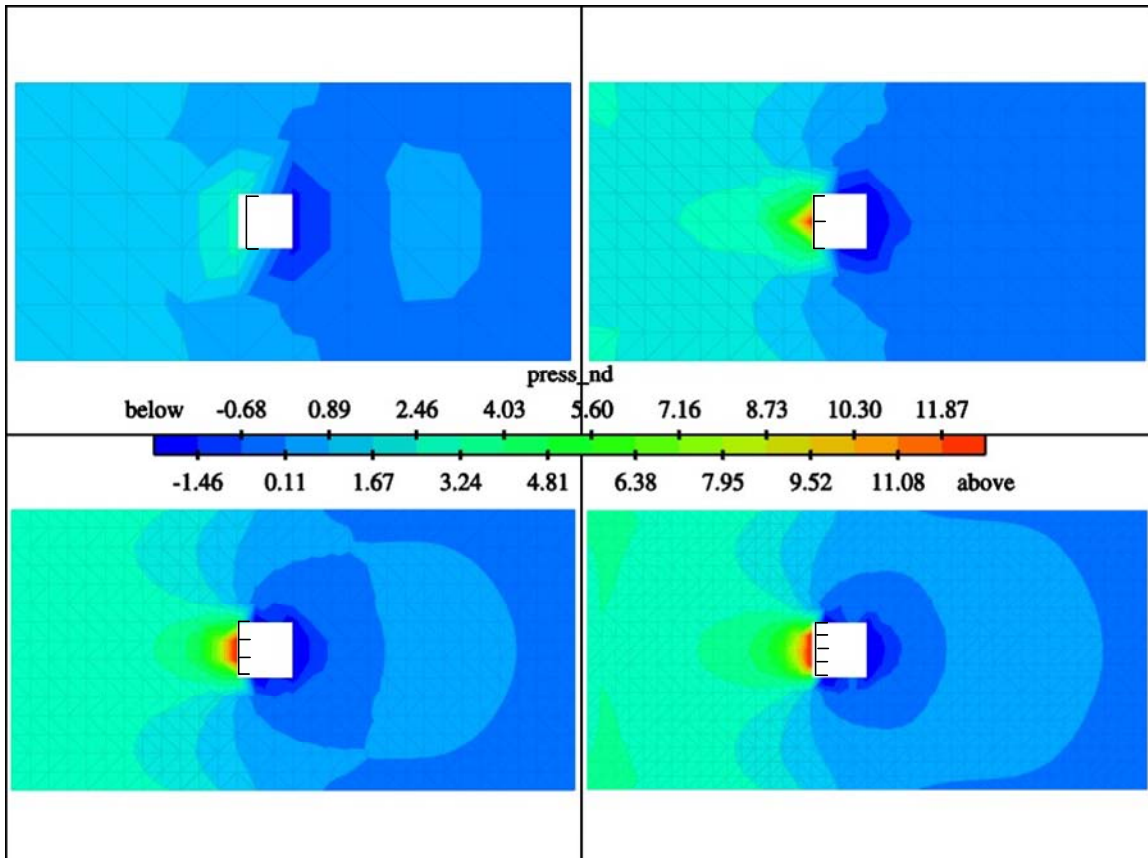Figure 10-1 An illustration of the test case geometry

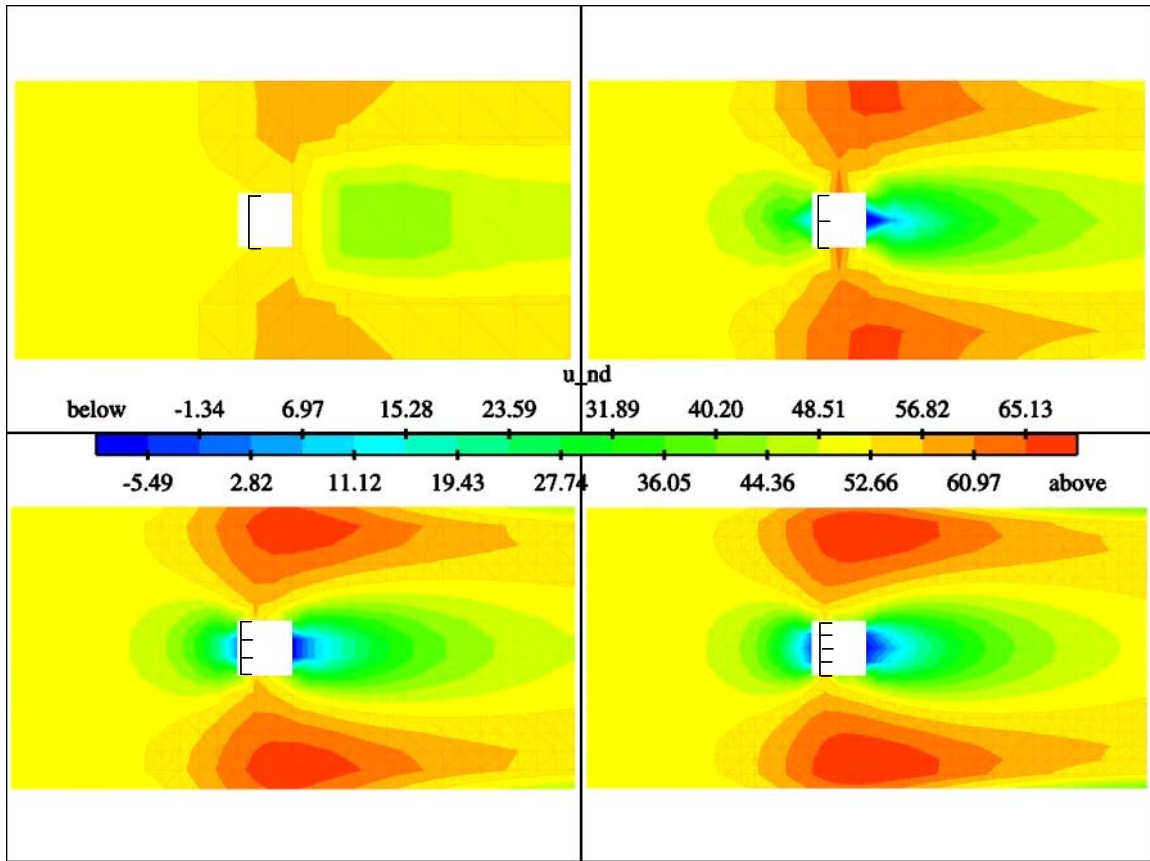Figure 10-2 Pressure predictions for the test case meshes

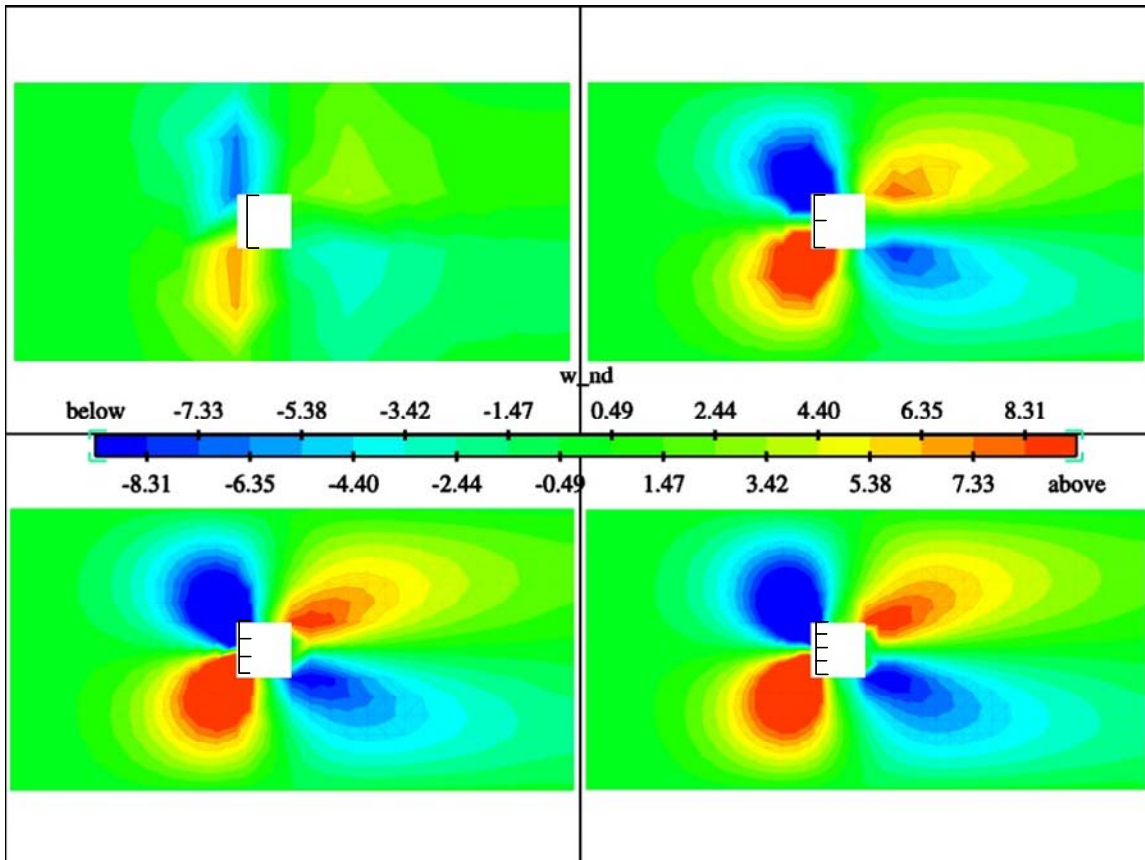Figure 10-3 x-velocity predictions for the test case meshes

Figure 10-4 z-velocity predictions for the test case meshes

The pressure plot suggests the pressure differential is severely under-predicted by the case with just one node across the object. The prediction with two is dramatically improved, and the difference between 3 and 4 is comparatively subtle. Similar observations are seen in the velocity plots.

The net effect of the low resolution is that the pressure drop and the velocity perturbations are substantially under-predicted from what they would be with improved resolution. This test case is at a Reynolds number of around 500, whereas in the experiments the Reynolds number for the objects in question might be as high as 20,000. It is not clear how this affects the findings. Without further refinement and more substantial testing at different Reynolds number conditions, it is difficult to know the required resolution to properly resolve an object in a flow. This test case succeeds at illustrating the significance of the assumptions that have been made to attempt to model the experimental system.

Appendix C. The inlet profile for the TFNS simulations

Modeling an inlet boundary condition with the TFNS turbulence model is different from modeling with the k-epsilon model. With k-epsilon, the inlet turbulence is specified with inlet conditions on the k and epsilon equations. The TFNS model requires turbulent scales above the specified filter to be explicitly modeled at the inlet by varying the velocity according to a

function or profile. The time filter used was 0.02 seconds, and data response from the gages used to measure inlet profiles was not sufficiently sensitive to provide these data.

A function was constructed to vary the stream-wise velocity using 2-dimensionally and time varying sinusoidal functions. The equation employed in this study is evident in the printout of the user subroutine that was compiled with Fuego and used to generate the varying inlet condition. The printout is at the end of this section. Each sine function varies temporally, and two of the functions project the functions spatially in a diagonal direction, while the third projects the sine function in a circular direction. The function was run with parameters that kept the mean velocity to 13 m/s, and allowed decreasing probability for velocities to be found at magnitudes further from the mean with a maximum range of about 10-16 m/s. Figure 10-5 shows a representation of the function applied across the inlet at a single time. The constants used were: period = 1.0 [s]; amplitude = 80.0 [cm/s]; and unot = 1300.0 [cm/s].
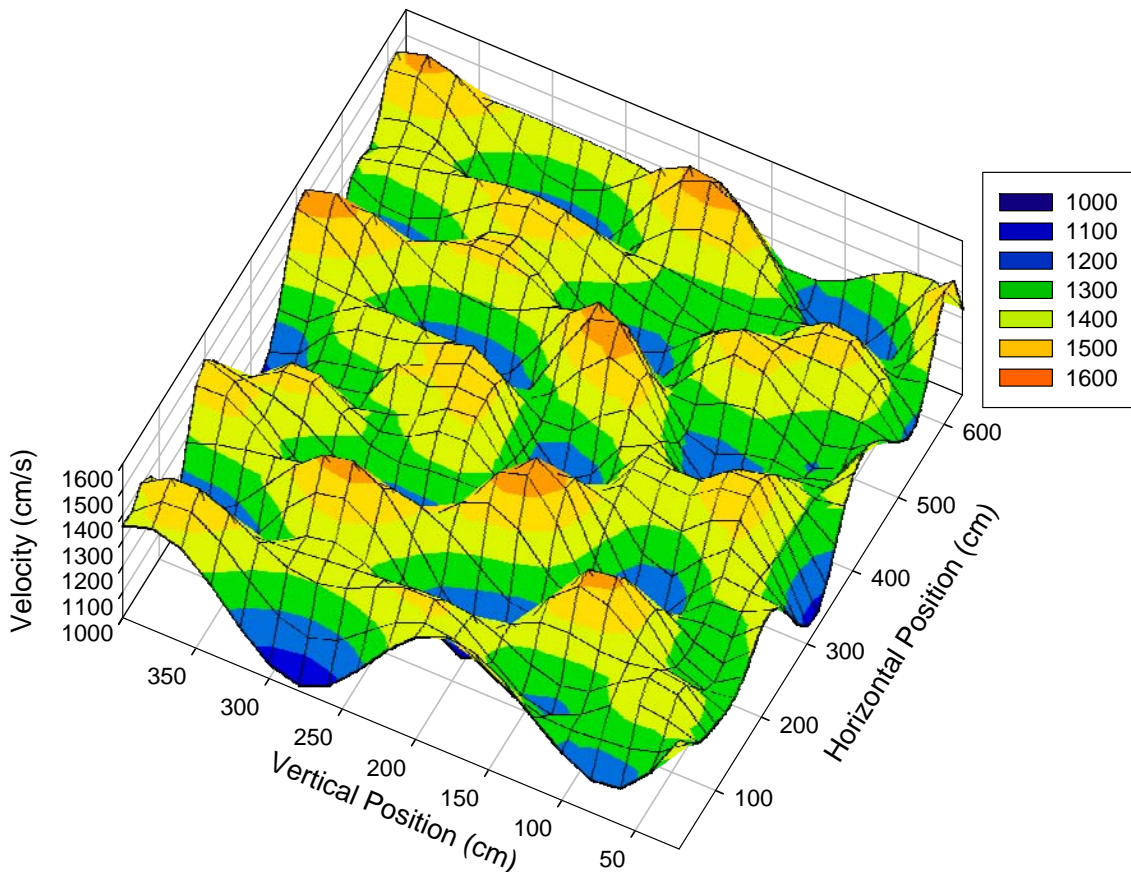
Figure 10-5 An illustration of the inlet profile for the TFNS simulation

A listing of the user subroutine:
```
      SUBROUTINE wtl_u_vel (NPTS, TIME, COORDS, VALUES,
     $               ICONST, ILEN, RCONST, RLEN)
C***********************************************************************
C
C*-----------------------------------------------------------------*C
C*    Copyright 2001 Sandia Corporation.                          *C
```

144

```
C*      Under the terms of Contract DE-AC04-94AL85000, there is a      *C
C*      non-exclusive license for use of this work by or on behalf     *C
C*      of the U.S. Government.  Export of this program may require     *C
C*      a license from the United States Government.                    *C
C*------------------------------------------------------------------*C
C
C       PURPOSE:
C
C
C       INPUTS:
C
C         NPTS      - number of points to evaluate
C         TIME      - current time
C         COORDS()  - coordinate locations for each point
C                      COORD(3,NPTS)
C                           COORD(1,I) is x
C                           COORD(2,I) is y
C                           COORD(3,I) is z
C       OUTPUTS:
C
C         VALUES()  - user-defined value for each point
C                      VALUES(NPTS)
C
C       DESCRIPTION:
C         Load in time varying inlet w-component of velocity at pool
C
C       AUTHOR:
C
C         Alex Brown
C         Sandia Nat. Lab
C         albrown@sandia.gov
C
C       REFERENCES:
C
C          NONE
C
C       LOCAL VARIABLES:
C
C
C       ROUTINES CALLED:
C
C
C       COMMON BLOCKS USED:
C
C
C       REVISION HISTORY (MM/DD/YY):
C
C
C
C**********************************************************************
C
C
#include <Afgo_numbers.h>

        INTEGER          NPTS, ICONST, ILEN, RLEN
C
        DOUBLE PRECISION TIME, COORDS, VALUES, RCONST
C
        DIMENSION        COORDS(3,NPTS), VALUES(NPTS), ICONST(ILEN)
        DIMENSION        RCONST(RLEN)
C
C------------------------------------------------------------------------
C

        INTEGER J
        DOUBLE PRECISION period, amp, unot, pi
C
C************* FIRST EXECUTABLE STATEMENT OF wtl_u_vel ******************
C
        period = RCONST(1)
        amp    = RCONST(2)
```

```fortran
      unot   = RCONST(3)
C
      pi = four*atan(one)
C
      DO 200 J=1, NPTS
C
          VALUES(J) = unot + amp*sin(two*pi*(time/period)+(COORDS(2,J)+
     &    COORDS(3,J))/(five*five*two))
     &    +amp* sin(two*pi*(time/period)+(COORDS(2,J)-
     &    COORDS(3,J))/(five*five*two))
     &    +amp*two/three* sin(two*pi*(time/period)
     &    +(((COORDS(2,J)-830.)**two+
     &    (COORDS(3,J)-600)**two)**(one/two))/(three*three*two*2))


  200 CONTINUE
C
      RETURN
C
C************* LAST EXECUTABLE STATEMENT OF wtl_u_vel *******************
C
      END
```

Appendix D. Pre-test Simulations

Appendix D. Pre-test simulations

Sandia National Laboratories

Operated for the U.S. Department
of Energy by   **Sandia**
Corporation

Albuquerque,   New
Mexico 87185-0836

date: June 13, 2003

to: Distribution

from: Walt Gill and Alex Brown, Org 9132

subject: Selection of Calorimeter Locations in the Waterloo Cross Wind Fire Test

Background and Summary. The wind/object/fire interaction experimentation in preparation at the Waterloo Cross Wind Fire Test Facility will subject calorimeters and associated fire instrumentation to a series of fire scenarios involving a large blocking object (Figure 1). The blocking object, a 9 ft diameter culvert, is sized and oriented to represent a truck tank trailer, aircraft fuselage, or some building structure. A burning pool of liquid hydrocarbon fuel is placed up-wind of the blocking object, with the fire instrumentation on both sides. A major element of the fire instrumentation suite is the passive calorimeter, which is used to determine the heat flux from the fire to an object involved with the fire environment.
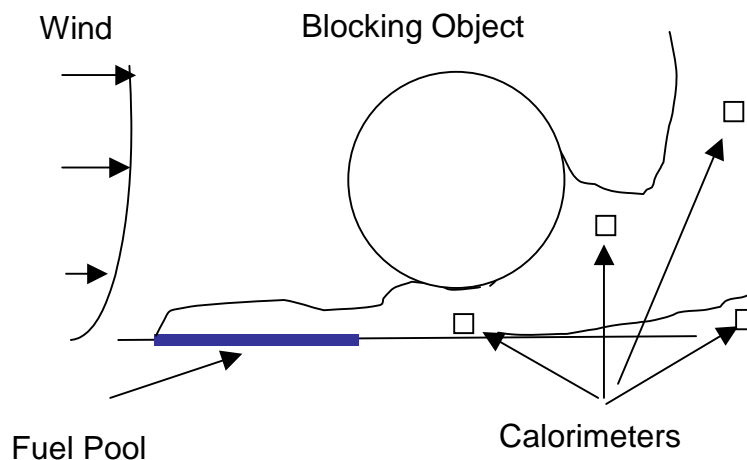
Figure1. Heat flux to objects in a pool fire involving a large blocking object in a crosswind.

The calorimeters have an appropriate dimension and geometry (12" OD x 24" long x 3/8" wall SS304 tube) to represent objects of current interest in fire safety studies. The size and thermal characteristics of the calorimeter are mindful of a variety of small cargo hazardous

147

materials packagings. There are 10 calorimeters available. One is being held back for further characterization at the Radiant Heat Facility in Albuquerque, leaving 9 to be deployed in the test at Waterloo.

The location of the calorimeters in the fire test are based on environments that would interest package designers. These are the environments and object orientations that result in heating that fully exercise packaging performance.

Because objects in fires are coupled with the fire plume dynamics and thus create their own environment, it is not possible to choose a location with the desired characteristics prior to the test. It is necessary to choose locations based on educated guesses and run the test to confirm that the desired results are obtained. Experimentally this would prove costly and likely not to yield a result even with multiple iterations. This is because it is physically not possible to capture a global view of the fire environment experimentally. To get around this limitation, we appeal to the fire codes VULCAN and FUEGO. The process is still iterative, however with the model, the entire fire environment (including immeasurable parameters) is available to aid in making educated guesses.

In what follows, the calorimeter configuration requirements are first reviewed. Then the results of VULCAN simulations of three fires in the Waterloo facility are explored for locations that potentially create the desired environment. It is found that the same locations serve for all three fires. The next step, to be reported on at a later date is to perform simulations with the calorimeters in the chosen locations, and confirm the desired environments are obtained.

Calorimeter Configuration Requirements. One thermal environment that is of interest to a package designer is intense heating, which is to be expected in regions of high fire plume temperature. To represent a shipping container, the object location and orientation in such a region would be ~ 1 m above the ground and oriented with the axis vertical. Another location which would represent a shipping container on the side would be the calorimeter lying on the ground with the axis oriented parallel to the flow. Both of these configurations can be either up-wind or down-wind of the blocking object and represent containers thrown from a vehicle in a transportation accident.

Another potentially challenging thermal environment provides a high thermal gradient around the periphery of the object. This can be expected to occur in three possible ways. The first is the object on the ground with the lower half of the object covered. The second is the object near the edge of the fire plume, and the third is the object interacting with the flow and enhancing mixing of fuel and air creating a local region of high temperature. This latter way would occur in the plume where the object Reynolds number is between 100 and 100,000. The Reynolds number range corresponds to the object generating vortices in the flow wake. Simultaneously, the turbulence length scale needs to be larger than the object. If the turbulent length scale is larger than the object, the vortices will enhance fuel air mixing leading to intense burning in the wake of the object and potentially a high heat flux on the down-wind side.

Thus, there are three desired locations for a non-uniformly heated object. The first is directly under the blocking object on the ground and oriented with the axis perpendicular to the flow. This could represent fallen hazardous cargo in an aircraft accident scenario. The second location is up-wind of the blocking object near the leading edge of the fire plume, 2 m above the ground, and oriented perpendicular to the flow. This could correspond to a munitions or fuel tank on an aircraft wing. The third location is down-wind of the blocking object 2 m above the ground. This corresponds to a similar situation on the down-wind side of the aircraft. These requirements are summarized in Table 1.

Calorimeter Designation	Calorimeter Configuration	Height Above Ground	Axis Orientation wrt to Ground	Axis Orientation wrt to Flow	Flow Environment
A	Cargo on Ground	0 m	Horizontal	Perpendicular	High Velocity
B	Munitions on Up-wind Wing	2 m	Horizontal	Perpendicular	High Velocity
C	Munitions on Down-wind Wing	2 m	Horizontal	Perpendicular	High Velocity
D	Upright Shipping Container	1.5 m	Vertical	NA	High Temperature
E	Upset Shipping Container	0 m	Horizontal	Parallel	High Temperature

Table 1. Required Calorimeter Configurations.

Expected Fire Environment. Preliminary runs with VULCAN in the Waterloo facility for a 2 meter diameter fire upwind of the 2.47 m (9 ft) diameter blocking object were calculated. Three wind speeds were considered; 2 m/s, 6 m/s, and 10 m/s. Figure 2 shows the boundary of the computational domain, the location of the blocking object and the pool fire.
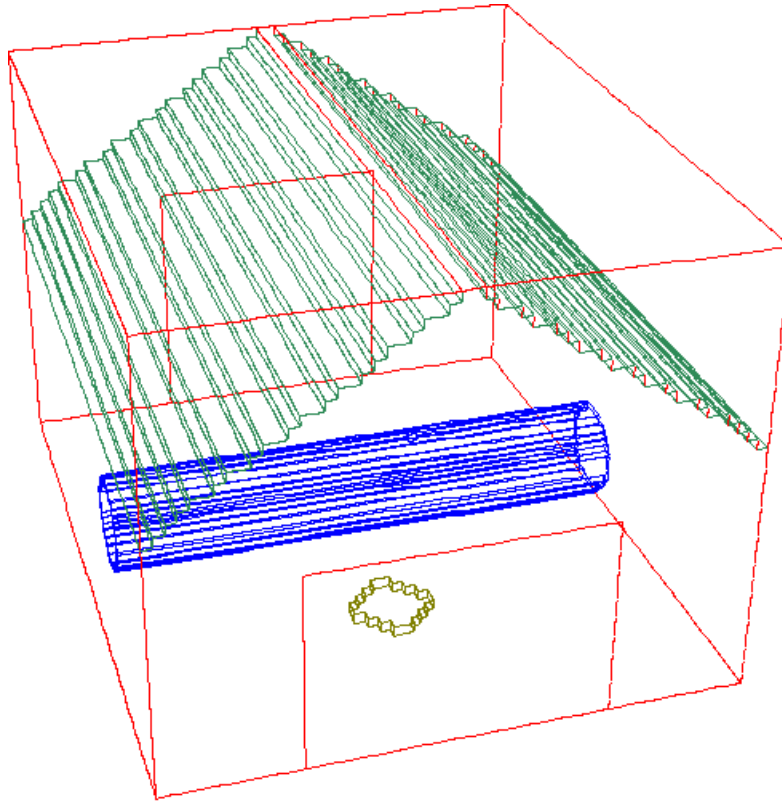
Figure 2. Computational domain for VULCAN simulations of the Waterloo facility. The view is from the inlet end. The pool is on the floor in front of the blocking body.

Figure 3 shows the flow temperatures along the center plane of the facility for the three chosen wind velocities. Figure 4 shows potential values of Reynolds number for a 0.3048 m (1 ft) dia cylinder, and Figure 5 shows turbulent length scales for the same wind speeds.

Turbulent length scale predictions in Figure 5 are dependent on the assumed inlet turbulence parameters, which for these simulations were based on an assumption of low turbulence. The length scale is based on the standard assumed definition for turbulence length scale ($L \equiv k^{3/2}/\varepsilon$). As more detailed information about the actual flow in the facility becomes available, improved predictions will be necessary to provide improved input to the experimental design.
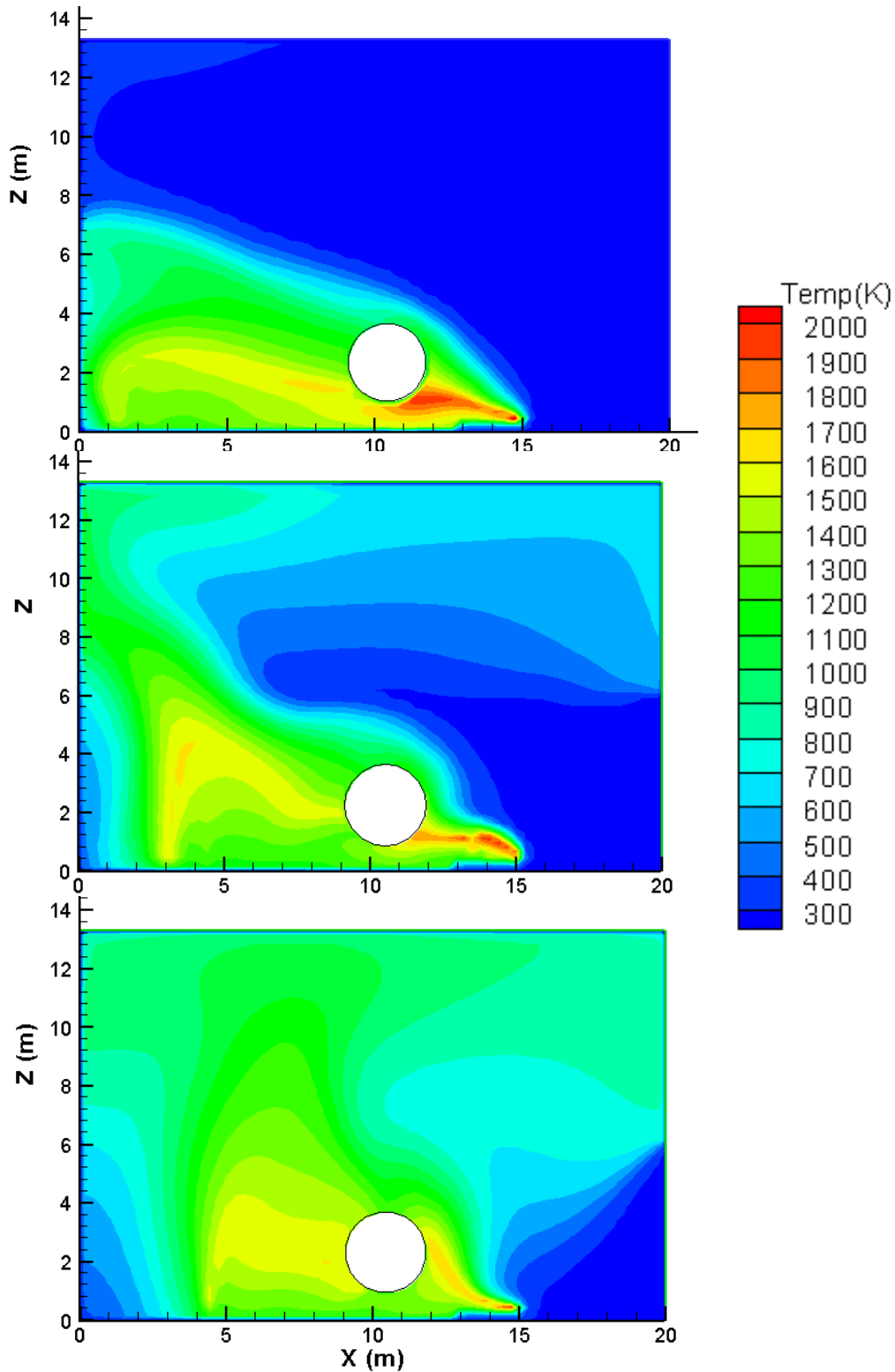
Figure 3. Flow temperatures along center plane for the three wind velocities 10 m/s (top), 6 m/s (middle) and 4 m/s (bottom).
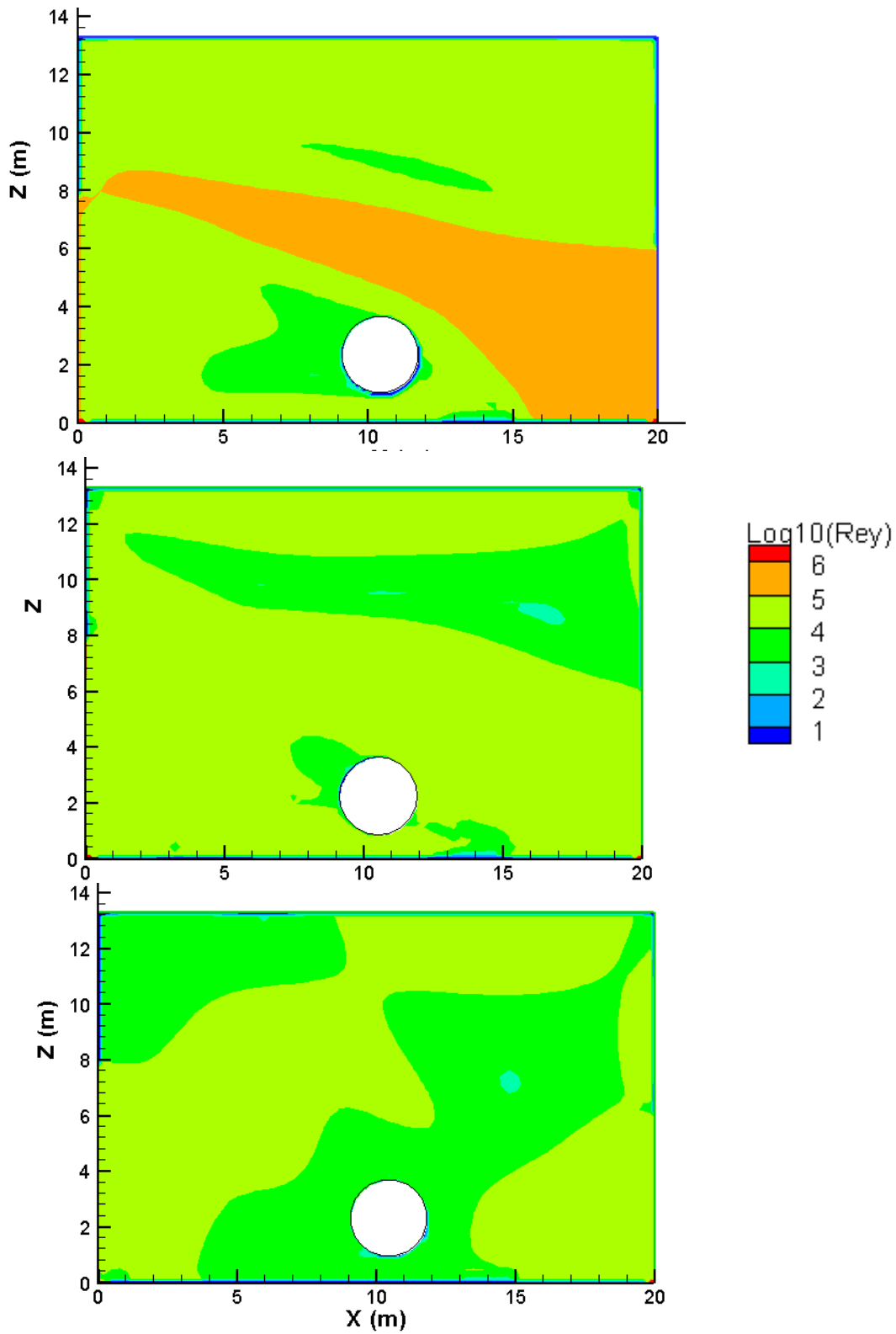
Figure 4. Log$_{10}$(Reynolds Number) of a hypothetical 0.3048 m dia cylinder along center plane for the three wind velocities 10 m/s (top), 6 m/s (middle) and 4 m/s (bottom).
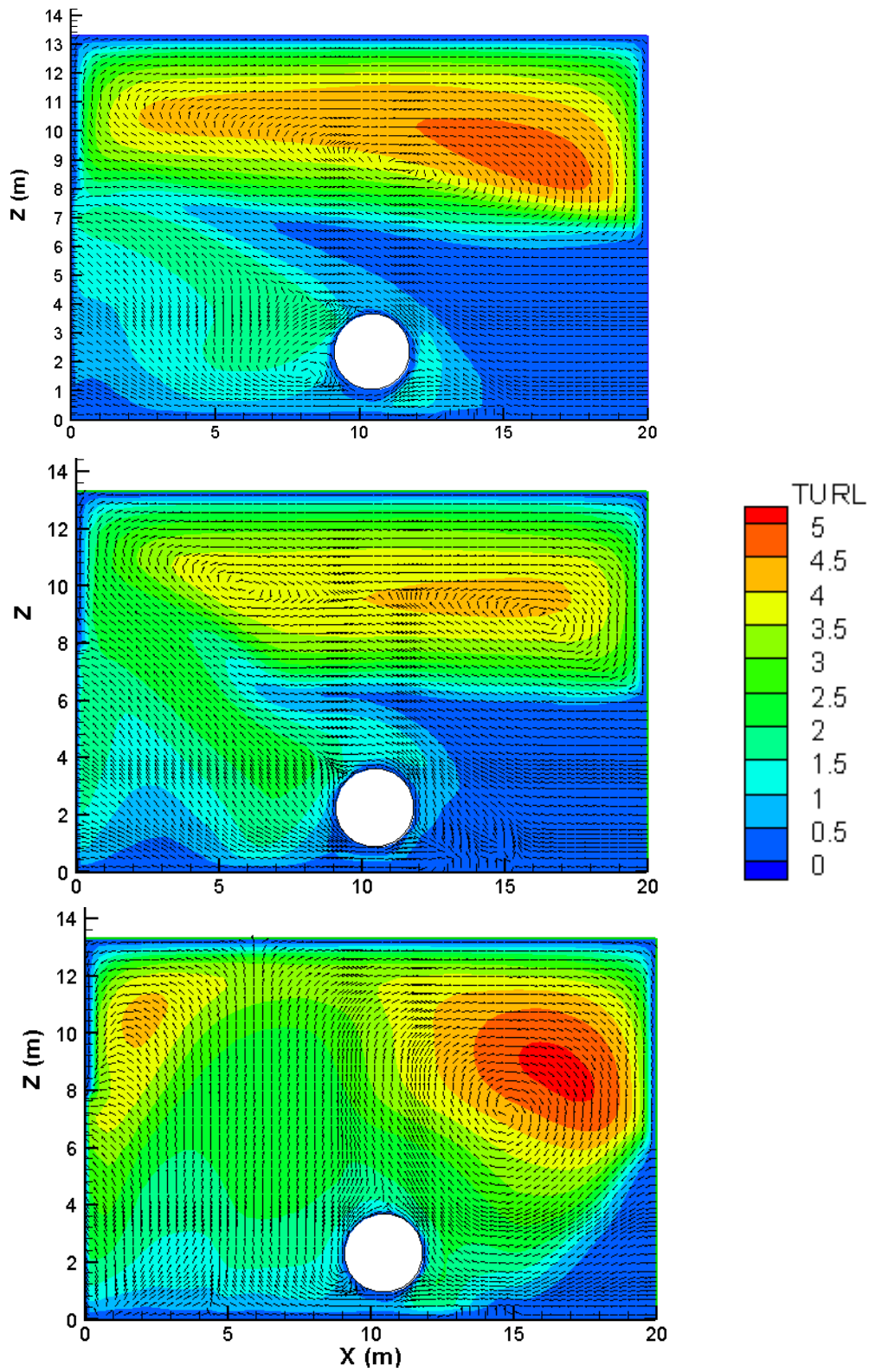
Figure 5. Flow turbulent length scale along center plane for the three wind velocities 10 m/s (top), 6 m/s (middle) and 4 m/s (bottom). The vectors indicate the average flow velocity.

Calorimeter Locations.   For the non-uniformly heated calorimeters, the flow criteria are met almost anywhere in the fire plume. Therefore, calorimeters B and C are placed at the 2 meter height in locations that correspond to 1) being at the edge of the fire, and 2) being in a flow situation that is amenable to the creation of a wake with enhanced mixing. Calorimeter A is placed directly under the blocking object.

The other calorimeters are placed in regions of intense heating where the local flow temperature is high. The locations for both types of calorimeters are shown in Figure 6 for each of the flow conditions. The contours are of the representative emission temperature raised to the 4th power and multiplied by the Stefan-Boltzman constant to give an indication of the potential local emissive power of the flames.

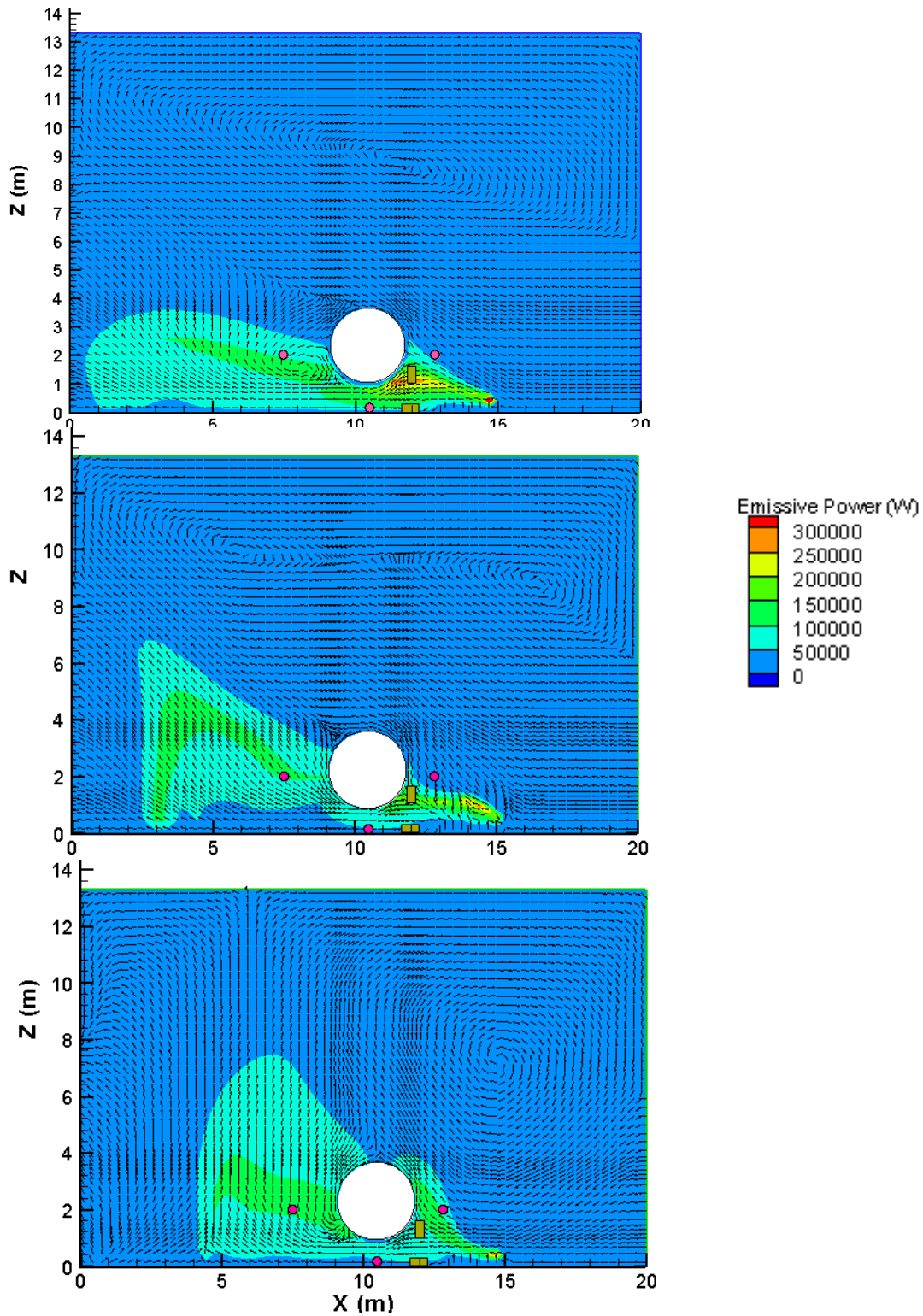| Calorimeter Designation	Height Above Ground	X Location	Axis Orientation wrt to Ground	Axis Orientation wrt to Flow
A	0 m	10.5 m	Horizontal	Perpendicular
B	2 m	12.8 m	Horizontal	Perpendicular
C	2 m	7.5 m	Horizontal	Perpendicular
D	1.0 m	11.85 m	Vertical	NA
E	0 m	11.65 m	Horizontal	Parallel

Table 2. Calorimeter locations

Figure 6. Location of the calorimeters for the wind speeds of 10 m/s (top), 6 m/s (middle), and 2 m/s (bottom). Contour map is the local emissive power of the flames and the vectors indicate the average flow velocity.

These locations are the first iteration of the calorimeter placement. The next step will be to include them in simulations to determine the heat flux from the fire to the object surface. For the calorimeters A, B, and C it is anticipated that the heat flux will vary significantly circumferentially about the object. For the D and E calorimeters, a high flux is expected.

Currently, five locations are selected for the calorimeters on the center-plane of the domain. The center-plane generally yielded the most severe results in computational results reviewed thus far. We presently plan to locate the remaining four calorimeters at similar locations to the first five except at an off-set (~1m) from the center-plane to test this finding experimentally. We remain, however, open to alternative suggestions as to placement of these four remaining objects.

Closure. The placement of fire instrumentation and test objects has historically been based on a mix of correlations, hands-on experience, and outcome expectations. Often, the end results have been disappointing if not misleading. With access to high fidelity computational models, a quality thinking aid is now available for properly instrumenting a fire experiment.

It is recognized the level of quality is dependent on the validity of the fire model, and that VULCAN has not been properly validated for this purpose. However, we believe these results can be viewed as hypotheses to be tested in the experimentation that is to be used to design validation and qualification experiments.

Distribution:

Elizabeth Weckman	University of Waterloo
Lou Gritzo	SNL 9132
Alex Brown	SNL 9132
Walt Gill	SNL 9132
Chuck Hanks	SNL 9132
Anay Luketa-Hanlin	SNL 9132
Barry Boughton	SNL 9116
Don Chenoweth	SNL 8728
Greg Evans	SNL 8728
Richard Simpson	SNL 6423

-- end of memo --

11. Distribution